PIERS 2007 Prague

Progress In Electromagnetics Research Symposium

Abstracts

August 27–30, 2007
Prague, Czech Republic

www.emacademy.org
www.piers.org

PIERS 2007 Prague Abstracts

Published by

The Electromagnetics Academy
777 Concord Avenue, Suite 207
Cambridge, MA 02138

www.emacademy.org
www.piers.org

ISSN: 1559-9450
ISBN: 978-1-934142-01-1

Progress in Electromagnetics Research Symposium

August 27–30, 2007

Prague, CZECH REPUBLIC

PIERS 2007 PRAGUE ORGANIZATION

PIERS Chair

J. A. Kong, MIT, USA

PIERS 2007 Prague General Chair

J. Vrba, Czech Technical University in Prague, Czech Republic

PIERS 2007 Prague General Vice-Chair

M. Mazanek and Z. Skvor, Czech Technical University in Prague, Czech Republic

PIERS 2007 Prague International Advisory Committee

L. C. Botten, W. C. Chew, H.-T. Chuah, G. D'Inzeo
N. Engheta, A. K. Fung, F. Giannini, T. M. Habashy
M. Hallikainen, Y. Hara, H.-C. Huang, E. Jakeman
R. Jansen, L.-W. Li, I. V. Lindell, K.-M. Luk
S. Mano, Y. Miyazaki, P. Pampaloni, M. Persson
A. Priou, L. X. Ran, K. Senne, R. Sorrentino
M. Tateiba, L. Tsang, K. Yasumoto, J. Zehentner
W. X. Zhang

PIERS 2007 Prague Technical Program Committee

A. Baghai-Wadji, H. Bartik, G. Berginc, H. Braunisch
H.-S. Chen, K.-S. Chen, T. J. Cui, H. C. Fernandes
L. Gurel, K. Hoffmann, P. Hudec, K. Kobayashi
J. Lettl, S. Lucyszyn, A. Massa, M. Mazanek
E. L. Miller, M. Moghaddam, R. Muttukrishnan, Z. P. Nie
L. Oppl, V. Pankrac, P. Pechac, P. Peschke
J. Pistora, J. Pokorny, M. Polivka, J. Pribetich
Z. Raida, G. S. N. Raju, R. Ramer, L.-X. Ran
C. M. Rappaport, A. Richter, C. Seo, X.-Q. Sheng
A. H. Sihvola, J. Sistek, L. Vannucci, J. Vokurka
B.-I. Wu, G. Xie

PIERS 2007 Prague Organization Committee

M. Cifra, J. Cvek, T. Drizdal, J. Herza
J. Holis, K. Novotna, M. Pourova, P. Togni
L. Visek, D. Vrba, J. Vrba(jr.), O. Zak
R. Zajicek

PIERS 2007 Prague Administrative Committee

J. J. Bao, Z. Y. Li, P. L. Xie, L. Y. Yu

PIERS 2007 PRAGUE SESSION ORGANIZERS

H. Aniolczyk	Y. N. Barabanenkov	R. De Leo	V. K. Devabhaktuni
K. Ito	S. Kar	H. Kikuchi	K. Kobayashi
J. Lettl	Y. Okuno	M. Oristaglio	M. Polivka
Z. Raida	K. Saito	Y. Shestopalov	Y. Strelniker
R. Talhi	J. Vrba	C.-J. Wu	G. Xie

PIERS 2007 PRAGUE SPONSORSHIP

- ☐ Czech Technical University in Prague
- ☐ Czechoslovakia Section of IEEE
- ☐ EMBS Chapter of Czechoslovakia Section of IEEE
- ☐ The Electromagnetics Academy at Zhejiang University
- ☐ MIT Center for Electromagnetic Theory and Applications/Research Laboratory of Electronics
- ☐ The Electromagnetics Academy

PIERS 2007 SESSIONS

Session 1P1
Computer-Aided RF/Microwave Modeling and Design

A New Computer Aided LNA Design Approach Targeting Constant Noise-figure and Maximum Gain

N. Roy and V. K. Devabhaktuni
Department of ECE, Concordia University, 1455 de Maisonneuve W, Montreal, H3G 1M8, Canada

Abstract— Low-noise amplifiers (LNAs) are critical to a variety of electronic circuits ranging from aerospace to Bluetooth applications. Typically, in the design phase preceding fabrication, an LNA needs to be optimized for a given set of user-specifications [1] (e.g., noise-figure, power consumption, voltage-gain etc.). Traditional approaches based on trial-and-error (e.g., those using Smith-charts) are often human-intensive and not particularly accurate. As such, computer aided design (CAD) approaches for LNAs are in great demand.

In this paper, we present a new and systematic RF/microwave-oriented CAD approach for LNA design. Consider Fig. 1 below. Given the S-parameters (e.g., an .s2p data file) for the transistor to be used in the LNA, the proposed approach finds input/output reflection coefficients that maximize the LNA gain for a specified noise-figure. It is to be noted that such a problem is typically solved by RF/microwave engineers using a trial-and-error approach based on the Smith-chart [2], in which several gain circles are manually plotted until an acceptable solution is found. Such an approach can take several iterations and the accuracy of the solution often replies critically on the expertise of the engineer. In the proposed approach, we accomplish the afore-mentioned task by solving for "the point" on the constant noise-figure circle, i.e., in the complex Γ plane, which intersects with the desired/maximum voltage-gain circle. The proposed CAD approach uses a "constrained line-search optimization technique" to find the exact/precise point (within a user-specified resolution) at which the two circles meet, thereby eliminating the need for a "trial-and-error" scenario.

The proposed CAD approach is illustrated *via* practical LNA example(s). The resulting LNA designs will be shown to meet the user-specifications.

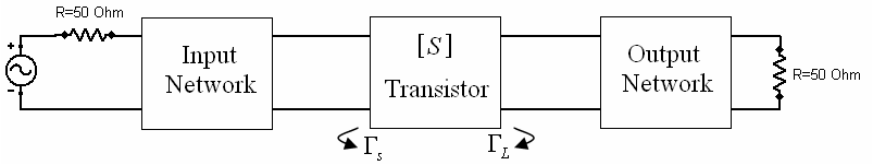

Figure 1: Block diagram of a typical LNA from an RF/microwave perspective.

REFERENCES

1. Lee, T. H., *The Design of CMOS Radio Frequency Integrated Circuits*, Cambridge University Press, Cambridge, UK, 1998.
2. Pozar, D. M., *Microwave and RF Design of Wireless Systems*, John Wiley & Sons, New York, NY, 2000.

EDA Designs of RFIC Inductors

Tianquan Deng

School of Computer Science & Engineering
University of Electronic Science & Technology of China
Chengdu 610054, China

Abstract— IC Inductor Design Tools (IDT) is an interactive software package that employs the quasi-static based full-wave analysis method. Its functionality may include analysis, synthesis, optimization, interpolation, and modeling of spiral inductors with any shape on any material substrate for microwave and wireless applications.

As dramatically increasing IC demand of computer and wireless communication industry, especially when CPU goes to high speed, thus high frequency up to a few GHz processor ICs will be going to the market, inductors will pay more important role in such high frequency ICs, for example, in RFICs and MMICs. It is noted that any kinds of ICs are basically constructed by four components: resistor (R), capacitor (C), inductor (L), and transistor (T). Among them, resistors and capacitors are easily analyzed and designed by simple formulas. Transistors are mainly modeled by measurement ways due to their process dependency and not easy scalability. So far, it really lacks an effective tool for inductor design. Here, only **IDT** fills in this blank with full functionality.

Feature:

- For PCs running Microsoft Windows
- Interactive graphical user interface
- Functions of analyzer, calculator, synthesizer, optimizer, and interpolator
- Use of the real design flow, i.e., from initial design, fabrication and calibration, re-design, till the specified accuracy obtained
- Dependent process design is more practical by the unique calibration technique

Metal Geometry:

- Rectangular, any polygon shape, and round spiral inductors
- No need to manually draw the layout, just to key in the dimension numbers
- Multiple-layer metals
- Considering ohmic loss, skin effect, and metal thickness of any kind of metals

Substrate Material:

- Hybrid fabrication materials such as alumina, ceramic, duroid, etc., and any other PCB
- Semi-conductor materials such as GaAs, Silicon, CMOS, BiCmos, Bipolar, etc.
- And user-defined, as well as, multiple-layer substrates

An unique calibration technique has been used for RFIC inductor design having advantages of high accuracy with independent process technologies. Comparisons with experimental results shows that IDT is a practical EDA tool with one more choice for RFIC designers.

REFERENCES

1. Deng, T., "CAD model for coplanar waveguide synthesis," *IEEE Trans. Microwave Theory Tech.*, Vol. 44, No. 10, 1733–1738, 1996.
2. Deng, T. Q., M. S. Leong, P. S. Kooi, and T. S. Yeo, "Synthesis formulas for coplanar lines in hybrid and monolithic MICs," *Electron. Lett.*, Vol. 32, No. 24, 2253–2254, 1996.
3. Deng, T. Q., M. S. Leong, P. S. Kooi, and T. S. Yeo, "Synthesis formulas simplify coplanar-waveguide design," *Microwaves & RF, Wireless Technology Issue*, Vol. 36, No. 3, 84–98, March 1997.

maximum change in f_r is around 4% when external loading (ice) thickness changes from 1 to 5 mm for $w/h_2 = 5$ and $h_3/h_2 = 0.01$ but as h_3/h_2 ratio increases the effect of external loading on resonant frequency decreases. And as w/h_2 ratio increases, the effect of external loaded is less. For external loading (ice) thickness changes from 1 to 5 mm for $w/h_2 = 20$, the effect is less than 1% with $h_3/h_2 = 0.01$. It shows that change in the resonant frequency for large w/h_2 and h_3/h_2 is small due to external loading.

The resonant frequency of microstrip antenna with one substrate and unwanted air-gap are shown in table with different air-gap. It is seen that there is a slight increase in resonant frequency due to air-gap. The increment is around 0.4% as air-gap h_3 varies from 0 to 4 mm. The experimental and PM calculated resonant frequency are in good agreement as shown in table.

Table 1: Rectangular patch for spaced superstrates.

$L = 28.6$ mm, $W = 36.7$ mm, $h_1 = 0$, $\varepsilon_{r1} = 1$, $h_2 = 1.52$ mm, $\varepsilon_{r2} = 2.986$, h_3 (variable), $\varepsilon_{r3} = 1$, $h_4 = 1$ mm				
h_3 (mm)	ε_{r4}	f_r (exp) GHz [6]	f_r GHz [6]	f_r (PM) GHz
3.5	2.35	2.940	2.937	2.9412
7.5	2.35	2.931	2.946	2.9466
12.8	2.35	2.948	2.952	2.9488
3.5	2.98	2.949	2.930	2.9423
7.5	2.98	2.940	2.943	2.9480
12.8	2.98	2.954	2.951	2.9503
3.5	10.4	2.922	2.891	2.9448
7.5	10.45	2.905	2.925	2.9051
12.8	10.45	2.954	2.944	2.9534
$L = 22.5$ mm, $W = 33.75$ mm, $h_1 = 0$, $\varepsilon_{r1} = 1$, $h_2 = 1.55$ mm, $\varepsilon_{r2} = 4$, $\varepsilon_{r3} = 1$, $h_4 = 0.76$ mm, $\varepsilon_{r4} = 2.32$				
h_3 (mm)	f_r (exp) (GHz) [2]		f_r (PM) (GHz)	% Dev.
0	3.150		3.1968	−1.485
0.1	3.157		3.1836	−0.84
0.2	3.161		3.1706	−0.30

REFERENCES

1. Bahl, I. J. and P. Bhartia, *Microstrip Antennas*, Artech House.
2. Lee, H. F. and W. Chen, *Book Wiley Series in Microwave & Optical Engineering.*
3. Munson, R. E., *IEEE AP-22*, 74–78, Jan. 1974.
4. Kirsching, M., et al., *Electron Lett.*, Vol. 17, 123–5, Feb. 1981.
5. Drordjevic, R., et al., *LINPAR for Window.*
6. Zhong, S.-S., *IEEE on AP-42*, No. 9, Sept. 1994.
7. Bhal, I. J., et al., *IEEE AP-30*, March 1982.

CAD Models for Estimating the Capacitance of a Microstrip Interconnect: Comparison and Improvisation

Sudarshan R. Nelatury[1], **Matthew N. O. Sadiku**[2], **and Vijay K. Devabhaktuni**[3]

[1]School of Engineering, Pennsylvania State University, Erie, PA 16563, USA
[2]College of Engineering, Prairie View A&M University, Prairie View, TX 77446, USA
[3]Department of ECE, Concordia University, Montreal, Quebec, H3G 1M8, Canada

Abstract— Although the field of numerical electromagnetics (EM) has come almost to a level of maturity, RF/microwave design engineers seem to prefer a simple yet accurate closed-form expression for a parameter/quantity of interest. For instance, a frequent scenario is the use of empirical formulae for the estimation of capacitance per unit length of microstrip interconnects. A survey of existing literature reveals that several formulae have been proposed in the past 40 years or so. Each of those works involves building of a CAD model (or formula) based on assumptions that seem reasonable. However, it is these assumptions that differentiate one work from another in some respect, e.g., model accuracy, valid frequency range etc.. A comparison of these formulae against experimentally measured results indicates to an RF/microwave engineer as to which of those several formulae best-suits a given CAD scenario. This paper compares 12 such formulae, which estimate the same quantity (i.e., capacitance). It is observed that cross-fertilization of certain intermediate steps of the above works could potentially lead to composite models that offer relatively better accuracies. For example, employing Schneider's formula (for calculating the effective permittivity of the substrate) in the CAD models proposed by four others leads to improved accuracies of those models. The work is of practical significance to the area of EM as applied to high-frequency circuit design, simulation and optimization.

REFERENCES

1. Bogatin, E., "Design rules for microstrip capacitance," *IEEE Trans. Components, Hybrids, and Manufacturing Tech.*, Vol. 11, No. 3, 253–259, Sept. 1988.
2. Sadiku, M. N. O., *Elements of Electromagnetics*, 4th ed., 236, 553, Oxford University Press, New York, 2007.
3. Knapp, H. R., "Characteristics of microstrip transmission lines," *IEEE Trans. Energy Conversion*, Vol. EC-16, No. 2, 185, April 1967.
4. Schneider, M. V., "Microstrip lines for microwave integrated circuits," *Bell Systems Technical Journal*, Vol. 48, No. 5, 1421, May 1969.
5. Kumar, A., et al., "A method for the calculation of the characteristic impedance of microstrips," *Int. J. Electronics*, Vol. 40, No. 1, 45, 1976.
6. Wheeler, H. A., "Transmission line properties of a strip on a dielectric sheet on a plane," *IEEE Trans. Microwave Theory Tech.*, Vol. 25, No. 8, 631, Aug. 1977.
7. Poh, S. Y., W. C. Chew, and J. A. Kong, "Approximate formulas for line capacitance and characteristic impedance of microstrip line," *IEEE Trans. Microwave Theory and Techniques*, Vol. 29, 135–142, Feb. 1981; and the erratum in Vol. 29, No. 10, 1119, Oct. 1981.
8. Sakurai, T. and K. Tamaru, "Simple formulas for two and three dimensional capacitances," *IEEE Trans. Electron Devices*, Vol. 30, No. 2, 183–185, Feb. 1983.
9. Edwards, T. C., *Foundations for Microstrip Circuit Design*, 45, John Wiley & Sons, New York, 1983.
10. Bogatin, E., "A closed form analytical model for the electrical properties of microstrip interconnects," *IEEE Trans. Components, Hybrids, and Manufacturing Tech.*, Vol. 13, No. 2, 258–266, June 1990.
11. Abuelma'atti, M. T., "An improved approximation to the microstrip line capacitance," *Int. J. of Infrared and Millimeter Waves*, Vol. 13, No. 11, 1795–1800, Nov. 1992.
12. Chow, Y. L. and W. C. Tang, "CAD formulas of integrated circuit components by fuzzy electromagnetics-simplified formulation by rigorous derivation," *Proc. IEEE Int. Symp. APS*, Vol. 3, 16–21, 1566–1569, Salt Lake City, UT, July 2000.
13. Shapiro, A. A., M. L. Mecartney, and H. P. Lee, "A comparison of microstrip models to low temperature co-fired ceramic-silver microstrip measurements," *Microelectronics Journal*, No. 33, 443–447, Jan. 2002.

14. Kwok, S. K., K. F. Tsang, and Y. L. Chow, "A novel capacitance formula of the microstrip line using synthetic asymptote," *Microwave and Optical Technology Lett.*, Vol. 36, No. 5, 327–330, March 2003.

Spacecraft Power Systems Design to Minimize Electro Magnetic Interference (EMI) Effects

Krishna Shenai
Electrical and Computer Engineering Department, Utah State University, Logan, UT, USA

Abstract— The electrical power system in a spacecraft more or less determines the payload, spacecraft size, cost, operating life, and mission efficiency [1]. Hence, it represents the most critical part of the overall spacecraft architecture. Typical components in a spacecraft power system include the power source (a solar array), energy storage system (a battery), power distribution and control unit, power conversion and voltage regulation unit, and payloads as illustrated in Fig. 1. The output voltage derived from the power source is generally variable in nature. There is also a battery charging circuitry to ensure adequate energy storage capability to power the spacecraft at times when the power source is not available. Depending on the mission objectives, high DC as well as AC voltages and currents may be generated on-board from the power source. Consequently, electro-magnetic interference (EMI) and signal integrity are important design constraints.

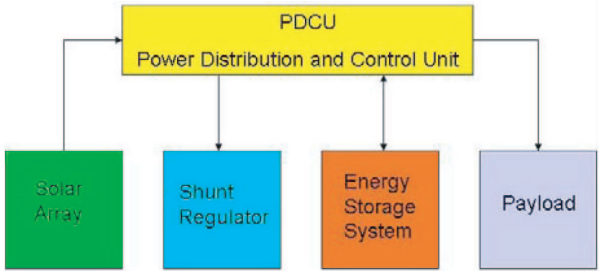

Figure 1: Block diagram of a spacecraft electrical power system.

The main objective in the design of a spacecraft electrical power system is two-fold. The first goal is the reduction of overall power consumption within the spacecraft so that minimum heat is dissipated, which in turn ensures minimal thermal management and cooling requirements, and improved reliability. This will guarantee prolonged operation of the mission and overall reduction of the payload. To reduce the overall power consumption, the spacecraft power system must be designed to obtain the highest power conversion efficiency under all loading conditions. The second consideration pertains to the overall reduction in size and weight of the spacecraft. To achieve this objective, the power system must be designed to operate at the highest power conversion frequency so that power passives and magnetics become small, thereby leading to an increase in power density [2]. The main problem here is that at higher power conversion frequencies, power system components become excessively lossy, and thereby result in increased on-board heating. Hence, a careful tradeoff in power density and power loss is needed to optimize the power system design [3].

The overall power loss in a spacecraft power system may be reduced by ensuring that the power conversion efficiency is at the highest under all loading conditions. Two approaches are used in spacecraft power systems as illustrated in Fig. 2 [4]. In either case, power loss reduction will require increased peak power efficiency and excellent load regulation. The efficiency may be increased by reducing the conduction power loss and the load regulation is improved by ensuring good power switching and control strategies. Further reduction in spacecraft power consumption can result from on-board power management of various loads. Spacecraft power management is in its infancy, and there is a great deal that can be done in this regard. Adaptive intelligent power management (AIPM) is a promising approach where the power system is capable of delivering on-demand efficient point-of-load power [5]. However, AIPM requires the ability to sense local power requirements within finite-state architecture and then delivering the right amount of power at the right time. Such advances are rapidly being accomplished in the commercial applications [6], and hence, tremendous opportunities to adapt AIPM in designing next generation spacecraft power systems exist.

The performance and reliability of the spacecraft power system critically hinges on minimizing application-level electro-thermal stresses [7]. The power system design and layout must be carried

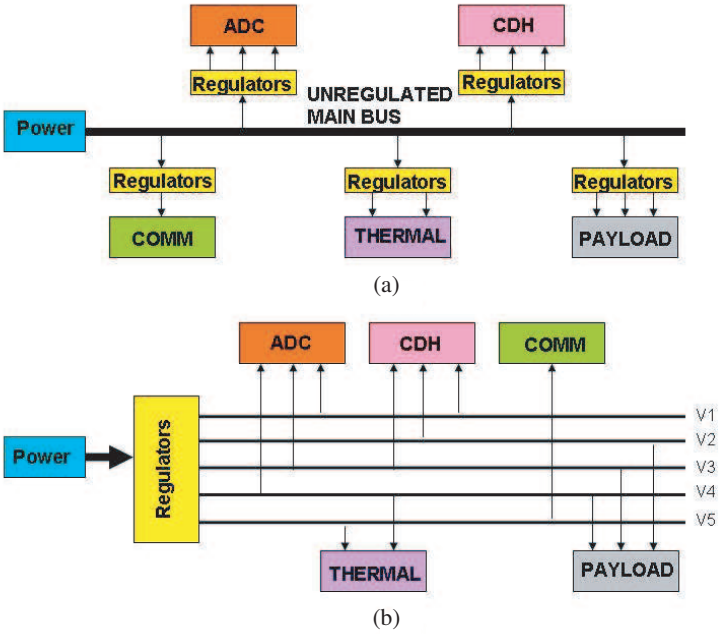

Figure 2: (a) Decentralized voltage regulation approach and (b) centralized voltage regulation approach used in spacecraft power systems.

out to minimize interconnect and package parasitic elements, including the parasitic resistances, capacitances and inductances. The circuit models used for various components (power switches, control electronics, resistors, inductors, capacitors, batteries, solar array, packaging, cooling, thermal management, and so on) must be accurate and physics-based. Such models are not generally available for space-qualified applications because they are technology-dependent. The component non-linearity, charge generation and storage within circuit components, and thermal problems further complicate the design of the spacecraft power system.

An increase in the spacecraft power density generally causes on-board EMI to increase. The spacecraft power system design must then account for EMI considerations in addition to conventional reliability issues pertaining to harsh environmental operation in space.

Past attempts to model the spacecraft electrical power system have generally neglected many of the effects described above, and hence, cannot be used to design reliable and compact power systems. These methodologies have been either circuit-oriented [8] or general purpose state-flow or signal-flow simulators [9]. A more recent approach focuses on a more integrative environment in a virtual test bed approach wherein some aspects of both methods have been applied [10]. However, the problem remains intact in that none of these approaches have the ability to design and model a spacecraft electrical power system to obtain the performance and reliability required. As a result, component specifications are severely de-rated to ensure power system reliability, thus causing significant performance penalty.

In the commercial arena, the SABER circuit simulator has become an industry-standard design tool in power system development [11]. It has the ability to perform a wide range of electrical, thermal and mechanical simulations and consists of state-of-the-art component models. The most important feature of SABER is its behavioral modeling and simulation capability using the MAST language. Component models and physical phenomena can be modeled using behavioral descriptions, thus allowing for tremendous flexibility in the design of complex circuits and systems. There is an opportunity to adapt SABER simulator to design and model advanced spacecraft power systems.

We have developed an approach to power management of devices within a power system that holds out the potential for significant reductions in power consumption. We will present a novel methodology for the design and modeling of next generation spacecraft electrical power systems. Our approach is unique and consists of the following essential elements. We have implemented advanced physics-based models for spacecraft power system components in SABER. We have developed an advanced integrated power system computer-aided design (CAD) infrastructure by integrating SABER simulation environment with two-dimensional (2-D) electromagnetic (EM) and semiconductor device simulation tools to facilitate circuit-level analysis and optimization of

EMI, non-linear charge storage and parasitic effects. We will demonstrate the utility of the new simulation infrastructure to model and design compact and reliable spacecraft power systems. We will further demonstrate the flexibility and scalability of the new CAD infrastructure for application in large spacecraft power system design.

A Novel Neural Smith Chart for Using Transmission Line Impedance Transforming and Impedance Matching

M. Fatih Çağlar[1] and Filiz Güneş[2]
[1]Department of Electronics and Communication Engineering, Süleyman Demirel University
Isparta, Turkey
[2]Department of Electronics and Communication Engineering, Yıldız Technical University
Beşiktaş, Istanbul, Turkey

Abstract— The Smith chart has become an icon of microwave engineering. It was originally intended to be a graphical aid for eliminating the drudgery of computation with complex numbers. A great deal of knowledge can be acquired from a Smith chart, e.g., standing wave ratio, single and double stub tunings and much more. Also, it is very useful in conveying input impedance variations along a transmission line as the observation point moves away from the load. Although Smith charts are valuable and contain significant amount of information, inaccurate observations can lead to erroneous results and frustration. Already, the manual analysis and design of microwave circuits are generally tedious and error prone. In this work, an artificial neural network (ANN) model of the Smith chart is achieved for an alternative solution to traditional calculations. In this model, the two bilinear transformations between the rectangular Z(Y)-plane and the reflection coefficient Γ-plane can be employed in both directions for the training data. Furthermore, translation of the reflection coefficient along the lossless transmission line from the load is also used. In the current work, the feed-forward Multilayer Perceptron (MLP) type of neural network is utilized with the two hidden layers, three inputs and twenty-three outputs. Real and imaginary part of load impedance, physical length and characteristic impedance of the transmission line, operation frequency are inputted to this network, while the magnitude and the phase of the input reflection coefficient, real and imaginary part of input impedance, single stub matching lengths and reactance, double stub matching lengths, position lengths and VSWR are taken as the outputs. Hidden layers activated by the hyperbolic tangent sigmoid function. The output neurons are linearly activated, also. Great generalization ability of the neural networks results in very good accuracy. Input impedance variations along the transmission line and impedance matching application samples are given as the typical examples for the utilization of the Neural Smith chart. Furthermore, Neural Smith chart can be employed Neural Unit Element (NUE) and Neural Stub Element (NSE) to be used in microwave circuitry.

Intertwined Two-section Dual-polarized Log Periodic Dipole Antenna

A. Tran and M. C. E. Yagoub
School of Information Technology and Engineering, University of Ottawa
800 King Edward, Ottawa, ON K1N 6N5, Canada

Abstract— Broadband dual-polarized antenna design is motivated by the needs for a measurement antenna for spherical antenna-measurement systems. In all spherical measurement systems, the positioning unit should often rotate on both axis (ϕ and θ) to measure and generate spherical data tables and 3D radiation pattern plots. Often the total radiated power (TRP) and total isotropic sensitivity (TIS) are the required figures of merit. The TRP calculation involves the discrete integration of the measured radiated power due to E_θ and E_ϕ. To reduce the time duration of a wireless device, it is desirable to have a measurement antenna that can be electronically switched to transmit and receive both field polarizations. Usually, measurement antennas are mechanically rotated for each polarization, making the test twice as long, and increasing the possibility of measurement uncertainties due to variations in the positioning of not only the antennas but also of the mechanical support. Dual polarized dipoles have been used to achieve dual polarization. Cross-polarization isolation of at least 20 dB can be achieved with these dual dipoles. However, as the frequency gets higher (over 5.2 GHz), the dipoles are very short (length less than 2 cm) and more difficult to build. Also, dipoles are inherently narrow-band; therefore it is preferable to replace them with a broadband dual-polarized antenna.

The dipole array antenna is a well known broadband planar antenna. To achieve dual-polarization, two printed log-periodic dipole antennas (LPDA) were placed orthogonally (Fig. 1).

In this paper, we investigated the orthogonally positioned (double-section) dual-polarized log-periodic dipole antenna within the frequency band from 0.8 GHz to 2.1 GHz. The antenna was designed using a 3D electromagnetic simulator (Ansoft-HFSS) and then fabricated with Rogers RT/Duroid 5880 substrate. Part of substrate of the fabricated antenna was then cut-out so that two similar cut-out LPDA can be mounted together. The measured pattern of the double-section LPDA is shown in Fig. 2. The measured gain was 8.3 dB.

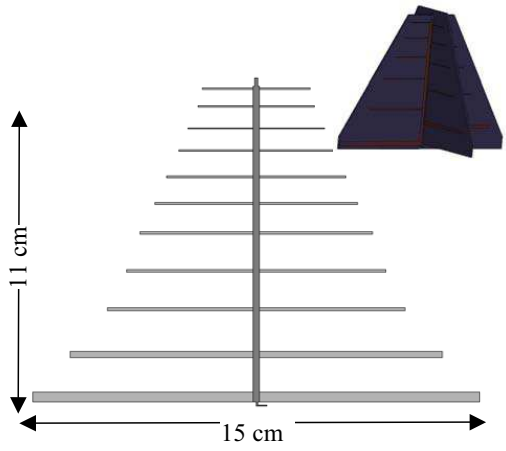

Figure 1: Single section LPDA (in inset: Double-section LPDA).

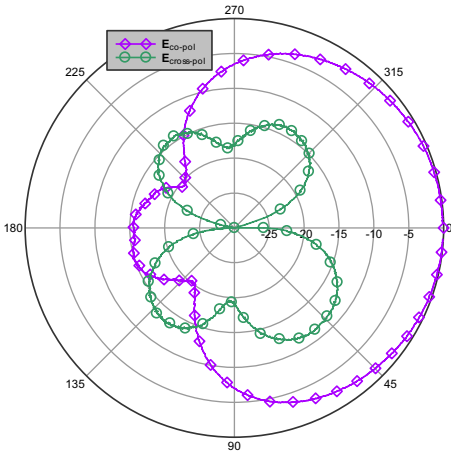

Figure 2: Measured radiation pattern of the double-section LPDA.

A Complete Simulation of a Radiated Emission Test according to IEC 61000-4-20

X. T. I Ngu, **A. Nothofer**, **D. W. P. Thomas**, **and C. Christopoulos**
University of Nottingham, United Kingdom

Abstract— In a radiated emission test according to IEC 61000-4-20 the radiated power of the equipment under test (EUT) is calculated from three measurements. The algorithm used to calculate this power assumes the EUT to be electrically small and have the radiation characteristics of a set of dipoles. Since this assumption is not always valid, the calculated power by this method may be different from the total power radiated by the EUT. This work presents a complete simulation of a radiated emission test according to IEC 61000-4-20 using the TLM method. This is then compared to the total radiated power of the EUT in free space, space above ground plane and in the GTEM cell. The differences in these power values are analyzed to predict a contribution to the uncertainty budget of the radiated emission test.

Design and Modeling of Planar Power Switching Inductors for Monolithic and Single Chip DC-DC Power Converters

Mohamad Hamoui and Krishna Shenai
Microsystems Design Laboratory
Department of Electrical and Computer Engineering
Utah State University Logan, UT, 84322, USA

Abstract— Engineers are continuously trying to integrate active circuit components of dc-dc converters on chip, while leaving behind the passive components because of their limited capabilities under small-scale integration. This document describes several key issues and design considerations relating to dc-dc converters under high frequencies. Inductor modeling and design of a buck converter are investigated, and a performance plot of the inductor under high switching frequency is presented.

Session 1P2
Negative Refraction and Metamaterials

Geometrically Caused Emergence and Metamaterials in Electromagnetics

A. Sihvola
Helsinki University of Technology, Electromagnetics Laboratory
P.O. Box 3000, FI-02015 TKK, Espoo, Finland

Abstract— The fuzzy concept of metamaterials will be critically discussed in connection with electromagnetics.

Introduction: For metamaterials, the web-based dictionary Wikipedia contains the following definition [1] (at present, March 2007):

> A metamaterial (or meta material) is a material that gains its properties from its structure rather than directly from its composition. This term is particularly used when the material has properties not found in naturally-formed substances. Metamaterials are of particular importance in electromagnetism (especially optics and photonics), where metamaterials are promising for a variety of optical and microwave applications, such as new types of beam steerers, modulators, band-pass filters, lenses, microwave couplers, and antenna radomes.

which is already slightly transformed from the four month older definition (December 2006):

> *In electromagnetism (covering areas like optics and photonics), a meta material (or metamaterial) is an object that gains its (electromagnetic) material properties from its structure rather than inheriting them directly from the materials it is composed of. This term is particularly used when the resulting material has properties not found in naturallyformed substances. Metamaterials are promising for a diversity of optical/microwave applications, such as new types of beam steerers, modulators, band-pass filters, superlenses, microwave couplers, and antenna radomes.*

The *Metamorphose* Network of Excellence by the European Union [2] has provided the definition:

> *Metamaterials are artificial electromagnetic (multi-)functional materials engineered to satisfy the prescribed requirements. The prefix meta means after, beyond and also of a higher kind. Superior properties as compared to what can be found in nature are often underlying in the spelling of metamaterial. These new properties emerge due to specific interactions with electromagnetic fields or due to external electrical control.*

and in the USA, the DARPA Technology Thrust program on metamaterials [3]:

> *MetaMaterials are a new class of ordered nanocomposites that exhibit exceptional properties not readily observed in nature. These properties arise from qualitatively new response functions that are: (1) not observed in the constituent materials and (2) result from the inclusion of artificially fabricated, extrinsic, low dimensional inhomogeneities.*

These definitions and other issues regarding the essence of metamaterials [4] will be discussed in the presentation.

REFERENCES

1. http://www.wikipedia.org.
2. http://www.metamorphose-eu.org.
3. http://www.darpa.mil/dso/thrust/matdev/metamat.htm.
4. Sihvola, A., "Metamaterials in electromagnetics," *Metamaterials*, Vol. 1, No. 1, 2–11, 2007.

Electromagnetic Fields in the Presence of an Infinite Meta-material Wedge

Mohamed A. Salem[1], **Aladin H. Kamel**[2], **and Andrey V. Osipov**[3]

[1]New Jersey Institute of Technology, Newark, NJ 07102, USA
[2]Advanced Industrial, Technological and Engineering Center
P. O. Box 433, Heliopolis Center, Cairo 11757, Egypt
[3]DLR Microwaves and Radar Institute, Oberpfaffenhofen, Wessling 82234, Germany

Abstract— The Kontorovich-Lebedev transform is applied to determine the electromagnetic fields in the presence of an infinite wedge of arbitrary doubly-negative (negative electric and negative magnetic) constants excited by an electric line-source. Uncoupled singular integral equations for the spectral amplitudes inside and outside the meta-material wedge are derived by analytically continuing those of an ordinary material wedge [1] and numerically solved by a successive approximation scheme. Near fields inside and outside the wedge are asymptotically approximated by a residue series. The far field inside the wedge is obtained by direct integration of the Kontorovich-Lebedev integrals; the far field outside the wedge is asymptotically approximated by a residue series. Extension to the plane wave illumination case is also given. Numerical results, for the near and far fields, showing the influence of a meta-material wedge on the directivity of an electric line source as well as the scattered fields due to an incident plane wave are presented. The results are also compared with those reported by [2] in the limit of an ideal (lossless unit-index) meta-material wedge.

REFERENCES

1. Salem, M. A., A. H. Kamel, and A. V. Osipov, "Electromagnetic fields in the presence of an infinite dielectric wedge," *Proc. R. Soc. A*, Vol. 462, 2503–2522, 2006.
2. Monzon, C., D. W. Forester, and P. L. Loschialpo, "Exact solution to lin source scattering by an ideal left-handed wedge," *Phys. Rev. E*, Vol. 72, 056606, 2005.

Metamaterials from Inherently Non-magnetic Materials for Deep Infrared to Terahertz Frequency Ranges

Vassilis Yannopapas[1] and Alexander Moroz[2]

[1]Department of Materials Science, School of Natural Sciences, University of Patras
Patras, GR-26504, Greece
[2]Wave-scattering.com, Germany

Abstract— Left-handed metamaterials come in two basic types, namely those based on purely dielectric periodic photonic crystal structures, or as periodic metallic microstructures exhibiting electric and magnetic resonances. The purely dielectric metamaterials are characterised by rather low wavelength-to-structure ratio (typically less than 2:1). On the other hand, the metamaterials based on metallic microstructures, the most prominent example of which are those consisting of split ring resonators (SRRs) and wires, are truly subwavelength structures with wavelength-to-structure ratio at least 5:1. Here we present a new set of artificial structures, which can exhibit a negative refractive index band in excess of 6% in a broad frequency range from deep infrared to terahertz range [1]. The structures are composites of two different kinds of non-overlapping spheres, one made from inherently non-magnetic polaritonic and the other from a Drude-like material. The polaritonic spheres are responsible for the existence of negative effective magnetic permeability whilst the Drude-like spheres are responsible for negative effective electric permittivity. The resulting isotropic negative refractive index structures are truly subwavelength structures with wavelength-to-structure ratio 14:1, which appears almost by 50% higher than it has been achieved so far. Therefore, the structure can maintain a negative refractive index even in a disordered state. Our results are explained in the context of the extended Maxwell-Garnett theory and reproduced by the calculations based on the layer Korringa-Kohn-Rostoker method, an ab initio multiple scattering theory. Various mechanism of tunability of the proposed structures are investigated.

REFERENCES

1. Yannopapas, V. and A. Moroz, "Negative refractive index metamaterials from inherently non-magnetic materials for deep infrared to terahertz frequency ranges," *J. Phys.: Condens. Matter*, Vol. 17, 3717–3734, 2005.

Metamaterial Collaborated with Active Components

Dongxing Wang, **Lixin Ran**, **and Jin Au Kong**
The Electromagnetics Academy at Zhejiang University, Zhejiang University, 310058, China

Abstract— Electromagnetic metamaterials have been hot topics in various research communities in recent years. Being with independently adjustable permittivity and permeability from negative to positive, metamaterials are attracting more and more attentions in the applications concerning the control of electromagnetic fields, such as high directive antennas, radomes and cloakings.

In this presentation, we discuss one method to obtain the controllable metamateirals, i.e., to collaborate lumped active element, such as varactors, into metal based microwave metamaterials. Different structures suitable for the collaborating are investigated, and the simulation and experimental researches for several controllable active metamaterials are presented.

Proper Leaky Modes in DNG Ridge Waveguides

António L. Topa, **Carlos R. Paiva**, **and Afonso M. Barbosa**

Department of Electrical and Computer Engineering and Instituto de Telecomunicações
Instituto Superior Ténico, Lisboa, Portugal

Abstract— Proper leaky modes, i.e., with field amplitude transversely attenuating at infinity, are know to propagate in double-negative (DNG) metamaterial slabs, in which both permittivity and permeability assume negative values. The modal properties of metamaterial slabs, either in free space or above a ground plane, have been already analyzed and a number of novel properties concerning propagation regimes and modal-field configurations were reported (see, e.g., [1–5]). The unusual properties exhibited by these planar structures exhibit are due to the fact that the Poynting vector is anti-parallel to the phase velocity. Other waveguiding structures based on DNG metamaterials media have been addressed in the literature showing that the presence of both negative constitutive parameters may give rise to unexpected and interesting propagation features [6].

In this paper, we investigate the modal properties of the proper leaky waves supported by three-dimensional metamaterial waveguides, in order to completely assess their propagation features. As an example, a DNG ridge waveguide is considered. To analyze this waveguide, we use the method proposed by Peng and Oliner in [7] for common dielectric planar waveguides. As the non-surface-wave modes comprise a continuous spectrum, we apply a discretizing procedure which consists on placing a perfectly-conducting wall at a distance $d = 2\lambda$ above the waveguide. In addition to the surface waves, the waveguide will then support an infinite number of higher non-surface modes, some propagating and the remainder non-propagating.

A lossless dispersive metamaterial DNG medium is considered throughout the paper, exhibiting a permeability and permittivity modelled as in [2], and working in a frequency range of simultaneously negative values. The operational diagram depicted in Fig. 1, is for a DNG ridge waveguide with inner and outer thicknesses $t_1/\lambda = 0.32$ and $t_2/\lambda = 0.14$, respectively, working at a frequency $f = 4.445\,\mathrm{GHz}$.

At this point of operation, the modes propagating in the inner region of the waveguide are backward modes, exhibiting a power flux which is opposite to that of the modes propagating in the outer region, therefore generating proper leaky modes.

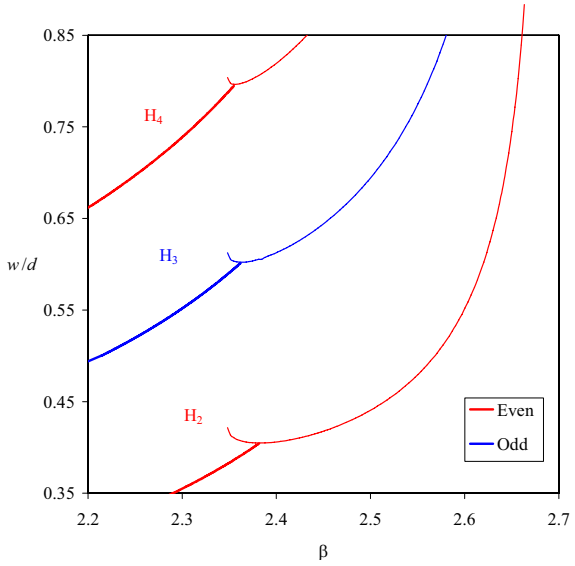

Figure 1: Normalized phase constant of the first leaky (thick) and surface (thin lines) hybrid modes of a DNG ridge waveguide as a function of the normalized width of the inner region.

REFERENCES

1. Nefedov, I. S. and S. A. Tretyakov, "Waveguide containing a backward-wave slab," *Radio Sci.*, Vol. 38, No. 6, 1101–1110, Nov.–Dec. 2003.
2. Shadrivov, I. W., A. A. Sukhorukov, and Y. S. Kivshar, "Guided modes in negative-refractive-index waveguides," *Phys. Rev. E, Stat. Phys. Plasmas Fluids Relat. Interdiscip. Top.*, Vol. 67, 57602-1–57602-4, May 2003.
3. Wu, B.-I., T. M. Grzegorczyk, Y. Zhang, and J. A. Kong, "Guided modes with imaginary transverse wavenumber in a slab waveguide with negative permittivity and permeability," *J. Appl. Phys.*, Vol. 93, 9386–9388, Jun. 2003.
4. Baccarelli, P., P. Burghignoli, G. Lovat, and S. Paulotto, "Surface-wave suppression in a double-negative metamaterial grounded slab," *IEEE Antennas Wireless Propag. Lett.*, Vol. 2, No. 19, 269–272, 2003.
5. Alú, A. and N. Engheta, "Guided modes in a waveguide filled with a pair of single-negative (SNG) double-negative (DNG) and/or double-positive (DPS) layers," *IEEE Trans. Microw. Theory Tech.*, Vol. 52, No. 1, 199–210, Jan. 2004.
6. Topa, A. L., C. R. Paiva, and A. M. Barbosa, Novel propagation features of double negative H-guides and H-guide couplers," *Microwave Opt. Technol. Lett.*, Vol. 47, No. 2, 185–190, October 2005.
7. Peng, S.-T. and A. A. Oliner, "Guidance and leakage properties of a class of open dielectric waveguides: Part I — Mathematical formulations," *IEEE Trans. Microwave Theory Tech.*, Vol. MTT-29, No. 9, 843–855, Sept. 1981.

Miniaturization of Resonant Particles Suitable for Metamaterial and Left Handed Media Design

F. Aznar, **M. Gil**, **J. Bonache**, **F. Martín**, **and J. García-García**

Departament d'Enginyeria Electrònica, Univeritat Autònoma de Barcelona
Bellaterra 08193, Barcelona, Spain

Abstract— In this work, new sub-wavelength resonant particles are proposed. With these new particles a stronger sub-wavelength character, and hence smaller dimensions, are obtained. The use of two metallic layers together with via holes is proposed to increase the coupling between the constituent parts of the resonators. Two new particles (Fig. 1(a)) based on a broad-side coupled spiral resonator are proposed and analysed: the BC-SR(2) and the BC-SR(4) (in both cases the number in brackets refers to the number of turns of the BC-SRs). As illustrative example of the utility of the new particles, negative permeability transmission lines based on microstrip lines periodically loaded with broad-side coupled spiral resonators (BC-SR) are designed and analyzed (Fig. 1(b)). Electromagnetic simulations and experimental results show that the dimensions of BC-SR(2) and BC-SR(4) are decreased in a factor of 2 and 4, respectively, as compared to that of a BC-SRR, as can be observed in Fig. 1(c). Thus, it is demonstrated that the electrical size of metamaterial resonant elements can be substantially reduced by combining spiral topologies with coupling enhancement. The analysis and results of the work, point out that the proposed resonant particles can be of interest for the synthesis of effective media with negative permeability as well as for the synthesis of filters or other passive devices based on electromagnetic resonators, with the consequent miniaturization benefit.

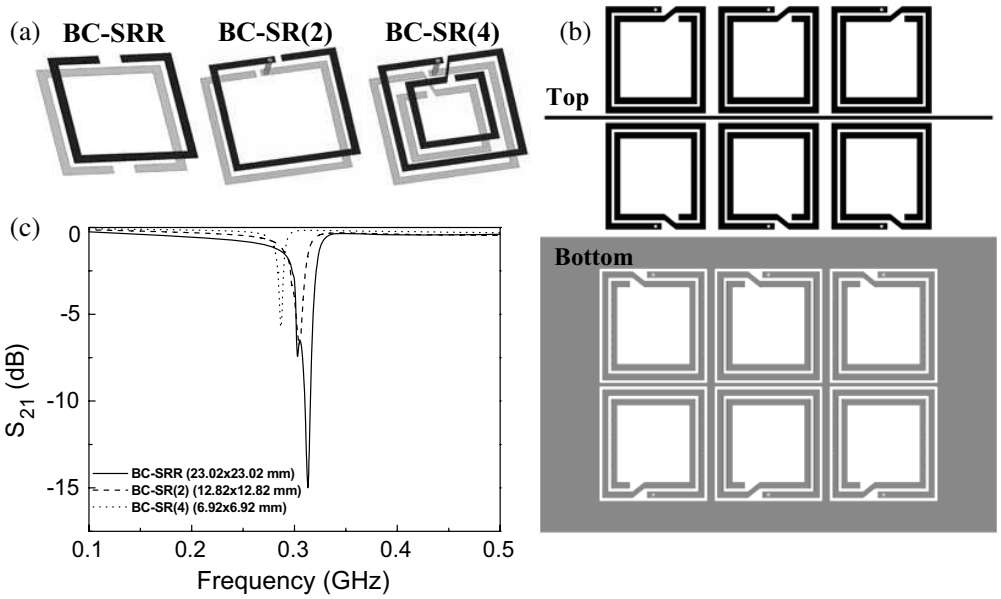

Figure 1: (a) Resonant particles topology, (b) layout of the BC-SR(4) loaded microstrip lines, (c) electromagnetic simulation of the three loaded microstrip lines designed.

Session 1P3
Electromagnetic Compatibility

Mobile Telecommunication Base Stations on Hospital Buildings — The Safety Aspect of Medical Equipment and Individuals

Halina Aniołczyk
Physical Hazards Department, Nofer Institute of Occupational Medicine, Lodz, Poland

Abstract— Recent years have brought a rapid development of electronics and advanced technologies, which found their use in many areas, including wireless communication and modern medical diagnostics with magnetic resonance devices, microwave tomography, and most of all, in tasks characteristic of medical technology, such as monitoring, registration and processing of biological signals. Hospital buildings often have such architectural configuration that they tower over their surroundings. Moreover, they are often situated in urban areas, which makes them good localizations for *Base Transceiver Station* (BTS) of mobile telecommunication. Hospitals, due to their function, are equipped in different devices and medical apparatuses with more or less complex electric and electronic structure. Used devices and installations, especially telecommunication and teleinformatics ones, have to demonstrate a particular level of resistance to different types of interference occurring in environment, and they themselves cannot be a source of such interference. These questions concern electromagnetic compatibility (EMC). Legal regulations of the EMC phenomenon in relation to medical products on the one hand, and mobile telecommunication BTS devices on the other, are indirectly one of the protective barriers for, for example, patients, by ensuring safety of operation of these devices. Transmitting aerials of BTS are a direct source of EMF emission to environment. Thus, EMF produced by BTSs undergo particular requirements of national legislature, defined in legal acts and regulations, as well as directives and recommendations of the EU. Every owner, the so called operator, is obliged to rigorously follow these rules. Does installation of mobile telecommunication BTSs on roofs of hospitals, or, if the need arises, also on the buildings' elevations, affect work of medical devices, as well as, indirectly, safety and health of individuals? To answer this question, the analysis of EMF levels occurring in the vicinity of BTSs installed on 20 hospital buildings was carried out.

The Electromagnetic Compatibility of Cellular Telephony Devices and Medical Equipment

Marian Wnuk
Military Academy of Technology, Warsaw, Poland

Roman Kubacki
Military Institute of Hygiene and Epidemiology, Warsaw, Poland

Abstract— Harmful influence of some forms of electricity on safety of people and work of devices hale been known for years. True, serious and common threats have occurred since introducing in industry, households, hospitals etc. electronic devices, made in digital and microprocessor technology. Possibility of electromagnetic disturbances causes mutual interferences, even causing serious threats for people and property.

One of the most developing domains of modern civilisation is domain dealing with transmitting information, especially cellular telephony. Installed base stations close to hospitals may be a source of potential disturbances of medical devices. Authors have made analyse of factors influencing the level of signal reaching medical devices. Various models of propagation both for internal (indoor) and external (outdoor) areas have been analysed. The useful ranges were appointed and disturbance the base station, for different band of frequency.

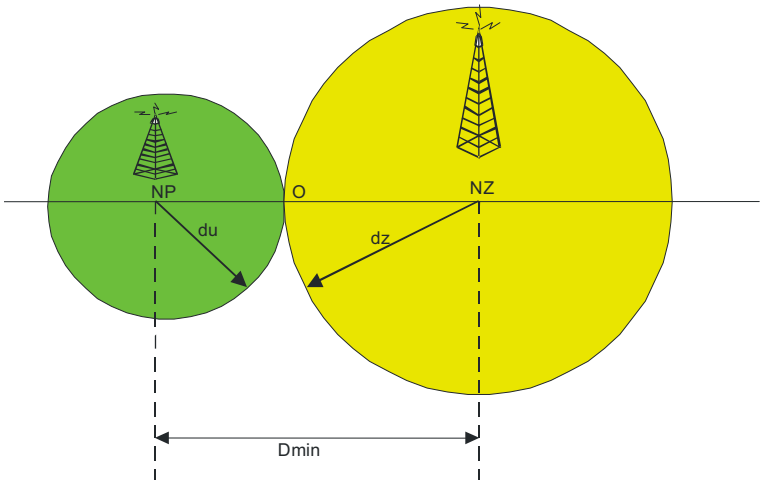

Conducted analyse takes into account also frequency of work of medical devices and radiocommunication systems. Levels of signal reaching medical devices have been defined and compared with sensitivity of the equipment.

The Determination of Minimal Safety Requirements for Base Station Antennas Localizations on the Hospital Roofs

Roman Kubacki[1], **Marian Wnuk**[2], **and Aleksander Dackiewicz**[3]

[1]Military Institute of Hygiene and Epidemiology, Warsaw, Poland
[2]Military Academy of Technology, Warsaw, Poland
[3]PTC ERA, Warsaw, Poland

Abstract— The increasing popularity of mobile phones in our live has aroused interest about potential health risk due to exposure to microwave energy. The results of investigate of the problem of safety localization of base stations antennas on the hospital roof have been presented. In this case the direct safety conditions for human on the roof as well as for patients inside the hospital were taken into consideration. On the other hands indirect safety conditions, i.e., the possible interaction of electromagnetic field on medical devices are also important. There exist three main types of localizations of base station antennas on the hospital roofs: antennas of all 3 sectors are mounted on the one common mast, antennas of each sector are mounted on individual masts and antennas are fitted up directly to the building walls. Each sector is equipped with 2 or 3 antennas operating at GSM, DCS or UMTS system frequencies, then the electric field strength at any point is a sum of all systems.

Values of electric field strength emitted from antennas have been calculated using electric and magnetic potentials and suitable equations have been adopted to calculate the field distribution in the vicinity of the antenna, i.e., in the near field. This model of calculation allows to determined the electric field strength just below the antennas, near the masts. It should be underlined that well known formulas are in fact the far field approximation and can not be used in the near field. With the proposed near field approximation formulas and taking into account not only the incident ray but also ray reflected from the roof it is possible to simulate the values of electric field strength on the roof surface in function of distance from antenna. Taking into account the attenuation of roof (in case of antennas on the roof) or wall (when antennas are mounted to the wall) it is possible to determined the level of exposure in internal rooms. The received values can be used to assess the possible health hazard or interaction on medical devices. The safety altitude of antennas above roof and safety localization on the wall taking into account the permissible value of microwave radiation of 7 V/m have been discussed.

Study of Magnetic Field Distribution in Infant Incubators

H. Aniolczyk[1] and P. Bieńkowski[2]

[1]Department of Physical Hazards, The Nofer Institute of Occupational Medicine, Lodz, Poland
[2]Institute of Telecommunication, Teleinformatics and Acoustics
Electromagnetic Environment Protection Laboratory
Wroclaw University of Technology, Wroclaw, Poland

Abstract— All electrical and electromagnetic devices and installations are a source of electromagnetic fields (EMF); they can be also a source of interference, or their work may cause interference in the work of other devices. Preliminary analysis of construction and equipment of incubators for infants shows that energy power lines and devices that use their power are the main source of EMF. In this range of extremely low frequencies (ELF) the magnetic component becomes the most important due to the use of relatively low voltage. It limits the electric field intensity to several dozen–several hundred V/m. The second frequency range that can be observed in incubators are very low frequency fields (VLF). The source of fields in this range are mainly switching power supplies and DC/DC voltage converters. These devices are the source of both magnetic and electric fields. 24 epidemiological studies showed increased incidence of leukemia in children with environmental (residence) exposure to 50 Hz magnetic field with magnetic induction above 0.3–0.4 μT. 50/60 Hz magnetic field is on the IARC list in the 2B group as a probable carcinogenic factor for humans.

An infant can stay in the incubator for as long as several months. The source of 50 Hz magnetic field are: electronic controlling systems, heating system, ventilation system, lighting system, as well as other devices, such as, for instance, a respirator or a phototherapy device for infants.

Measurements were carried out for 17 incubators of different types installed at the Pathology and Emergency Ward of the Neonatology Clinic. Measurements of magnetic field intensity inside and in the vicinity of incubators were carried out during simulation of the normal work of the device (empty incubator with temperature stabilization switched on), as well as during the actual work of the device (incubator with an infant inside). In order to determine spectral parameters of the measured magnetic field induction (H), spectral analysis with the use of oscilloscope with the FFT function was carried out. It was shown that the energy power line magnetic field component, i.e., 50 Hz, plays the most important part. The continuous monitoring of the H field induction in a selected area of the incubator's chamber (with the infant inside) was carried out. The study aimed at defining the field's variability in time, during the regular infant caretaking activities. The 24-hour monitoring, with observation of characteristic activities performed by the medical staff and the infant's mother, was carried out. The following values have been established on the basis of the study results: H field induction average value on the level of 0.325 μT with standard deviation 0.26 μT, H field induction maximum value on the level of 2.050 μT, and H field induction minimum value on the level of background level (c. 0.05 μT). The uncertainty of measurements was estimated as 20%. Value close to the average is also the value most often registered during measurements. For comparison, background level measurements in Room A showed: inside — 0.05 μT, in the window plane — 0.14 μT, near distribution board — 0.44 μT, whereas background level measurements inside Room B showed 0.15 μT.

Scientific Thematic Network "Electromagnetic Compatibility of Devices, Systems and Installations for IT Community EMC-Net"

S. Lysiak, **T. Reczek**, **and T. W. Więckowski**
Wrocław University of Technology, Poland

Abstract— This article describes in short the history, structure and scope of activities of the scientific thematic Network EMC-net, which unites several academic institutions, laboratories and other organizations involved in electromagnetic compatibility issues. The authors present an overview of the Network's developments so far as well as current joint projects involving it's members and the Network's activities as an opinion-setting authority.

Development of Research Works Pertaining to Textile Shields

Joanna Koprowska
Textile Research Institute, 92-103 Łódź, Brzezińska 5/15, Poland

Abstract— Plastics or textiles with conductive coat are more often applied as shielding materials. In our area of interest and research scope can be found light and flexible shielding materials like textiles covered with absorbing layer. These materials, owing to their flexibility, are considered as promising materials for the protection of equipment and persons against electromagnetic radiation (as covers, protective clothing and wallpapers).

Research work concerned textile shielding materials have been carried out at Textile Research Institute since 1995. At the beginning these materials were produced from Nitril-Static electroconductive fibres, according to our own technology. They were electrically conductive textiles (nonwovens: WOM-E Maliwatt-type and needled IG-NS) differing in technology of production, but also in electric properties. Attenuation of these electroconductive materials was measured in some Polish and also European EMC laboratories. Shielding effectiveness laboratory examinations proved possibility to apply electrically conductive textiles as electromagnetic shields.

The level of this efficiency allowed to apply these technical textiles also in different applications.

Presently research works are carried out on composite materials using the selected textile raw materials and coating layers. The paper presents our own test results in reference to the state-of-the art in the world.

Session 1P4
Biomedical Applications of Electromagnetic Waves

Planar Applications for Local Thermotherapy

J. Vrba, T. Drizdal, P. Togni, R. Zajíček, L. Víšek, K. Novotná, J. Vedralova L. Pergl, and L. Oppl

Department of Electromagnetic Field, Faculty of Electrical Engineering
Czech Technical University in Prague
Technická 2, 166 27 Prague 6, Czech Republic

Abstract—

Introduction: During last years we work on theory and applications of various types of applicators for microwave thermotherapy. In this paper we would like to describe some of our results for planar applicators. Here mentioned examples of applicators are designed for working frequency either 434 or 2450 MHz and optimized by aid of 3D electromagnetic field simulator SEMCAD. Impedance matching measurements were done by aid of vector analyzer and SAR distributions were evaluated using infrared camera.

Methods: All discussed applicators are developed on the 1,5 mm thick dielectric substrate with relative permittivity $\varepsilon_r = 4,2$. Two centimetre thick water bolus ($\varepsilon_r = 78$) is inserted between the irradiating part of the planar applicator and agar phantom ($\sigma = 0,8\,\mathrm{S/m}$, $\varepsilon_r = 54$). The dimensions of the applicators were analytically calculated with respect to the working frequency 434 resp. 2459 MHz and then optimized by aid of 3D electromagnetic field simulator SEMCAD. First example of these applicator is circular microstrip resonator which is placed on the square substrate with dimensions 78×78 mm. The active part is composed of circular patch with radius of 19 mm. The position of the feeding point is 17 mm from the center of the circular patch. Next applicator is the circular slot-line resonator which is developed on the square substrate with dimensions 80×80 mm. In this case the radius of the circular patch (active part) is 17 mm. The width of the slot-line (7.5 mm for both applicators) gives the correct impedance matching for the working frequency. The rest of the metallization which surrounds the slot lines forms the ground planes. The last one is the rectangle microstrip line applicator with the dimensions 95×55 mm of the substrate. The circumference of the microstrip line, which is equal to wavelength together with 3 mm width of the microstrip line provides good impedance matching at the working frequency.

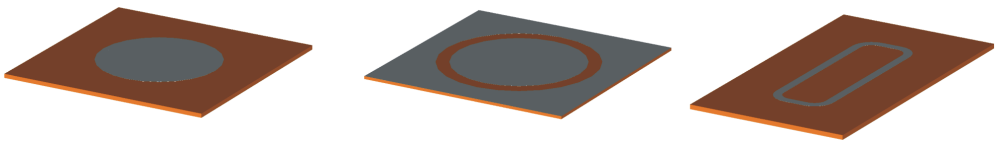

Figure 1: Model of circular microstrip, circular slot-line and rectangle microstrip line applicator.

Conclusion: Different planar applicators were designed and evaluated. As an example three selected applicators were described here, in our presentation we would like to give more informations on impedance matching and 3D SAR distribution of each of these applicators.

ACKNOWLEDGMENT

This research is supported by Czech Research Program: "Transdisciplinary Research in the Area of Biomedical Engineering II" (MSM6840770012) and by Grant Agency of the Czech Republic project: Medical Applications of Microwaves: "Therapy and Diagnostics" (102/05/0959).

Shorted Microstrip Applicators for Local Hyperthermia

Tomas Drizdal, **Paolo Togni**, **Megela Alexandr**, **and Jan Vrba**
Department of Electromagnetic Field, Czech Technical University in Prague
Technická 2, 166 27 Prague 6, Czech Republic

Abstract— Hyperthermia is a type of cancer treatment in which body tissue is exposed to temperatures up to 45 C, in order to damage and kill cancer cells, or to make cancer cells more sensitive to the effects of radiation and certain anticancer drugs. Local hyperthermia is used to heat small areas which are mainly placed at the surface of the body. As we can quite simply localize these tumours, thus the area which must be heated is clearly defined. The type of the applicators selected for treatment depends on their radiated EM field patterns which give different thermal distribution in the treatment area (our task is uniformly the tumour and minimize the temperature enhancement in the healthy tissue).

This paper describes a circular microstrip (CMSA) and rectangular microstrip (RMSA) applicators for local hyperthermia which are designed for a working frequency of 434 MHz. Applicators are developed on a 78 mm square dielectric board with a metallization on both sides. This board (substrate) has permittivity $\varepsilon_r = 4.1$ and thickness of 1.5 mm. To reduce the geometrical dimensions of both applicators the patch is shorted to the ground plane in one point of the patch. The designed geometrical dimensions as well as the position of feeding point were optimized using a 3D electromagnetic field simulator. The active part is in the first case composed of a circular patch with radius of 19 mm and in the second case of a 36 mm square patch. The distance of feeding point from the center is 17 mm for CMSA and is 16 mm for RSMA. Using these modifications the Shorted CMSA and RSMA were developed. An agar phantom ($\varepsilon_r = 54$, $\sigma = 0.8\,\mathrm{S/m}$) was used as a model of biological tissue during the simulations. To protect the surface of the agar phantom a two centimeters thick water bolus ($\varepsilon_r = 78$) is inserted between applicator and agar phantom.

Impedance matching was measured using a network analyzer and 3D SAR distribution was obtained using IR-camera and the results shows that this type of applicators can be used for local hyperthermia.

Evaluation on Heating Performances of Antennas for Interstitial Thermal Therapies by Use of Tissue-equivalent Solid Phantom with Capillary Blood Flow

Kazuyuki Saito[1], **Atsushi Hiroe**[2], **Satoru Kikuchi**[2], **Masaharu Takahashi**[1], **and Koichi Ito**[3]

[1]Research Center for Frontier Medical Engineering, Chiba University, Japan
[2]Graduate School of Science and Technology, Chiba University, Japan
[3]Faclty of Engineering, Chiba University, Japan

Abstract— In recent years, various types of medical applications of microwave have been extensively investigated and developed. In particular, the minimally invasive microwave thermal therapies using thin applicators are of great interest. Until now, the authors have been studying the heating performances of coaxial-slot antenna, which is one of the thin microwave antennas for interstitial thermal therapies. In order to estimate the heating performances of the antenna, numerical simulations and experiments by use of tissue-equivalent solid phantoms are performed. It is possible to calculate the SAR (specific absorption rate [W/kg]) and the temperature distributions around the antenna inside biological tissue by the numerical calculations. However, in the experiments, although the SAR can be estimated, measurement of temperature rise around the antenna is difficult, because it is not easy to realize a tissue-equivalent solid phantom with cooling effect by blood flow. Until now, the authors developed the tissue-equivalent solid phantom with a thick blood vessel and estimated the temperature rise by the coaxial- slot antenna. In this study, the tissue-equivalent solid phantom with capillary blood flow was developed and the temperature rise around the coaxial-slot antenna inside this developed phantom was experimentally measured. As a result of measurement, good agreement was observed between the measured and the calculated temperature rise under some assumptions.

Implementation of Active Antennas in Medical Microwave Radio-thermometry

S. Jacobsen and Ø. Klemetsen
Department of Physics and Technology, University of Tromsø, Tromsø, Norway

Abstract— Microwave radiometry is a spectral measurement technique for resolving black-body radiation of heated matter above absolute zero. The emission levels vary with frequency and medical radio-thermometers are short range instruments that can provide temperature distributions in subcutaneous biological tissues when operated in the microwave region. However, a crucial limitation of the microwave radiometric observation principle is the extremely weak signal level of the thermal noise emitted by the lossy material ($-174\,\mathrm{dBm/Hz}$ at normal body temperature). Requirements of long integration time (∼3–5 secs) and wide integration bandwidth (∼300–50,MHz) result in a maximum of 5–6 radiometric bands per antenna within the usable frequency scan range from 1 to 4 GHz.

To improve the radiometer signal-to-noise ratio, we propose to integrate a tiny, moderate gain, low noise amplifier (LNA) close to the antenna terminals as to obtain increased detectability of thermal gradients within the volume under investigation. The concept is verified experimentally in a lossy phantom medium by scanning the active antenna across a thermostatically controlled water phantom with a hot object embedded at $d = 38\,\mathrm{mm}$ depth. The temperature gradient between the target and environment was only $0.9^{\circ}\mathrm{C}$. Analysis shows a marked increase in signal-to-clutter ratio of the brightness temperature spatial scan profile when comparing active antenna operation with a conventional passive setup.

Implanted Antenna for an Artificial Cardiac Pacemaker System

Tamotsu Houzen[1], **Masaharu Takahashi**[2], **and Koichi Ito**[3]

[1]Graduate school of Science and Technology, Chiba University, Japan
[2]Research Center for Frontier Medical Engineering, Chiba University, Japan
[3]Graduate School of Engineering, Chiba University, Japan

Abstract— Recently, medical implant telemetry system (MITS) monitoring medical information such as a cardiac beat has been investigated with a great interest. A wireless telemetry system which can transmit medical information without a wire piercing the skin has advantage to prevent the infection with a germ in a medical diagnosis. An antenna embedded into the human body which can be transmitted vital signals of a patient to the external equipment is fundamentally necessary for the realization of this system. In this paper, a planar inverted-F antenna (PIFA) on the surface of an artificial cardiac pacemaker as an implanted antenna is proposed. For the design of the antenna, the human body is substituted by the 2/3 muscle-equivalent phantom and the analysis by finite-differential time domain (FDTD) method is used. The communication link budget is additionally calculated for the estimation of the antenna in a real environment. As a result, it is confirmed that the proposed antenna operating at 400 MHz-band can build up the communication link of MITS with the external equipment which is located within 6 m distance and 58 deg. altitude.

Measurements of Dielectric Properties of Biological Tissues in Mm-wave Band by Free-space Reflection Method, Ellipsometry Method and Coaxial Probe Method

T. Sakai[1], **M. Hanazawa**[1], **H. Wakatsuchi**[1,2], **S. Watanabe**[1], **A. Nishikata**[3], **and O. Hashimoto**[2]

[1]National Institute of Information and Communications Technology, Japan
[2]Aoyama Gakuin University, Japan
[3]Tokyo Institute of Technology, Japan

Abstract— Permittivity of tissues is required to calculated electromagnetic dosimetry and it is well known that permittivity has frequency dispersion. Therefore a number of measurement methods of dielectric constant have been studied at many frequency bands. However, to our knowledge, permittivity of tissues have not been reported in 20 GHz or more. There have been strongly demands for a dielectric constant of tissues at millimeters wave band. In this study we applied three methods to permittivity measurement of tissue in millimeter wave band.

There are many tissues that are difficult to obtain in large amount and to be cut in precisely required shape for measurement. Open-ended coaxial prove methods have advantages with respect to these points. We employed the coaxial probe kit (Agilent 85070E 200 MHz–50 GHz) to measure, because permittivity of tissues can be obtained even small volume i.e., 1 cm^3 or without cutting the tissues. Variations of measurement results are caused by several factors for example hardness of a sample, evaporation on the surface of a sample, pressing power of the probe against a sample etcetera. In actual measurement it is difficult to realize these factors. Therefore measurement results should be compared with other method's results for reliability.

We developed two free-space measurement systems for permittivity of biological tissues. One is reflection method and the other is ellipsometry method.

The reflection method measured a complex reflection coefficient from a flat sample at 18–50 GHz using focus lens antenna. Measured reflection coefficients contain an effect of optical flat glass which is set on the sample as cover of the holder. To remove the effect, S-parameter of cover glass was also measured and was translated to T-parameter. And permittivity is estimated from the reflection coefficient without the effect of glass.

The ellipsometry method is based on measurement of electromagnetic scalar value and observes ellipsoidal polarized reflection wave which is caused by linear polarization wave exposure to a sample. In millimeter wave measurement system, a horn antenna works as a polarized analyzer, we can choose the "rotating antenna method" which corresponds to the rotating analyzer method in optical region.

To confirm the validity of three methods, measurement results of water were compared with each others at room temperature. And these data have a good agreement with each other although the results of free-space methods have ripple.

Effects of Parameters of a Dosimetric Human Model on Temperature Elevation Due to Millimeter-wave Exposure

A. Kanezaki[1,2], **T. Sakai**[2], **S. Watanabe**[2], **and H. Shirai**[1]

[1]Chuo University, Japan
[2]National Institute of Information and Communications Technology, Japan

Abstract— In recent year, expectations for millimeter-wave (30 GHz–300 GHz) technology are rising with significant progress on information society. Because the exposure to millimeter-wave will increase, it is important to evaluate the safety of millimeter-wave exposure. Most of millimeter-wave power is absorbed within the surface of a human body and the absorbed power causes temperature elevation in the body. Safety guidelines for millimeter-wave exposure are based on warmth sensation and ocular effects. Especially, the warmth sensation is the fundamental basis of the safety guidelines in millimeter-wave band although details of characteristics of the threshold of the warmth sensation has not been investigated. As one of basic analyses, we investigated effects of parameters of a dosimetric human model on temperature elevation due to millimeter-wave exposure using a threelayers model that consists of skin, fat and muscle.

Transmission-line theory was used to analyze the specific absorption rate (SAR [W/kg]) distribution in the human-body model. The temperature distribution in the human-body model exposed to millimeter-wave has been calculated with bioheat equations [1]. We applied a constant temperature at the boundary in the deep region of the layer model and a heat transfer at the boundary between the skin surface and air as described in [2]. The difference forms were numerically calculated with an implicit method which accelerates the difference calculation [3]. We investigated effects of thickness of each layer of the human model and skin water content on temperature elevation due to millimeter-wave exposure. The dielectric properties of biological tissue were set for the degree of the water content as described in [4].

We found higher temperature elevation when skin thickness decreases and fat thickness increases. We also found that the temperature elevation increases with decreasing skin water content. In this study we investigated the effects of the physical parameters of the human model, i.e., the width and water content of the tissues, on the temperature elevation due to the millimeter-wave exposure. Our study is useful to establish the worst case of the human model to investigate the safety of the millimeter-wave exposure although further investigations, e.g., the effects of physiological parameters such as blood flow and the effects at other frequencies, are necessary.

REFERENCES

1. Hoque, M. and O. P. Gandhi, "Temperature distribution in the human leg for VLF-VHF exposures at the ANSI recommended safety levels," *IEEE Trans. Biomed. Eng.*, Vol. 35, No. 6, 442–449, 1988.
2. Bernardi, P., M. Cavagnaro, S. Pisa, and E. Piuzzi, "Specific absorption rate and temperature elevation in a subject exposed in the far-field of radio-frequency sources operating in the 10–900-MHz range," *IEEE Trans. Biomed. Eng.*, Vol. 50, No. 3, 295–304, 2003.
3. Patankar, S. V., *Numerical Heat Transfer and Fluid Flow*, Hemisphere Publishing Corporation, New York, 1980.
4. Wang, J., O. Fujiwara, and S. Watanabe, "Approximation of aging effect on dosimetric tissue properties for SAR assessment of mobile telephones," *IEEE Trans. Electromagn. Compat.*, Vol. 48, No. 2, 408–413, 2006.

Induced Current Density in Adults and Children Exposed to Homogeneous Magnetic Field in Intermediate Frequency Band

K. Maruyama[1,3], **Y. Suzuki**[2], **K. Wake**[3], **T. Sakai**[3], **S. Watanabe**[3], **M. Taki**[2], **and O. Hashimoto**[1]

[1]Aoyama Gakuin University, Japan
[2]Tokyo Metropolitan University, Japan
[3]National Institute of Information and Communications Technology, Japan

Abstract— Currently, electrical appliances like IH hob have been used in various places. Therefore, public concern have been rising for the possibility of biological effect caused by magnetic field due to such a electrical appliances. IH hob uses time varying magnetic field around 20 kHz for fundamental heating frequency. In ICNIRP guideline [1], magnetic field strength with intermediate frequency is limited by induced current density to protect nerve system. A lot of analyses have been done [2, 3] to investigate the relationship between the strength of incident magnetic field and induced current inside of human body. There are a few studies to compare current densities between adult and child induced by intermediate frequency magnetic field. The purpose of this study is to clear the differences of induced current density distribution for the realistic numerical models with wide range of age group.

We applied the impedance method [4] to calculate current density induced by uniform magnetic field within adult male and children models for various ages. In this calculation, we use four numerical human models, which are adult male, 3, 5, and 7 years old, respectively. The adult male was developed based on MR images [5]. The child models were built on the adult male model by reduction and deformation. Each model has 51 tissues and spatial resolutions are 2 mm. Calculation conditions are as follows. The strength of magnetic flux density is 1 μT. The frequency is 20 kHz. Three types of incident magnetic field are employed to investigate dependence of current density distribution on the direction. The directions of magnetic field are from front to back, right to left and top to bottom against to human models. Results of current density distribution are averaged over a cross-section of 1 cm^2 perpendicular to the current direction. The maximum values of averaged current density are compared for each model and each incident direction. The maximum values of current density also compared within central nerve system.

As a result, maximum value of current density obtained by child models do not exceeded that value for the adult male model. Maximum values inside of nerve organizations were much lower than the maximum value within trunk and head.

REFERENCES

1. International Commission on Non-Ionizing Radiation Protection, "Guidelines for limiting exposure to time-varying electric, magnetic, and electoromagnetic fields (up to 300 GHz)," *Health Phys.*, Vol. 74, 494–522, 1998.
2. Dimbylow, P. J., "Induced current densities from low-frequency magnetic fields in a 2 mm resolution, anatomically realistic model of the body," *Phys. Med. Biol.*, Vol. 43, 221–230, 1998.
3. Xi, W., et al., "Induced electric currents in models of man and rodents from 60 Hz magnetic fields," *IEEE Trans. Biomed. Eng.*, Vol. 41, 1018–1023, 1994.
4. Orcutt, N. and O. P. Gandhi, "A 3-D impedance method to calculate power deposition in bioloical bodies subjected to time vaying magnetic fields," *IEEE Trans. Biomed. Eng.*, Vol. 35, 577–583, 1988.
5. Nagaoka, T., et al., "Development of realistic high-resolution whole-body voxel models of Japanese adult males and females of average height and weight, and application of models to radio-frequency electromagnetic-field dosimetry," *Physicsin Medicine and Biology*, Vol. 49, 1–15, 2004.

Session 2A1
Novel Mathematical Methods in Electromagnetics 1

Extension of the Finite Network Method to Magnetic Materials and Its Application to Eddy-current Testing

A. Farschtschi and T. Richter

Chemnitz University of Technology, Germany

Abstract—

$$\begin{bmatrix} \underline{\mathbf{Z}}_{cc} & j\omega\underline{\mathbf{M}}_{ec} \\ j\omega\underline{\mathbf{M}}_{cm}^{T} & j\omega\underline{M}_{em} \\ j\omega\underline{\mathbf{M}}_{ec}^{T} & \underline{Z}_{ee} \end{bmatrix} \begin{bmatrix} \underline{\mathbf{I}} \\ \underline{I}_e \end{bmatrix} = \begin{bmatrix} \mathbf{0} \\ \underline{U}_m \\ 0 \end{bmatrix} \tag{1}$$

n: number of current loops

$\underline{\mathbf{Z}}_{cc}$: $n \times n$ matrix of the impedances and mutual inductances of the short-circuit loops of the massive conductor

$\underline{\mathbf{M}}_{ec}$: vector of length n of mutual inductances between the loops of the massive conductor and the primary excitation coil

$\underline{\mathbf{M}}_{cm}$: vector of length n of mutual inductances between the loops of the massive conductor and the exploring coil

$\underline{M}_{em}$: mutual inductance between primary and exploring coil

$\underline{Z}_{ee}$: impedance of the excitation coil

$\underline{I}_e$: vector of loop currents of the massive conductor

$\underline{U}_m$: measurement voltage of the exploring coil

Eddy-current methods are common in non-destructive material testing. The authors apply the finite network theory (FNM) to material testing including boundary conditions to magnetic interfaces. FNM discretises massive conducting volumes into cuboid volume elements. The mid-nodes of neighboring cuboid volume elements are connected by branches and form a staggered grid with respect to the volume discretisation. The resulting network of resistor elements is solved by the mesh current method. In the case of low frequencies it is sufficient to neglect free charges, but we have to take into consideration inductances. Figure 1 illustrates the steps in network generation. Usually, self and mutual inductances are defined for closed current loops. In the presence of magnetic ma- terials additional magnetic boundary currents are introduced to fulfill the tangential continu- ity of the magnetic field at boundaries.

Figure 2 and Table 1 show the problem sketch. An exploring coil and a coincident measurement coil are moved along the surface of a magnetic workpiece. The application of FNM to eddy-current testing results in the system of matrix Equations (1).

The aim of the simulation is the variation of the induced voltage in the exploring coil with the position of the coil center. The induced voltage is normalized to that voltage, which occurs at the absence of cracks:

$$\left|\frac{\Delta U_m(x)}{U_{m,oc}}\right| = \left|\frac{U_{m,wc}(x) - U_{m,oc}(x)}{U_{m,oc}}\right| \tag{2}$$

x is the position of the coil centers of the coin- cident coils with respect to the position of the deepest crack at $x = 0$ (see Figure 2). $U_{m,wc}(x)$ is the induced measurement voltage varying with the coil position. $U_{m,oc}$ is the measurement voltage without cracks and serves as reference value for the normalized voltages in Equation (2). A couple of simulation runs where performed to determine $U_{m,wc}(x)$ against the coil center position x. The results are shown in Figure 3. As expected, we obtain a maximum induced voltage, when the coil center is situated above a crack.

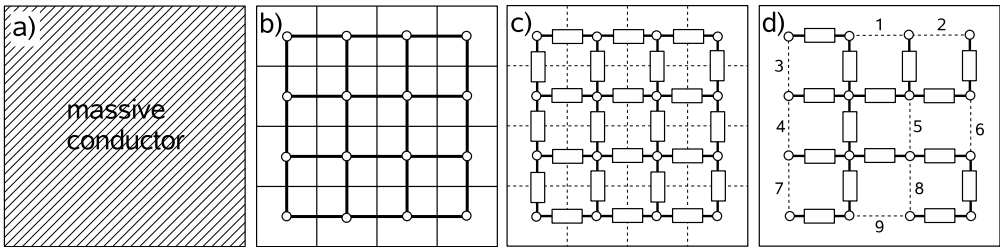

Figure 1: 2D example of the generation of the electric network: (a) conducting volume, (b) volume discretisation and staggered grid for network generation, (c) electric network of inductive coupled resistors (consisting of the half of neighboring volume elements), (d) spanning tree of the network and co-tree (dotted lines, branches 1–9).

Table 1: Crack geometry of the ferromagnetic block, see Figure 2.

Crack No. (label)	x [cm]	l [cm]	w [cm]	h [cm]
1 (c1)	0.0	12.6	0.28	1.2
2 (c2)	2.4	12.6	0.28	0.8
3 (c3)	3.6	12.6	0.28	0.4
4 (c4)	4.8	12.6	0.28	0.2

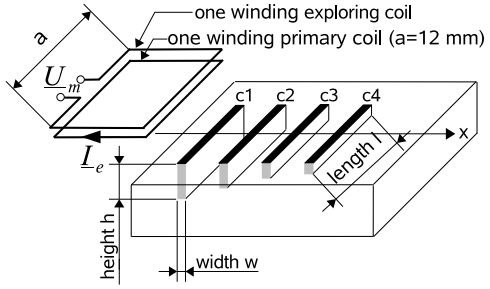

Figure 2: Geometry of the sample problem. The cracks have the same width $w = 0.28\,\text{mm}$, same length $l = 12.6\,\text{mm}$ and are positioned at $x = 0\,\text{mm}$, $x = 24\,\text{mm}$, $x = 48\,\text{mm}$ and $x = 48\,\text{mm}$. The cracks vary in height ($1.2\,\text{mm}$, $0.8\,\text{mm}$, $0.4\,\text{mm}$, $0.2\,\text{mm}$ from lower to upper x).

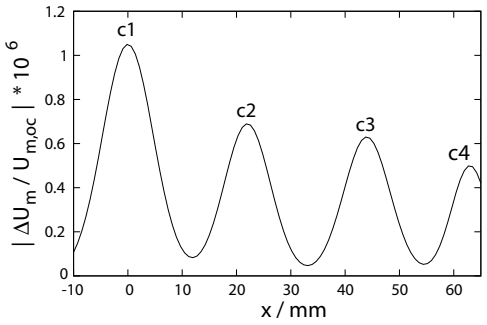

Figure 3: Variation of normalized measurement voltage given by Equation (2) ($\mu_r = 200$ and $f = 300\,\text{Hz}$).

On an Extension of the Layer and Bulk Photonic KKR Methods for Nonspherical and Noncylindrical Scatterers

Alexander Moroz

Wave-scattering.com, Germany

Abstract— Computer implementations of the layer and bulk photonic KKR methods, which are both ab initio multiple scattering theories, have been extended to the case of nospherical and noncylindrical scatterers. The computer implementations enable one to perform a fast and high-precision computations of diffraction and band structure properties of various photonic systems involving photonic crystals, array patterned surfaces for plasmonic and sensing applications, and photonic heterostructures. An advantageous feature of the methods is that material dispersion does not cause any increase in computational time. A two-dimensional version of the layer and bulk photonic KKR methods enables one to perform various optimization tasks by scanning over 15.000 different configurations per day.

A Study on Numerical Dispersion of CIP Method for EM Problems

Y. Ando and M. Hayakawa
Department of Electronic Engineering, The University of Electro-Communications
1-5-1, Chofugaoka, Chofu, Tokyo, 182-8585, Japan

Abstract— The constrained interpolation profile (CIP) method is a computational scheme for problems including different phases [1], and it provides possibilities to reduce computational resources for solving electromagnetic problems. The method is based on the upwind scheme with the profiles between two grid points, interpolated in terms of cubic polynomials which allow us to calculate fields at the next time step with good precision. However, propagating waves suffer from numerical dispersion, like other schemes.

We consider a wave propagating to $+x$-direction with the velocity of c_0. The field value is indicated by $f(x,\, t)$ and the derivative is expressed as $g(x,\, t) = \partial f/\partial x$. Their discretized forms are given by $f_i^n \equiv f(i\Delta x,\, n\Delta t)$ and $g_i^n \equiv g(i\Delta x,\, n\Delta t)$, where Δx and Δt are the spatial and temporal discretization, respectively. Therefore, the explicit form of the CIP updating scheme is given by the following equations:

$$f_i^{n+1} = A_1 f_i^n + A_2 f_{i-1}^n + A_3 g_i^n + A_4 g_{i-1}^n, \quad g_i^{n+1} = B_1 f_i^n + B_2 f_{i-1}^n + B_3 g_i^n + B_4 g_{i-1}^n, \qquad (1)$$

where the coefficients A_α and B_α are given by

$$\begin{aligned} A_1 &= 1 + 2\xi^3 - 3\xi^2, \quad A_2 = 3\xi^2 - 2\xi^3, \quad A_3 = \Delta x(2\xi^2 - \xi^3 - \xi), \quad A_4 = \Delta x(\xi^2 - \xi^3), \\ B_1 &= \frac{6}{\Delta x}(\xi - \xi^2), \quad B_2 = -B_1, \qquad B_3 = 1 + 3\xi^2 - 4\xi, \qquad B_4 = 3\xi^2 - 2\xi, \end{aligned}$$

and ξ is the so-called the Courant number, and is given by $\xi = \frac{c_0 \Delta t}{\Delta x}$.

Consider a plane wave at an angular frequency ω in order to derive the numerical dispersion of the CIP method: $f_i^n = f_0 \exp(j\omega t - j\tilde{k}x)$, $g_i^n = g_0 \exp(j\omega t - j\tilde{k}x)$, where f_0 and g_0 are constants, and $\tilde{k}$ is the numerical wave number. Substituting f_i^n and g_i^n into the updating equations, we have

$$e^{j\omega\Delta t} \begin{bmatrix} f_0 \\ g_0 \end{bmatrix} = \begin{bmatrix} A_1 + A_2 e^{j\tilde{k}\Delta x} & A_3 + A_4 e^{j\tilde{k}\Delta x} \\ B_1 + B_2 e^{j\tilde{k}\Delta x} & B_3 + B_4 e^{j\tilde{k}\Delta x} \end{bmatrix} \bullet \begin{bmatrix} f_0 \\ g_0 \end{bmatrix} = \mathbf{F}_2 \bullet \begin{bmatrix} f_0 \\ g_0 \end{bmatrix} \qquad (2)$$

The dispersion relation is the condition to satisfy the above equation, that is, $|e^{j\omega\Delta t}\mathbf{I}_2 - \mathbf{F}_2| = 0$; where $\mathbf{I}_m$ is the identity matrix of $m \times m$. The equation is written explicitly in the following form.

$$\{e^{j\omega\Delta t} - A_1 - A_2 e^{j\tilde{k}\Delta x}\}\{e^{j\omega\Delta t} - B_1 - B_2 e^{j\tilde{k}\Delta x}\} = \{A_3 + A_4 e^{j\tilde{k}\Delta x}\}\{B_3 + B_4 e^{j\tilde{k}\Delta x}\}. \qquad (3)$$

For the analysis of the numerical dispersion, the more important parameters are the sampling density and the Courant number ξ. The sampling density D is the number of the discretization per wavelength: $D = \frac{\lambda_0}{\Delta x} = \frac{2\pi}{k_0 \Delta x}$, where λ and k_0 are the physical wavelength and the physical wavenumber. Introducing the normalized numerical wavenumber $\tilde{k}_n = \tilde{k}/k_0$, we can rewrite the numerical dispersion relation (3) into

$$\{e^{j\xi P} - A_1 - A_2 e^{j\tilde{k}_n P}\}\{e^{j\xi P} - B_1 - B_2 e^{j\tilde{k}_n P}\} = \{A_3 + A_4 e^{j\tilde{k}_n P}\}\{B_3 + B_4 e^{j\tilde{k}_n P}\}, \qquad (4)$$

where $P = 2\pi/D$. The numerical dispersion relation is obtained by finding $\tilde{k}_n = \tilde{k}_n^r + j\tilde{k}_n^i$ which satisfies Eq. (4) for given ξ and D.

The straightforward extension of the CIP method is easily obtained by using the second derivatives to interpolate the profiles with the polynomials of the 5th order.

REFERENCES

1. Yabe, T., F. Xiao, and T. Utsumi, *J. Comp. Phys.*, Vol. 169, No. 2, 556–593, 2001.
2. Schneider, J. B. and C. L. Wagner, *IEEE Microwave Guided Wave Lett.*, Vol. 9, No. 2, 54–56, Feb. 1999.

A Neural Network Model for Phased Antenna Arrays

Fikret Tokan, Filiz Güneş, and Burak Bardak
Department of Electronics and Communication Engineering, Yıldız Technical University
İstanbul, Turkey

Abstract— In this work, a CAD model of linear antenna arrays is carried out using the Artificial Neural Network (ANN)s. Linear arrays are used widely in practice and their operating principles can be used to understand more complex array geometries. The pattern characteristics of an array can be explained for operation as a transmitter or receiver, whichever is more convenient, since antennas usually satisfy the conditions for reciprocity.

The basic array antenna model consists of two parts, the pattern of one of the elements by itself, the element pattern, and the pattern of the array with the actual elements replaced by isotropic point sources, the array factor. The total pattern of the array $F(\theta, \phi)$ is then the product of the element pattern $G(\theta, \phi)$ and the array factor $AF(\theta, \phi)$ which is called principle of pattern multiplication:

$$F(\theta, \phi) = G(\theta, \phi)AF(\theta, \phi) \tag{1}$$

$AF(\theta, \phi)$ of a general N-element antenna array can be expressed in terms of its geometrical configuration $\mathcal{G}$ and feeding conditions $\mathcal{F}$ as follows:

$$AF(\theta, \phi) = \sum_{i=1}^{N} C_i e^{j\alpha_i + jk_0 \vec{a}_r \cdot \vec{r}_i} \tag{2}$$

where and C_i and α_i are the excitation amplitude and phase of the ith antenna and the other parameters have the well-known definitions.

In this work, the array factor $AF(\theta, \phi)$ of the phased antenna arrays will be treated in a black-box using Artificial Neural Network (ANN)s as given. In the other words, the array factor of this array will be investigated as the function of element number N, interelement spacing d, and feeding conditions $[C, \alpha]$. Since each of these parameters is independent, so it is possible to obtain linear arrays with a large variety of the pattern characteristics. In the today's technology, the mechanical problems associated with a single large antenna are traded for the electrical problems of feeding small antennas of array. However, with the advancements in solid-state technology, it is possible to realize the feed networks required for the excitation with reasonable cost. In fact, arrays offer the unique capability of electronic scanning of the main beam. By changing the phase of the exciting currents in each element antenna of the array, the radiation pattern can be scanned through space. The array is then called a phased array. Phased arrays have many applications, particularly in radar.

As it is well-known, ANNs have emerged as a powerful linear learning machine for accurately modeling highly nonlinear input/output relationships in the large amount without requiring any knowledge. At the same time, ANNs have been used bidirectionally by reverse training and later this has also found an application into the design of the microstrip antennas. In this work, an expert machine is generated on the phased antenna arrays using a powerful linear learning machine, the Artificial Neural Network (ANN). It is a Multi-Perceptron Layer (MLP) network with two hidden layers each of which consists of ten neurons activated by the tangent sigmoid. In this way, the phased antenna arrays are modeled as a system approach. Inputs of this system are the number of elements, excitation and the geometry, and while the outputs are the array radiation characteristics. Thus it is possible to analyze and design the phased antenna arrays without requirement any knowledge of electromagnetism and neural network. Furthermore, behaviors of the phased arrays are obtained and then demonstrated by rectangular and polar patterns, changing all the system parameters.

Support Vector Machines for Use in the Device Modeling

Nurhan Türker Tokan and Filiz Güneş
Department of Electronics and Communication Engineering, Yıldız Technical University
İstanbul, Turkey

Abstract— Adequate modeling of nonlinear microwave devices still remains a complex but unavoidable step towards the achievement of a good circuit design. Even the characterization of passive elements, which is relatively simple for low frequencies, can be difficult for microwave frequencies. In the case of semiconductor devices, that are characterized by highly nonlinear models with a large set of parameters and complicated relationships between them, a proper selection of values for these parameters is a nontrivial task. Indeed, if performed inadequately this can significantly distort the simulation results. Usually these model parameters cannot be obtained by direct measurements because of the device nonlinearities. For our case, let us consider a microwave transistor as the semiconductor device. As it is well-known, there are two approaches to model its small-signal and noise behaviors: (i) The lumped equivalent electrical circuit approach, in which signal and noise performance has generally been separated from each other and device is characterized within a sub-region of its operation domain. (ii) The black-box modeling approach which can consider together both signal and noise behaviors of the device in its whole operation domain.

Today's, advances in the computational sciences make "learning machines" possible, which enable to generalize 'discrete' data into the 'continuous' data domain. Neural Networks are typical learning machines and used in the black-box modeling of non-linear devices. Neural transistors are typical black-box models of microwave transistor that generalizes the signal- and noise parameters from N-measured samples accurately over the whole operation domain of the device, which consists of bias conditions (V_{DS}, I_{DS}) and the operation frequency f. These black-box models are employed successfully in designing microwave devices and circuits.

On the other hand, within the last decade Support Vector Machines (SVM) emerge as a competitive learning machine, which are based on a judicious and rigorous mathematics combining the generalization and optimization theories together and verified to be computationally very efficient. In SVM, a nonlinear function is learned by a linear learning machine in a kernel-induced feature space while the capacity of the system is controlled by a parameter that does not depend on the dimensionality of the space. The learning algorithm minimizes a convex functional which guarantees the global minimum in the optimization procedure. The solution has sparseness that means it can be represented by means of a small subset of training points and ensures enormous computational advantages. This reduced number of non-zero parameters together with the guaranteed global minimum marks a clear distinction between this system and other pattern recognition algorithms, such as neural networks.

In this work, a SVRM model of Small — Signal and Noise behaviors of a microwave transistor is presented to the microwave world to be replaced by its ANN model. A worked example is also completed demonstrating highly nonlinear regression ability of the SVM comparatively with its ANN model. Thus, it can be concluded that SVM can conveniently be used in modeling of the highly nonlinear microwave devices with better accuracy and efficiency than ANN models.

ACKNOWLEDGMENT

This work was supported by The Scientific and Technological Research Council of Turkey.

Calculation of Electromagnetic Field with Integral Equation Based on Clifford Algebra

A. Chantaveerod[1], **A. D. Seagar**[2], **and T. Angkaew**[1]

[1]Department of Electrical Engineering, Chulalongkorn University, Thailand
[2]Department of Telecommunication, Srivijaya University of Technology, Thailand

Abstract— Multidimensional Cauchy integrals are used to calculate numerically the electromagnetic field radiated internally and externally from surfaces on which the field is specified. The calculations are carried fully in the form of Clifford arithmetic and the results appear in the form of Clifford numbers, which are subsequently separated into electric and magnetic fields and compared directly with known analytical results.

Wiener-Hopf Analysis of the Diffraction by a Terminated, Semi-infinite Parallel-plate Waveguide with Four-layer Material Loading

E. H. Shang and K. Kobayashi
Department of Electrical, Electronic, and Communication Engineering, Chuo University
1-13-27 Kasuga, Bunkyo-ku, Tokyo 112-8551, Japan

Abstract— Analysis of the scattering from open-ended waveguide cavities has received much attention recently in connection with the prediction and reduction of the radar cross section (RCS) of a target. A number of two- and three-dimensional (2-D and 3-D) cavity diffraction problems have been analyzed thus far by means of high-frequency ray techniques and numerical methods, but the solutions obtained by these approaches are not uniformly valid for arbitrary cavity dimensions.

In the previous papers [1, 2], we have considered a terminated, semi-infinite parallel-plate waveguide with three-layer material loading as a canonical 2-D cavity geometry, and analyzed the plane wave diffraction rigorously by means of the Wiener-Hopf technique. As an important generalization to the geometry in [1, 2], we shall consider, in this paper, a terminated, semi-infinite parallel-plate waveguide with four-layer material loading, and analyze the E-polarized plane wave diffraction using the Wiener-Hopf technique.

The geometry of the waveguide is shown in Figure 1, where ϕ^i is the incident field of E polarization, the waveguide plates at $x = \pm b$ and the planar termination at $z = -d_1$ are perfectly conducting and of zero thickness, and the four material layers I, II, III, and IV are loaded on the terminated plate. Introducing the Fourier transform of the scattered field and applying boundary conditions in the Fourier transform domain, the problem is formulated in terms of the simultaneous Wiener-Hopf equations. The Wiener-Hopf equations are then solved via the factorization and decomposition procedure leading to the exact solution. Taking the inverse Fourier transform of the solution in the complex domain, the scattered field inside and outside the waveguide is explicitly evaluated. Numerical examples on the monostatic RCS are presented, and the backscattering characteristics of the waveguide are discussed in detail.

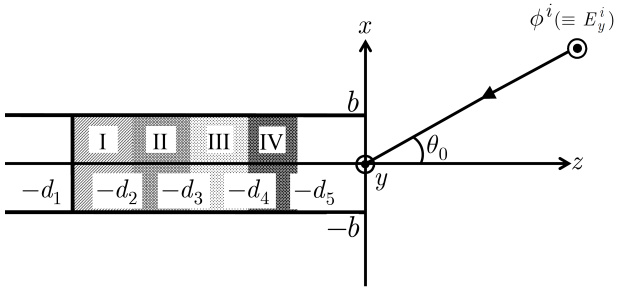

Figure 1: Geometry of the problem.

REFERENCES

1. Koshikawa, S. and K. Kobayashi, "Diffraction by a terminated, semi-infinite parallel-plate waveguide with three-layer material loading," *IEEE Trans. Antennas Propagat.*, Vol. 45, 949–959, 1997.
2. Koshikawa, S. and K. Kobayashi, "Diffraction by a terminated, semi-infinite parallel-plate waveguide with three-layer material loading: the case of H polarization," *Electromagnetic Waves & Electronic Systems*, Vol. 5, 13–23, 2000.

Combined Perturbation and Wiener-Hopf Analysis of the Diffraction by Two Parallel, Corrugated Half-planes

J. P. Zheng and K. Kobayashi
Department of Electrical, Electronic, and Communication Engineering, Chuo University
1-13-27 Kasuga, Bunkyo-ku, Tokyo 112-8551, Japan

Abstract— The analysis of wave scattering by gratings and waveguides with periodic structures is important in electromagnetic theory and optics. Various analytical and numerical methods have been developed so far and the diffraction phenomena have been investigated for many kinds of periodic structures. The Wiener-Hopf technique is known as a powerful tool for analyzing electromagnetic wave problems rigorously, and can be applied efficiently to the diffraction by specific grating geometries. However, most of the Wiener-Hopf analyses are restricted to periodic structures of infinite extent and plane boundaries. Therefore, it is important to investigate scattering problems involving periodic structures without these restrictions.

As an example of infinite periodic structures with non-plane boundaries, Chakrabarti and Dowerah [1] analyzed the plane wave diffraction by two parallel sinusoidal half-planes by means of the Wiener-Hopf technique together with the perturbation method. In [2], we have considered a finite sinusoidal grating as an example of finite periodic structures with non-plane boundaries, and analyzed the plane wave diffraction using a method similar to that employed in [1]. In this paper, we shall reconsider the problem solved by Chakrabarti and Dowerah [1] for the H-polarized plane wave incidence, and analyze the E-polarized plane wave diffraction by two parallel corrugated half-planes using the Wiener-Hopf technique.

The problem geometry is shown in Figure 1, where ϕ^i is the incident field of E polarization, and the waveguide surface is infinitely thin and perfectly conducting. Assuming that the corrugation amplitude is small compared with the wavelength, we replace the original problem by the problem of diffraction by two parallel half-planes with impedance-type boundary conditions. Taking the Fourier transform of the wave equation and applying approximate boundary conditions in the transform domain, the problem is formulated in terms of the simultaneous Wiener-Hopf equations. The Wiener-Hopf equations are then solved approximately via the factorization and decomposition procedure together with the perturbation scheme leading to the efficient zero- and first-order solutions. The scattered field in the real space is evaluated by taking the inverse Fourier transform and applying the saddle point method.

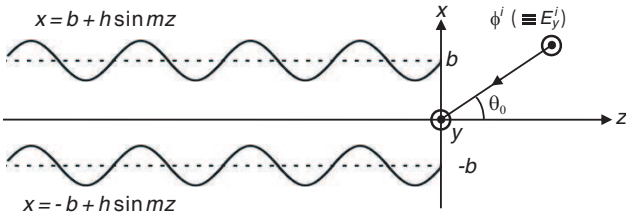

Figure 1: Geometry of the problem.

REFERENCES

1. Chakrabarti, A. and S. Dowerah, "Traveling waves in a parallel plate waveguide with periodic wall perturbations," *Can. J. Phys.*, Vol. 62, 271–284, 1984.
2. Kobayashi, K. and T. Eizawa, "Plane wave diffraction by a finite sinusoidal grating," *IEICE Trans.*, Vol. E74, 2815–2826, 1991.

Polarization Evolution in Weakly Anisotropic Media: Quasi-Isotropic Approximation (QIA) of Geometrical Optics Method and Its Recent Generalizations

Yu. A. Kravtsov[1,2], **P. Berczynski**[3], **B. Bieg**[2], **K. Yu. Bliokh**[4,5], **and Z. H. Czyz**[6]

[1]Space Research Institute, Profsoyuznaya St. 82/34, Moscow 117997, Russia
[2]Institute of Physics, Maritime University of Szczecin
1-2 Waly Chrobrego St., Szczecin 70500, Poland
[3]Institute of Physics, Szczecin University of Technology, Szczecin 70-310, Poland
[4]Institute of Radio Astronomy, 4 Krasnoznamyonnaya St., Kharkov 61002, Ukraine
[5]A. Ya. Usikov Institute of Radiophysics and Electronics, Kharkov 61085, Ukraine
[6]Telecommunications Research Institute, Warsaw 04051, Poland

Abstract— Quasi-isotropic approximation (QIA) of geometrical optics method is presented, which describes evolution of electromagnetic waves in weakly anisotropic media, and its recent generalizations are discussed. It is shown that in combination with complex geometrical optics QIA is able to describe not only polarization, but also diffraction phenomena in weakly anisotropic media. Being applied to inhomogeneous magnetized plasma, QIA embraces both Faraday effect and Cotton-Mouton phenomenon. QIA equations can be presented in a compact form by using the complex polarization angle. Relations between complex polarization angle and traditional parameters of polarization ellipse are established. In conclusion the Segre's equations for Stokes vector evolution are derived directly from QIA, what establishes deep unity, if not equivalence of these two approaches.

Quasi-isotropic approximation (QIA): Quasi-isotropic approximation of the geometrical optics method [1–3] describes propagation of electromagnetic waves in weakly anisotropic media, where all the components of the anisotropy tensor $\hat{\nu} = \hat{\varepsilon} - \varepsilon_0\hat{1}$ are small as compared with permittivity ε_0 of the isotropic background medium.

According to [1–3], solution of the Maxwell equations in the frame of QIA can be presented as $\mathbf{E} = A\mathbf{\Gamma}\exp(ik_0\Psi)$, where A and Ψ are correspondingly amplitude and eikonal of the electromagnetic wave in isotropic medium and $\mathbf{\Gamma}$ is a unit polarization vector. The latter obeys the QIA equations in the form

$$\frac{d\mathbf{\Gamma}}{d\sigma} = \frac{1}{2}ik_0\varepsilon_0^{-1/2}\hat{\nu}\mathbf{\Gamma}. \tag{1}$$

Combination of QIA with complex geometrical optics (CGO): In frame of CGO eikonal Ψ and amplitude A become complex valued and thereby allow describing propagation and diffraction of the Gaussian beam. In the case of paraxial CGO [4, 5] eikonal Ψ can be presented as a quadratic form $\Psi = \Psi_c + \frac{1}{2}B_{ij}\xi_i\xi_j$, where Ψ_c is an eikonal along the central ray and ξ_i are deviations from central ray. Matrix elements B_{ij} becomes complex valued in frame of CGO and satisfy nonlinear matrix Ricatti equation

$$\frac{dB_{ij}}{d\tau} + B_{ik}B_{kj} = \alpha_{ij}, \tag{2}$$

where parameters α_{ij} are the derivatives of the dielectric permittivity trannsverse the ray. The real parts $\mathrm{Re}B_{ij}$ of parameters B_{ij} describe the curved phase front of the beam, whereas imaginary parts $\mathrm{Im}\,(B_{ij})$ corresponds to Gaussian profile of the electromagnetic beam and describe its diffraction in inhomogeneous plasma.

Complex polarization angle (CPA): Tangent of CPA is involved as a ratio of complex amplitudes $\tan\gamma = \Gamma_2/\Gamma_1$. The components of CPA $\gamma = \gamma' + i\gamma''$ characterizes the angular parameters ψ, χ of the polarization ellipse: real part γ' defines polarization angle, $\gamma' = \psi$ and imaginary part — its ellipticity: $\tanh\gamma'' = \tan\chi = e$.

In the case of weakly anisotropic plasma γ obeys the equation

$$\dot{\gamma} = \frac{1}{2}\Omega_3 + \frac{1}{2}i\Omega_1\sin 2\gamma - \frac{1}{2}i\Omega_2\cos 2\gamma = \frac{1}{2}\Omega_3 + \frac{1}{2}i\Omega_\perp\sin(2\gamma - 2\alpha_\perp), \tag{3}$$

where $v = \omega_p^2/\omega^2$, $u = \omega_c^2/\omega^2$ are standard plasma parameters, $\Omega_1 = \frac{1}{2}k_0vu\sin^2\alpha_{||}\cos 2\alpha_\perp$, $\Omega_2 = \frac{1}{2}k_0vu\sin^2\alpha_{||}\sin 2\alpha_\perp$, $\Omega_3 = k_0vu^{1/2}\cos\alpha_{||}$ and $\Omega_\perp = \sqrt{\Omega_1^2 + \Omega_2^2}$.

Equation for Stokes vector evolution, derived from QIA: According to [6], the components $s_1 = \cos 2\chi \cos 2\psi, s_2 = \cos 2\chi \sin 2\psi, s_3 = \sin 2\chi$ of the Stokes vector $\mathbf{s} = (s_1, s_2, s_3)$ satisfy the Segre's equation

$$\dot{\mathbf{s}} = \mathbf{\Omega} \times \mathbf{s}, \tag{4}$$

where $\mathbf{\Omega} = [\Omega_1, \Omega_2, \Omega_3]$. It can be shown that Equation (4) follow directly from QIA Equation (1). In turn, solutions of the Equation (4) can be expressed through complex polarization angle $\gamma = \gamma' + i\gamma''$.

Evolution of the polarization vector in inhomogeneous plasma is described on the basis of quasi-isotropic approximation of the geometrical optics method. QIA equations take into account: i) curvature and torsion of the ray; ii) longitudinal and lateral inhomogeneity of plasma; iii) torsion of the static magnetic field; iv) weak absorption and dichroism. QIA equations are the basis for consequent derivation of the equation for the complex polarization angle, which promises to become an effective instrument for hot plasma polarimetry. Besides, equation for the complex polarization angle are proved to be equivalent to the Segre's equation for the Stokes vector. As a result, QIA equations are favorable basis for substantiation of the Segre equation for evolution of the Stokes vector. The results under consideration might be quite helpful for solution of the inverse problems of plasma diagnostics, presented in [7].

REFERENCES

1. Fuki A. A., Yu. A. Kravtsov, and O. N. Naida, *Geometrical Optics of Weakly Anisotropic Media*, Gordon & Breach, Lond., NY, 1997.
2. Kravtsov, Yu. A. and Yu. I. Orlov, *Geometrical Optics of Inhomogeneous Media*, Springer, Berlin, 1990.
3. Kravtsov, Yu. A., *Geometrical Optics in Engineering Physics*, Alpha Sci. Int., London, 2005.
4. Berczynski, P. and Yu. A. Kravtsov, Combination of quasi-isotropic approximation with complex geometrical optics. VI Intern. Workshop and School "Towards fusion energy-plasma physics, diagnostics, spin-offs," Kudowa Zdroj, Poland, September 18–22, 2006.
5. Berczynski, P., K. Yu. Bliokh, Yu. A. Kravtsov, et al., *JOSA A*, Vol. 23, No. 6, 1442–1451, 2006.
6. Segre, S., *Plasma Phys. Contr. Fusion*, Vol. 48, 339, 2006.
7. Guenther, K., *Plasma Phys. Contr. Fusion*, Vol. 46, 1423–1441, 2004.

Numerical Methods for the Solution of Volume Integral Equations of Electromagnetics

A. B. Samokhin[1] and A. S. Samokhina[2]

[1]Moscow Institute of Radio Engineering, Electronics and Automatics
78, Vernadsky av., Moscow 117454, Russia
[2]Institute of Control Science of Russian Academy of Sciences
65, Profsouznaya st., Moscow 117997, Russia

Abstract— We consider volume integral equations with the kernels depending on the difference of arguments

$$a(x)u(x) + \int\limits_Q \frac{K(x-y)}{r^3} u(y)dy = f(x) \tag{1}$$

Here $u(x)$, $f(x)$ are l-dimensional vectors, and $a(x)$ and $K(x)$ are $l \times l$ matrices; $r = |x - y|$ is the distance between points x and y of the three-dimensional Euclidean space E_3 with Cartesian coordinates $x = (x_1, x_2, x_3)$ and $y = (y_1, y_2, y_3)$, and Q is a bounded three-dimensional domain. Many important classes of problems of mathematical physics can be described by equations of the form (1); for example, this is the case for problems of electromagnetic and acoustic scattering on three-dimensional transparent bodies. The corresponding integral operator is scalar ($l = 1$) and compact in acoustic problems and singular and vector ($l = 3$) in electromagnetic problems.

To solve the integral Equation (1) numerically, one reduces it to a system of linear algebraic equations (SLAE). The solution of that system must approximate the solution of the original problem with prescribed accuracy. Let h be a typical length on which the solution u varies only slightly. Then the dimension N of the SLAE can be estimated as $N \approx l(mesQ/h^3)$. In the following, we consider the numerical solution of the integral Equations (1) that can be reduced to a very large SLAE, $N >> 1000$. It is clear that we must apply only an iteration method. Number T of arithmetic operations that guarantees the required accuracy of solution and memory volume M required for the implementation of the algorithm are the main efficiency criteria for any numerical algorithm. Multiplication of matrix SLAE by vector is the most laborious operation of the iteration method. Therefore, the number of multiplications for the implementation of a particular algorithm will be called the number of iterations. Then, the value of T is estimated by the formula

$$T \approx LT_A \tag{2}$$

Here, L is the number of iterations and T_A is the number of arithmetic operations required for multiplication of a matrix by a vector. In this report we solve the problems related with the minimization of the values T_A, L and M by using the fact that the kernel of the integral operator depends only on the difference of Cartesian coordinates of x and y.

REFERENCES

1. Samokhin, A. B., "Integral equations and iteration methods in electromagnetic scattering," VSP., Utrecht, The Netherlands, 2001.

Session 2A2
Plasmonics, Nano-composites and Metamaterials, Extraordinary Light Transmission 1

Field Propagation in Nanoporous Metal Waveguides

A. J. Viitanen[1], **I. S. Nefedov**[2], **and S. A. Tretyakov**[2]

[1]Electromagnetics Laboratory, TKK Helsinki University of Technology, Finland
[2]Radio Laboratory/SMARAD Center of Excellence, TKK Helsinki University of Technology, Finland

Abstract— In recent years a lot of attention is paid for metal nanoscale structures because of new phenomena and potential applications for waveguide and antenna techniques. Especially in optical region new effects arise based on plasmon resonances. In this study field propagation in nanoporous metal structures is considered. It is known that in optical region some noble metals behave like plasma which are almost lossless. Inserting pores in such metal we have effectively a resonant material with Lorentz type resonance. The resonant properties depend on the plasma frequency of the metal and on the volume fraction of pores in metal. A thin layer of such material behaves as a guided wave structure at the frequency range near the resonance. Actually near the resonance a huge change in propagation properties happend. These properties also depend on the thickness of the slab. With a proper choise of these parameter values there exist backward waves.

Another structure which is considered is a metal with regular arrays of pores. Actually, this structuce can be analyzed in a similar way as the arrays of dipoles. Now in this case, the surrounding medium is metal while the inclusions are empty spheres. It is seen that the inclusions resonate at the frequency where the relative permittivity is $\epsilon_r = -\frac{1}{2}$. Making a linear chain of such particles we have a waveguide. Although the field is decaying outside the pores, these inclusions are so close to each other that there is interaction with the neighbouring pores. Near the resonance this interaction is strong enough that there exist guided wave modes along the array. Properties of these modes are investigated. The allowed frequency range where the guided modes exist depend on the geometry, i.e., how close the pores are. There exist two propagating modes, transversal and longitudinal polarizations. The transversally polarized field propagates as a forward wave and the longitudinally polarized field as a backward wave.

Eigenmode Analysis of the Plasmonic Modes in Periodic Metal Nanoparticle Arrays

Kin Hung Fung, **Yurong Zhen**, **and C. T. Chan**
The Hong Kong University of Science and Technology, Hong Kong

Abstract— We demonstrate an efficient eigen-decomposition method to analyze the plasmonic modes in metal nanoparticle structures. The proposed method has the advantage of simultaneously showing the dispersion relation and the mode quality. It can also separate the material properties from the geometrical properties. Its efficiency therefore does not depend on the complexity of the material polarizability. We used the method to analyze the guided plasmonic modes of metal nanoparticle chains in various configurations. For the 1D system, the rigorous dynamic dipole polarizability typically gives a red-shift compared with the results obtained from the broadly used quasistatic dipole polarizability with radiation correction. We also applied the method to 2D and 3D structures, and we will discuss the evolution of the dispersion relations as the complexity of the structure increases.

Role of Resonances in Amplification of Faraday Effect

Alexey P. Vinogradov[1], **Alexander M. Merzlikin**[1], **Alexander V. Dorofeenko**[1]
Alexander B. Granovsky[2], **Alexander A. Lisyansky**[3], **and Mitsuteru Inoue**[4]

[1]Institute for Theoretical and Applied Electromagnetics, Russian Academy of Sciences, Russia
[2]Faculty of Physics, Moscow State University, Russia
[3]Department of Physics, Queens College, the City University of New York, USA
[4]Department of Electrical and Electronic Engineering, Toyohashi University of Technology, Japan

Abstract— Enhancement of the magnetooptical (MO) Faraday effect by means of different resonant structures is considered. It is well known that in a gyrotropic system we can observe a rotation of the plane of polarization of the incident linearly polarized wave traveling along the gyrotropic axis (in our case it is the direction of the magnetization of a MO medium). A linearly polarized wave can be presented as a sum of two circular polarized waves, which are eigenwaves in MO medium. Since the phase velocities of these eigenwaves are different, the plane of the polarization of the linearly polarized wave rotates in space when the z-coordinate increases (MO Faraday effect). If at zero magnetization the system has a transmittance resonance, like the Fabry-Perot filter has, at non-zero magnetization the resonance line splits into resonance lines for the left and right circular polarizations (Fig. 1). At the frequency at which these lines are crossing, the transmitted wave is linearly (not elliptically) polarized and one can observe the rotation of the plane of polarization.

A well-known realization of such a resonant structure is a MO defect in a photonic crystal [1]. We consider another realization, which is related to an excitation of a Tamm surface state existing at an interface of photonic and magnetophotonic crystals with intersecting band gaps [2] and with a plasmon resonance [3]. In the case of the Tamm-state resonance, the angle of the polarization plane rotation θ is shown in Fig. 1. It has an order of π because it is related to phase change at the resonance rather than to the weak Faraday rotation of wave passing the structure. Treating the structures as an open resonator, we consider a transfer function as a sum of simple fractions and analyze how the parameters of resonances influence the rotation angle.

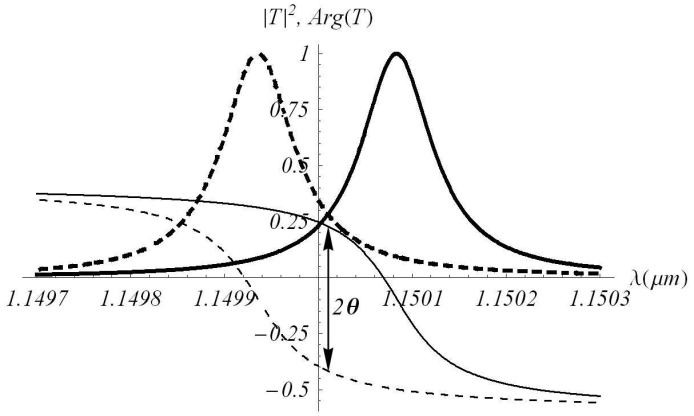

Figure 1: Peaks of the transmission coefficient (thick lines) and corresponding phases (thin lines) for two circular polarizations at the presence of magnetization.

REFERENCES

1. Vinogradov, A. P., S. G. Erokhin, A. B. Granovsky, and M. Inoue, *Journal of Communications Technology and Electronics*, Vol. 49, 88, 2003.
2. Vinogradov, A. P., A. V. Dorofeenko, S. G. Erokhin, M. Inoue, A. A. Lisyansky, A. M. Merzlikin, and A. B. Granovsky, *Phys. Rev. B*, Vol. 74, 045128, 2006.
3. Hermann, C., V. A. Kosobukin, G. Lampel, J. Peretti, V. I. Safarov, and P. Bertrand, *Phys. Rev. B*, Vol. 64, 235422, 2001.

Metal Dielectric Constant Influence on Extraordinary Optical Transmission through Hole Arrays

Sergio G. Rodrigo[1], **F. J. García-Vidal**[2], **and Luis Martín-Moreno**[1]
[1]Departamento de Fisica de la Materia Condensada-ICMA, Universidad de Zaragoza
E-50009, Zaragoza, Spain
[2]Departamento de Fisica Teorica de la Materia Condensada, Universidad Autonoma de Madrid
E-28049, Madrid, Spain

Abstract— In this work we compare recent experiments [1] on the influence of the metal chosen on extraordinary optical transmission (EOT) against calculations performed with the Finite Difference Time Domain (FDTD) method. We analyze transmission spectra through hole arrays drilled in several optically thick metal films (viz. Ag, Au, Cu, Al, Ni, Cr and W) for several periods and hole diameter proportional to the period ($d = P/1.75$). Theoretical calculations are in excellent agreement with experimental results (see figure below and Ref. [1]).

If the metal were a Perfect Electric Conductor, the transmission properties would be scale free if the metal thickness was *also* scaled. Therefore, in order to reveal even more clearly the effect of the metal dielectric constant, the case in which the film thickness is scaled as $h = P/2.0$ (compared with experiments where metal thickness was fixed) is also considered.

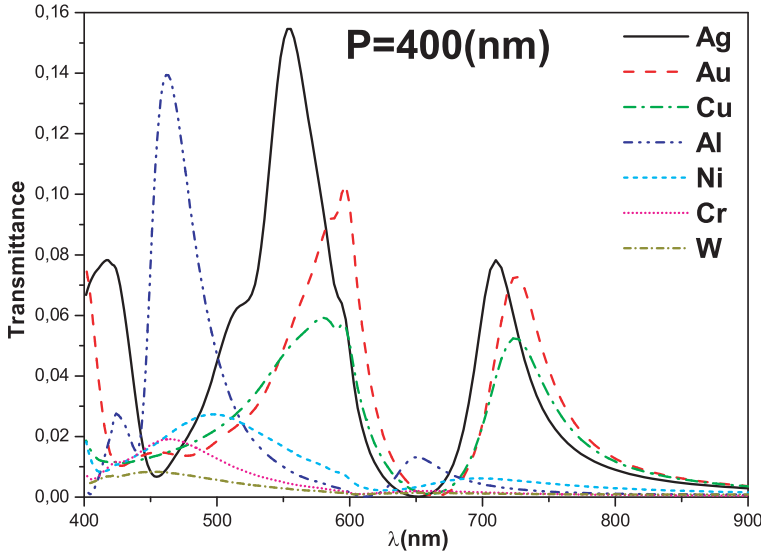

Figure 1: FDTD calculated transmission spectra for metals studied at a given period $P = 400\,(\mathrm{nm})$, $w = 250\,(\mathrm{nm})$ and $d = P/1.75$.

REFERENCES

1. Przybilla, F., A. Degiron, J.-Y. Laluet, C. Genet, and T. W. Ebbesen, *J. Opt. A: Pure Appl. Opt.*, Vol. 8, 458–463, 2006.

Metamaterial Comprising Plasmonic Nanolasers

Andrey K. Sarychev, **Alexander A. Pukhov**, **and Gennady Tartakovsky**

Institute of Theoretical and Applied Electrodynamics RAS, Izhorskaya 13, Moscow 125412, Russia

Abstract— We consider plasmonic nanoantennas immersed in active host medium. Specifically shaped metal nanoantennas can exhibit strong magnetic properties in the optical spectral range due to the excitation of the magnetic plasmon resonance. At the magnetic plasmon resonance the magnetic component of the em field excites collective electron oscillation in the plasmonic nanoantenna. The excitation of the circular current $\boldsymbol{I}$ in the horseshoe plasmonic antenna is shown in the figure,

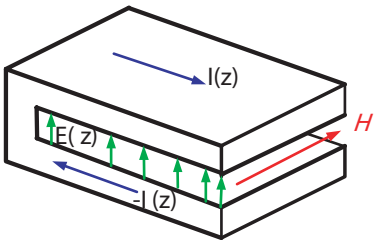

where the magnetic field $\boldsymbol{H}$ is applied parallel to the gap between two arms. The current $\boldsymbol{I}$ is shorted by the displacement currents flowing in the gap. When the frequency of the impingent light is larger than the resonant frequency, the current $\boldsymbol{I}$ inside the horseshoe induces the magnetic field which direction is opposite to the direction of the field of the impingent wave. Therefore, the metamaterial, composed from the horseshoe nanoantennas have negative effective magnetic properties at optical frequencies: the effective magnetic susceptibility is negative and the permeability could be negative when the concentration of the horseshoe nanoantennas is large enough. A metamaterial comprising such nanoantennas can demonstrate "left-handiness" in the optical range.

We show that high losses predicted for the optical "left-handed" metamaterials can be compensated by the gain medium, which is staffed in the gap of the horseshoe. We have derived condition under which the nanoantennas filled with highly efficient gain medium can demonstrate low absorption or even gain sufficient for lasing, namely,

$$G\lambda/(2\pi n_d\gamma) > 1,$$

where G and n_d are the gain and refractive index of the active medium correspondingly, λ is wavelength, and $\gamma = \varepsilon_m^{''}/|\varepsilon_m|$ is the metal loss factor. As soon as this condition is fulfilled the interaction between gain medium and the plasmonic nanoantenna leads to coherent oscillations in the electric charge and the magnetic moment of the horseshoe, even in the absence of the external electromagnetic field. Thus we propose plasmonic nanolaser, where the metal nanoantenna operates like a resonator. The size of the proposed plasmonic laser is much smaller than the wavelength. Therefore, it can serve as a very compact source of EM radiation.

Sequence-dependent Phase Transition of DNA-linked Gold Nanoparticle Assemblies

Ching-Hwa Kiang and Nolan C. Harris
Department of Physics and Astronomy, Rice University, Houston, TX 77005, USA

Abstract— DNA-linked gold nanoparticle systems offer a unique opportunity for studying the phase behavior of biological particles with tunable interactions. Melting of these nanoparticles exhibit an unusual trend not found in other colloidal systems [1–3]. I will present experimental studies of reversible phase transition of DNA-linked gold nanoparticle assemblies. Single-stranded DNA-capped gold nanoparticles are linked by complementary linker DNA to form the assemblies. Compared to free DNA, a sharp melting transition is observed for the DNA-linked gold nanoparticle assemblies. Using optical spectroscopy, we observed unusual melting transitions when there are disorder [4] and defects [5] in the DNA duplex sequence.

REFERENCES

1. Kiang, C.-H., *Physica A*, Vol. 321, 164, 2003.
2. Sun, Y., N. C. Harris, and C.-H. Kiang, *Physica A*, Vol. 350, 89, 2005.
3. Sun, Y., N. C. Harris, and C.-H. Kiang, *Physica A*, Vol. 354, 1, 2005.
4. Harris, N. C. and C.-H. Kiang, *Phys. Rev. Lett.*, Vol. 95, 046101, 2005.
5. Harris, N. C. and C.-H. Kiang, *J. Phys. Chem. B*, Vol. 110, 16393, 2006.

Extraordinary Phenomena in Metal-semiconductor Hybrid Structures

S. A. Solin, Charles M. Hohenberg, K. A. Wieland, Y. Wang, and A. K. M. S. Newaz

Center for Materials Innovation and Department of Physics, CB 1105
Washington University in St. Louis
1 Brookings Drive, St. Louis, MO 63130, USA

Abstract— Following the discovery of room temperature extraordinary magnetoresistance (EMR) as large as 3,000,000% in macroscopic narrow-gap metal-semiconductor hybrid (MSH) structures formed from InSb and Au [1], and the quantitative explanation of this new phenomenon based on geometric effects [1, 2], much effort has been expended to scale EMR devices to the nanoscopic regime in order to impact technologies such as ultra-high-density magnetic recording. The miniaturization of EMR devices has been successful [3, 4] and has revealed surprising new aspects of the mesoscopic physics of these nano-hybrid structures. The EMR effect in macroscopic and nanoscopic structures will be described and explained using both analytic and finite element analysis. It will be shown that EMR is but one example of a broad class of phenomena that result from the interplay of geometry and interfaces in simple MSHs. Three further examples will be described. 1. Extraordinary Piezoconductance — EPC [5]: MSHs are found to exhibit a large change in conductance with applied strain. Like EMR, the magnitude of this EPC depends strongly on the unstrained device geometry, and is more than 500% greater than the piezoconductance of the homogeneous semiconductor alone at a strain of 3×10^{-4}. 2. Extraordinary Optoconductance — EOC [6]: Using a Van der Pauw plate setup, the voltage of the bare semiconductor is compared directly to that of the MSH to determine the EOC. In GaAs-In at 30 K EOC $\sim$ 500% has been observed. Bulk InSb-In structures have a room temperature EOC $\sim$ 50%. Prior research has shown that one may increase the EOC by using a semiconductor with a large differential e-h mobility. Te doped n-type InSb thin films ($n = 2.11 \times 10^{22}\,\mathrm{m}^{-3}$ and $\mu_e = 4.02\,\mathrm{m}^2/\mathrm{Vs}$) are therefore prime candidates for room temperature EOC. These MSHs were illuminated with Ar focused 488.0 nm light and studied as a function of the position of the laser spot and temperature. 3. Extraordinary Electroconductance — EEC [7]: We have developed a new design for a microscopic thin film EEC sensor, which is a van der Pauw plate structure consisting of a heavily doped n-type GaAs epi layer (500 nm) with a metallic shunt (50 nm) on top. EEC arises from the current redistribution between the shunt and GaAs when an external E field lowers the interfacial Schottky barrier height (SBH). By defining the EEC effect to be the percentage change in sample conductance with and without the E field, we have obtained a 20% change in a field of 12 kV/cm at 300 K. We also compared the response of a sample with a Schottky barrier to an unshunted sample and to a shunted sample with an Ohmic interface. We propose that by applying a new surface treatment to the GaAs mesa, the surface state density can be remarkably reduced, so that the SBH is controlled by judicious choice of the metal. This allows more electron transport over the barrier and results in a geometrically enhanced conductance change. By varying the geometry of the structure and the material of the shunt, we can optimize the design of the EEC sensor. Time permitting, the potential (and kinetic) impact of "EXX" effects on a wide range of sensor technologies will be highlighted.

REFERENCES

1. Solin, S. A., et al., *Science*, Vol. 289, 1530, 2000.
2. Zhou, T., D. R. Hines, and S. A. Solin, *Appl. Phys. Lett.*, Vol. 78, 667, 2001.
3. Solin, S. A., et al., *Appl. Phys. Letters*, Vol. 80, 4012, 2002.
4. Solin, S. A., *Scientific American*, Vol. 291, 70, 2004; *Physics Highlights of 2002*, APS News, 6, Feb. 2003; *IEEE Spectrum*, 19, Feb. 2003; *Nature*, News and Views, 392, May 23, 2002.
5. Rowe, A. C. H, D. R. Hines, and S. A. Solin, *Applies Physics Lett.*, Vol. 83, 1160, 2003; A. C. H. Rowe and S. A. Solin, *Phys. Rev.*, Vol. B71, 235323, 2005.
6. Wieland, K. A., Y. Wang, S. A. Solin, A. M. Girgis, and L. R. Ram-Mohan, *Appl. Phys. Lett.*, Vol. 88, 52105, 2006.
7. Wang, Y., K. A. Wieland, and S. A. Solin, *J. Appl. Phys.*, in press.

Spectroscopic Properties of a Two-level Atom Interacting with a Complex Spherical Nanoshell

Alexander Moroz

Wave-scattering.com, Germany

Abstract— Frequency shifts, radiative decay rates, the Ohmic loss contribution to the nonradiative decay rates, fluorescence yield, and photobleaching of a two-level atom radiating anywhere inside or outside a complex spherical nanoshell, i.e., a stratified sphere consisting of alternating silica and gold concentric spherical shells, are studied. The changes in the spectroscopic properties of an atom interacting with complex nanoshells are significantly enhanced, often more than two orders of magnitude, compared to the same atom interacting with a homogeneous dielectric sphere. The detected fluorescence intensity can be enhanced by 5 or more orders of magnitude. The changes strongly depend on the nanoshell parameters and the atom position. When an atom approaches a metal shell, decay rates are strongly enhanced yet fluorescence yield exhibits a well-known quenching. Rather contra-intuitively, the Ohmic loss contribution to the nonradiative decay rates for an atomic dipole within the silica core of larger nanoshells may be decreasing when the silica core-inner gold shell interface is approached. The quasistatic result that the radial frequency shift in a close proximity of a spherical shell interface is approximately twice as large as the tangential frequency shift appears to apply also for complex nanoshells. Significantly modified spectroscopic properties (see computer program freely available at http://www.wave-scattering.com) can be observed in a broad band comprising all (nonresonant) optical and near-infrared wavelengths.

REFERENCES

1. Moroz, A., "Spectroscopic properties of a two-level atom interacting with a complex spherical nanoshell," *Chem. Phys.*, Vol. 117, No. 1, 1–15, 2005, [quant-ph/0412094].
2. Moroz, A., "A recursive transfer-matrix solution for a dipole radiating inside and outside a stratified sphere," *Annals of Physics (NY)*, Vol. 315, 352–418, 2005.

Beam Splitter Using a One-dimensional Metal Photonic Crystal with a Parabola-like Equi-frequency Contour

Linfang Shen[1], **Tzong-Jer Yang**[2], **and Yuan-Fong Chau**[3]

[1]Department of Information Science and Electronic Engineering
Zhejiang University, Hangzhou, Zhejiang Province, China
[2]Department of Electrophysics, National Chiao Tung University, Hsinchu, Taiwan
[3]Department of Electronic Engineering, Chin Yun University, Jung Li, Taiwan

Abstract— The spatial dispersion properties of a one-dimensional metal photonic crystal (1D MPC) consisting of Ag films and SiO2 layers stacked alternatively with a period a along x-direction for the thickness of silver films much smaller than a is analyzed. Five types of dispersion curves for a 1D MPC at a normalized frequency less than one has been shown. By exploiting one of five types — the parabola-like dispersion behavior, a MPC slab can be used to realize an exactly 50/50 beam splitter based on the symmetry of the geometric structure. The spatial separation of the output beams at the exit surface is linearly proportional to the thickness of slab, while the total output power varies almost periodically. The numerical results are simulated by FDTD (Finite Difference Time Domain) method. Finally, we find that a better splitting performance can be achieved by only optimizing the thickness of slab.

*This work is supported by NSC of ROC.

Wave Interaction with Double-negative and Double-positive Plates

F. Urbani[1], **C. Sabah**[2], **and S. Uckun**[2]

[1]Department of Engineering, University of Texas at Brownsville
80 Fort Brown, Brownsville TX 78520, USA
[2]Electrical and Electronics Engineering Department, University of Gaziantep
27310, Gaziantep, Turkey

Abstract— In this study, wave interaction with double-negative (DNG) and double-positive (DPS) plates is presented. Theoretically, the structure is composed by DNG and DPS plates with different material properties and thicknesses forming an N-tier structure. The DNG plates are described by using the Lorentz and Drude media parameters while the DPS plates are defined by known dielectric materials. The incident electric field is assumed to be a monochromatic plane wave with any arbitrary polarization. After obtaining the electric and magnetic fields both inside and outside the plates and imposing the boundary conditions, the reflected and transmitted powers are calculated using the transfer matrix method in order to observe their behaviors. In this paper, the frequency response of the DNG and DPS plates is deeply analyzed both analytically and numerically. Finally, the computations of reflected and transmitted powers are analyzed numerically with the purpose of designing efficient filters at the microwave, millimeter wave, and optical frequency regions.

Session 2A3a
Medium Effects on Electromagnetic Wave Propagation and Applications

Prediction of Some Ionospheric Effects on Radio-waves Propagation

R. Talhi[1,2], **A. Lebrere**[1,2], **F. Li**[1,2], **and F. Costen**[3]

[1]C.N.R.S-UMR 6115, 3A, Avenue de la recherche scientifique, 45071 Orleans Cedex 2, France
[2]University of Tours, France
[3]School of Electrical and Electronic Engineering, University of Manchester, Manchester, M601QD, UK

Abstract— The design and performance of radio communication systems (terrestrial, maritime, earth-space links) and satellite navigation systems (GPS, EGNOS, GLONASS, MSAS), are as we know, directly related to the properties of the radio propagation channel. Radio waves propagating through a turbulent medium with fluctuations of refractive index, such as ionosphere, suffer from various distortions like intensity and phase scintillations, group delay, broadening of pulses, Faraday rotation effect, etc. The ionosphere (mainly regions E and F) is the one of the most difficult region to study theoretically or to make measurements because of its ion and electron densities which change dramatically with many factors like time of day, season and variations in solar and geomagnetic activity, magnetic latitude of the observation point. For example, in the equatorial region, when solar activity is maximum, GPS observations show that the strength of random ionospheric irregularities (of different scales), may be very large after sunset and gives rise to intensity fading as large as 20 dB, which cause failing of most receivers to acquire GPS signals. In the same solar conditions, at polar, auroral and middle latitudes, the ionospheric irregularities with speeds as large as 1 km/s, may cause significant phase scintillations, and make GPS receivers to lose phase lock [1]. In addition, one of the major contributions to some navigation errors, is the ionospheric delay, also induced by random irregularities of the ionosphere. It is shown that this propagation delay can exceed 85 ns, which corresponds to approximately 155 TECU (Total Electron Content Unit $= 10^{16}$ electrons/m^2) or to 25 m error in the range, reducing the accuracy of the GPS user position [2].

This paper is focused on the impact of some ionospheric effects on radio waves propagation in H.F band (3 to 30 MHz); fluctuations of intensity and polarization are analyzed taking into account the influence of turbulence and electron density variations; a brief description of the used method is given, and some results are presented and discussed.

In order to assess some of the previous ionospheric effects and their contribution to degradation of radio signals, we have developed a stochastic model, based on generalized radiative transfer theory, and using a Monte-Carlo method. Then we tested our model in various simulations. As concerns prediction of fluctuations of scattered intensity and polarization effects in the angular area $(\theta, \phi) = [0, \pi] \times [0, 2\pi]$, using typical ionospheric parameters, turbulence spectrum, and electron density profile, the results analysis confirm our preliminary approach [3], and show that the statistical characteristic of the intensity fluctuations seems to follow a Weibull distribution for small incidence angles ($\theta \cong 6$ degrees), with a maximum-likelihood close to 99.7%; and for large incidences angles ($\theta \cong 30$ degrees), the approximation law corresponds to Lognormal distribution with an estimator close to 97.6%. While the statistic relative to the degree of polarization may be represented by a Hill distribution mainly for small angles of incidences, with an estimator of the order of 99.2%. Furthermore, if we look how electron density and turbulence may influence the intensity fluctuation, we can observe that the angular position of the maximum scattered intensity is governed by the maximum electron density (typically 10^{12} e/m^3), and the angular width (at mid-height) of the scattered energy is dominated by the turbulence strength. The latter result corresponds to broadening of the differential scattering cross-section, which is related, in particular, to multiple scattering effect due to ionospheric turbulence as is proven in [4].

REFERENCES

1. Basu, S., "Ionospheric scintillations," *URSI-GA 2005*, New Delhi, India, 2005.
2. Oliveira, A. B. V., et al., "Ionospheric equatorial anomaly studies during solar storms," *URSI-GA 2005*, New Delhi, India, 2005.
3. Talhi, R., et al., "Electromagnetic scattering and polarization: theory and application," *Piers 2005*, Hangzhou, China, 2005.
4. Ishimaru, A., et al., "Ionospheric effects on synthetic aperture radar at 100 MHz to 2 GHz," *Radio Science*, Vol. 34, 1999.

Mutual Coupling Effects on the Mean Capacity of MIMO Antenna Systems

Andrea Farkasvolgyi and Lajos Nagy
Department of Broadband Infocommunications and Electromagnetic Theory
Budapest University of Technology and Economics
H-1111 Budapest, Goldmann sq 3, Hungary

Abstract— We would like to show in this article the effect of the antenna position changing on the capacity of the multiple-input-multiple-output (MIMO) system considering effect of the mutual coupling. In the course of the simulation we analyzed a 3×3 MIMO antenna system.

We chose low elements-number-antenna-system because this system is the most suitable design on the end-user-market. We are supposing this antenna buildup (three elements on both receiver and transmitter) issues in the simplest structure with the highest mean capacity. With other antenna-number-reduction capacity of so-called multiple antenna system would have a beyond measure low level. Goal of this simulation is the capacity maximization by changing antennas position and observe the effects of mutual coupling for mean capacity. Orthogonal parallel transmission links can be found by eigenvectors of the channel matrix. Eigenvectors of the channel are generated from singular value decomposition (SVD) of the channel matrix. The parallel transmission links coexist in the frequency band named eigenchannels. The capacity of a multiple antenna system depends on the number of eigenchannels. The MIMO channel is similar to a low correlation diversity channel. MIMO systems generally operate in an indoor rich scattering environment and takes advantage of uncorrelated electric and magnetic fields. In the paper we present that the channel capacity is affected by the antenna structures. We can maximize the efficiency of transmission by changing the antenna positions. We will demonstrate channel-capacity-variation versus angles between antenna elements and show the effect of mutual coupling for channel capacity. We make these optimizations for an unmitigated indoor environment. In the paper for these optimizations we take the three dimension (3-D) double bouncing (DB) stochastic scattering model with wide angular spread as a basis at both ends in order to that by this method we can calculate with scattering surfaces between the transmitter and the receiver.

The waves launch from the transmitter antennas and first they reach the elements of the primary reflection surface and from here they re-scatter to the second group of scatterers (which are around the receiver antennas) and finally they are reflected to the receiving antennas. The transmission channel matrix H consists of nine transmission links. At the start of the simulation the antennas were orientated in the Z axis and later they were rotated toward the X-Y axes (the structure was opened like an umbrella). The radiated electric field of each dipole is applied for the calculation of the transmitter matrix. The current distribution for each electric dipole is sinusoidal, which is often supposed for finite length dipoles. The radiated far field can be derived using the excitation current and it is generally expressed in spherical coordinate system.

The complete MIMO transmission matrix, H may be given as $H = H_{sc2-re} \cdot H_{sc1-sc2} \cdot H_{sc1-tr}$, where H is of size $N_r \times M_t$ (in this case the element number of H is 9) with entries $H[n, m]$ which describe the path from nth transmitter to mth receiver (where H_{tr-sc1} means the transfer between the transmitter unit and the first surface of scatterers; $H_{sc1-sc2}$ is the connection between the first group and the second group of scatterers; H_{sc2-re} is like the first matrix can describe the path from the second group of scatterers to the receiver).

The original channel matrix H will be modified when mutual coupling is included. The channel matrix including mutual coupling, H_{mut}, is given by $H_{mut} = C^r_{mut} * H * C^t_{mut}/C_r * C_t$ (where, $C^r_{mut} = Z_l(Z_{re} + Z_l)^{-1}$ and $C^t_{mut} = Z_{tr}(Z_{tr} + Z_s)^{-1}$; $C_t = Z_t(1, 1)/(Z_t(1, 1) + Z^*_t(1, 1))$ and $C_r = Z_r(1, 1)/(Z_r(1, 1) + Z^*_r(1, 1))$; the mutual impedance matrix on transmitter and receiver units $Z_{tr}\, Z_{re}$; load impedance Z_l and source impedance Z_s). From this definition, in the case of zero-mutual coupling H_{mut} converges to H.

For a MIMO radio channel the channel capacity comes from SVD and water filling algorithms by $C = \sum_{i=1}^{r`} \log_2(1 + \lambda_i SNR_i)$.

By results of the simulation we can show, at first variation of the channel capacity by the antenna position and secondly effect of the mutual coupling for the channel capacity.

Ultrashort Electromagnetic Pulse Dynamics in the Singular and Weak Dispersion Limits

K. E. Oughstun and N. A. Cartwright

College of Engineering & Mathematical Sciences, University of Vermont, USA

Abstract— The asymptotic description of the dynamical evolution of an ultrashort electromagnetic pulse in a dispersive medium has shown that the temporal pulse structure evolves into a set of so-called precursor fields that are characteristic of the dispersive medium. Of particular interest is the evolution of the Brillouin precursor whose peak amplitude experiences zero exponential decay with propagation distance $z > 0$, decreasing algebraically as $z^{-1/2}$ in a dispersive, absorptive medium. The limiting behavior of this algebraic peak amplitude decay in both the zero damping (or singular dispersion) limit as well as the zero density (or weak dispersion) limit is investigated here for a single resonance Lorentz model dielectric in order to establish whether or not this rather unique behavior persists in these two different limits.

Low Latitude Ionospheric Turbulence Observed by the Micro-satellite DEMETER

F. Li, **F. Lefeuvre**, **M. Parrot**, **and R. Talhi**
C.N.R.S (National Center for Scientific Research), Orleans, France

Abstract— The paper is related to a statistic performed with the electrostatic turbulence observed by the micro-satellite DEMETER (Detection of Electro Magnetic Emissions Transmitted from Earthquake Regions) in the ionosphere.

Electrostatic (ES) turbulence at mid-latitudes and in the equatorial region of the ionosphere has been studied with the help of satellite, sounding rocket, and coherent scatter radar observations. It is known that electron density irregularities (Equatorial spread-F), equatorial density anomalies (each side of the magnetic equator) and plasma bubbles occur in these regions.

The study is done to check if the seismic activity can influence the turbulence. Following previous works from Molchanov et al. [2–5] and Hobara et al. [1], data bases dedicated to the systematic analysis of the power and spectral indices of the electric field have been elaborated.

DEMETER is the first scientific micro-satellite which was launched by CNES in June 2004 with a payload under the responsibility of LPCE. DEMETER measures the electric field and the magnetic field in the ionosphere in diverse bands of frequency (6 components of the electromagnetic field to investigate from DC up to 3.5 MHz), as well as the characteristic plasma parameters (ion composition, electron density and temperature, energetic particles) at the satellite altitude. DEMETER is low-altitude satellite (710 km) with a polar and circular orbit which measures electromagnetic waves all around the Earth except in the auroral zones (invariant latitude $> 65°$). Data are recorded at two different local times (around 10.00 and 22.00 LT). The main object of this micro-satellite is to study the ionospheric perturbations related with the seismic activity.

In this work, two data bases are considered: one for the survey mode and the other for the burst mode. For the survey mode, estimations of the turbulence parameters are performed from the 8 first Fourier components of the averaged power spectra (0–150 Hz frequency band). A single slope power law model ($f^{-\alpha}$) is assumed. A quality factor allows to test that hypothesis. For the burst mode, the power spectra are derived from the waveforms.

The study of the electrostatic turbulence by the DEMETER data was done as function of two characteristic parameters: the power density and the slope of the spectrum of the electric field until a hundred Hz. This study was done in all the zones covered by the satellite and particularly in the zones of mi-latitude and in the equatorial region. The following works have been done:

- creation of a data base for the statistics work,
- study of electrostatic turbulence as function of geophysical parameters,
- study of electrostatic turbulence as function of seismic activity,

This paper is principally related to the statistics study of electrostatic turbulence as function of seismic activity. The processing involves sixteen months (from August 2004 until December 2005, only spurious data and data recorded during high magnetic activity (the irregular disturbances of the geomagnetic field caused by solar particle radiation: $K_p > 7$) have been removed) of data and more than 2000 earthquakes of magnitude larger than 4.8. The data base is organised as function of the universal time, the local time, and the geographic latitude and longitude. In order to know the geographic variations of the two parameters which characterize the ES turbulence, geographic maps (see Figure) have been plotted by averaging data in bins of 2.5° in latitude and 5° in longitude.

The statistics results are shown with a superposed epoch method. Two methods are used: the ratio between the values of the parameters measured along an orbit which is close to an earthquake epicentre and the reference values of the maps obtained at the same location in the same conditions; the normalized cumulative probability of the parameters measured comparing with the histograms. The method of superposed-epoch is used to represent all these ratios and normalized cumulative probability. All earthquakes occur at the time zero and the time scale has been chosen from 3 days before the time of the earthquakes until 1 day after the shock with a resolution of 2 hours. The results are presented as function of the distance between the projection of the satellite orbit on the Earth's surface and the epicentres (maximum = 2000 km, resolution = 200 km). At the end, all ratios and all normalized cumulative probability in a given cell have

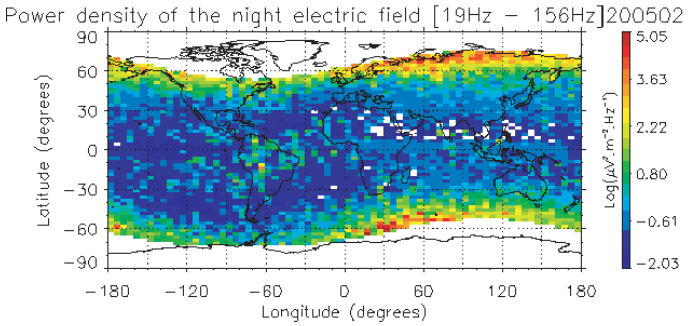

Figure 1: Geographical map of the power density of the ES turbulence during night time in February 2005.

been averaged. A comparison is done between the results obtained with the earthquake data set and a random data set.

In this study we have shown that: the electrostatic turbulence could vary as function of seismic activity, there is an influence of the seismic activity on the ES turbulence at an altitude of 700 km both before and after the earthquakes. The perturbations are observed until 2 days before the earthquakes. The perturbations are real but they are weak and only statistically revealed (in average the power density increases at the maximum by a factor of 2, the average change of the slope is at the maximum equal to 20%). Up to now nothing can be said about the possibility to predict earthquakes with the analysis of the ES turbulence.

REFERENCES

1. Hobara, Y., F. Lefeuvre, M. Parrot, and O. A. Molchanov, "Low-latitude ionospheric turbulence observed by Aureol-3 satellite," *Annales Geophysicae*, Vol. 23, 1259–1270, 2005.
2. Molchanov, O. A., M. Hayakawa, V. V. Afonin, O. A. Akentieva, and E. A. Mareev, "Possible influence of seismicity by gravity waves on ionospheric equatorial anomaly from data of IK-24 satellite 1. Search for idea of seismo-ionosphere coupling," *Seismo Electromagnetics: Lithosphere-Atmosphere-Ionosphere Coupling*, 275–285, edited by: Hayakawa, M. and Molchanov, O. A., Terrapub, Tokyo, 2002.
3. Molchanov, O. A., M. Hayakawa, V. V. Afonin, O. A. Akentieva, E. A. Mareev, and V. Yu. Trakhtengerts, "Possible influence of seismicity by gravity waves on ionospheric equatorial anomaly from data of IK-24 satellite 2. Equatorial anomaly and small-scale ionospheric turbulence," edited by: Hayakawa, M. and Molchanov, O. A., *Seismo-Electromagnetics (Lithosphere-Atmosphere-Ionosphere Coupling)*, 287–296, Terrapub, 2002.
4. Molchanov, O. A., "On the origin of low- and middle-latitude ionospheric turbulence," *Physics and Chemistry of the Earth*, Vol. 29, 559–567, 2004.
5. Molchanov, O. A., O. S. Akentieva, V. V. Afonin, E. A. Mareev, and E. Fedorov, "Plasma density-electric field turbulence in the low-latitude ionosphere from the observation on satellites; possible connection with seismicity," *Physics and Chemistry of the Earth*, Vol. 29, 569–577, 2004.

Session 2A3b
Power Electronics

Optimizing of System Partition and Software Architecture of Distributed Control Computer of Power Electronics Facility

J. Zdenek

Faculty of Electrical Engineering, Czech Technical University in Prague
Technicka 2, 166 27 Prague 6, Czech Republic

Abstract— The principles and methodology of system and software architecture design of the distributed network control computer (DNCC) of a mid-range complexity power electronics facility are presented. The system design is based on such criteria as functionality, reliability and maintainability. To reach these properties special emphasis is placed on correct and optimal system functions partition among distributed computer nodes to be minimized the overall communication overhead and on minimizing the hardware parts of the system by moving maximum of facility user and system functions into the software. As an examples of such design task the DNCC structure of two implemented power systems is introduced. These are the scientific high temperature material processing equipment for research in space orbital station and the electric locomotive.

EMI in Induction Motor Drive Fed from IGCT Voltage Source Inverter

S. Bartoš[1], **V. Jehlička**[1], **J. Škramlík**[1], **and V. Valouch**[2]

[1]Institute of Thermomechanics, Department of Electrical Machines, Drives, and Power Electronics
Academy of Sciences of the Czech Republic, Prague, Czech Republic
[2]Department of Electrical Drives and Traction, Faculty of Electrical Engineering
CTU Prague, Czech Republic

Abstract— The paper summarizes the experience acquired during laboratory experimental operation of an IGCT inverter feeding a 3-phase induction machine (IM) as well as practical knowledge gained from the employment of the IGCT switching devices in vehicles of city mass transportation. Among others, overvoltage phenomena occurring between the inverter and the IM, the influence of the feeding cables, and the causes of electromagnetic interference (EMI) were traced.

PWM Strategy Applied to Realized Matrix Converter System

J. Lettl and S. Fligl

Department of Electric Drives and Traction, Faculty of Electrical Engineering
Czech Technical University in Prague, Czech Republic

Abstract— The presented paper deals with the realized matrix converter induction motor drive with emphasis on the PWM strategy design. Sophisticated pulse width modulation strategies in terms of various optimization criteria are known in case of indirect frequency converters, whereas both the inverter and the rectifier can be operated with pulse width modulation. The instantaneous states of both the output and the input converter waveforms depend at any time on the switch state of the converter power switches. Suitable switch states sequence of the nine matrix converter switches can be indirectly derived from the given switch states sequence of the twelve switchers of the indirect frequency converter. However, the main goal is to achieve the maximal possible output voltage by overmodulation employment. The special digital control system consisting of two personal computers was designed. The first PC serves for monitoring purposes only, the second one is equipped with a common interface card and works in real time.

Technological Aspects of Noise-suppressing Filter Design

K. Künzel and V. Papež
Czech Technical University in Prague, Czech Republic

Abstract— The noise suppression is up to date problem of power electronic devices like power sources, power converters etc. Paper deals with suppression of conducted disturbances. Main topic is filter design and it's assembling from real devices with theirs real characteristics. Filter topology and device wiring are very important too. Paper calls attention to selected questions and proposes their solution.

Testing of Robust Control Characteristics for Traction PMSM

O. Černý, J. Šimánek, R. Doleček, and J. Novák

University of Pardubice, The Czech Republic

Abstract— The paper deals with our research in the field of control of drive with permanent magnet synchronous motor (PMSM), particularly verification of control characteristics. We focus to development the robust control algorithm for direct drive PMSM. We have designed and simulated an algorithm of phase current control.

Session 2A4
Remote Sensing & Scattering

Electromagnetic Wave Scattering from a Random Layer with Randomly Rough Interfaces

Gerard Berginc[1] and Claude Bourrely[2]

[1]Thales Optronique, rue Guynemer, BP 55, 78233 Guyancourt Cedex, France
[2]Centre de Physique Theorique, CNRS-Luminy Case 907, 13288 Marseille Cedex 9, France

Abstract— Volume and surface scattering is a topic which has been studied in different domains such as radio-physics, geophysical remote sensing, plasmonics and surface optics. But few works deal with the scattering of electromagnetic waves when volume and surfaces of the slab are described by random processes. In this paper, we consider a rough inhomogeneous slab.

By using Green functions, we have obtained an integral equation, called the Bethe-Salpeter equation, on the intensity inside the slab. By applying the Wigner transform to this equation and by considering the ladder approximation, we obtained the integral formulation of the radiative transfer theory.

The main goal of this paper is to introduce the boundaries in the derivation of the radiative transfer equation. We have shown that this can be done by replacing the Green function for an infinite medium, which describes the propagation between two scattering events for particles inside the medium, with the Green functions taking into account the wave diffusion by the boundaries. Furthermore, we were able to incorporate the correlations between the scatterers by multiplying the scattering operator of one particle, which appears in the radiative transfer equation, by a structure factor which is identical to the factor describing the scattering of X-rays by crystals. Finally, we can take into account the enhanced backscattering phenomenon by integrating the "most-crossed" contributions in our theory.

In our paper, we calculate the incoherent bistatic cross-sections up to the approximation of order 2. We are interested in two phenomena of coherence which can appear for slightly dense media. The first is the coherent retro-diffusion which we highlight by calculating the "most-crossed" double diffusion term. We calculate this term for diffusers placed in a general dielectric substrate. This point deserves to be noted because it illustrates the great generality of the obtained equations which allow us to calculate the intensity diffused for a great number of cases. We then study another phenomenon of coherence in the random media which is only due to the process of single diffusion in a dielectric substrate bounded with interfaces. Some numerical examples are given in this paper.

A Hybrid Analytical-numerical Algorithm of Scattering from a 3D Target above Randomly Rough Dielectric Surface

Ya-Qiu Jin and Hongxia Ye
Key Laboratory of Wave Scattering and Remote Sensing Information (MOE)
Fudan University, Shanghai 200433, China

Abstract— Electromagnetic scattering from the target above or beneath a rough surface has attracted much interest during recent years because of extensive applications to radar surveillance, target identification, GPR (ground-penetration radar) probing, and so on. The studies on scattering from volumetric target (as a deterministic scatter) and from environmental background, e.g., land surface (as distributed scatters) were usually separated in different research groups. However, identification of the target from complicated background needs fully understanding of interactions between the target and background.

Most of numerical studies for scattering from the composite model of target and underlying rough surface are based on 2D model, such as general forward backward method with spectrum accelerate algorithm (GFBM/SAA), finite element method and domain decomposition method (FEM-DDM) etc. A 3D model of a target above a flat (smooth) surface was studied using the specular image and multilevel fast multipole algorithm (MLFMA). Interaction between a slender cylinder and a slightly rough surface was also studied using the reciprocity theorem and stationary phase method under some approximation restrictions.

To find the difference scattering due to the target presence above rough surface, a 2D model was studied. It has been found that scattering due to surface contribution took most of computation time. To resolve this difficulty, a hybrid algorithm to apply analytic Kirchhoff approximation (KA) to rough surface and numerical MoM (method of moment) to the target is developed.

In this paper, the aforementioned KA-MoM is generalized to the 3D model. Firstly, the coupling integral equations for difference scattering from a non-regular conducting target above randomly rough dielectric surface model are derived. Then, MoM with Conjugate Gradient (CG) approach is employed to solving the target's IE, and KA is applied to rough surface scattering. Coupling iterations take account the target-surface interactions. Since only one integral is operated for rough surface scattering with KA, much memory and computation time is reduced. Convergence and error analysis are also discussed. Some examples of bistatic difference scattering are presented and discussed.

Propagation-Inside-Layer Expansion Method for Scattering by a Stack of Two Rough Surfaces: Acceleration with the Forward-backward Method Combined to the Novel Spectral Acceleration

Nicolas Déchamps and Christophe Bourlier

Radar Team, IREENA Laboratory, Polytech'Nantes
Rue Christian Pauc, La Chantrerie, BP 50609, 44306 Nantes Cedex 3, France

Abstract— The modeling of the electromagnetic scattering from a stack of two rough surfaces is investigated by using the recent PILE (Propagation-Inside-Layer Expansion) method of Déchamps et al. [1] combined to the Forward-Backward Novel Spectral Acceleration (FBNSA) method developed for a single interface, of Chou and Johnson [2–5]. The method is valid for configurations such as mono-dimensional surfaces separating homogeneous media. In this case the integral equations of the system can be cast into to $\overline{\overline{Z}}\,\overline{X} = \overline{X}^{inc}$ where $\overline{\overline{Z}} = \begin{bmatrix} \overline{\overline{Z}}^{A} & \overline{\overline{C}}^{B\to A} \\ \overline{\overline{C}}^{A\to B} & \overline{\overline{Z}}^{B} \end{bmatrix}$ is the impedance matrix [1].

PILE method is based on the following expansion of the field X on the upper surface:

$$\overline{X} = \sum_{k=0}^{P} \overline{\overline{M}}^{k} \left(\overline{\overline{Z}}^{A}\right)^{-1} \overline{X}^{inc}, \tag{1}$$

where $\overline{X}^{inc}$ is the incident field on the upper surface and $\overline{\overline{M}} = \left(\overline{\overline{Z}}^{A}\right)^{-1} \overline{\overline{C}}^{B\to A} \left(\overline{\overline{Z}}^{B}\right)^{-1} \overline{\overline{C}}^{A\to B}$ is the characteristic matrix of the layer. The physical interpretation of the method is shown in Fig. 1. This expansion converges to the exact solution if the spectral radius of $\overline{\overline{M}}$ is less than 1 [1].

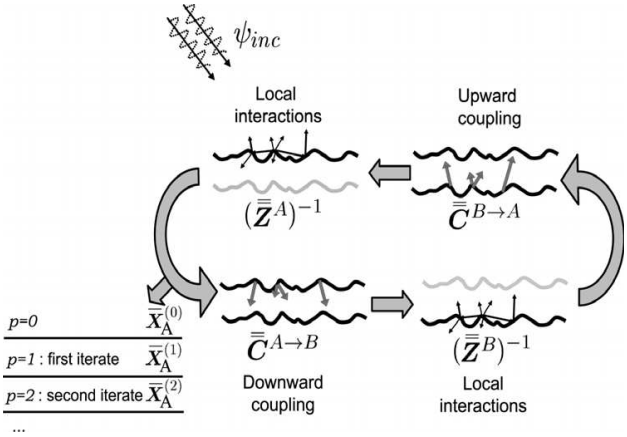

Figure 1: Scheme of PILE method.

When applying iteration (1), fast efficient methods valid for single rough surfaces can be applied to speed up the inversions $\left(\overline{\overline{Z}}^{A}\right)^{-1}$ and $\left(\overline{\overline{Z}}^{B}\right)^{-1}$. In this paper, the FBNSA is applied. The products involving, $\left(\overline{\overline{C}}^{A\to B}\right)$ and $\left(\overline{\overline{C}}^{B\to A}\right)$, the coupling matrices, is also accelerated, using the NSA. The PILEFBNSA method reaches then a complexity of $O(N)$, where N is the number of samples per interface.

Graphs showing the convergence of the PILE-FBNSA method versus different parameters will be presented; furthermore, the method will be compared to the FBNSA method specially developed for a layer by Moss et al. [6].

REFERENCES

1. Déchamps, N., C. Bourlier, N. de Beaucoudrey, and S. Toutain, "A fast numerical method for electromagnetic scattering by rough layered interfaces: Propagation-Inside-Layer Expansion (PILE) method," *JOSA A*, Vol. 23, No. 2, 359–369, 2006.
2. Chou, H.-T. and J. T. Johnson, "A novel acceleration algorithm for the computation of scattering from rough surfaces with the Forward-Backward method," *Radio Science*, Vol. 33, 1277–1287, 1998.
3. Chou, H.-T. and J. T. Johnson, "Formulation of forward-backward method using novel spectral acceleration for the modeling of scattering from impedance rough surfaces," *TGRS*, Vol. 38, No. 1, 605–607, 2000.
4. Torrungrueng, D. and J. T. Johnson, "Some issues related to the novel spectral acceleration method for the fast computation of radiation/scattering from one-dimensional extremely large scale quasi-planar structures," *Radio Science*, Vol. 37, No. 2, 2002.
5. Iodice, A., "Forward-Backward method for scattering from dielectric rough surfaces," *IEEE TAP*, Vol. 50, No. 7, 901–911, 2002.
6. Moss, C. D., T. M . Grzegorczyk, H. C. Han, and J. A. Kong, "Forward-Backward method with spectral acceleration for scattering from layered rough surfaces," *EEE TAP*, Vol. 54, No. 10, 2917–2929, 2006.

An Effective Method for the Scattering of Electromagnetic Waves by Periodic Rough Surfaces

Selda Yıdız, Yasemin Altuncu, and Funda Akleman

Electrical and Electronics Engineering Faculty, Istanbul Technical University
Maslak 34469, Istanbul, Turkey

Abstract— Scattering of electromagnetic waves from rough surfaces is of importance from both theoretical and practical points of view. One of the main applications of such problems is the ground wave propagation modeling of the electromagnetic waves. Although several methods have been developed for the solution of such kind of problems it still needs to be treated with effective methods. For the periodic surfaces having a slow variation one can obtain the solution under the Rayleigh hypothesis in terms of Floquet modes. On the other hand, for surfaces which does not satisfy the Rayleigh condition it is required to develop new methodologies.

The main objective of this work is to extend the method given in [3] to the scattering problems connected with the periodic rough surfaces between two dielectric media. The basic idea here is to consider the irregularities of the rough surface as buried objects in a two half-spaces medium with planar interface, which allows one to formulate the problem as a scattering problem related to periodically buried cylindrical bodies of arbitrary cross sections. Through the periodic Green's function of two half spaces media with planar interface, the problem is reduced to the solution of a Fredholm integral equation of second kind which can be treated by using one of the known techniques. In this work, we solved the integral equation via an application of Method of Moments (MoM) by reducing it to a linear system of equations. Since the Periodic Green's function can be obtained in terms of Floquet modes, the computational cost of the method is very low. Such an approach can also be used for the non-periodic locally rough surfaces. In such a case one takes a sufficiently large region which contains the rough surface and assumes that this structure is repeated periodically with a period that is equal to length of the region, which allows us to formulate the problem as a scattering from periodic rough surfaces. The method permits us to obtain both the near and far field expressions of the scattered wave. It is compared with existing methods and observed that it yields quite good results.

REFERENCES

1. Hastings, F. D., J. B. Schneider, and S. L. Broschat, "A Monte-Carlo FDTD technique for rough surface scattering," *IEEE Trans. on Anten. and Prop.*, Vol. 43, No. 11, 1183–1191, 1995.
2. Demir, M. A. and J. T. Johnson, "Fourth-and higher-order small-perturbation solution for scattering from dielectric rough surfaces," *Journal of the Optical Society of America A-optics Image Science and Vision*, Vol. 20, No. 12, 2330–2337, 2003.
3. Altuncu, Y., A. Yapar, and I. Akduman, "On the scattering of electromagnetic waves by bodies buried in a half-space with locally rough interface," *IEEE Trans.on Geoscience and Remote Sensing*, Vol. 44, No. 6, 1435–1443, 2006.

High Resolution Multispectral Photogrammetric Imagery: Enhancement, Interpretation and Evaluations

Arthur Roberts, **Charles Bostater**, **and Thomas Becker**

Department of Geography, Simon Fraser University, Burnaby, BC V5A 1S6, Canada

Abstract— A variety of aerial mapping cameras were adapted and developed into simulated multiband digital photogrammetric mapping systems. Two multiband cameras (IIS 4 band and Itek 9 band) and 3 pairs of mapping and reconnaissance cameras were evaluated for digital spectral performance and photogrammetric mapping accuracy in an intertidal environment.

Aerial films (24 cm × 24 cm format) tested were: Agfa color negative and extended red (visible and near infrared) panchromatic, and Kodak color infrared and B&W (visible and near infrared) infrared. All films were negative processed to published standards and digitally converted at either 16 (color) or 10 (B&W) microns. Excellent precision in the digital conversions was obtained with scanning errors of less than one micron. Radiometric data conversion was undertaken using linear density conversion and centered 8 bit histogram exposure. This resulted in multiple 8 bit spectral image bands that were unaltered (not radiometrically enhanced) "optical count" conversions of film density. This provided the best film density conversion to a digital product while retaining the original film density characteristics.

A series of underwater geometric line targets were imaged across a 3.5 meter tidal range for shell sand, eelgrass and sandstone benthic environments. Imagery varied from completely exposed targets (very low tide) to greater than 3 meters depth for all targets. Spectral and photogrammetric evaluations were undertaken for substrate and bathymetry determinations (spectral) and target spatial accuracy, stereoscopic depth evaluations and capillary and gravity wave line target distortions.

Results indicate that multispectral photogrammetric systems offer improved intertidal feature mapping capability.

Computation of the Polarimetric Bistatic Signature of Trihedral Corner Reflector Arrays in High-frequency Domain

G. Kubické, C. Bourlier, and J. Saillard
IREENA, Université de Nantes, Polytech'Nantes, Rue Christian Pauc
La Chantrerie, BP 50609, 44306 Nantes Cedex 3, France

Abstract— In this paper, the polarimetric bistatic signature of Trihedral Corner Reflector (TCR) arrays is considered. These arrays are supposed to be embedded in absorbing material, as example in Figs. 1 and 2, and composed of several TCRs which correspond rigorously to faceted trirectangular tetrahedrons. These elementary reflectors, shown in Fig. 3, are formed by three isosceles right triangular faces mutually orthogonal. Corner reflector is a very interesting radar target because it exhibits a large bistatic and monostatic Radar Cross Section (RCS) over a wide angular range. Thus, a TCR array can still increase the RCS and could be more interesting for some applications using reference radar target as calibration of Synthetic Aperture Radar (SAR) images [1] for example, and for radar test target as for missile seeker test.

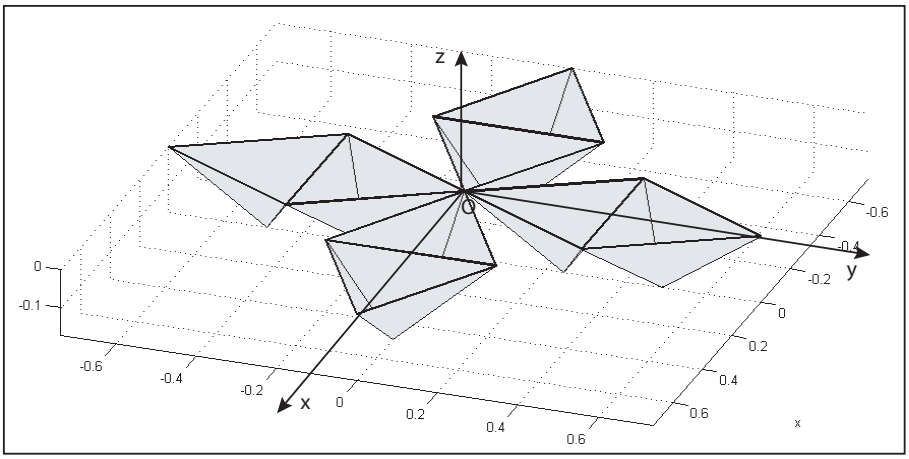

Figure 1: Example of TCR array composed by 8 TCRs (2 by branches) — Perspective view.

The elementary reflectors, present in the array, were studied in a restricted domain [2, 3], for which the TCR is excited and observed in the interior region. This corresponds, as shown in

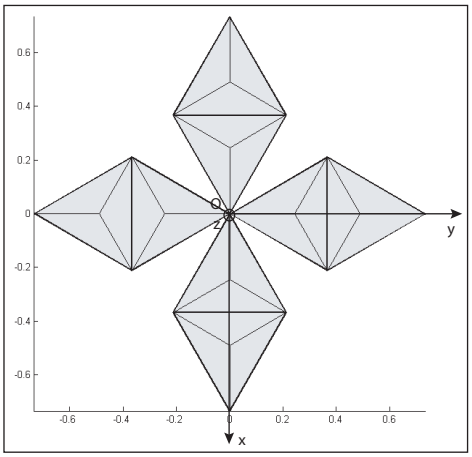

Figure 2: Example of TCR array composed by 8 TCRs (2 by branches) — View from above.

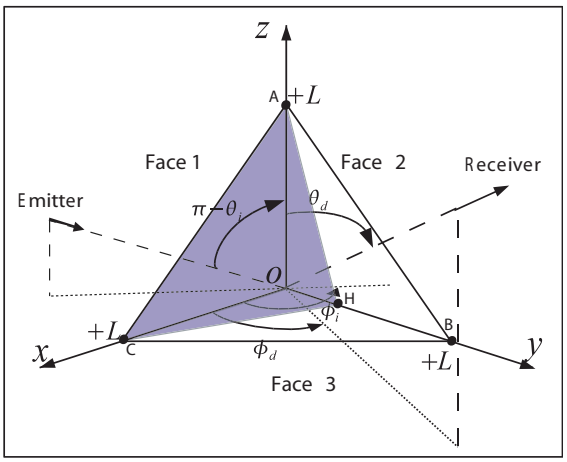

Figure 3: Illustration of the shadowed area in excitation (FSA convention).

Fig. 3, to elevation angles $\{\pi - \theta_i; \theta_d\}$ and azimuth angles $\{\phi_i + \pi, \phi_d\}$ defined with respect to the transmitter and the receiver, respectively, and ranging from 0 to $\frac{\pi}{2}$ radians. However, TCRs in the array can be illuminated and/or observed laterally and thus the shadowing effect must be included. Consequently, the computation of the bistatic signature of TCR arrays, in high-frequency domain, has never been studied until now.

In this paper, the authors present the computation of the bistatic signature of TCR arrays, obtained from coherent summations of the Sinclair matrix of each TCR expressed in the global system of coordinates. The TCR is evaluated for any excitation and observation angles, by taking into account shadowing effect with the help of Geometrical Optics (GO) approximation. Fig. 3 gives an axemple of shadowing effect in excitation. The Physical Optics (PO) approximation is used to evaluate the bistatic signature for single reflections and for the last reflection of double and triple reflections. GO is also used for the first, and the first two reflections of double and triple reflections, respectively. The first-order edge diffraction contribution is evaluated by using the Method of Equivalent Currents (MEC) [4].

In the final paper, the method will be explained in more details, several TCR arrays will be studied, and results will be discussed, by evaluating the statistical approach.

REFERENCES

1. Van Zyl, J. J., "Calibration of polarimetric radar images using only image parameters and trihedral corner reflectors responses," *IEEE Trans. Geos. Rem. Sens.*, Vol. 28, No. 3, 337–348, 1990.
2. Corona, P., G. Ferrara, C. Gennarelli, and G. Riccio, "A physical optics solution for the backscattering by triangularly shaped trihedral corners," *Ann. Télécom.*, No. 5–6, 557–562, 1995.
3. Polycarpou, A. C., C. A. Balanis, and C. R. Birtcher, "Radar cross section of trihedral corner reflectors using PO and MEC," *Ann. Télécom.*, No. 5–6, 510–516, 1995.
4. Knott, E. F., "The relationship between Mitzner's ILDC and Michaeli's equivalent currents," *IEEE Trans. Ant. Prop.*, Vol. 33, No. 1, 112–114, 1985.

A Hybrid Method for the Scattering of Electromagnetic Waves from Coatings of Variable Thickness

Birol Aslanyürek[1], **Mehmet Çayören**[2], **Hülya Şahintürk**[1]

[1]Mathematical Engineering Department, Yıldız Technical University
34210 Davutpasa, Istanbul, Turkey
[2]Electrical and Electronics Engineering Faculty, Istanbul Technical University
34469 Maslak, Istanbul, Turkey

Abstract— Scattering problems related to coatings located on a perfectly conducting objects are of importance due to their potential applications of antenna design. The results of such studies can be used to determine the dielectric coatings to obtain a desired antenna radiation pattern. Although there are a number of methods for coatings with simple geometries in literature, limited number of works exist for coatings with variable thickness [1–3]. While the scattering problems related to homogeneous and simple shaped such as spherical and elliptical coatings can be solved analytically, this is not possible for arbitrary varying coatings. In such a case, one has to apply a hybrid or numerical methods such as Method of Moments.

In this paper we present a hybrid method for the scattering of electromagnetic waves by a coating of arbitrary shape located on a perfectly conducting object. For the sake of simplicity we consider coatings located on perfectly conducting circular cylinders which leads to reduce the problem to a 2D scalar one. The method presented here is based on separating the whole region outside the perfectly conducting cylinder into four parts by two fictitious circles which are located inside and outside the coating. Then the scattered field in the regions between the circles are expanded into Taylor series while in the other regions it is represented by series in terms of Bessel and Hankel functions. The use of the boundary conditions reduces the problem to the solution of a liner system. The method is simple and easy to apply for even coatings which are large in size. The numerical implementations show that the method is very effective and accurate for coatings having a large dielectric coefficient. For the large scale coatings the number of unknowns in the proposed method is much more less than those in the Method of Moments as a result the new method produces results much faster.

REFERENCES

1. Tanyer, S. G. and R. G. ve Olsen, "High-frequency scattering by a conducting circular cylinder coated with a lossy dielectric of nonuniform thickness," *IEEE Transactions on Antennas and Propagation*, Vol. 45, No. 4, 689–697, 1997.
2. Sebak, A. R., "Scattering from dielectric-coated impedance elliptic cylinder," *IEEE Transactions on Antennas and Propagation*, Vol. 48, No. 10, 1574–1580, 2000.
3. Strifors, H. C. and G. C. ve Gaunaurd, "Scattering of electromagnetic waves by a perfectly conducting cylinder with a thin lossy magnetic coating," *IEEE Transactions on Antennas and Propagation*, Vol. 48, No. 10, 1528–1532, 2000.

Monitoring of Satellite Thermal Basin in a Slope of Mountain Range

S. Nakamura

Kyoto University, Japan

Abstract— This work concerns to a problem of a satellite thermal basin in a slope of mountain range. First, a model is introduced in a simple geometrical model for a basin in a slope of mountain range. It is necessary to consider a combined effect of several factors which are infrared radiation out of a slope of mountain range as an assumed black body. The infrared radiation transfers its energy as a form of radiated beam normal to the surface of the model basin. When the beam out of the basin concentrats just neighbor the thermal sensor mounted on a satellite with a polar orbit, the thermal pattern covering the area of the interested basin shows an unexpected abnormal high temperature.

This abnormal high temperature is a result of monitoring the thermal pattern on the land and the ocean. As for the problems on the ocean, the author has had reported and noted by this time. These apparently abnormal thermal patterns must have been taken not to be obtained under a correct operational condition, though the author has found that such the thermal pattern has been monitored under the normal operation for the direct receiving of the satellite signal at the station settled on the land just neighbor the ocean.

For this problem, it is considered to be effective at understanding a thermal patch of a high temperature in a basin in a slope of mountain range on land. Then, an application of the physical criteria for radiation could be introduced for the considering problem. That is, an application of Kirchhoff's law. Plack's radiation law tells us that the intensity of radiation out of the surface of the black body in a unit time is related well to the factors, i.e., Planck's constant $h = 6.55 \times 10^{-27}$ ergsec, propagation speed of electromagnetic ray c as 3×10^{10} cm/sec, Boltzmann's constant $k = 1.37 \times 10^{-16}$ erg/deg, and the absolute temperature T of the interested material of the black body. Considering the total radiation intensity which is an integral of Planck's radiation formula for wave length of the beam. With this, the interested problem can be solved by Stefan-Boltzmann's law. Stefan-Boltzmann's law for what the author interested in is expressed, in this case, as $\mathbf{B} = \sigma \mathrm{T}^4$ (where, the numeral σ is 5.70×10^{-5} erg/cm^2/sec/deg).

Then, the total radiation flux in the author's interest is proportional to T^4. Then, we have a relation $\mathrm{d}\mathbf{B}/\mathbf{B} = \mathrm{dT}/\mathrm{T}$. This relation is independent of the wave length of the beam.

When dt = 40K and T = 273K, dT/T = 0.416. Then, $\mathrm{d}\mathbf{B}/\mathbf{B} = 0.584$. This means that the beam out of the interested basin concentrated at the rate of 0.584 at one of the pixels in the directly monitored satellite thermal sea surface pattern.

This thermal anomary of 40K had been supported by the practical satellite monitoring of the thermal pattern covering a basin in a slope of mountain range, when the author has directly monitored the earth's surface to find what noted first under a normal operation.

Automated Passive Ground Remote Surveillance of Critical Oil & Gas Transport Infrastructures

F. Kaspareck and E. Poggiagliolmi
Entec Integrated Tech., UK

Abstract— Gas transport presents less risk to disruption when compared to oil transport. In case of accident, oil flow can be restored quickly and represents a limited loss, unlike gas that is normally linked to contracted quantities. Any gas interruption affects downstream and consumer supply, whereas any incident on a crude or product line carries a high environmental risk and associated remedial costs.

Pipelines are more vulnerable than what assessed and perceived at present. This is confirmed by the extremely high number of IT attacks on pipeline operating systems, but also by recent accidents caused by assaults in remote areas. Threats mostly affect operational systems but in other cases they imply physical and mechanical damage to the pipeline. Most hydrocarbon transport infrastructures are not equipped with physical perimeter security because threats are not apparent and there are opex and construction capex limitations with respect to available technology. Automated perimeter surveillance, when in place, is carried out by satellite with limitations of resolution and logistics, besides involving high costs for image processing and interpretation.

This paper introduces a new, reliable, fully automated and cost effective pipeline passive surveillance system that, when installed and interfaced with the pipeline operational system, can virtually eliminate the risk of physical perimeter intrusions. Intrusion detection is achieved by means of a large number of sensors deployed on or below the ground surface. The transmitted sensors signals are analyzed in pseudo real time by means of neural nets and pattern recognition algorithms. Adaptable beam forming transforms are utilised in real time processing and analysis to output type of intrusion, position, azimuth and approaching speed with reference to the infrastructure. The results can be automatically correlated to a signature database for automated alarm triggering decision and, or displayed on monitor screens. In case of noisy background, pattern recognition techniques are also employed to isolate the signal. The system works in hibernation mode until it detects a meaningful signal. The system can be ported also to offshore and sub sea application and it is virtually effective on any type of terrain.

Other advantages of this method are that surveillance is carried out without high profile protections such as barbed wire and fences, the system is entirely unmanned, it is not visible from the air or from land, it is instrumentally undetectable and it draws electric power from photovoltaic solar panels.

Session 2AP
Poster Session 1

Time Reversal Telecommunication in a Reflective Environment

G. Collin, **J. de Rosny**, **G. Lerosey**, **A. Tourin**, **and M. Fink**
Laboratoire Ondes et Acoustique, E.S.P.C.I., Universite Paris 7
C.N.R.S, UMR 7587, 10 rue Vauquelin, 75005 Paris, France

Abstract— The aim of this article is to prove inter-symbol-interference reduction by using the time reversal technique in a telecommunications system.

Introduction: In a reflective environment, the radiofrequency signal shows many distortions. One of them is temporal spreading of symbols due to the different arrival times of the multiple reflexions. If the spreading time is larger than the repetition time between symbols, one symbol interferes with its closest neighbours. These inter-symbol interferences (ISI) make extremely difficult the decoding of information. Here we show that the time reversal technique, thanks to pulse compression effect, can be solution to strongly decrease the ISI.

Time Reversal and Temporal Focusing: We have developed a time reversal wireless communication system at 2.45 GHz. Various modulations (4 QAM, 8 QAM and 16 QAM) can be tested. One symbol-frame contains 200 symbols. After demodulation, the symbols are plotted in I/Q constellations (see Fig. 1).

We observe that the symbol spreading in the I/Q diagram is much smaller with time-reversal technique. Hence, there is no error when the message in transmitted when time reversal is used.

A complete study of the error rate with respect to several parameters such as data rate, symbol length, time-spreading have been carried out. These results are compared to simple theoretical models.

Conclusion: The application of the time reversal can be seen as a pre-processing step implemented in the emitter to decrease the ISI in a strong reflective environment. As for the receiver, it remains the same. Hence implementation of time reversal can be a good solution to increase the data rate in reflective environment without modifying the receiver.

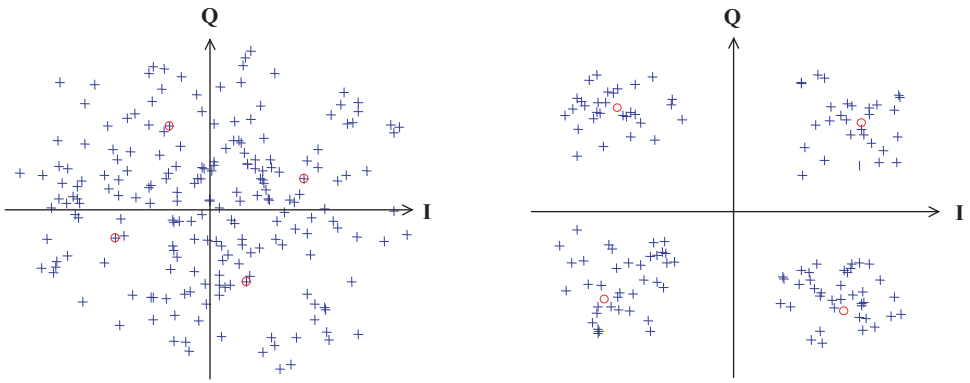

Figure 1: Two I/Q constellations. (a) [respect. (b)] is obtained without [respect. with] time-reversal. The modulation is 4 QAM (4 state modulations, see the circles). A cross represents each transmitted symbol. The bit rate equals 37 Mbits/s. With time reversal, the error rate is 0% while it reaches 33.3% without Time Reversal.

Comparative Analysis of WLAN, WiMAX and UMTS Technologies

Aktül Kavas

Department of Electronics & Communication Engineering
Electrical and Electronics Faculty, Yıldız Technical University
Beşiktaş 34349, Istanbul, Turkey

Abstract— Wireless broadband technologies promise to make all kinds of information available anywhere, anytime, at a low cost, to a large portion of population. From the end user perspective the new technologies provide the necessary means to make life more convenient by creating differentiated and personalized services. In the last decade we were primarily used to accessing people via voice, but there are of course other forms of communication like gestures, facial expressions, images and even moving pictures. Today we increasingly need user devices wireless for mobility and flexibility with total coverage on small light and affordable terminals then ever.

Evolving of circuit switched networks towards packet switched technology high data rates is acquired and this evolution has opened new opportunities. 2.5 and 3G networks provide high mobility for the packet domain users. The commercial UMTS networks defined by 3GPP are launched by major telecom operators. Communication over UMTS networks provides broadband voice, data and video traffic to mobile users.

On the other hand the development of the technology has opened new era like WLAN, WiMAX and HSDPA communication. Therefore the merging IP based services provide broadband data access in fixed, mobile and nomadic environments supporting voice, video and data traffic with high speed, high capacity and low cost per bit.

At the moment the main question would be to find out whether these new emerging technologies are competitive or complementary technologies to UMTS.

In this study WLAN, WiMAX and UMTS technologies are introduced and comparative analysis in terms of peak data rate, bandwidth, multiple access techniques, mobility, coverage, standardization, market penetration is presented.

WiMAX Cell Planning and Coverage Prediction

Aktül Kavas
Electrical and Electronics Faculty, Yildiz Technical University
34349, Beşiktaş-İstanbul, Turkey

Abstract— The development of internet access and broadband multimedia services to residential users via wireless communication systems attracted an increasing interest of the service providers and the telecommunication industry. The emerging technology is WiMAX which is defined as Worldwide Interoperability Microwave Access, based on IEEE 802.16-2004 Air Interface Standard and is rapidly proving itself as a technology that will play a key role in fixed broadband wireless metropolitan area networks. Wimax broadband wireless solution enables convergence of mobile and fixed broadband networks through a common wide area broadband radio access technology and flexible network architecture. The scalable architecture, high data throughput and low cost deployment make WiMAX also a leading solution for wireless broadband services.

In areas without pre-existing physical cable or telephone networks, WiMAX will be a viable alternative for broadband access that has been economically unavailable.

The bandwidth and reach of WiMAX make it suitable for the following potential applications:

- Connecting Wi-Fi hotspots with each other and to other parts of the internet.
- Providing a wireless alternative to cable and DSL for last mile broadband access
- Providing high-speed mobile data and telecommunications services
- Providing a diverse source of internet connectivity as part of a business continuity plan. That is, if a business has a fixed and a wireless internet connection, especially from unrelated providers, they are unlikely to be affected by the same service outage.
- Providing nomadic connectivity.

The radio wave propagation model or path loss model plays a significant role in cell planning and coverage prediction of the wireless communication systems. The properties of base and the mobile station as well as communication channel propagation environment properties are required to calculate the radio coverage for chosen base station. Path loss models represent a set of mathematical equations and algorithms, which are applied for radio signal propagation prediction in certain propagation environment. Propagation algorithms can be classified in three basic groups

- empirical,
- semi-deterministic and
- deterministic.

In this study semi deterministic models are used for the allocated frequency bands for WiMAX systems. Calculations are realized for urban, suburban and rural areas for different terrain types. Analyzing the coverage of the WiMAX system in different propagation environment for selected frequencies is presented. Finally in conclusion some remarks on system capacity are given.

Research on Asymmetric Characteristics of Mobile Communications System Based on Electromagnetic Radiation

Weidong Wang, **Yinghai Zhang**, **Kaijie Zhou**, **and Heng Zhang**

Information & Electronics Technology Lab, Beijing University of Posts and Telecommunications
P. O. Box 116, Beijing 100876, China

Abstract— The influence on environment caused by electromagnetic radiation is always a controversial problem. With the large-scale application of mobile communications system, the total amount of electromagnetic radiation will increase and people will have to re-evaluate the social effect of mobile communications. The mobile terminal is a small transceiver, which is close to human body. The distance from mobile terminal to human body ranges from several centimeters to dozens of centimeters. Compared to that, the distance from base station to human body is longer, which ranges from dozens of meters to several kilometers. So the radiations caused by the mobile terminal and base station to human body are different.

This article discusses the asymmetric transmission characteristics of mobile communications system in view of the effects of electromagnetic radiation to human body. By calculation of human's Specific Absorption Rate (SAR) which is caused by uplink and downlink electromagnetic radiation, it shows that: under the restriction of electromagnetic radiation, the downlink rate is much higher than that of uplink, the ratio of downlink rate bound to uplink rate bound is up to 10^5. It is termed Electromagnetic Asymmetry (EA) between uplink and downlink, which must be taken into account in the future mobile communications system.

To protect people from electromagnetic radiation, the resource allocated to uplink must be restricted. According to Shannon Theory, it means that effective bandwidth of uplink should be narrower than that of downlink. So in TDD system, the number of uplink timeslot should be less than that of downlink timeslot. In FDD system, the uplink bandwidth should be narrower than downlink bandwidth. In present, it is well known that the data-service requirements also result in the asymmetric frequency or timeslot allocation between uplink and downlink, which is called as Service Asymmetry (SA). However, EA is different from SA. The ratio of downlink to uplink bandwidth caused by EA is 10^5, while the ratio caused by SA is less than 10^2. EA and SA will be both taken into account in future mobile system, but EA will has higher priority to SA.

An Analytical Approach for Improving the Quality Factor of RFIC Spiral Inductors

Hao-Hui Chen[1], **Huai-Wen Zhang**[2], **Hui-Ching Sung**[1], **Shyh-Jong Chung**[3], **and Jen-Tsai Kuo**[3]

[1]Department of Electronic Engineering, Huafan University, Taipei, Taiwan
[2]United Microelectronics Corporation (UMC), Hsinchu, Taiwan
[3]Department of Communication Engineering, National Chiao Tung University, Hsinchu, Taiwan

Abstract— With the rapid growth of the demand for low-power, low-cost, and high-integration wireless communication systems, the development of on-chip passive devices for radio frequency integrated circuits (RFICs) has emerged as a critical issue recently. Among the passive circuits, the on-chip spiral inductor is one of the key elements in various RFIC designs such as mixers, amplifiers, and oscillators. One important issue concerned in the design of a spiral inductor is the improvement of the quality factor (Q-factor). Since the Q-factor is primarily governed by the losses of the metal strip and substrate, much research has been devoted to improve the Q-factor by reducing the metal or substrate loss. One possible approach is the variable line width design reported in [1, 2]. As shown in Fig. 1, this technique modifies a conventional spiral inductor with fixed line width to be the one with the line width increasing from the inner to the outer turns. By narrowing the width of the inner coils, the losses due to the eddy-current on the metal strip, which is induced by the time-varying magnetic flux passing through the metal lines and is significant in the inner coils, can be alleviated. The metal loss is therefore reduced leading to the increase of the Q-factor. Although this technique is effective and can be easily implemented by standard IC fabrication technologies, it is generally difficult to find the proper line width of each metal coil. In this work, an analytical formula is developed to efficiently determine the line width in the variable line-width inductor design. Since this design increases the Q-factor by reducing the metal loss, which can characterized by an equivalent series resistance R_s, an analytical expression of the series resistance for a spiral inductor is first derived as $R_s = \sum_{n=1}^{N} R_{s,n} = \sum_{n=1}^{N} (R_{ohm,n} + R_{ed,n})$, where N is the number of turns and $R_{s,n}$ is the resistance of the n-th coil. Furthermore, $R_{s,n}$ can be decomposed into the ohmic resistance $R_{ohm,n}$ and the eddy-current resistance $R_{ed,n}$. With suitable field analyses, $R_{ohm,n}$ and $R_{ed,n}$, and thus $R_{s,n}$, can be written as functions of the line width (W_n) of the considered metal coil. By minimizing $R_{s,n}$, an analytical formula for determining the proper line width of the n-th coil is then formulated. With the obtained analytical formula, the variable line width design can be a very efficient and user-friendly method for improving the inductor performance. Several Si-based spiral inductors have been tested. The results and the detailed formulation will be presented and discussed in the symposium.

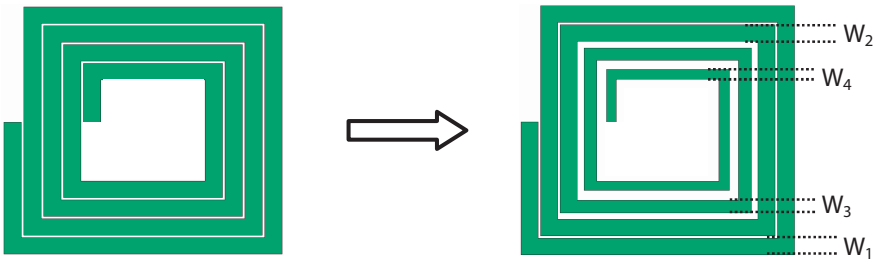

Figure 1: Modified inductor design for improving the Q-factor: (a) conventional inductor design, (b) variable line width design.

REFERENCES

1. Hsu, H.-M., "Improving the quality factor of a broadened spiral inductor with arithmetic-progression step width," *Microw. Opt. Tech. Lett.*, Vol. 45, 118–120, Apr. 2005.
2. Bahl, I. J., "Improved quality factor spiral inductors on GaAs substrates," *IEEE Microw. Guided Wave Lett.*, Vol. 9, 398–400, Oct. 1999.

Reflectarray with Variable-patch-and-slot Size

The Nan Chang and Bor-Tsong Chen
Tatung University, Taipei, Taiwan R. O. C.

Abstract— Reflectarray using a variable-patch-and-slot (VPS) size method is presented. A slot as a new variable is added to the original variable patch (VP) size configuration. The slot plays a role to modify the original phase diagram. In some cases, it optimizes both sensitivity and bandwidth of a reflectarray. Based on this observation, we designed a reflectarray on an FR4 substrate. Experimental results show a maximum gain of 24.5 dB at 11.4 GHz with an aperture size of 19.5 cm×25 cm. It has a 1.5 dB bandwidth of 19.3% and has an aperture efficiency of 31.48%. The cross-polarization level is bellow 25 dB.

Design of an UWB Antenna with Band-rejection Characteristic

H. J. Lee, Y. H. Jang, and J. H. Choi

Department of Electrical and Computer Engineering, Hanyang University
17 Haengdang-Dong, Seongdong-Gu, Seoul 133-791, Republic of Korea

Abstract— This paper proposes an ultra-wideband (UWB) antenna with band-rejection characteristic. By inserting a notch on the ground, extremely wide impedance bandwidth is obtained. However, band-rejection technique needs to employed to avoid the possible interference between UWB system and wireless local area network (WLAN) service since frequency band from 5.15 GHz to 5.825 GHz has been allocated for WLAN. Various band-rejection methods applicable to planar antenna structures have been reported recently. In this paper, the band-rejection performance is achieved by embedding the spur-lines on the ground. The geometrical configuration of the proposed antenna is illustrated in Fig. 1. As shown in Fig. 2, by controlling the length (L_S) of a pair of about quarter wavelength long spur-lines, the band-rejection performance can be obtained. Fig. 3 shows the simulated and measured VSWR characteristics of the proposed antenna. The designed antenna has a rejection band from 4.7 GHz to 5.9 GHz while maintaining the wide impedance bandwidth from 2 GHz to 10.6 GHz for VSWR less than 2.0. The proposed antenna also shows omnidirectional radiation patterns and has good gain flatness for the desired frequency band outside of the rejection band.

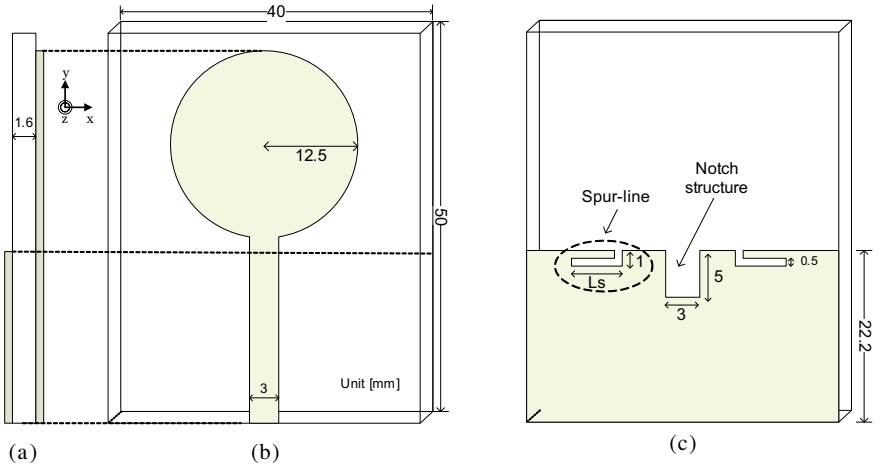

Figure 1: Geometry of proposed antenna, (a) side view, (b) top view, (c) bottom view.

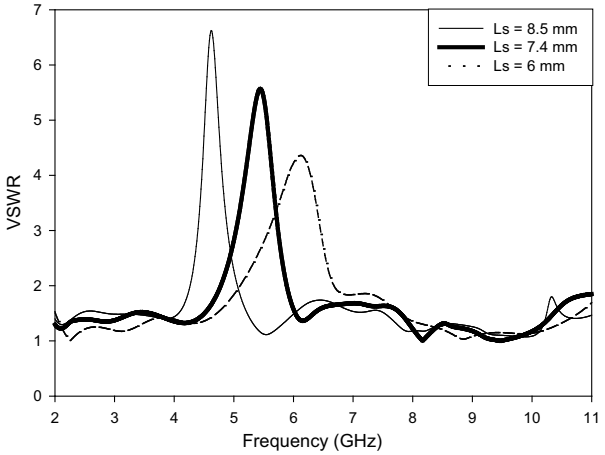

Figure 2: Simulated VSWR for various lengths of a pair of spur-lines.

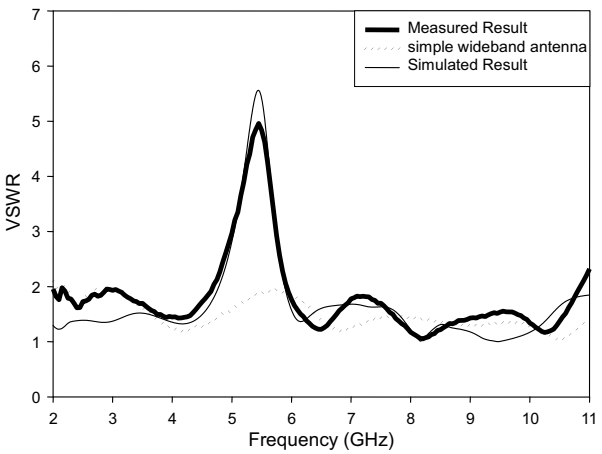

Figure 3: Comparison of simulated and measured VSWR.

A Novel Antenna Design for UHF RFID Tag on Metallic Objects

Youngman Um[1], **Uisheon Kim**[1], **Wonmo Seong**[2], **and Jaehoon Choi**[1]

[1]Department of Electrical and Computer Engineering, Hanyang University, Republic of Korea
[2]E.M.W. Antenna Co., Ltd., Gasan-dong, Geumcheon-gu, Seoul 459-2, Republic of Korea

Abstract— In Radio Frequency IDentification (RFID) system, tags are usually attached to objects having various material properties. Among them, metallic objects strongly affect the performance of antenna including radiation efficiency, gain, etc.. Planar inverted-F and microstrip patch antennas have been proposed for RFID tag application. However, these antennas have narrow impedance bandwidth and resonant frequency can be easily shifted due to the characteristics of objects that tag antennas are attached to.

In this paper, a novel microstrip patch RFID tag antenna with wideband characteristic is proposed. It has a less sensitive characteristic against size of metallic object, wide impedance bandwidth and a long reading distance. The antenna consists of shorting strip, open stubs, tag IC and radiating patch having I-shaped slits. The proposed antenna illustrated in Figs. 1(a) and 1(b) is located on the finite ground plane and is constructed on FR4 substrate ($\varepsilon_r = 4.4$, $\tan\delta = 0.02$) with thickness of 6 mm ($= 3 \times 2$ mm). Overall dimension of the proposed antenna is 100 mm $\times$ 26 mm $\times$ 6 mm. A width of the open stub and I-shaped slit is 1 mm and tag IC has input impedance of 43-j800 Ω at 915 MHz. The resonant frequency and impedance bandwidth can be controlled by adjusting the lengthes of I-shaped slits and open stubs, or a gap distance between the open stub and feed line. The -3 dB impedance bandwidth is from 664 MHz to 955 MHz as shown in Fig. 1(c). High radiation efficiency and peak gain are achieved by using shorting strip and three substrates. The radiation pattern is shown in Fig. 1(d). Peak gain, radiation efficiency and maximum reading distance are simulated and measured for 200 mm $\times$ 200 mm, 400 mm $\times$ 400 mm, and 600 mm $\times$ 600 mm metallic plates. Peak gain and radiation efficiency are listed in Table 1. The maximum reading distances are 4.4 m, 4.7 m and 3.25 m, respectively. The results show that the proposed antenna operates well on metallic objects with various sizes.

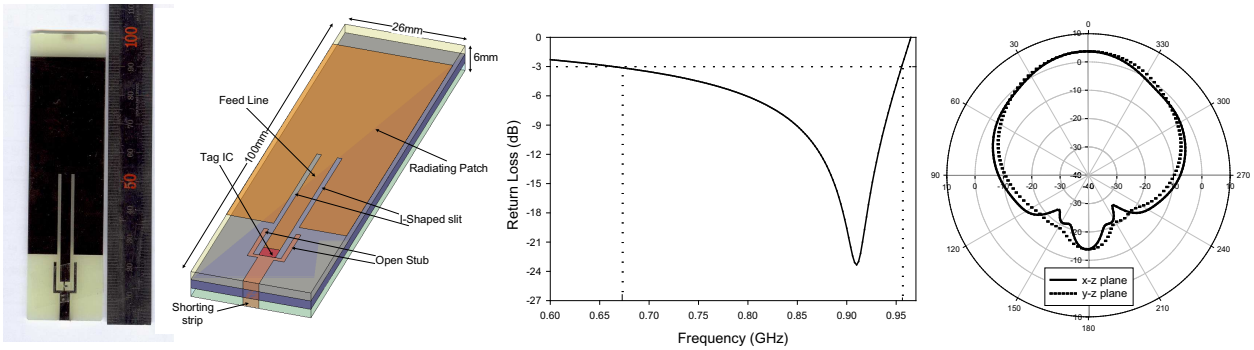

Figure 1: Proposed RFID tag antenna: (a) fabricated antenna, (b) 3D view, (c) return loss characteristic, (d) radiation pattern at 910 MHz.

Table 1: Simulated peak gain and radiation efficiency.

Metallic plate size	200 mm $\times$ 200 mm	400 mm $\times$ 400 mm	600 mm $\times$ 600 mm
Peak Gain (dBi)	2.4	2.10	1.6
Radiation Efficiency (%)	36	34	34.7

A Neural Network Approach to the Prediction of the Propagation Path-loss for Mobile Communications Systems in Urban Environments

S. P. Sotiroudis, K. Siakavara, and J. N. Sahalos
Radiocommunications Lab, Department of Physics, School of Sciences
Aristotle University of Thessaloniki, Thessaloniki 54124, Greece

Abstract— The prediction of electromagnetic wave propagation is of great importance in the design and planning of a cellular-network both for mobile and fixed wireless-access systems. A prediction, based on theoretical models, is really valuable since it offers the capability of determining optimum base locations, in order to obtain suitable data rates, to estimate their coverage and evaluate the quality of the wireless network without the need of expensive and time consuming measurements.

The theoretical models used for the estimation of the path-loss in various urban or suburban areas, even within buildings, are grouped in two categories: the empirical or statistical models (e.g., the COST-231-Walfisch-Ikegami model, the Hata model, etc.) and the site-specific or deterministic ones (e.g., the Ray Tracing technique, the Image Method, the FDTD or the Moment Method, etc.). The models of the former category are easier to implement and require less computational effort but are less sensitive to the environment's physical and geometrical structure. Those of the latter category have a certain physical basis and are more accurate but at the cost of more computations and at the necessity of more detailed information about the coverage area.

In the present work, prediction models based on Neural Network (NN)-architectures are proposed. Published works have introduced the NN-methodologies as efficient techniques for indoor and outdoor estimation of path-loss propagation. They have given solutions to the prediction problem, feeding the input of the NN by the values of some of the geometry parameters of the environment, e.g., the mean height and mean dimensions of the buildings and the mean width of the roads. In the work at hand Multiple Layer Perceptron (MLP) and Radial Basis Function (RBF) neural networks were composed, and the collections of data, by which they were trained, include the detailed environment profile. These data were produced using empirical models and/or the Ray Tracing technique. Although the calculation for the training collections were made for simple and uniform distribution of the manmade structures, the appropriate grid modeling of the build-up area as well as the way by which the input data were presented to the NNs made them efficient to give, in the generalization phase, results for arbitrary environments, provided that a digital map of the area is available.

Results for urban and suburban areas, received by the proposed procedure, along with the associate ones yielded by empirical and/or deterministic models, will be presented, for comparison reasons. The general NNs' performance shows their effectiveness to give results with satisfactory accuracy in a short time. Furthermore, since they are trained with results received via the Ray Tracing method, they have inherently, a certain physical basis, and that is why they are flexible to adapt to arbitrary environments.

Calculation of EM Characteristics of a Cellular Phone Handset by Time-domain MoM

R. Sarraf[1], **R. Moini**[1], **S. H. H. Sadeghi**[1], **and A. Farschtschi**[2]

[1]Amirkabir University of Technology, Iran
[2]Chemnitz University of Technology, Germany

Abstract— The effect of cellular phone handset dimensions on radiation pattern, impedance and resonance frequency is investigated. The handset body is modeled by an appropriate three-dimensional wiregrid structure with a $\lambda/4$ monopole antenna as its radiating source. The governing electric field integral equation (EFIE) is solved in the time domain, using the method of moments (MoM). The integral equation form of the electric field due to a filamentary current is derived (see Figure 1):

$$\mathbf{E}(\mathbf{r},t) = -\frac{\mu_0}{4\pi}\int_C \left[\frac{\mathbf{s}'}{R}\frac{\partial}{\partial t'}I(s',t') + c\frac{\mathbf{R}}{R^2}\frac{\partial}{\partial s'}I(s',t') - c^2\frac{\mathbf{R}}{R^3}q(s',t')\right]ds' \tag{1}$$

By applying the boundary condition on the tangential electric field at the conductor surface of Equation (1) the electric field integral equation for thin conducting wires is obtained

$$\mathbf{s}\cdot\mathbf{E}^A(\mathbf{r},t) = \frac{\mu_0}{4\pi}\int_C \left[\frac{\mathbf{s}\cdot\mathbf{s}'}{R}\frac{\partial}{\partial t'}I(s',t') + c\frac{\mathbf{s}\cdot\mathbf{R}}{R^2}\frac{\partial}{\partial s'}I(s',t') - c^2\frac{\mathbf{s}\cdot\mathbf{R}}{R^3}q(s',t')\right],\ \mathbf{r}\in C(\mathbf{r})+a(\mathbf{r}), \tag{2}$$

where q can be expressed in terms of I as $q(s',t') = -\int_{-\infty}^{t'}\frac{\partial}{\partial s'}I(s',\tau)d\tau$ and $a(\bar{\mathbf{r}})$ denotes the wire radius at point $\bar{\mathbf{r}}$ (see Figure 1). Since the integration path in Equation (2) is along $C(\bar{\mathbf{r}})$ while the wire radius displaces the field evaluation path, it is always true that $R > 0$ and the integral in Equation (2) thus has no singularity. The model described above is used to compute the electromagnetic field intensity around the handset. The handset body is approximated by a metallic box of dimension $a \times b \times c$ (Figure 2). A $\lambda/4$ monopole wire antenna of length h and radius r is placed at the top center of the handset body along the z-axis ($w = 3\,\text{cm}$). The validity of this approach is verified by comparing our simulated results by those reported by Luebbers et al. [1]. Figure 3 shows the input impedance of the antenna when $c = 5\,\text{cm}$. The

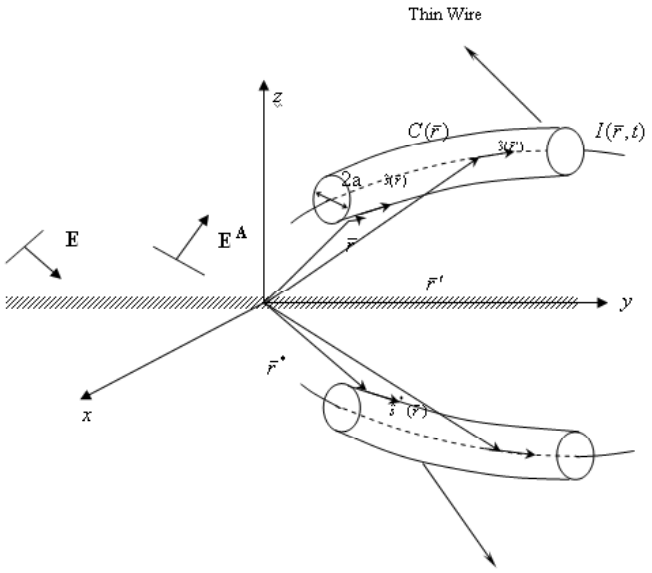

Figure 1: Thin wire geometry.

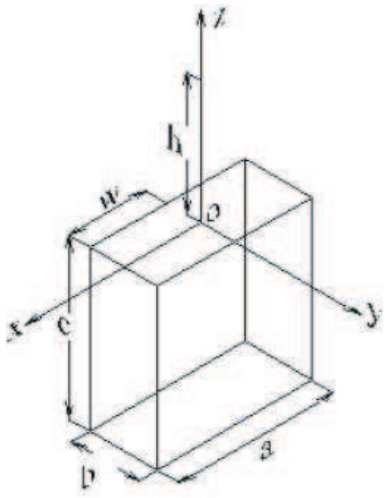

Figure 2: The geometric structure of the handset body together with its radiating monopole antenna.

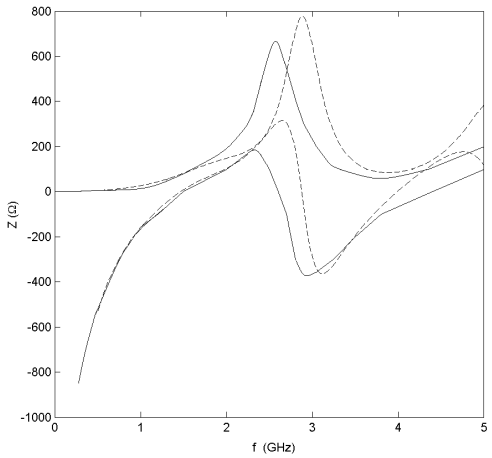

Figure 3: Computed input impedance of the monopole antenna mounted on the handset with height $c = 5\,\text{cm}$ for the proposed method (solid lines) and the method given in [6] (dashed lines).

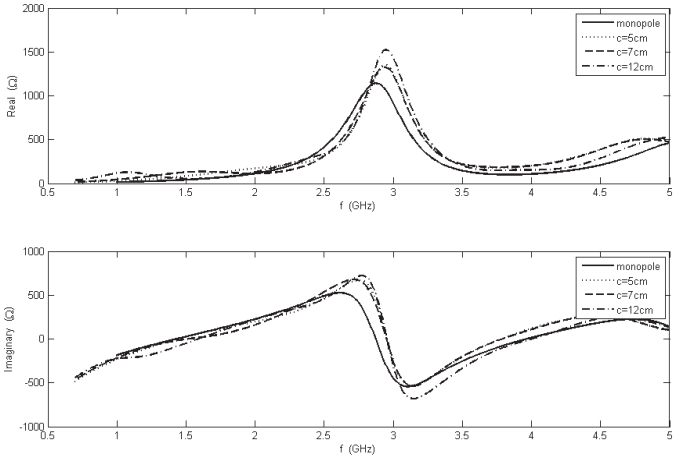

Figure 4: Input impedance of the monopole antenna without conducting box and with conducting box with various heights (dashed).

operating frequency varies from 0 to 2 GHz. The results are in good agreement with each other. Figure 4 depicts the variation of impedance versus frequency for the cases of single monopole ($c = 5, 7, 12\,\text{cm}$) with the resonant frequencies of 1450, 1470 and 1580 MHz respectively. As vividly seen in this figure, except for the case of $c = 12\,\text{cm}$, the first resonant frequency (first occurrence of the imaginary part being zero) appears to be in the close vicinity of our design frequency (i.e., 1.5 GHz). Figure 5 illustrates the impact of the monopole position w on the radiation pattern. The position of the monopole antenna shifts the main lobe of the antenna to the side. This affect could be used to reduce the amount of the radiation reaching human brain which is considered to be the most harmful.

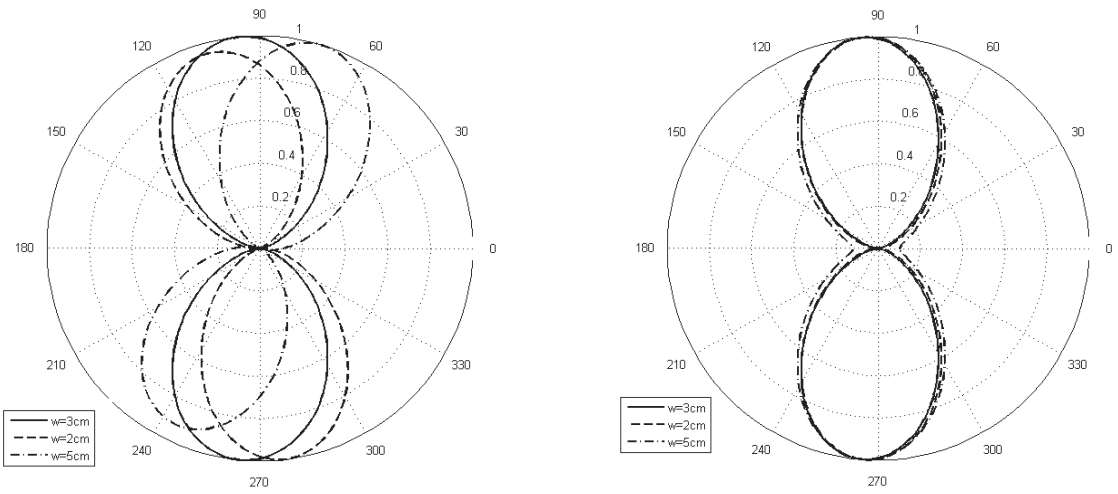

(a) x-z plane ($\Phi = 0^o$) (b) y-z plane ($\theta = 90^o$)

Figure 5: Radiation pattern of the monopole antenna mounted on the headset with $w = 3\,\text{cm}$ (solid), $w = 2\,\text{cm}$ (dashed), $w = 5\,\text{cm}$ (dashed/dotted).

REFERENCES

1. Luebbers, R., L. Chen, T. Uno, and S. Adachi, "FDTD calculation of radiation patterns, impedance, and gain for a monopole antenna on a conducting box," *IEEE Trans. Ant. and Propagat.*, Vol. 40, No. 12, 1992.

Topology Finite Element Method for Field Calculation Problems

Shizuo Li[1] and Yong Lu[2]

[1]College of Electrical Engineering, Guangxi University, Nanning 530004, China
[2]Guangxi Electric Power Institute of Vocational Training, Nanning 530007, China

Abstract— Topology finite element method (TFEM) represents the coefficient matrix of usual finite element method (FEM) with multiplication of several more simple matrixes, which can save more memories. So if the algorithm in the next step of solving simultaneous equations only involves matrix multiplication, it can take the advantages of TFEM. In this paper we show that by combining TFEM with a new preconditioning conjugate gradient method (PCGM), the calculating program needs much less memories than before while the computation is speeded up. It provides us a new approach for calculating large scale finite element problems on microcomputer.

Topology Finite Element Method

A: Topology Finite Element Method

Relation of the coefficient matrix of TFEM with the one of usual FEM is:

$$WHW^T = -M \tag{1}$$

Here M is the coefficient matrix of usual FEM, W is the node-edge incident matrix reflecting the relation between nodes and edges, W^T is the rotate matrix of W, H is the effect degree matrix. So the model of the field problem with TFEM can be derived as follows:

$$WHW^T\varphi = -M\varphi = P \tag{2}$$

P is a known matrix.

TFEM have a lot of advantages as bellow:

1. H is a diagonal matrix, and can be saved with a one-dimension array.
2. Each column of W has only two entries that equal to 1 and -1 respectively, while the others equal to zero. This can be saved with two one-dimension integer arrays whose length is equal to the number of edges, the first array saves the numbers of the starting nodes of directed edges, and the second array saves the numbers of the ending nodes of directed edges.
3. It needs much less memories than bandwidth-saving technique of usual FEM, and it need not optimize the node numbers, and can save much CPU time.
4. It needs fewer memories than nonzero-entry-saving technique, and it can save the addressing time of non-zero entries in the next step of solving simultaneous equations.

B: Combining TFEM With a New PCGM

In this paper, a new preconditioning conjugate gradient method is applied to take full advantages of TFEM.

Introduce a diagonal matrix Q:

$$q_{ii} = \frac{1}{\sqrt{m_{ii}}} \tag{3}$$

m_{ii} is the ith diagonal entry of coefficient matrix M in usual FEM. Multiply Equation (2) by Q, so

$$QWHW^T\varphi = QWHW^TQQ^{-1}\varphi = QP$$

Rewrite this equation as:

$$\begin{aligned} A\varphi' &= P' \\ A &= QWHW^TQ \quad \varphi' = Q^{-1}\varphi \quad P' = QP \end{aligned}$$

Substituting this equation in conjugate gradient method, a new PCGM iterative form is developed:

1. $\gamma^{(0)} = Q\left(P - WHW^T\varphi^{(0)}\right)$
2. $\xi^{(0)} = \gamma^{(0)}$

3. i=0
4. $\zeta^{(i)} = QWHW^TQ\xi^{(i)}$
5. $a = \gamma^{(i)T}\gamma^{(i)}/\xi^{(i)T}\zeta^{(i)}$
6. $\varphi^{(i+1)} = \varphi^{(i)} + aQ\xi^{(i)}$
7. $\gamma^{(i+1)} = \gamma^{(i)} - a\zeta^{(i)}$
8. Let $\delta = Max\left(\gamma^{(i+1)}\right)$

If $\delta \leq \varepsilon$ iteration terminates, otherwise continues.

9. $b = \gamma^{(i+1)T}\gamma^{(i+1)}/\gamma^{(i)T}\gamma^{(i)}$
10. $\xi^{(i+1)} = \gamma^{(i+1)} + b\xi^{(i)}$
11. Let $i = i + 1$ turn to 4th step.

Assuming that the mesh graph has N nodes and K edges, the calculating amount for one iteration is: $10N$+K multiplication or divisions and $7N$+$3K$ additions or subtractions. So total calculating amount $T(N)$ of this method is:

$$T(N) \sim O(N) \tag{4}$$

This is much less than the $O(N \log N)$ of ICCG.

The total memories required is $7N + 2K$ real number memory units and $2K$ integer number memory units.

Obviously, after combining this new PCGM with TFEM, because of no need for doing incomplete CHOLESKY factorization and addressing, not only can be simplified the calculating program, saved the memories and reduced the matrix calculating amount in each iteration, but also the fault that conjugate gradient method is difficult to converge can be overcome.

C. Example:

An example is calculated to show the advantages of topology finite element method.

Conclusion

In this paper, the advantages of combination of topology finite element method and a new preconditioning conjugate gradient algorithm have been shown. Undoubtedly this combination is a simple and systematic approach that leads to a substantial gain in memory volume and computational cost, especially in the situation with node number increasing.

REFERENCES

1. Song, G. and H. Shi, "Topology finite element method for solving electromagnetic field problem," *Electronics Letters (IEE)*, Vol. 19, No. 15, 529–551, Jul. 1983.
2. Henneberger, G., "An accelerated N-R method associated with the ICCG algorithms," *IEEE Trans. on Mag.*, Vol. 26, No. 2, 709–711, 1990.
3. Cui, X., "An new preconditioning conjugate gradient algorithm," *Trans. of North China Electric Power University*, No. 2, 1–7, 1989.

Effect of Radar Beam Pattern on Determination of Echo Center Using Coherent Radar Imaging

Jenn-Shyong Chen[1], **Peter Hoffmann**[2], **and Marius Zecha**[2]

[1]Department of Computer and Communication Engineering, Chienkuo Technology University, Taiwan
[2]Leibniz-Institut für Atmosphärenphysik, Kühlungsborn, Germany

Abstract— Multiple-receiver radar interferometry, termed as coherent radar imaging (CRI) in the MST radar community, provides the ability of studying the atmosphere from the view of multiple scattering/reflecting centers of the echoes. However, previous works of CRI concentrated on small zenith angles of echo centers within the beam width. For large zenith angles outside of the main beam, the error of the estimated angles of echo centers may be significant due to the transmitted and receiving beam patterns, which should be examined in more detail although such problem may occur occasionally in observations or be crucial only for some radar systems. This issue was examined by simulation calculation in this study. Moreover, a study of the atmospheric echoes received by the OSWIN 53.5 MHz radar in Kühlungsborn (54°N, 12°E), Germany, was carried out. The atmospheric echoes were collected in the height interval of mesosphere and by different observational modes, namely, vertical and oblique radar beams with the receiving configurations of 3×2, 6×1 (north-south alignment) and 1×6 (east-west alignment) antenna groups. We found that in the 6×1 and 1×6 antenna groups many echoes returned from large off-zenith angles (ranging between several and 20 degrees) and their off-zenith angles became larger as range height increased. Based on the observation and simulation calculation, the relationship between observed off-zenith angles of echo centers and radar beam pattern were investigated.

Design of Conformal Tapered Leaky Wave Antenna

O. Losito

Department of Innovation Engineering, University of Salento
Via per Monteroni, Lecce 73100, Italy

Abstract— Since the first microstrip leaky wave antenna (LWA) introduced by Menzel much progress has been made regarding the development of leaky wave antennas based on the higher order mode of microstip. The LWAs possess the advantages of low-profile, easy matching, fabrication simplicity, and frequency/electrically scanning capability. Nevertheless, in some applications especially with regard to communication applications, the main beam variation of LWA should be as low as possible. A tapered steps microstrip LWA in which each step can irradiate in subsequent ranges of frequency and designed by running a simple algorithm which uses an FDTD code, is a possible first solution studied to obtain a broadband and fixed mainbeam LWA. But the impedance mismatch between subsequent steps, reduces the bandwidth. Furthermore the excitation of a higher order mode without dominant mode perturbation, requires a more elaborate feeding scheme. Subsequently, we studied a curved design of tapered antennas, as shown in Fig. 1, from 8 to 11 GHz with a physical grounding structure along the length of antenna which allows a reduction of the impedance mismatch and a suppression of the dominant mode (the bound mode). Moreover, this solution allows the adoption of a simple feeding, and also the reduction of sidelobes. The length of CTLWA was chosen to be 120 mm, with a 15 mm start width, and 8.9 mm of final width, for a substrate of thickness of 0.787 mm and $\varepsilon_r = 2.32$. Finally, due to the image theory it is also possible to design only half of an antenna with the same property of one in its entirety, reducing up to 60% the antenna's dimensions, as shown in Fig. 2. This layout therefore, improves the band, as shown in Fig. 3, (33% for VSWR < 2), the gain (12 dBi) and the efficiency (up to 85%) with reference to conventional uniform microstrip LWAs (which have band of 22% for VSWR < 2, peak gain up to 10 dBi and efficiency up to 75%). The leakage radiate phenomena can only be noted above the cutoff frequency of higher order mode and below the frequency such that the phase constant of complex propagation constant is equal the free space wave number.

Figure 1: Layout of curve tapered leaky wave antenna (CTLWA).

Figure 2: Layout of half curve tapered leaky wave antenna (HCTLWA).

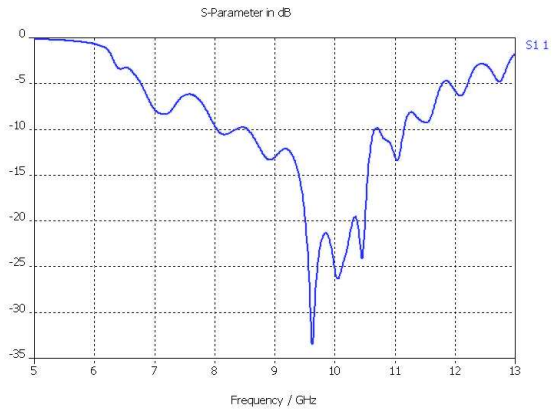

Figure 3: S11 of HCTLWA.

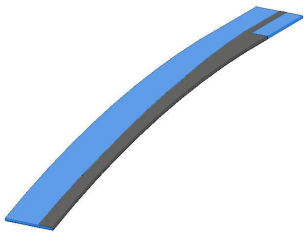

Figure 4: Layout of bend curve tapered LWA (BCLWA).

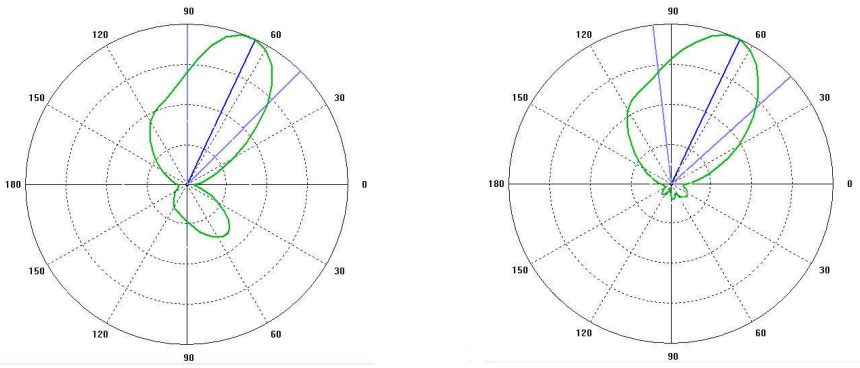

(a) (b)

Figure 5: (a) Radiation pattern of E field (H plane) at 8 GHz of CLWA, (b) radiation pattern of E field (H plane) at 8 GHz of BCLWA.

Nevertheless, we note that a tapered LWA for a fixed frequency, changes the main beam radiation angle. This occurs because the phase constant β and attenuation constant α vary with a cross section along the length of antenna. This allows a corresponding angolar radiation range [$\vartheta_{\min}$, $\vartheta_{\max}$] can be obtained. For linear tapered LWA we can predict the angle of main beam using a simple geometrical-optical approach. This paves the way to prediction of the main beam angle of curve tapered LWAs. Furthermore this focusing phenomena of the radiation pattern of a tapered LWA can obtain a wide-beam pattern in a radiation range which is evident when the antenna length is increased ($L \cong 50\lambda_0$). To obtain a broad beam pattern without the use of a longer LWA, we can bend a tapered curve LWA as shown in Fig. 4, allowing the electromagnetic waves to diverge. This increases the beam noticing a major reduction of the back lobes, as shown in Fig. 5. The performance of the efficiency and the band of this LWA can be improved further, if we use a substrate with relative dielectric constant that approached 1, highlighting that this structure is attractive for the design of high performance microstrip leaky-wave antennas for microwave and millimeter wave applications.

Analysis of the Gain and Linearity Characteristics in Bias Controlled Push Pull Power Amplifier

Young-Huang Chou, **Chao-Yu Huang**, **Chin-Chih Yeh**, **Hao-Hui Chen**, **and Rong-Chan Hsieh**

Department of Electronic Engineering, HuaFan University
No. 1, Huafan Rd. Shih-Ting, Taipei 223, Taiwan, R. O. C.

Abstract— Linearity of the power amplifier is an important specification to judge the quality of signal transmitted in modern wireless communication system. Single amplified path with Class A operation using power back off technology is a major method now used to implement the miniaturized linear power amplifier design. However, it suffers the disadvantage of lower efficiency. In this work, gain and linearity performance of two paths push pull power amplifier were investigated. Fig. 1 show the proposed ideal of circuit block diagram. Compared to the traditional configuration, modification was made by controlling the DC biases of two sets of HBT devices embedded in the individual path. Different types of operating points from deep class A to deep class AB would be used with setting strategy of optimal compensated gain response. By using the specific combination of deep class A and class AB bias setting in two sets of HBT devices, overall amplifier gain having higher level and flatness response would be obtained, which proved the enough dynamic range and linearity for system applications. Because of mixed operating points (class A and class AB) together with differential operation with even harmonics cancellation, efficiency could be improved effectively compared to the original single path class A design. In addition, the P1dB gain compression point would be moved to higher power region, which revealed extended power range for linear operation. Finally, the DC bias in one set of HBT devices with class AB operation would be varied gradually to class A condition. After combining to another set of HBT devices with fixed class A operation, a minimum IMD3 could be generated significantly at a specific input power level. This controllable minimum IMD3 could be useful in some applications with higher linearity requirement.

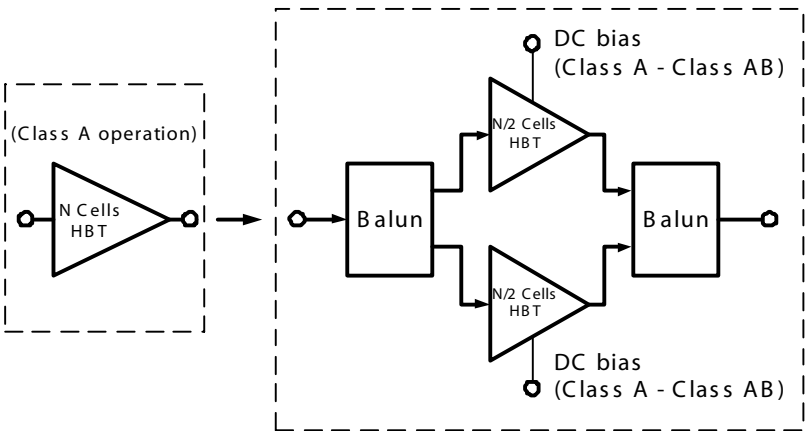

Figure 1: Modification of the single path class A power amplifier to the proposed bias controlled push pull configuration.

Design of an Internal Wideband Antenna for DTV Laptop Application

S. G. Jeon, D. H. Seo, and J. H. Choi

Department of Electrical & Computer Engineering, Hanyang University
17 Haengdang-Dong, Seongdong-Gu, Seoul 133-791, Republic of Korea

Abstract— An internal antenna for DTV laptop application should how low profile and wideband (470 MHz∼740 MHz) characteristic. A low profile antenna for DTV signal reception in the UHF band for laptops has been reported recently [1, 2]. The key issue in the design of an internal antenna is the size reduction while maintaining the antenna performance the same as that of an external antenna.

In this paper, a folded planar dipole antenna [3] with meandered metal plate is proposed as shown in Fig. 1. To achieve the low profile and compact structure on finite ground, the metal plate dipole antenna is folded and has meandered shape. The two arms of the proposed structure are designed asymmetrically to obtain the wide bandwidth by generating the two different resonance modes. Proposed antenna has a length of 60 mm, which is only 0.13 wavelength of 630 MHz (center frequency of the desired band). It is fed by 50 Ω coaxial line. Fig. 2 shows the simulated and measured return losses the proposed antenna. Measured return loss bandwidth for VSWR less than −7.5 dB is 366 MHz (451 MHz∼817 MHz). Design parameters of the antenna are experimentally optimized and the measured radiation and return loss characteristics of the antenna are good enough for DTV application. This antenna can be a good candidate for internal receiving antenna for DTV laptop application due to its low-profile, small size and wide impedance characteristic.

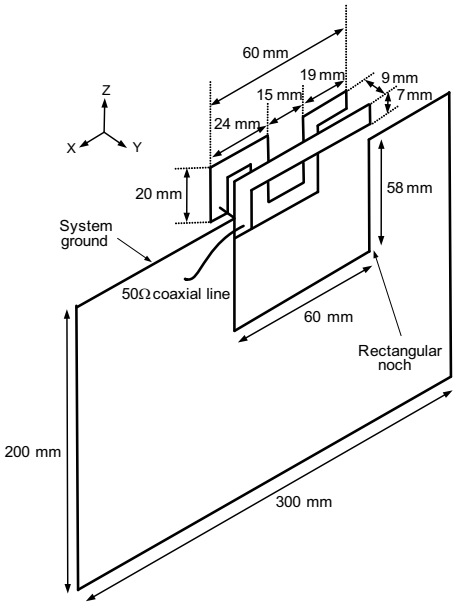

Figure 1: Proposed antenna for laptop.

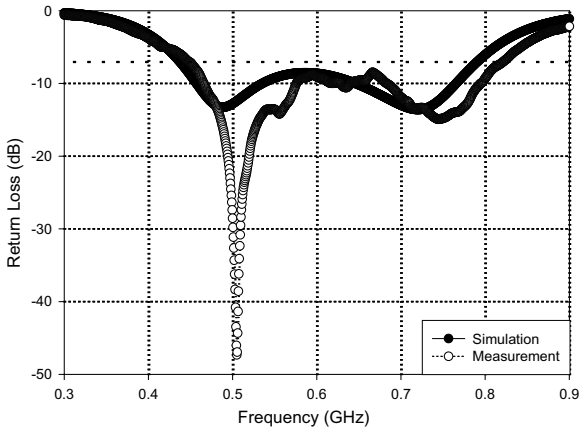

Figure 2: Simulated and measured return loss characteristics.

REFERENCES

1. Su, C. M., L.-C. Chou, C.-I. Lin, and K.-L. Wong, "Embedded DTV antenna for laptop application," *Antennas and Propagation Society International Symposium, 2005 IEEE*, Vol. 4B, 68–71, 3–8 July, 2005.
2. Su, C. M., L.-C. Chou, C.-I. Lin, and K.-L. Wong, "Internal DTV receiving antenna for laptop application," *Microwave Opt. Technol. Lett.*, Vol. 44, 4–6, 2005.
3. Stutzman, W. L. and G. A. Thiele, *Antenna Theory and Design*, 2nd ed., John Wiley & Sons Inc., 1998.

Development of Voltage Controlled Oscillators Using 2-μm GaAs HBT Monolithic Integrated Circuit Technology for Atacama Large Millimeter/Submillimeter Array Application

Hong-Yeh Chang[1], **Yan-Liang Yeh**[1], **Chi-Hsein Linand**[1], **Kung-Hao Liang**[1]
Chau-Ching Chiong[2], **and Eric Bryerton**[3]

[1]Department of Electrical Engineering, National Central University, Chungli 32001, Taiwan
[2]Academia Sinica, Institute of Astronomy and Astrophysics, P. O. Box 23-141, Taipei 10617, Taiwan
[3]National Radio Astronomy Observatory, 1180 Boxwood Estate Road, Charlottesville, VA 22903, USA

Abstract— The development of voltage controlled oscillators (VCOs) using 2-μm GaAs HBT monolithic integrated circuit (MMIC) technology is presented in this paper for Atacama large millimeter/submillimeter array (ALMA) application. The VCOs will be applied to the local oscillator (LO) chain of the ALMA receivers to replace yttrium-iron-garnet (YIG) oscillator. The YIG oscillator demonstrates excellent phase noise, but they usually consume much dc power with high cost. In ALMA receivers, a lot of oscillators are required to perform the measurement of electromagnetic spectrum in millimeter and submillimeter bands, therefore the overall dc power consumption and the cost are crucial for the instrument. The MMIC technology provides many advantages of compact size, low weight, high performance, high repeatability, and low cost in high volume production. By utilizing the technology for the ALMA receivers, the drawback of the YIG oscillators can be resolved. So far, a few VCOs using the 2-μm GaAs HBT MMIC technology have been developed, and the frequency of the VCOs is from 15 to 32 GHz with dc power consumption of lower than 40 mW. The overall chip sizes of the VCOs are within $1 \times 1\,\mathrm{mm}^2$. The measured phase noise of the VCOs is better than -100 dBc/Hz at 1-MHz offset frequency. The VCOs features a maximum tuning range of 30%, and a figure-of-merit (FOM) of -168 dBc/Hz.

ACKNOWLEDGMENT

This work was supported in part by the National Science Council of Taiwan, under Grant NSC 95-2221-E-008-170, and the ALMA-T research project in ASIAA, Taipei, Taiwan. The chip was fabricated by the WIN Semiconductors Inc. Taiwan. The authors would like to acknowledge Chip Implementation Center (CIC) of Taiwan for providing EDA design software.

A Modified Formulation for the Band Structure Calculation of Metallic Photonic Crystals

K.-H. Chi and Y.-P. Chiou
Graduate Institute of Electo-Optical Engineering and Department of Electrical Engineering
National Taiwan University, Taipei 10617, Taiwan

Abstract— Conventional frequency domain methods are mostly derived for lossless and dispersiveless materials, which is ineffective or/and inefficient in the analysis metallic photonic crystals. Instead, time domain methods, such as finite-difference time-domain (FDTD) method is adopted. However, the required computation resource is large and the resolution in band structure calculation is relatively rough. In this paper, we derive a formulation directly from Maxwell equations to calculate the band structure calculation of metallic photonic crystals. Since less assumption is assumed, the limitations are alleviated. The sampling rate in the proposed method is flexible along with frequency, while conventional methods use same samplings in all frequency regions. Therefore, it is more efficient since better accuracy in high frequency region is achieved and computation resources are economic in low frequency region. The proposed formulation is verified by comparing the results with conventional frequency and time domain methods.

Signal and Energy Velocity of EM-waves in Dispersive Media

Hiroyuki Hosono[1] and Toshio Hosono[2]

[1]Department of Engineering Science, Junior College of Nihon University, Japan
[2]Nihon University, Japan

Abstract— Ever since the study by Sommerfeld and Brillouin, the physical meaning of the group and energy velocities had been misunderstood.

In 1970 Garrett and McCumber showed that the superlumial group velocity is really the velocity of the envelope of a Gaussian wave packet.

Since then, the study of group velocity has been intensified; the studies of signal and energy velocities have been left behind.

The present situation of understanding of the energy velocity is represented by the Jackson's statement [1]: "In a dispersive medium, the velocity of energy flow may lack precise meaning.". Against this statement, we show that, even in an anomalous dispersion band in which the group velocity is superluminal, the signal velocity is always equal to the energy velocity of the carrier, and that every frequency component of a signal travels at its own energy velocity. Thus, we show that the energy velocity has precise physical meaning even in anomalous dispersion bands.

This conclusion is simple and clear, but has been difficult to obtain by analytical method such as the steepest descent method. The analysis using Gaussian wave packet can not be used to determine the signal velocity because it is too smooth. On the other hand, the analysis using square modulated wave packet suffers from the interference due to the Sommerfeld-Brillouin precursors.

In order to find out the signal velocity, it is essential to have the high precision graphics of propagating signal that enables us to distinguish the main signal clearly from the Sommerfeld-Brillouin precursors.

Using FILT, a numerical algorithm of Faithful Inversion of Laplace Transform, we can obtain the waveform of the propagating signal with sufficient information to conclude that the signal velocity is always equal to its energy velocity.

Although the study of superluminal group velocity has been very active, people have not understood its true meaning because they do not know the velocity of carrier.

We show that the group velocity plays its role only after the arrival of the carrier that travels at its subluminal energy velocity.

The faster the group velocity becomes, the slower the energy velocity. So, the carrier of a superluminal Gaussian wave packet moves at very slow energy velocity.

REFERENCES

1. *Jackson's Classical Electrodynamics*, Wiley, 1999.

Design of the Broadband Bandpass Filter Using Slow Wave Characteristics

Jin-Sup Kim and Sang-Gi Byeon
Wireless Communication Research Center, Korea Electronics Technology Institute, R. O. Korea

Abstract— The broadband suspended substrate filter is proposed and implemented using slow wave characteristics, aiming at transmitting the signals in the passband of 6–10 GHz. It is composed of two quarter-wavelength resonators and K-inverter. The K-inverter is composed of two short-circuited stubs. After optimization of this filter, a good bandpass behavior with transmission poles is theoretically realized and experimentally confirmed. Within the whole bandpass filter passband, the return loss is found higher than 14 dB, and the insertion loss is less than 1.9 dB.

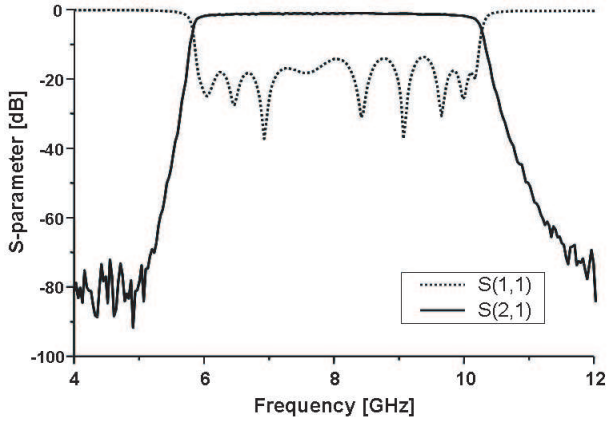

Figure 1: Measured results of suspended substrate stripline BPF.

REFERENCES

1. Rhodes, I. D., "Suspended substrate filters and multiplexers," *Proceedings of 1986 European Microwave Conference*, 16th EuMc, 8–18.
2. Bhartia, P. and P. Pramanick, "Computeraided design models for broadside-coupled striplines and millimeter-wave suspended substrate microstrip lines," *IEEE Transactions on Microwave Theory and Techniques*, Vol. 36, No. 11, November 1988.

Compact Representation of the Inductance Coefficients in Presence of Uncertain Parameters

B. De Vivo, L. Egiziano, P. Lamberti, and V. Tucci
Department of Electrical and Information Engineering, University of Salerno, Italy

Abstract— The realization of power electronic circuits employed for the energy conversion process in a great number of applications involves the design of inductors and transformers. However, the relevant parameters of such electromagnetic components obtained by performing a nominal value design are rarely correspondent to those available from market devices. For this reason an appropriate realization of such components may be required for each application. Besides, the quality of the obtained electromagnetic component sensibly affects the characteristics of the overall system, especially in terms of power consumption and dimensions. The availability of a compact and efficient model of the electromagnetic component able to keep into account the inevitable uncertainty associated to its physical realization is useful to guarantee an appropriate design of the circuit.

In order to pursue this objective in this paper the representation of the inductance coefficients in presence of uncertain parameters is presented in a simple and compact form. In particular the self and mutual inductance coefficients are obtained by applying the Interval Arithmetic to the Hopkinson's law. This approach leads to inductance coefficients which are not expressed as point-values but as sets expressed by *intervals*. Such intervals certainly include all the possible values that the coefficients can assume in presence of tolerances on physical and/or geometric parameters. The procedure is applied firstly to a simple wound component in order to put in evidence the validity of the proposed approach in presence of geometric tolerances. Then the non linearity of the ferromagnetic material characteristics is considered and the analysis from the actual data-sheet value is performed. Finally, a compact representation of the self and mutual inductance coefficients in presence of multiple couplings is given by considering a linear actuator. The correctness of the resultant intervals that include the actual values of the coefficients is evaluated by using a FEM commercial software.

Microstrip Patch Antenna Using an Aperture-coupled Waveguide

Se-Hwan Choi, **Jae-Young Lee**, **and Jong-Kyu Kim**
Korea Electronics Technology Institute, Korea

Abstract— Millimeter-wave antennas are important for the sensor system and low-cost communication. In recent years, planar antennas are widely used in the millimeter-wave range due to low cost and profile, simple and lightweight construction, ease of fabrication and reproducibility. While it is often desirable to select planar antennas and circuits, there are still many applications that need the waveguide circuitry because the waveguide bulkiness becomes less a factor and its losses are smaller than those of a microstrip line in millimeter-wave the range. So waveguide-to-microstrip transitions are needed to connect the waveguide and a microstrip line or antenna. Traditionally, waveguide-to-microstrip transitions use types of microstrip probes or fin-line transitions. Although these types have a wideband characteristic, they suffer from several disadvantages such as manufacturing complexity and large bulk. In this paper, we use the waveguide endwall coupler as a waveguide-to-microstrip transition. The endwall coupler has narrower bandwidth than microstrip probes or fin-line transitions. But it shows excellent performance as a microstrip patch antenna feeder. Because this technique has simple structure and high tolerance, it is suited for low cost and high volume production for commercial millimeter-wave applications. Besides, the n-by-n array antenna can be designed if needed.

This paper describes the 2 by 2 array microstrip patch antenna using an aperture-coupled waveguide at 24 GHz. The antenna consists of a waveguide feed and four patches that are excited by the endwall coupler. Feeding waveguide uses the WR-42 (10.7 mm × 4.3 mm) standard waveguide. Patterns for patches are fabricated on the Taconic TLX-9 ($r = 2.5$ and $t = 31$ mil) substrate. Microstrip pattern is coupled with waveguide through a slot on the ground plane. The size of a metallic plate and a slot decides a degree of coupling. Next, a transformer with the high impedance and a patch with a half wavelength are located. A metallic plate is coupled simultaneously as the phase of a rectangular waveguides dominant mode (TE10) changes. Seeing at the center of a metallic plate, both sides of a plate have a phase difference of 180 degree. This field excites four patches that are located symmetrically, finally it makes a 2 by 2 array antenna. Spurious radiation from the slot is not an issue because it should be co-polarized and combined with the radiation of the patch.

The antenna is simulated by Ansoft HFSS V9.1 and is analyzed by a network analyzer HP8510c and a measurement system. As measurement results, this antenna has the gain of 10 dBi and the bandwidth of 1.3 GHz. And half power beamwidth is 35 degree on the E-plane and 31 degree on the H-plane.

Balancing the Interference Probability between Systems for Sharing Frequency Spectrum

Taekjin Hwang[1], **Sanggee Kang**[2], **and Heonjin Hong**[1]

[1]ETRI, Korea
[2]Kunsan National University, Korea

Abstract— In order to share frequency spectrum, balancing the transmitting parameters, such as power, bandwidth, duty factors etc., is necessary for using the limited frequency resources efficiently. In this paper we study how to adjust transmitting parameters for sharing frequency bands in two cases. First we consider that a frequency band is already allocated to the specific communications. The second is the case of allocating new frequency bands to communication systems having interference mitigation techniques. For each case we investigate the conditions for sharing frequency bands and suggest a balancing factor for adjusting the interference effects between systems using different interference mitigation techniques.

Impulse Response of Seafloor Hydrocarbon Reservoir Model

Jingtian Tang and Weibin Luo
School of Info-physics and Geomatics Engineering, Central South University, China

Abstract— In recent years marine controlled source electromagnetic (CSEM) were on the increase applied to identify seafloor hydrocarbon reservoirs. For this method provide for the possibility of electromagnetic based discrimination between oil-filled and water-filled reservoirs. It is also a direct indicator to thin resistive layers. In this paper, We examine the underlying physics of the CSEM method in time domain by forward modeling. The step response and impulse response of homogeneous earth half space, marine double half space and four-layer earth models to horizontal electric dipole source (HED) were computed using Gaver-Stehfest inverse Laplace transforms and numerical integration related Hankel transforms. Because the EM response of resistive hydrocarbon reservoirs is a frequency dependent function of source-receiver offsets and seafloor conductivity, so a wideband low frequency signal is suitable in marine oil and gas survey due to electromagnetic (EM) attenuation in conductive sea water. The EM wave propagate in conductive medium satisfies diffusion equation. A concept of transient impulse time was put forward. It is confirmed that the transient impulse time of the conductive medium to horizontal electric dipole can directly indicate the conductivity of the earth. The HED can generate both galvanic effects currents and inductive effects currents, so it is sensitive to thin resistive layers, and inline dipole-dipole configuration is a main survey system, it sounds with geometry and works with multi offsets. Multi receiver dipoles and transmitter dipoles can be laid in line with different space. Moving the inline system can perform both profile and sounding explorations. The transient impulse time of different offsets can be used to map the seafloor conductivity. For the high resolution to both thin resistor and good conductor, this method can applied for hydrocarbons and metal deposits explorations on land, also in marine.

Generalized Approach for Phase Interferometric Measurements of Electromagnetic Field

Jan Zela, **Karel Hoffmann**, **and Premysl Hudec**
Department of Electromagnetic Field, Czech Technical University
Technicka 2, 166 27 Prague 6, Czech Republic

Abstract— A new generalized approach for microwave phase interferometric measurement of electromagnetic field using an antenna matrix (AM) was developed. The approach allows correction of most significant measurement errors caused by mutual couplings of closely spaced antenna elements. It is based on vector measurements of the AM designed for the frequency 2.60 GHz and Matlab simulations.

Artificial Neural Network Employment in the Design of Multilayered Microstrip Antenna with Specified Frequency Operation

K. Siakavara

Radiocommunications Lab., Department of Physics, Aristotle University of Thessaloniki
Thessaloniki 54124, Greece

Abstract— Microstrip antennas are used in a wide range of wireless communications systems which demand multiple and/or wide band frequency operation, high power gain, omni-directional radiation patterns etc. and the design of printed antennas suitable to meet the requirements of multiple operational features is a difficult task.

Various techniques are employed for the synthesis of multi-band microstrip antennas, as the utilization a) of printed elements loaded with varactors or slots b) of stacked elements c) of EBG substrates or the application of the fractal design technique. Recent works have shown that the fabrication of the radiating elements in multilayered substrates is an effective method to achieve multi-frequency operational characteristics.

The difficulty in all the above methods is to solve the inverse problem, that is to find out the appropriate geometry and the proper values and positions of the lumped elements in order the antenna to exhibit a desired performance. The present work focuses to this problem. An Artificial Neural Network(ANN) procedure was employed for the synthesis of a microstrip antenna with pre-specified frequency response. The ANN algorithms have been proved to be a useful tool for the design of printed antennas and have been applied to the evaluation of the resonate frequency of the radiating element for specific structural parameter values and also to the inverse problem, namely the finding of the values of these parameters for a specific resonate frequency. Furthermore ANN have been employed in the calculation of the radiation pattern or the input impedance of this antenna type. In the work at hand a printed ring antenna was designed in a three layered substrate. The inherent advantage of a ring antenna is its property to resonate for a diameter less than $\lambda g/2$ (λg is the guiding wavelength of the equivalent linear microstrip line having width equal to that of the ring). This attribute means a physical size smaller than the size of the respective circular disc resonating at the same frequency. The modification of the ring shape, via slits, would increase the frequency bandwidth if the slits are notched on proper positions and have suitable dimensions. The frequency response is also affected by the dielectric constant values and the heights of the substrates. The difficulty in designing the antenna is due to the large number of the physical parameters, the values of which have to be calculated in order the radiating element to exhibit the desired response.

The problem was solved via a neurocomputational algorithm. The MLP-NN architecture was used and the composed network was trained via the backpropagation algorithm. The calculation of the training data set was based on the theoretical analysis of the antenna scheme and was made via simulation. The input of the ANN receives the desired pattern of the antenna's input reflection coefficient versus frequency and gives the appropriate values of the twelve parameters of the structure by which this pattern would be obtained. The results of the procedure were verified by simulation of the antennas, synthesized via the parameter values yielded from the ANN.

It was ascertained that the MLP-ANN methodology can efficiently give solution to the problem and respective examples will be presented. In all cases the ANN gave correct answer when, in the desired reflection coefficient pattern, the frequency separation between the resonate regions was at least 1GHz. This fact and also the upper limit values of the obtained bandwidths depend mainly on the shape of the printed elements and also on the regions of the antenna's parameter values by which the ANN was trained.

Microwave Probes for Dielectric Measurements

Radim Zajíček, **Ladislav Oppl**, **and Jan Vrba**
Department of Electromagnetic Field, Faculty of Electrical Engineering
Czech Technical University in Prague, Czech Republic

Abstract— Dielectric properties of biological tissues are determining factors for the dissipation of electromagnetic energy in the human body and therefore they are important parameters in hyperthermia cancer treatment, microwave detection of tumors and in assessment of exposure doses in basic research of interactions between electromagnetic field and biological tissues.

If we want to use broadband measurement method which is nondestructive, noninvasive and which can offer possibilities for in vivo as well as in vitro measurements, we should choose reflection method. The reflection method on the open end of the coaxial line is the well known method of determination of dielectric parameters. The method is based on the fact that the reflection coefficient of an open ended coaxial line depends on dielectric parameters of material which is attached to it. A typical measurement system using a coaxial probe method consists of the network or impedance analyzer, the coaxial probe and software.

The main aim of the project is to design convenient measurement probes for frequency range from 30 kHz to 3 GHz. Three types of measurement probes were under investigation: coaxial, planar and waveguide. The coaxial probe was created by adapting the standard N and SMA connector from which the parts for connecting to a panel were removed. The planar probe is created by a section of three conductor coplanar line. As a possible waveguide probe is under analyses the section of metal waveguide with rectangular cross section. The material can be measured by touching these probes to the flat face of a material and by determining the reflection coefficient.

This feasibility study of measurement method involves numerical modeling and simulations. The system that we modeled consisted of two parts, i.e., the sensor and the biological tissue sample. The biological tissue sample was modeled based on available published data of complex permittivity. Numerical simulation based on Finite Integration Technique (FIT) is used to calculate reflection coefficient on interface between measurement probe and sample of biological tissue.

Reported measurement method is convenient method for the determination of dielectric parameters of biological tissues. It was found that coaxial probe is useful in frequency range from 40 MHz. The description by two element equivalent circuit (fringing capacitance and radiating conductance) is necessary because of the probe radiation at higher frequencies. The planar probe excited by SMA connector was found as suitable. The waveguide probe is suitable in the construction as a section of waveguide with the rectangular cross section with added dielectric cotter. Generally the waveguide is a narrowband microwave component but dielectric cotter with defined conductivity makes it more broadband. And also achieved reflection coefficient is sufficient. The waveguide probe is useful from the frequency 1 GHz.

Electrical Vibrations of Yeast Cell Membrane

M. Cifra[1,2], J. Vaniš[2], O. Kučera[1,2], J. Hašek[3], I. Frýdlová[3], F. Jelínek[2] J. Šaroch[2], and J. Pokorný[2]

[1]Department of Electromagnetic Field, Czech Technical University
Technická 2, 166 27 Prague, Czech Republic
[2]Institute of Photonics and Electronics, Academy of Sciences of the Czech Republic
Chaberská 57, 182 51, Prague 8, Czech Republic
[3]Institute of Microbiology, Academy of Sciences of the Czech Republic
Vídeňská 1083, 142 20 Prague 4-Krč, Czech Republic

Abstract— Local nanomechanical motion of yeast cell (*Saccharomyces Cerevisiae*) wall has been measured by Pelling et al. with atomic force microscope (AFM). By means of the Fourier transform of the measured signal they have found oscillations with amplitude of a few tenths of nm to a few nm's lying around the frequency of 1 kHz. Frequency of these oscillations was temperature dependent. Background noise of the AFM was of the order of magnitude of 10^{-2} nm. Oscillations at a single frequency have been detected on the normal yeast cell wall and those at multiple frequencies different from the frequency on the normal cell wall have been detected on the bud scar. Oscillations of the yeast cell wall and of the bud scar ceased after addition of metabolic inhibitor, which suggests cellular metabolism is involved in the generation of motion. These findings correspond to the Frőhlich's postulate of coherent electrically polar longitudinal vibrations in biological systems. Vibrations of the electrically polar structures in the cell membrane imply generation of electromagnetic field.

This paper reports on the measurements of the electrical vibrations of the yeast cells in the region of kHz. The measurement system consists from:

- temperature stabilized, triple screened box (electrically and electromagnetically by mumetal) with a sensor and preamplifiers
- spectral analyzer Rohde-Schwarz (FSEA30 20 Hz–3,5 GHz) controlled by PC via GPIB

Point measurement was carried out with a sensor containing obliquely cut tip whose width at the end was ca. 30–50 nm.

The evaluated signals display electromagnetic activity of the yeast cell plasma membrane. The cell strain used was different from that used by Pelling et al. The yeast cells were measured with AFM as well.

Effect of High-Q Ba4Ti13O30 Materials on the Dielectric Properties of (Bax, Sr(1-x))TiO3 Films for Microwave Communication

Hsiu-Fung Cheng[1], **Thomas Joseph Palathinkal**[2], **Yen-Chih Lee**[2], **and I-Nan Lin**[3]

[1]Department of Physics, National Taiwan Normal University, Taipei 116, Taiwan, R. O. C.
[2]Department of Materials Science and Engineering, National Tsing-Hua University, Hsinchu 300, Taiwan, R. O. C.
[3]Department of Physics, Tamkang University, Tamsui 251, Taiwan, R. O. C.

Abstract— Nano-sized BaTiO3, SrTiO3 and TiO2 powders have been used to synthesize (Bax, Sr$(1-x)$)TiO3 materials via mixed oxide process. Then (Bax, Sr$(1-x)$)TiO3 (BST) ($x = 0.5$ and 0.6) with addition of high-Q (quality factor) Ba4Ti13O30 (BT) materials were screen printed on Al2O3 substrates. The prepared thick films of BST/BT with three layered and five layered composite materials were sintered at 1275°C (4 h). The microwave dielectric properties of the bulk ceramics and the thick films were measured by resonant cavity method at higher microwave frequencies (~ 9.5 GHz). The three layered thick films have dielectric constant ~ 13.4 for $x = 0.5$ and 15.5 for $x = 0.6$. The five layered thick films possess dielectric constant ~ 12.7 for $x = 0.5$ and 15.8 for $x = 0.6$. The frequency $\times$ quality factor ($f \times Q$) increases markedly with a larger magnitude of 1600 for the three layered thick films than the five layered ones. The results imply that the BST/BT composite thick films have potential application in tunable microwave devices.

Pulsed-laser Deposited Ferroelctric Thin Films with Nanostructure for Nano Device Applications

Hsiu-Fung Cheng[1], **Thomas Joseph Palathinkal**[2], **and I-Nan Lin**[3]

[1]Department of Physics, National Taiwan Normal University, Taipei, Taiwan
[2]Department of Materials Science and Engineering, National Tsing Hua University, Hsinchu, Taiwan
[3]Department of Physics, Tamkang University, Tamsui, Taiwan

Abstract— Novel $SrBi_{4.25}La_{0.75}FeTi_4O_{18}$ (SBLFT) ferroelectric thin films have been synthesized by pulsed laser deposition (PLD) technique. The SBLFT thin films were grown on Pt/Si substrate electrodes for electrical measurement and analysis. The crystalline structure and microstructure of SBLFT thin films were examined and determined, respectively, using x-ray diffraction (XRD) and field emission scanning electron microscopy (FESEM). XRD and FESEM, respectively, show that the films are in (1111) preferred orientation and with nanometer grain size. The PLD SBLFT thin films have ferroelectric properties of saturated electric polarization, $P_s = 8.0\,\mu C/cm^2$, and coercive electric voltage, $V_c = 2.5\,V$. The results imply that these smart SBLFT ferroelectric thin films have potential applications in nano devices such as ferroelectric random access memories or electro-optic detectors.

An Innovative Permanently Implanted Wireless Intracranial Pressure Monitor Using Microwave Frequencies: Long Term Durability under Pressure in Aqueous Environment

F. A. Kralick[1], **U. Kawoos**[2], **R. V. Warty**[3], **M. R. Tofighi**[4], **and A. Rosen**[2]

[1]Department of Neurosurgery, Hahnemann University Hospital, Philadelphia, PA 19102, USA
[2]School of Biomedical Engineering, Drexel University, Philadelphia, PA 19104, USA
[3]Department of Electrical Engineering, Drexel University, Philadelphia, PA 19104, USA
[4]Penn State University, the Capital College, Middletown, PA 17057, USA

Abstract— Monitoring of intracranial pressure (ICP) is the most important issue in diagnosis and treatment of patients with neurosurgical issues. Current procedures include indirect methods that do not provide an accurate pressure measurement or invasive catheter based systems which provide accurate measurement but cannot be used for long durations. Current shortcomings of these catheter-based systems include infection, brain damage, and intensive care hospital stays. A novel permanent wireless epidural pressure sensor is proposed. The unit operates at an ISM band of 2.4 GHz and radiates a microwave signal as a function of pressure. In-vitro and in-vivo tests were performed to study the efficiency of this measurement technique with good result. In this study long term durability and stability were analyzed under varying pressures in air and aqueous environments. The aqueous environment was temperature controlled at 37 degrees to simulate the milieu of the intracranial compartment. The results demonstrated long-term sensitivity and accuracy as well as maintained proper electrical and wireless function under these conditions.

Session 2P1
Novel Mathematical Methods in Electromagnetics 2

Analysis of the Parallel Plate Waveguide with Finite Length Impedance Loading

Ayşegül Işıkyer, **İ. Hakkı Tayyar**, **and A. Büyükaksoy**

Gebze Institute of Technology, 41400 Gebze, Kocaeli, Turkey

Abstract— The geometry of the problem is depicted in Fig. 1. An incident TEM mode travelling in the positive x direction is confined between parallel planes located at $y = 0$ and $y = b$. The plates are perfectly conducting for $x < 0$ and $x > l$, and are characterized by constant surface impedances for $0 < x < l$. For the sake of generality we assume that the surface impedances of the lower and upper plates are different from each other and denoted by $Z_1 = \eta_1 Z_0$ and $Z_2 = \eta_2 Z_0$, respectively, with Z_0 being the characteristic impedance of the free space. The aim of this work is to determine the effect of the relative surface impedances η_1 and η_2 on the reflection and transmission coefficients.

This work may also serve as a first order approximation to the groove waveguide. A rectangular shallow groove filled with low loss material in a perfectly conducting plane may be simulated by the following impedance boundary condition $E_x = \eta Z_0 H_z$ applied at the opening of the groove, where $\eta = -i\sqrt{\frac{\mu_r}{\epsilon_r}}\tan(kt\sqrt{\epsilon_r\mu_r})$ is the normalized impedance. ϵ_r and μ_r are the relative constitutive parameters of the material filling the groove, while t denotes the groove's depth. In what follows we will assume that the depths and the materials filling the lower and upper grooves are different corresponding to the surface impedances η_1 and η_2, respectively.

The representation of the solution to the problem in terms of Fourier integrals leads to two simultaneous modified Wiener-Hopf equations which are uncoupled by using the analytical properties of the functions that occur and by introducing infinite sum over certain poles with unknown expansion coefficients. The solution involves two infinite sets of unknown coefficients satisfying two infinite systems of linear algebraic equations.which are solved numerically.

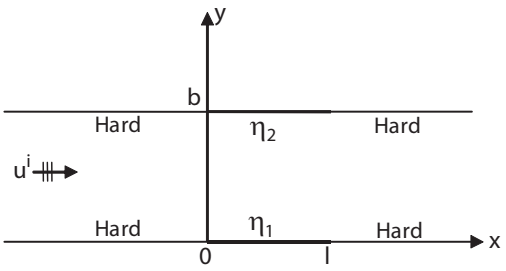

Figure 1: Geometry of the problem.

A New Spectral Method for Scattering by Impedance Polygons

J. M. L. Bernard
CEA-DIF, Département de Physique Théorique et Appliquée
91680, Bruyères le Châtel, France

Abstract— We study a new spectral approach for scattering by two-dimensional polygonal objects with arbitrary surface impedance conditions. In this delicate exterior problem, the Wiener-Hopf method cannot be applied, while asymptotic methods can only be used if corners are widely spaced compared to wavelength, and the presence of imperfectly reflective surfaces particularly complicates the problem.

We present here a general method to handle in a global manner the problem of n-part polygonal objects using the Sommerfeld-Maliuzhinets representation of the field. This representation has long been devoted to the rigorous analysis of isolated wedges. However, some of our recent developments permit us to consider a new integral expression of the spectral function, in some domain of complex angles, where it becomes possible to take globally account of boundary conditions on a complex geometry.

This generalisation of Maliuzhinets methods enables us to derive, for the first time, the functional equations for the spectral functions for scattering by a general impedance polygon with finite or infinite surface, and to reduce generally the problem to a system of Fredholm integral equations of the second kind with non-singular kernels, allowing approximations.

We apply in particular this approach to the important class of three-part impedance polygons composed of a finite segment attached to two semi-infinite planes, and show how to decouple the set of integral equations in some particular cases, then we study particular properties of kernels permitting approximations when the wave number k is large or small.

REFERENCES

1. Bernard, J. M. L., "Scattering by a three-part impedance plane: a new spectral approach," *Quarterly J. of Mech. and Appl. Mathematics*, Vol. 58, No. 3, 383–418, 2005.
2. Bernard, J. M. L., "A spectral approach for scattering by impedance polygons," *Quarterly J. of Mech. and Appl. Math.*, Vol. 59, No. 4, 517–549, 2006.

A Finite Difference Frequency Domain Study of Curvature Lifted Modes Degeneration

C. S. Lavranos and G. A. Kyriacou

Microwaves Lab., Department of Electrical & Computer Engineering
Democritus University of Thrace, 12 Vas. Sofias St., Xanthi 67100, Greece

Abstract— During the last decades conformal microwave circuits and systems received vast research interest, since they serve significant applications. A variety of applications, such as a moving airborne platform or a digital beamforming antenna carry microwave transmit-receive systems such as "smart skin" antennas with their main part asked to be made conformal to the objects surface. This is in agreement with the modern tendency toward miniaturization of printing or integrating the microwave devices on curved surfaces. This curvature varies from canonical objects as cylinders, to almost arbitrary (usually aerodynamic) curvatures. Moreover, a plethora of microwave devices can be considered as comprised of waveguiding sections. Therefore, the accurate design of conformal systems requires the knowledge of curved waveguides characteristics. This paper contributes exactly to this specific research field.

Several analytical methods aiming at the investigation of curved waveguides have been proposed in the literature, e.g., [1, 2]. However, these are restricted to the study of canonical geometries. Numerical methods like the two dimensional Finite Element Method (FEM) or the Method of Moments (MoM) are capable of handling curved geometries. Yet, FEM is unable to handle waveguide curvatures in the propagation direction. On the other hand, MoM involves the Green's functions of the structure which are not usually available for curved geometries. Hence, these methods by no means can serve as a general tool for the analysis of arbitrary curved waveguides.

Our research effort is based on a two-dimensional Finite Difference Frequency Domain (2-D FDFD) eigenvalue method formulated in orthogonal curvilinear coordinates. The theoretical basics have been presented in our previous works [3, 4]. This analysis is formulated as an eigenvalue problem for the complex propagation constants and it is restricted to structures uniform along the propagation direction. The waveguiding structure can be curved in all directions and this constitutes its main advantage. Besides that, it retains the classical FDFD method capability of handling arbitrary shaped curved geometries filled with either isotropic or anisotropic materials. The present work mainly focuses on the effects of curvature on microwave devices. Particular attention will be paid on mode degeneration and birefringence phenomena which are observed when the waveguiding structure is curved in the propagation direction, e.g., [1, 2].

The eigenvalues frequency spectrum (propagation constants dispersion curves) and the corresponding eigenvectors (electromagnetic field distributions) of numerous curved structures are studied. Mode degeneration and birefringence phenomena are observed in these numerical results. The accuracy of the method is examined through comparisons with already published results.

REFERENCES

1. Lewin, L., D. C. Chang, and E. F. Kuester, *Electromagnetic Waves and Curved Structures*, Peregrinus, London, U.K., 1977.
2. Fang, X.-S. and Z.-Q. Lin, "Birefringence in curved single-mode optical fibers due to waveguide geometry effect — Perturbation analysis", *Journal of Lightwave Technology*, Vol. LT-3, No. 3, June 1985.
3. Lavranos, C. S. and G. A. Kyriacou, "Eigenvalue analysis of curved open waveguides using a finite difference frequency domain method employing orthogonal curvilinear coordinates," *Progress In Electromagnetics Research Symposium*, 271–275, Hangzhou, China, August 2005.
4. Lavranos, C. S. and G. A. Kyriacou, "Eigenvalue analysis of curved waveguides employing FDFD method in orthogonal curvilinear co-ordinates," *IEE Electronic Lett.*, Vol. 42, Issue 12, 702–704, June 2006.

Three Dimensional Open Cavities Eigenanalysis, Employing Finite Elements in Conjunction with Spherical Harmonics

P. C. Allilomes and G. A. Kyriacou

Department of Electrical and Computer Engineering, Democritus University of Thrace
Vas Sofias 12str., Xanthi 67100, Greece

Abstract— One of the most active research fields in electromagnetics is the analysis of cavities. An open challenge of this research field is the eigenfrequency analysis of open radiating cavities. The broad applications of open cavities span from antenna design to optical laser cavities. Thus, a computer based analysis tool capable of computing the eigenfrequencies of arbitrary open cavities, will significantly shorten the design time of many electromagnetic devices.

Most of the computerized techniques able to solve cavity problems in a unified manner are based on numerical techniques such as the finite elements (FEM) and the finite difference method (FD). In principle these methods can handle any non radiating closed structure. Instead, in radiation problems FEM and FD are usually applied with success only for scattering problems and not for eigenvalue analysis. In the case of radiation problems FEM and FD can be applied after their hybridization with certain techniques that render the open/unbounded solution domain to an equivalent closed one. In fact, the mesh of FEM and FD must be truncated by an artificial boundary in a manner taking into account the radiation phenomena, preventing reflections of outgoing waves back to the cavity. The most common mesh truncation techniques are the use of a perfect matching layer (PML) and the employment of Turkel's type absorbing boundary conditions (ABC). The above remedies for the simulation of infinite solution domain with general numerical methods can not be applied easily to eigenvalue analysis problem. Particularly the Turkel's ABC's are local boundary conditions, so they are not exact and thus can not achieve the accuracy needed for the eigenfrequency analysis. The PML approach produces false or spurious resonances as it distorts the initial cavity geometry. An effort to applying FEM on open optical cavities can be found in, [1].

In the present work a hybrid FEM formulation capable of handling the eigenvalue analysis of open, arbitrary shaped cavities is described. The formulation is based on a vector Dirichlet-to-Newmann mapping. The mapping is derived considering a spherical fictitious boundary for the mesh truncation and an expansion to spherical harmonics. This leads to a non-linear "exact" eigenvalue problem, enabling the computation of the eigenfrequencies of the cavity. This approach is considered optimal due to the nonlocal exact nature of the vector Dirichlet-to-Newmann mapping boundary conditions [2]. The nonlinearity of the eigenvalue problem is handled by an extension of the techniques derived in the author's previous work, [3].

REFERENCES

1. Hyun, S., J. Hwang, Y. Lee, and S. Kim, "Computation of resonant modes of open resonators using the FEM and the anisotropic perfectly matched layer boundary condition," *Microw. Opt. Technol. Lett.*, Vol. 16, No. 6, 352–356, 1997.
2. Keller, J. B. and D. Givoli, "Exact non-reflecting boundary conditions," *J. Comp. Phys.*, Vol. 82, 172–192, 1989.
3. Allilomes, P. C. and G. Kyriacou, "A nonlinear eigenvalue hybrid fem formulation for two dimensional open waveguiding structures," *PIERS Online*, Vol. 1, No. 5, 620–624, 2005.

On the Theory of TM Electromagnetic Guided Waves in a Nonlinear Three-layer Dielectric Structure

H. W. Schürmann[1], **V. Serov**[2], **Yu. Shestopalov**[3], **and Yu. Smirnov**[4]

[1]Department of Physics, University of Osnabrück, Osnabrück D-49069, Germany
[2]Department of Mathematical Sciences, University of Oulu, P.O. Box 3000, FIN-90014, Finland
[3]Department of Mathematics, Karlstad University, Karlstad SE-65188, Sweden
[4]Department of Mathematics, Penza State University, Penza 440017, Russia

Abstract— We consider transverse-magnetic (TM) guided waves in a structure that consists of a homogeneous nonmagnetic dielectric film characterized by a (rather) general nonlinearity tensor and situated between two semi-infinite linear half-spaces. We derive the exact differential equation for the field components and the associated integrability condition. Evaluation of the field components and of the dispersion relation (DR) is reduced to an Abelian integral. The approach is elucidated by considering a Kerr-type nonlinear film.

The exact analytical solution of Maxwell's equations for a lossless nonlinear three-layer dielectric waveguide is a basic problem of classical electrodynamics. Compared with the mathematical treatment of TE-polarized waves the analysis in the case of TM-polarized guided waves is more difficult. In this case the magnetic field $\mathbf{B}$ is the appropriate quantity but the nonlinear dielectric function ε is simple if expressed in terms of the electric field $\mathbf{E}$. If expressed by the magnetic field, ε is determined by a complicated equation that contains $\mathbf{B}$ and derivatives of $\mathbf{B}$ [1]. The investigation is further complicated because, for TM-polarized waves, the occurrence of two field components in general leads to a dielectric tensor even for an isotropic film [2], and it seems that the approach developed by Leung to study p-polarized nonlinear surface polaritons cannot be generalized if ε is a tensor (see [1]). Another exact and analytical approach to the problem has been proposed in [3] where the guided TM-waves are considered in a structure consisting of two semi-infinite nonlinear dielectric media and the problem is reduced to a (decomposition) equation for the two field components and to a quadrature. Furthermore the solution is used for deriving a DR. To the best of our knowledge all other publications on waveguiding in a nonlinear three-layer structure are either numerical or use approximations. In this study we largely follow the lines proposed in [3] but consider a nonlinear slab structure. For (general) nonlinear tensorial permittivities that satisfy an integrability condition we reduce Maxwell's equations to an exact differential equation (for the two field components). Integration yields an equation so that one field component can formally be expressed in terms of the other, leading to the possibility of finding one field component by integration. Evaluation of the boundary conditions for the slab structure leads to a general DR. Finally, we elucidate the general approach by applying it to a Kerr-like nonlinearity.

REFERENCES

1. Leung, K. M., "P-polarized nonlinear surface polaritons in materials with intensity-dependent dielectric functions," *Physical Review B*, Vol. 32, No. 8, 5093–5101, 1985.
2. Seaton, C. T., J. D. Valera, B. Svenson, and G. I. Stegeman, "Comparison of solutions for TM-polarized nonlinear guided waves," *Optics Letters*, Vol. 10, 149–157, 1985.
3. Joseph, R. I. and D. N. Christodoulides, "Exact field decomposition for TM waves in nonlinear media," *Optics Letters*, Vol. 12, No. 10, 826–828, 1987.

A Hybrid Offset Moment Method and Mode Matching Technique for Cylindrical Horn Antennas Analysis

S. Diamantis, **A. P. Orfanidis**, **and G. A. Kyriacou**
Democritus University of Thrace, Xanthi, Greece

Abstract— Horn antennas are widely used as feeds of large reflectors and lens antennas, as elements in phased arrays and as standard-gain components in antenna measurements. A lot of works were devoted to horn antenna analysis during the last decades. However most of them do not take into account the discontinuity between the horn aperture and the free space. Most of these techniques describe the horn itself through a stepped waveguide approximation and each junction as well as the whole horn is analyzed employing the mode matching technique. The aperture is included in this scheme as an additional discontinuity for which different approaches are proposed for its analysis. Wriedt et al. [1] as well as Liu et al. [2] employed the Method of Moments (MoM), while Encinar et al. [3] considered a plane wave expansion for the field in the free space which was in turn matched (through the continuity conditions) to the field of the last waveguide section. The present effort aims at the analysis of the aperture discontinuity for cylindrical horn antennas.

In our previous work [4], a hybrid technique was employed for the analysis of the rectangular horn antenna including the discontinuity effect between the aperture and free space. The transition from the feeding waveguide up to the radiating aperture has been analyzed using the Mode Matching Technique (MMT), while the discontinuity between the horn aperture and free space has been modeled using an "offset moment method". First, a field equivalence principle is adopted in order to define an equivalent closed geometry by considering equivalent magnetic current densities on an auxiliary surface parallel to the aperture but slightly shifted toward the horn interior. In this paper the method proposed in [4] will be extended in order to analyze cylindrical horn antennas. Following a similar way, the interior conical region of the horn is approximated by circular waveguide sections, namely employing the stepped waveguide approach. Similar to [4], Love's field equivalence principle is employed for the definition of magnetic current densities on an auxiliary surface. This is again parallel to the aperture but slightly shifted inwards. The above procedure can be explained in a more rigorous mathematical formulation as a vector Diriclet-to-Neumann map. The generalized scattering parameters of the discontinuity between the horn aperture and the free space are obtained by enforcing the field continuity conditions on the aperture surface. Note that the offset moment method is actually a modification of the moment method, where the sources are displaced from the surface on which the boundary conditions are imposed. Numerical results for the input reflection coefficient, the antenna input impedance and the far field radiation patterns will be presented at the symposium.

REFERENCES

1. Wriedt, T., K. H. Wolff, F. Arndt, and U. Tucholke, "Rigorous hybrid field theoretic design of stepped rectangular waveguide mode converters including the horn transition into half space," *IEEE Trans. On Antenna and Propagation*, Vol. AP-37, No. 6, 780, June 1989.
2. Liu, K., C. A. Balanis, C. R. Birtcher, and G. C. Barber, "Analysis of pyramidal horn antennas using moment methods," *IEEE Transactions On Antennas and Propagation*, Vol. 41, No. 10, 1379–1389, October 1993.
3. Encinar, J. A. and J. M. Rebollar, "A hybridtechnique for analyzing corrugated and noncorrugated rectangular horns," *IEEE Trans. On Antenna and Propagation*, Vol. AP-34, No. 8, 961, August 1986.
4. Diamantis, S. G, A. P. Orfanidis, G. A. Kyriakou, and J. N. Sahalos, "Hybrid mode matching and auxiliary sources technique for horn antenna analysis," *Microwave and Optical Technology Letters*, Vol. 49, Issue 3, 734–739, March 2007.

Analysis of Electromagnetic Diffraction by a Dielectric Body in Several Domains Using the Volume Singular Integral Equations

Y. Smirnov and A. Tsupak
Penza State University, Russia

Abstract— The three-dimensional time-harmonic problems of diffraction of electromagnetic by an anisotropic dielectric body Q in 3D-domains P are examined. The following types of domains are considered: free space ($x_1,\ x_2,\ x_3 \in R$), half space ($x_3 > 0$) and infinite layer ($x_3 \in (0, a)$). The boundaries of the domains in cases 2 and 3 are considered to be perfectly conducting.

The surface of body Q is piece-wise smooth, i.e., conical and corner points are available.

The body Q has constant magnetic permeability μ_0 and positive 3-by-3 matrix (tensor) permittivity $\hat{\varepsilon}(x)$. The components of $\hat{\varepsilon}(x)$ are bounded functions in $\bar{Q}$: $\hat{\varepsilon} \in L_\infty(Q)$, and also $\hat{\varepsilon}^{-1} \in L_\infty(Q)$. The outside media $P \backslash \bar{Q}$ is characterized by constant permittivity and permeability $\varepsilon_0 (> 0),\ \mu_0 (> 0)$.

The diffraction problem is stated in terms of generalized boundary-value problem for the system of Maxwell's equations. The field $\vec{E}$, $\vec{H}$ is found in space $L_2(P)$. Maxwell's equations as well as boundary conditions on perfectly conducting surfaces are considered in distributional sense.

The method of volume integral singular equations is applied to solve the problem. In order to reduce the original problem to integral equation the Green function $\hat{G}_E$ is used. It can be defined in the following way

$$\hat{G}_E = \frac{1}{4\pi} \frac{e^{ik_0|x-y|}}{|x-y|} \hat{I} + \hat{g}(x, y), \quad x, y \in P,$$

where $\hat{g}(x, y)$ is a continuous tensor, dependent on the type of domain P.

The following integral equation is acquired:

$$\vec{E}(x) + \frac{1}{3}\left[\frac{\hat{\varepsilon}(x)}{\varepsilon_0} - \hat{I}\right]\vec{E}(x) - v.p.\int_Q \hat{\Gamma}_1(x, y)\left[\frac{\hat{\varepsilon}(y)}{\varepsilon_0} - \hat{I}\right]\vec{E}(y)dy - \int_Q \hat{\Gamma}_2(x, y)\left[\frac{\hat{\varepsilon}(y)}{\varepsilon_0} - \hat{I}\right]\vec{E}(y) = \vec{E}^0(x)$$

Tensor $\hat{\Gamma}_1$ has hypersingularity and $\hat{\Gamma}_2$ is continuous and depends on the type of domain P.

The equivalence of differential and integral problems is proved. The existence and uniqueness of solutions of the diffraction problem in free space is proved. The Fredholm property for integral operator of problems in half space and infinite layer is also proved.

Galerkin method is used for numerical solution of integral equation. Finite elements of low order are applied as basic and test functions in Galerkin method. The explicit expressions for augmented matrix are written. The convergence of Galerkin method is proved for a wide class of dielectric bodies.

ACKNOWLEDGMENT

This work is supported by Russian Foundation of Basic Research, grant 06-07-89063.

Optimization of a Microwave Amplifier Using Neural Performance Data Sheets with a Memetic Algorithm

Y. Cengiz[1], **F. Güneş**[2], **and U. Kılıç**[3]

[1]Department of Electronics and Communication Engineering
Süleyman Demirel University, Isparta, Turkey
[2]Department of Electronics and Communication Engineering
Yıldız Technical University, Beşiktaş, Istanbul, Turkey
[3]Akdeniz University, Antalya, Turkey

Abstract— Optimization is one of the fundamental processes frequently encountered in the engineering problems and is highly nonlinear in terms of the descriptive parameters of the system. An optimization process generally contains two fundamental problems:

(i) The first is to form a feasible Design Space which is defined in terms of the design variables and targets;
(ii) The second is that the global minimum of the error (objective) function governing the optimization must be obtained with respect to the design variables within the feasible design space.

For optimization of a microwave amplifier, design variables are generally the matching circuit parameters whose lower and upper limits are very often determined by the technology to be utilized in the realization stage of the design. Nevertheless, design targets are still one of the main problems of the amplifier optimization. Generally, the optimization is focused on the transducer power gain (G_T) over a frequency band of operation without controlling the other performance criteria such as the noise (F), the input standing wave ratio (V_i). Certainly, within the optimization process one can easily embed the desired performance goals without knowing the physical limits and/or compromise relations among F, V_i and G_T appropriately. Unfortunately this process often fails to attain the desired goals. However, the Neural Performance Data Sheets (NPDS) of the transistor overcomes all the above-mentioned handicaps and embeds the compatible (F, V_i, G_T) triplets with their source (Z_S) and load (Z_L) terminations together over a predetermined frequency band of operation, which is given in the accompanied paper [1]. So optimization of a microwave amplifier is a multi-objective design problem with a mix of equality and inequality constraints.

The Memetic algorithm with the decimal mode is utilized in the multi-objective optimization process for the global minimum of the objective function which is expressed as a function only gain of a matching circuit, in the negative exponential form to ensure the rapid convergence. Here optimization of a microwave amplifier with the different type matching circuits is given as a worked example and its resulted performance ingredients are compared with the design targets.

REFERENCES

1. Güneş, F. and C. Tepe, "Identification of a microwave transistor using 'neural performance data sheets'," submitted in the *Progress in Electromagnetics Research Symposium 2003*, Hawai, 2003.

Gain Gradients Applied to Design of the Terminations of the (Noise, Gain, Input VSWR) Triplets for a Microwave Transistor

Salih Demirel and Filiz Güneş

Department of Electronics and Communication Engineering, Yıldız Technical University
İstanbul, Turkey

Abstract— Characterization of active microwave devices and design of the wideband microwave amplifiers are still among the major interests in the communication engineering. Especially, in designing microwave amplifiers, many sophisticated numerical methods are utilized to optimize the system performance. In this work, a typical design application of a microwave amplifier is presented with the determined feasible design space and applied gradient algorithm using analytical gain gradients. Generally, the optimization is focused on the transducer power gain (G_T) over the frequency band of operation without controlling the other performance criteria such as the noise (F), the input VSWR (V_i), and the output VSWR (V_o). It should also be mentioned that the optimization process of the performance is highly nonlinear in terms of the descriptive parameters of the system. Certainly, within the optimization process, one can easily imbed the desired performance goals without knowing the physical limits and/or compromise relations among F, V_i and G_T and bandwidth B appropriately. But unfortunately, this process, often fails in hitting the desired goals. However, in this work to overcome all these above-mentioned handicaps firstly the potential performance characteristics of the active element employed in the amplifier are obtained to form the target space of the optimization. Physical lengths and characteristic impedances of the transmission lines used in the matching circuits are chosen as the design variables and their lower and upper limits are bounded by the limits of the planar transmission line technology, so that resulted microwave amplifier can be realized by this technology. Design Target Space is determined by the Compatible Performance [Noise (F), Input VSWR (V_i), Gain (G_T)] triplets and their source $Z_S(\omega_i)$ and load $Z_L(\omega_i)$ terminations resulted from the Performance Characterization theory of the active device. These triplets take into account the physical limitations of the device and realizibility conditions so that $F_{\mathrm{req}} \geq F_{\mathrm{min}}$, $V_{i\,\mathrm{req}} \geq 1$, $G_{T\,\mathrm{min}} \leq G_{T\,\mathrm{req}} \leq G_{T\,\mathrm{max}}$; and $Z_S(\omega_i)$ and $Z_L(\omega_i)$ terminations take place within the "Unconditionally Stable Working Area (USWA). Here, F_{min} is the minimum noise figure of the device and $G_{T\mathrm{min}}$, $G_{T\mathrm{max}}$ are the minimum and maximum gain values constrained by F (noise) and V_i (Input VSWR), which are also determined by the Performance Characterization theory. A simple design process is followed where the $Z_S(\omega_i)$ and $Z_L(\omega_i), i = 1 \ldots N$ terminations are synthesized using the Darlington theorem. So optimization of the amplifier is reduced to the gain optimization of two passive, reciprocal two-ports. The numerical results of amplifiers for the design targets of noise figure $F_{\mathrm{req}} = 0.46$ dB and $V_{i\mathrm{req}} = 1$, $G_{T\mathrm{req}} = 12$ dB in the frequency range 4–11 GHz are given in comparison to each other. A typical design example is given synthesized, target, simulated with the resulted, characteristics. Finally, the complete analysis of the whole system is done using the optimized parameters and the resulted performance are compared with the results of a Professional soft packet and shown that all of them are agreed well.

A Simple and Accurate Model for Wire Diagnosis Using Reflectometry

F. Auzanneau, M. Olivas, and N. Ravot
CEA LIST, France

Abstract— Reflectometry is provides useful information for the diagnosis, i.e., detection, localization and characterization of electrical defects in wired networks. We propose a theoretical model for the simulation of reflectometry signals for any kind of network topology. Based on microwave propagation theory, it provides explicit formulas for both Time Domain and Frequency Domain Reflectometry signals, and helps understand and explain reflectometry measurements results.

Today's automotive electronic systems rely heavily on wired networks, and their near-future counterparts ("by wire" functions) will be based on high reliability wired interconnections. Aging wire has been identified as a major risk factor for aircrafts, this is true for safety critical systems (systems whose failure may cause injury to human beings) such as cars, nuclear plant control systems, medical intensive care and life support systems.

To improve the reliability of wired networks or to help for maintenance purposes, the reflectometry method is the most promising approaches. Based on the injection of probe signal(s) into the network and the analysis of the reflected signals, this method provides useful information for the diagnosis of electrical defects in the wires.

This paper proposes an accurate model of reflectometry signals for any wired network. Based on standard microwave propagation theory, this model provides simple explicit formulas for the simulation of both time domain and frequency domain reflectometry signals. Comparison with experimentation is very good, and it can be applied to very complex network topologies to provide a clear explanation of measured TDR or FDR signals.

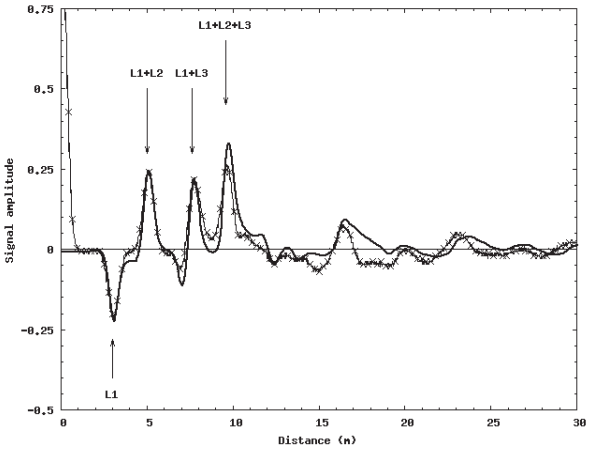

Figure 1: Simulation (solid) comparison with measurement (x) for a Y-shaped network.

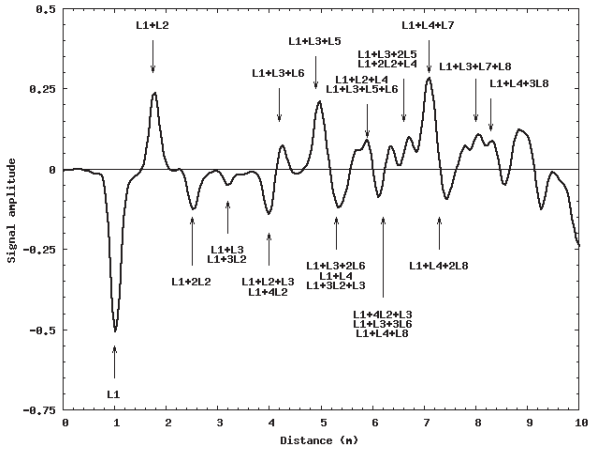

Figure 2: TDR simulation results for a very complex network topology.

REFERENCES

1. Furse, C. and R. Haupt, "Down to the wire: The hidden hazard of aging aircraft wiring," *IEEE Spectrum*, 35–39, Feb. 2001.
2. Hartebrodt, M. and, K. Kabitzsch, "Fault detection in fieldbuses with time domain reflectometry," *Proc. AFRICON2004 7th IEEE Africon Conference*, Vol. 1, 391–396, September 2004.

Propagation Characteristics of Multilayered Dielectric Gratings with the Air-hole Type Elliptic Cylinders

Ryosuke Ozaki, **Tsuneki Yamasaki**, **and Takashi Hinata**
Department of Electrical Engineering, College of Science and Technology, Nihon University
1-8-14, Surugadai Kanda Chiyoda-ku, Tokyo 101-8308, Japan

Abstract— Dielectric gratings are widely used in integrated optics and acousto-optics, such as optical gratings, optical couplers, optical waveguide filters, and Photonic Crystal. Recently, the refractive index can easily be controlled to make periodic structures by the development of manufacturing technology of optical devices. Accordingly, the numerical methods which are applicable to dielectric gratings have been proposed. However, it is not treated the propagation characteristic in detail for Photonic Band Gap.

In this paper, the guiding problems of electromagnetic waves by Multilayered Dielectric Gratings with the air-hole type elliptic cylinders are analyzed using the combination of Fourier series expansion method and multilayer method. Our approach for the multilayer method differs from that of other method, so that the order of characteristic matrix equation depends on the modal truncation number, but does not depend on the number of layers. Therefore our method is effective to the guiding problems.

Numerical results are given for the propagation characteristics for multilayer dielectric gratings with the air-hole type elliptic cylinders both for TE and TM modes. The differences in the propagation characteristics of the shape of elliptic cylinder are discussed.

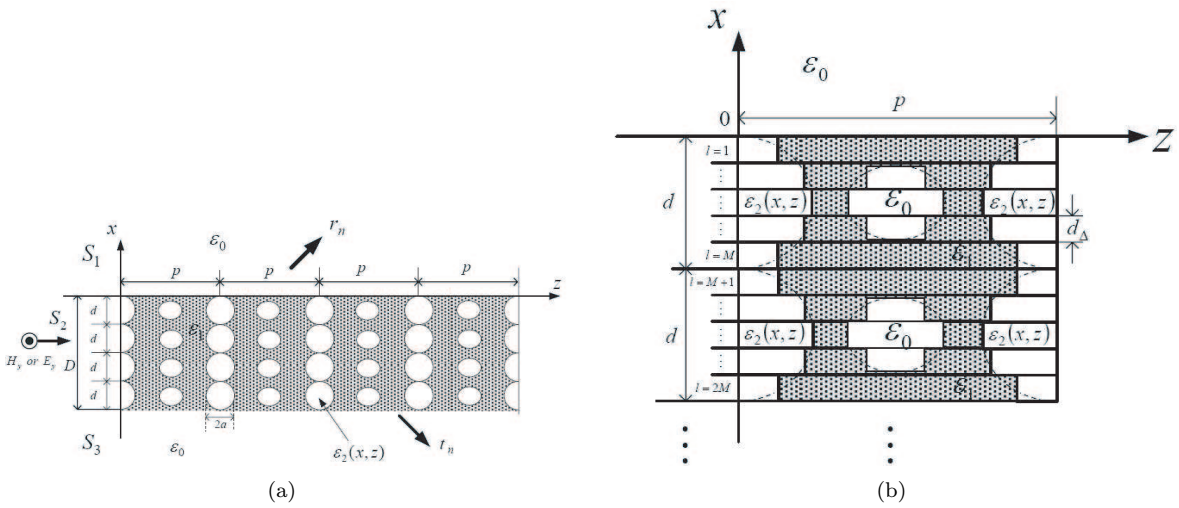

Figure 1: Multilayered dielectric gratings with the air-hole type elliptic cylinders, a) Coordinate system, b)Approximated inhomogeneous layers.

Scattering of Electromagnetic Waves by Periodically Inhomogeneous Dielectric Gratings Consisting of Inhomogeneous Layer

Tsuneki Yamasaki, **Ryosuke Ozaki**, **and Takashi Hinata**

Department of Electrical Engineering, College of Science and Technology
Nihon University, Tokyo, 101-8308, Japan

Abstract— Dielectric gratings have found applications in various areas such as integrated optics and acousto-optics, optical filters, and holography. Recently, the refractive index can easily be controlled to make the periodic structures such as fiber grating, photonic crystal waveguide, and frequency selective devices by the development of manufacturing technology of optical devices.

In this paper, the Fourier series expansion method using the plane multilayer method has been applied to the analysis of the scattering problems by periodically inhomogeneous dielectric gratings consisting of inhomogeneous layer.

In the grating region $S_2(-D < x < 0)$; Fig. 1(a) shows the configuration whose shape of the grating is inhomogeneous cylinder with the cross section of $(a \times a)$, the permittivity profile $\varepsilon_2(x, z)$ is generally not separable with respect to the x and z variables. Main process of our method to treat these problems is as follows: (1) The grating layer is approximated by an assembly of M stratified layers of modulated index profile with step size $d_\Delta \triangleq d/M$ in the grating region (2) Taking each layer as a modulated dielectric grating, electromagnetic fields are expanded appropriately by a finite Fourier series. (3) Finally, the gratings are matched using appropriate boundary conditions to get the multlayered grating using the solution of the first region.

In the region of inhomogeneous layer $S_3(-D < x < -D - d)$, the permittivity profile $\varepsilon_3(x)$ is different type rather than that of region S_2. Therefore, the main process of our method to treat these problems as well as region S_2 is as follows (see Fig. 1(b)): (1) The electromagnetic fields are expanded appropriately by a finite Fourier series with the period d. (2) The inhomogeneous layers are matched using appropriate boundary conditions between region S_2 and region S_4.

Although these inhomogeneous regions are different types of the inhomogeneous dielectric gratings, we have proposed the new approach using the solution of periodically inhomogeneous media.

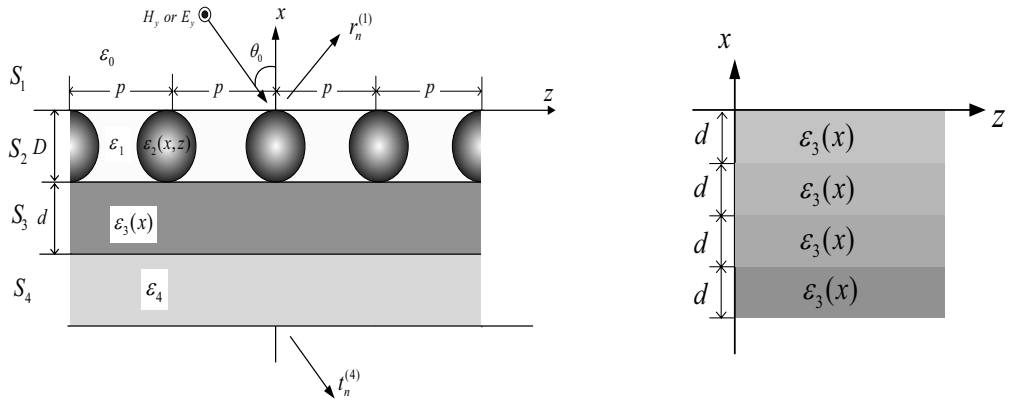

Figure 1: Structure of periodically inhomogeneous dielectric gratings consisting of inhomogeneous layer. (a) Coordinate system, (b) Periodically inhomogeneous layers in region S_3.

Comparative Studies on Amplitude and Phase Control Radiation Patterns

Y. V. Narayana[1] and G. S. N. Raju[2]

[1]Department of ECE, ANITS, Sangivalasa, Visakhapatnam, India
[2]Department of ECE, AU College of Engineering, Visakhapatnam, India

Abstract— Arrays are used to control gain and radiation characteristics to meet the requirements of a given application. It is possible to generate a narrow beam or a shaped beam either by amplitude [1, 2] or phase control [3, 4]. In fact, it is also possible to control the pattern characteristics by the element space distribution in the array [5]. Several methods are reported in the literature on the design of amplitude distribution to produce a specified beam. Similarly different techniques are available for the design of phase distribution function for fixed amplitude distribution for producing a specified beam shape.

However, in the present work the amplitude distribution is designed using Fourier Transform technique to produce sector beam over a few angular sectors. For predetermined amplitude distribution phase function is designed again to produce sector beams over the above mentioned set of angular regions. The patterns are numerically computed for a continuous line source. The patterns are overlapped for the sake of comparison. It has been possible to optimize the beam shapes by both the methods. It may be noted that the patterns of the first method are useful for non-scan applications and those with the second method are useful for fast scan applications if implemented using digital phase shifters.

REFERENCES

1. Balanis, C. A., *Antenna Theory Analysis and Design*, John Wiley & Sons, Inc., New York, 1982.
2. Stainberg., B. D., *Principles of Aperture and Array System Design*, John Wiley & Sons.
3. Orchard, H. J., R. S. Elliott and G. J. Stern, "Optimizing the synthesis of shaped beam antenna patterns," *IEE Proceedings*, Part H, 63–68, 1985.
4. Chakraborty A. and B. N. Das, "Scanning of sector and cosecant beams generated by a circular aperture," *IEEE Trans. Antennas Propagat.*, Vol. AP–32, No. 9, 1000–1003, September 1984.
5. King, D. D., R. F. Packard, and R. K. Thomas, "Unequally spaced broadband antenna arrays," *IRE Trans. Antennas and Propagation*, Vol. AP-8, No. 4, 380–385, July 1960.

Session 2P2
Plasmonics, Nano-composites and Metamaterials, Extraordinary Light Transmission 2

Effect of Motion of the Scatterers on Localization: Quasi Localization and Quasi Mobility Edge

E. Kogan
Jack and Pearl Resnick Institute, Physics Department, Bar Ilan University
Ramat Gan 52900, Israel

Abstract— We consider free quantum particle in a slowly changing scattering potential (the dimensionality of space is 3). It is well known that *static* scattering potential can cause localization. More exactly, there exists mobility edge — the energy which separates delocalized states (above the mobility edge) and localized states (below the mobility edge). The question which we address in this paper is what happens with this picture when the scattering potential is not static, but is weakly time-dependent. For example, we can consider two mixed gases, one of light quantum particles, and the other of heavy particles, which can be either quantum or classical.

To answer this question we calculate the diffusion coefficient of light particles states as a function of energy in the framework of Selfconsistent Localization Theory. We claim the existence of the crossover region, which we call the quasimobility edge, which separates states with high and low diffusion coefficient. The latter is determined by the dephasing time. The consideration is based on the calculation of Cooperon for the time-dependent scattering potential. For the Cooperon $C(\mathbf{R},t)$ we obtain equation

$$\left\{\partial/\partial t - D\nabla^2 + [f(0) - f(t)]\right\} C(\mathbf{R},t) = 0, \tag{1}$$

where

$$f(t) =< V(\mathbf{r},t)V(\mathbf{r},0) > \tag{2}$$

is the correlator for the time-dependent random scattering potential. Eq. (1) can be easily understood if we compare diagrams for the Diffuson and the Cooperon on Fig. 1. The Diffuson does not have any mass because of Ward identity. In the case of the Cooperon, the Ward identity is broken: interaction line which dresses single particle propagator is given by static correlator, and interaction line which connects two different propagators in a ladder is given by dynamic correlator. The difference $[f(0) - f(t)]$ shows how strongly the Ward identity is broken and, as we'll see below, determines the mass of the Cooperon. Solving Eq. (1) we get

$$C(r,t) = C_{\rm el}(r,t) \exp\left\{\int_0^t [f(t') - f(0)]\, dt'\right\}, \tag{3}$$

where $C_{\rm el}$ is the Cooperon calculated ignoring the in-elasticity of scattering. The time-reversal invariance in the system we are considering is broken due to dephasing; the diffusion pole of the particle-particle propagator disappears, although particle-hole propagator still has a diffusion pole, which is guaranteed by particle number conservation. For the diffusion coefficient D we obtain equation

$$\frac{D_0(E)}{D(E)} = 1 + \frac{1}{\pi\nu(E)} \int_0^\infty \sum_{\mathbf{k}} C(k,t) dt \tag{4}$$

where ν is the density of states, D_0 is the diffusion coefficient calculated in Born approximation and the momentum cut-off $|\mathbf{k}| < 1/\ell$, where ℓ is the mean free path, is implied.

Magnetooptical Effects in Plasmonic Nanoscale Structures

V. I. Belotelov[1,2], L. L. Doskolovich[3], and A. K. Zvezdin[1]

[1]A.M. Prokhorov General Physics Institute RAS, 38, Vavilov st., Moscow 119991, Russia
[2]M.V. Lomonosov Moscow State University, Leninskie gori, Moscow 119992, Russia
[3] Image Processing Systems Institute RAS, 151, Molodog. st., Samara 443001, Russia

Abstract— It was shown recently that the optical properties of the periodical arrays of the subwavelength holes in the metal films is mainly governed by the surface plasmon-polaritons (SPPs) leading to the effect of the extraordinary optical transmission (EOT) [1]. At the same time, magnetooptical properties of similar systems are also expected to demonstrate some interesting peculiarities and effects.

We have studied optical properties of a bilayer metal/dielectric heterostructure [2]. The metallic part of the structure is a diffraction grating of subwavelength period constituted by the arrays of either slits or holes. The dielectric layer is a ferromagnetic magnetized in polar geometry, i.e., perpendicularly to its plane. As test media for the metal and dielectric Au and BiYIG are used, respectively. Numerical modeling was performed on the basis of the rigorous coupled-wave analysis extended for the case of magnetic media. The effect of simultaneous enhancement of transmittance and MO Faraday and Kerr effect is found. It is shown that the proper choice of the gyrotropic nanostructure geometry allows acquiring the high transmittance (about 35%) and extraordinary Faraday effect (enhanced by an order of magnitude) for the wavelengths of the near-infrared range (850–1100 nm).

Though the problem of light interaction with perforated metal-dielectric systems is very complex, qualitative explanations for the revealed phenomena are given, suggesting SPPs coupling with quasi-guided waves in the thin dielectric layer being in its roots. It is shown that while the EOT phenomenon is largely due to the formation of the localized modes in the region of the metal/dielectric interface, the extraordinary Faraday rotation is mostly related to the conversion of the TM- and TE-modes in the dielectric layer. The difference in the origin of both effects allows adjusting optical and MO features of the heterostructure in the proper way and achieving the desired coincidence of the transmittance and Faraday rotation resonances. The latter makes considered heterostructures of great interest for possible application for the magnetic field sensors and new elements of the integrated optics.

ACKNOWLEDGMENT

This work was supported by RFBR (06-02-17507, 05-02-17064, 07-07-97601, 07-01-96602, 07-07-91580, 07-02-91588), and Russian foundation "Dynasty".

REFERENCES

1. Ebbesen, T. W., H. J. Lezec, H. F. Ghaemi, T. Thio, and P. A. Wolff, *Nature*, Vol. 391, 667, 1998.
2. Belotelov, V. I., L. L. Doskolovich, and A. K. Zvezdin, *Phys. Rev. Lett.*, Vol. 98, 77401, 2007.

Extraordinary Light Transmission through Nanohole Arrays in Presence of Magnetic Field

Yakov M. Strelniker[1], **David J. Bergman**[2], **and David G. Stroud**[3]

[1]Department of Physics, Bar-Ilan University, IL-52900, Ramat-Gan, Israel
[2]School of Physics and Astronomy, Tel Aviv University, Tel Aviv, IL-69978, Israel
[3]Department of Physics, Ohio State University, Columbus, OH 43210, USA

Abstract— We have developed a theory which explains (in the quasistatic limit) the experimentally observed by Gordon et al. [1] squared dependence of the ratio of polarizations on the aspect ratio of the holes, as well as other features of extraordinary light transition [2]. Several ways to control the extraordinary light transition are discussed [3, 4]. For example, we show that a magnetic field applied parallel to the film would significantly alter this transmission [3]. The alteration occurs because the magnetic field makes the metal dielectric tensor anisotropic. The other way is to dip the perforated metal film into a pool of nematic liquid crystals (NLC). A static electric field $\mathbf{E}_0$ (or a static magnetic field $\mathbf{B}_0$) would then be applied parallel to the film, causing the NLC's director, n, to line up parallel to the applied field both within the holes and in the two layers above and below the metallic film [4]. Since the transmission would differ substantially for n parallel and perpendicular to the polarization of the incident wave, the transmission coefficient through the film could be controlled simply by rotating $\mathbf{E}_0$ (or $\mathbf{B}_0$).

REFERENCES

1. Gordon, R., *et al*, *Phys. Rev. Lett.,* Vol. 92, 037401, 2004.
2. Genet, C., T. W. Ebbesen, *Nature*, Vol. 445, 39-46, 2007, and references therein.
3. Strelniker, Y. M., and D. J. Bergman, *Phys. Rev. B*, Vol. 59, R12763-R12766, 1999.
4. Strelniker, Y. M., D. Stroud, and A. O. Voznesenskaya, *Eur. Phys. J. B*, Vol. 52, 1-7, 2006.

Nano-magnetophotonics: Control of Light and Spin Waves by Introducing Artificial Nano-scaled Structures

M. Inoue[1,2], **R. Fujikawa**[1], **H. Uchida**[1], **K. H. Shin**[1], **A. Khanikaev**[1]
A. Baryshev[1], **A. Fedyanin**[2], **A. Granovsky**[2]

[1]Toyohashi University of Technology, Toyohashi, Aichi 441-8580, Japan
[2]M. V. Lomonosov Moscow State University, Leninskie Gory, Moscow 119992, Russia

Abstract— Introduction of artificial nano-scaled structures to magnetic materials gives us a variety of opportunities for controlling light and spin waves traveling in the structured materials. Magnetophotonic crystals (MPCs) [1, 2] can be classified into such materials, where optical-order periodic structures composed of magnetic and/or dielectric materials are introduced so as to create photonic band gap and to confine light in the vicinity of additional defects in the periodic structures. One- and two-dimensional MPCs have already found their optoelectronic applications such as magneto-optic (MO) spatial light modulator [3] and optical waveguide isolator [4].

Enhancement of MO Faraday and Kerr effects can be achieved by utilizing the surface plasmon resonance [5]: For instance, when Au nano-particles are embedded in magnetic garnet thin film, the Faraday rotation angle of film shows considerable enhancement at the wavelength of plasmon resonance. This is also the case for Kerr rotation, suggesting that the MO responses can be manipulated by the use of localized evanescent field associated with the plasmon resonance. More sophisticated structures for the plasmon-assisted magnetophotonics have been also proposed and discussed based upon the theoretical calculations [6, 7].

It was Nikitov et al. [8] who showed experimentally and theoretically that magnetostatic waves (MSWs) propagating in the YIG film with periodic magnetic domains exhibit band gap structure, similar to the case of photonic crystals. They call the materials as magnonic crystals, which are indeed attractive for controlling the propagation of MSWs and spin waves. This was also confirmed for the one-dimensional case [9], where electronic controllability of MSWs in magnonic crystals was discussed.

REFERENCES

1. Inoue, M., et al., *J. Phys. D: Appl. Phys.*, Vol. 39, No. 8, R151–R161, 2006.
2. Inoue, M., et al., "Magnetic Nanostructures," eds. B. Aktaş, L. Tagirov, and F. Mikailov, *Springer Series in Materials Science*, 29–43, 2007.
3. Shin, K. H., et al., *J. Appl. Phys.*, *10th Joint MMM/Intermag Proc.*, in press, 2007.
4. Wang, Z., et al., *Appl. Phys. B*, Vol. 81, 369–375, 2005.
5. Inoue, M., et al., in preparation for publication, 2007.
6. Fedyanin, A., et al., *Proc. Plasmonics 2006*, 76, Singapore, 2006.
7. Khanikaev, A., et al., *Proc. Plasmonics 2006*, 77, Singapore, 2006.
8. Nikitov, S., et al., *MRS Symp. Proc.*, Vol. 834, 87–96, 2005.
9. Inoue, M., et al., in preparation for publication, 2007.

Imaging Characteristics of a Left-handed Metamaterial Lens

Pi-Gang Luan[1], **Kao-Der-Chang**[1], **Hung-Da Chien**[1], **Chii-Chang Chen**[1], **and Chi-Shung Tang**[2]

[1]Department of Optics and Photonics, National Central University, Jhong-Li 32054, Taiwan
[2]Research Center for Applied Sciences, Academia Sinica, Taipei 11529, Taiwan

Abstract— We investigate in this paper the imaging characteristics of a left-handed metamaterial slab as a superlens. For an ideal, lossless slab, we use simple geometric concept based on phase continuity to explain why there is a thickness limitation that pointed out by some researchers [2]. For an absorptive slab, the field is determined by the Green's function, which we calculate numerically by summing over all the contributions from the Fourier components of the source field that correspond to different transverse k-vectors. The imaging characteristics are determined by several parameters, which include the ratio of wavelength to slab thickness, wavelength to source-surface distance, and the absorption effect. Varying these parameters the image width can be tuned from about one wavelength to subwavelength scale. In the former situation, the energy density is mainly concentrated at the two images that predicted by ray tracing. For the later case, although the image width is indeed subwavelength size along the focal plane, however, the field amplitude decays exponentially from the slab surface. The energy density of the field in this case is mainly concentrated at about the two surfaces of the slab, carried by the surface plasmon polaritons (SPPs) that excited by the near-field of the source. Heuristic discussion about the relation between the subwavelength imaging phenomenon and Heisenberg's uncertainty principle is given. We also discuss the time-evolution behavior of the imaging process of the superlens system. Based on the idea of force-driving double-oscillator model [3], we have found a natural explanation to the ideal problem of why perfect imaging is unachievable even in principle.

REFERENCES

1. Pendry, J. B., *Phys. Rev. Lett.*, Vol. 85, 3966, 2000.
2. García, N. and M. Nieto-Vesperinas, *Phys. Rev. Lett.*, Vol. 88, 207403, 2002.
3. Gómez-Santos, G., *Phys. Rev. Lett.*, Vol. 90, 077401, 2003.
4. Luan, P.-G., H.-D. Chien, C.-C. Chen, and C.-S. Tang, ArXiv/physics/0311122.

Multi-layered Fe Films for Microwave Applications

A. V. Osipov, **I. T. Iakubov**, **A. N. Lagarkov**, **S. A. Maklakov**
D. A. Petrov, **K. N. Rozanov**, **and I. A. Ryzhikov**

Institute for Theoretical and Applied Electromagnetics, Moscow, Russian Federation

Abstract— The microwave permeability of multi-layered Fe films is under study. The multi-layer films are found to possess more rigid magnetic structure and larger damping factor of ferromagnetic resonance compared to those of single-layer films. Bulk materials with high microwave permeability may be produced as laminated structures of these multi-layer ferromagnetic films. In the paper, experimental data are presented on the microwave permeability of such laminated regular structures based on Fe films. Possible technical applications of the materials under study include thin wideband radar absorbers and miniaturized patch antennas.

Two-dimensional Finite-difference Time-domain Study of Coupling Parameters in Different Nano-plasmonic Waveguides

Majid Rasouli Disfani, **Mohammad Sadegh Abrishamian**, **and Mehdi Zahedi**

Department of Electrical Engineering, K.N. Toosi University of Technology
P.O. Box 16315-1355, Tehran 16314, Iran

Abstract— In the recent years there has been a great interest in periodic structures like photonic crystals and metamaterials which exhibit novel optical properties because of their subwavelength structures. The aforementioned subwavelength structures can also find their applications like waveguides in the optical frequency range. These waveguides have also drawn a lot of attention because of their abilities of transporting energy with concentration of light below the diffraction limit. The transport of energy in such a kind of waveguide is based on the coupling of surface plasmons. Previous analysis of surface plasmons includes the plasmon propagation along metal strips, wires, or grooves in metal. Furthermore the coupling between plasmons on metal particles is investigated from the viewpoint of guided energy. The dimension of metal particles (d), lattice parameter (Λ) of the periodic structures, different patterns of metal particles, and the excitation frequency affect the coupling between plasmons.

In this paper, finite-difference time-domain (FDTD) method is applied to the problem of optimizing the coupling between surface plasmons in three different two-dimensional plasmon waveguides depicted in Fig. 1. These structures are in the form of rows of silver nanorods and nanosquares. In the analyzed waveguides, dimension effects of silver particles are investigated at optical frequencies. Based on the distributions of electric and magnetic fields and the energy transport for the waveguides, nano-plasmonic waveguides are designed and optimal operating conditions are found to enhance the coupling strength for nonlinear applications. The frequency dispersion of silver nanoparticles is characterized by Drude material model. It is taken into account in FDTD simulations by the auxiliary differential equation (ADE-FDTD) method. In order to minimize the reflection from outer boundaries, convolution perfectly matched layer (CPML) is applied to

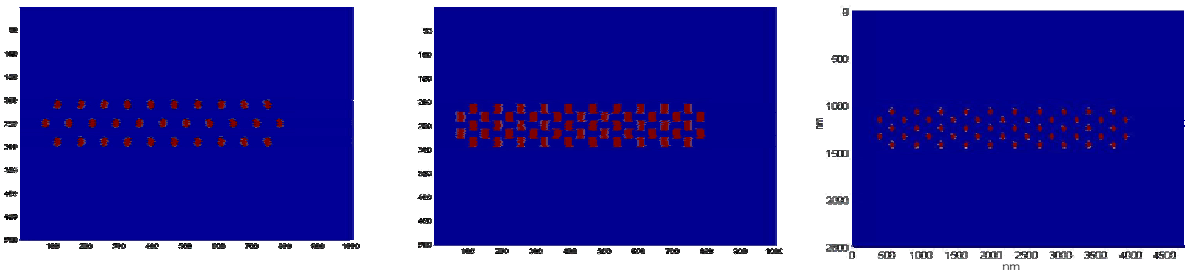

Figure 1: Two-dimensional nano-plasmonic waveguides.

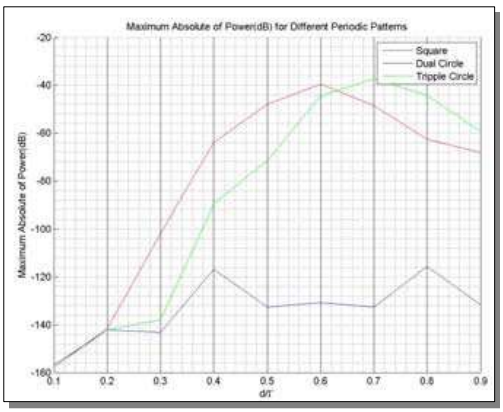

Figure 2: Maximum absolute power for three different plasmonic waveguides vs. d to Λ ratios.

introduce reflections as low as $-100\,\mathrm{dB}$. It is obvious from Fig. 2 that the maximum coupling strength and power enhancements are achieved for d to Λ ratios of 0.6 to 0.8 in the analyzed waveguides. Because of the plasma frequency of the silver nano-plasmonic particles, real part of dielectric function of silver can be positive and negative for different wavelength ranges. In this paper, the effect of excitation frequency on the maximum coupling strength and power enhancements is investigated. Furthermore the power distribution in an infinite number of nano-particles is calculated by applying Bloch's periodic boundary condition.

Modal Analysis of Extraordinary Transmission through Subwavelength Slits in a Silver Plate

G. Ghazi and M. Shahabadi
School of Electrical and Computer Engineering, Photonics Research Lab
University of Tehran, Iran

Abstract— The extraordinary transmission of light through arrays of subwavelength slits or holes is a topic of vast investigation since the paper by Ebbesen in 1998. In this work, we present a modal analysis along with the mode matching technique to determine the transmission coefficient of a one-dimensional array of slits made in a real metal which is assumed to be silver. We will use the measured data for complex refractive index of silver reported in a well-known paper by Johnson and Christy. With the help of this method, we will obtain the field distribution inside and outside the metallic plate as well as the transmission coefficient as a function of wavelength. We will also investigate different mechanisms of transmission and the effect of propagating and evanescent modes on the extraordinary transmission.

The Figure below illustrates a typical calculated transmission through a one-dimensional array of subwavelength slits.

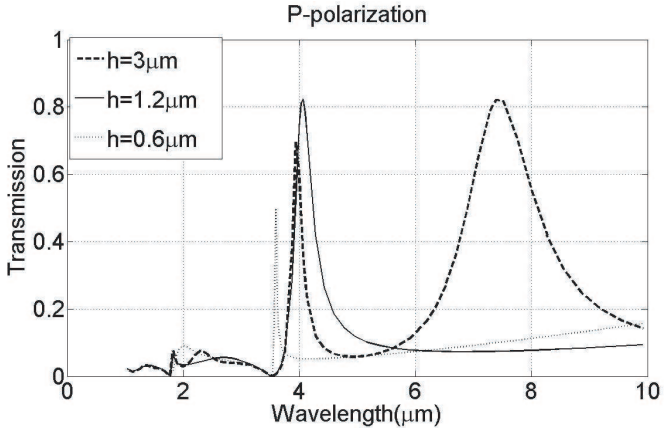

Figure 1: Zero-order transmission of a grating with a periodicity of $L_x = 3.5\,\mu\text{m}$ and slit width of $a = 0.5\,\mu\text{m}$ and thickness of $h = 0.6,\ 1.2,\ 3\,\mu\text{m}$.

Tunable Negative Index Metamaterial and Applications

Patanjali V. Parimi[1, 2], **Peng He**[1], **Carmine Vittoria**[1], **and Vincent G. Harris**[1]

[1]Department of Electrical and Computer Engineering, College of Engineering
Northeastern University, 360 Huntington Avenue, Boston, MA 02115, USA
[2]Department of Physics, Northeastern University, 360 Huntington Avenue, Boston, MA 02115, USA

Abstract— There has been considerable interest in the development of negative index metamaterials (NIM) that simultaneously possess negative permittivity (ε) and permeability (μ) giving rise to a negative index of refraction (n). Much of the fascination in NIM arises from their unusual electromagnetic properties that allow for several novel applications such as super lenses, miniature and leaky wave antennas, and phase shifters. Notable NIM are resonant metamaterials, photonic crystals and planar periodic arrays of passive lumped circuit elements. These NIMs are limited by inherent narrow bandwidth and are not at all tunable. In order to obtain negative n at different frequencies the periodicity and size of the elements need to be changed. Such limitations of the existing NIM urge investigation of tunable NIM. We have designed and fabricated a magnetic field tunable, low loss, negative refractive index metamaterial using yttrium iron garnet (YIG) and a periodic array of copper wires. The effect of the YIG film is to provide a tunable negative μ over a continuous range of frequencies on the high frequency side of the ferrimagnetic resonance. Complementary negative ε is achieved using a periodic array of copper wires. The tunability is demonstrated from 18–23 GHz under an applied magnetic field with a figure of merit of 4.2 GHz/KOe. The tuning bandwidth is measured to be 5 GHz compared to 0.9 GHz for fixed field. The insertion loss is measured to be 1 dB/cm at 22.3 GHz. The measured negative refractive index bandwidth of 0.9 GHz compares well with the transfer matrix theory and finite element method simulations. We further demonstrate a novel tunable NIM phase shifter and miniature antenna. The phase shifter is fabricated is using high quality Yttrium Iron Garnet films and copper strips etched on a circuit board. A phase shift of 180° for change in an applied field of 1.2 KOe is achieved at 24 GHz.

ACKNOWLEDGMENT

Work supported by the Defense Advanced Research Projects Agency and National Science Foundation.

Magnetic Coupling on Co-doped ZnO Films

H. Chou[1], **Cheng-Pang Lin**[1], **Y. H. Ho**[1], **J. C. A. Huang**[2], **and H. S. Hsu**[2]

[1]Department of Physics and Center for Nanoscience and Nanotechnology
National Sun Yat-Sen University, Kaohsiung 804, Taiwan
[2]Department of Physics, National Cheng Kung University
Tainan 701, Taiwan

Abstract— The magnetic and electric properties of Co-doped ZnO films by applied various external electric fields in room temperature (RT) were measured. It is found that both magnetization and electric resistance vary with gate voltages. The magnetization was saturated faster and the resistance was increases for lower negative gate voltages. Since the gate voltage equivalent to the carrier (electrons) density in the Co-doped ZnO film, the negative gate voltage indicates lower electron density and a lighter effective mass which results in a larger isolated polaron sphere. In this study, our result supports Bound Magnetic Polaron model as the mechanism of Oxide Dilute Magnteic Semiconductor.

Low Frequency Relaxation Oscillations in a Capacitive Discharge Chamber Connected to a Peripheral Grounded Chamber

Zhuwen Zhou[1], **M. A. Lieberman**[2], **Sungjin Kim**[2]
Shiyin Ji[1], **Guangyu Sun**[1], **and Mingsen Deng**[1]

[1]Department of Physics, Guizhou Educational College, Guiyang 550003, China
[2]Department of Electrical Engineering and Computer Sciences-1770
University of California, Berkeley, CA 94720, USA

Abstract— We have observed relaxation oscillations in an argon capacitive discharge connected to a peripheral grounded chamber through a slot with dielectric spacers. The oscillations, observed from time-varying optical emission of the main discharge chamber and the periphery, show, for example, some low frequency (2.72 Hz ∼ 3.70 Hz) relaxation oscillations at 100 mTorr, at higher absorbed power. We interpret the low frequency oscillations using an electromagnetic model of the slot impedance with parallel connection variational peripheral capacitance, coupled to a circuit analysis of the system including the matching network. The model results are in general agreement with the experimental observations, and indicate a variety of behaviors dependent on the matching conditions.

Session 2P3
Microwave and Millimeter-Wave Devices and Circuits

Computer-analytical Characterization of Resonant-cap Circuit for Microwave Oscillators and Power Combiners

Subal Kar, **S. Bhanja**, **and S. Sasmal**
University of Calcutta, India

Abstract— A detailed electromagnetic analysis of radial cavity formed by a resonant-cap circuit mounted in rectangular waveguide is carried out to characterize the properties of oscillators and power combiners at microwave frequency. The radial cavity with the active device embedded in it has been approximated to be equivalent to a circular disc microstrip patch antenna. The computer-analytical characterization based on this approach is found to be very close to the experimental results obtained with resonant-cap IMPATT oscillators and power combiners. The analysis is general and throws considerable insight regarding the properties of resonant-cap circuits which will be useful in the design of microwave and millimeter-wave oscillators and power combiners.

With this model for the resonant-cap circuit we have observed that the oscillation frequency can be changed both by changing the cap diameter (D) and cap height (h). However, the change of frequency with cap diameter is more practical and do not violate the basic assumption ($h \ll \lambda$) of the model. The real part of the impedance represented by the cap structure is found to be significantly dependent on the cap height. This is important because in the design of amplifier we need a larger R_c compared to that needed for oscillator operation, and this can be done with a small change in cap height, without violating the assumption mentioned above.

The cap structure is found to behave as a quarter-wave impedance matching element between the device and the waveguide in which both the device and the cap circuit is embedded. The normalized power plot shows that $D/\lambda = 0.55$ for optimum power out put from the oscillator. The cap cavity acting as an antenna shows that a sharp fall of radiation resistance with D/λ also takes place around a value of 0.55, indicating that the cap cavity is an efficient radiator with such optimized cap design.

The twin-cap power combiner analyzed with this model, taking the two cap sources as two elements of an antenna array, shows that the combining efficiency can be optimized by suitably choosing the separation between the caps (i.e., with small adjustments of cap height of the twin cap cavities) and almost 100% power combining efficiency is achievable with such optimization.

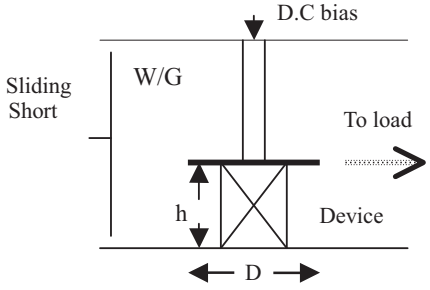

Cap Oscillator

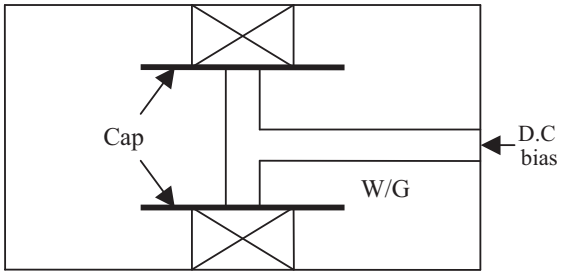

Twin Cap Combiner

Modeling of Multi Post Waveguide Structure Useful for Ka Band Cavity Oscillator Design

S. Dutta[1], **A. Majumder**[1], **and S. Kar**[2]

[1]SAMEER Kolkata Centre, Plot-L2, Block-GP, Sector-V Salt Lake, Kolkata PIN-700091, India
[2]Institute of Radio Physics & Electronics, University College of Science & Technology
92, A.P.C Road, Calcutta 700009, India

Abstract— The paper describes the analysis and modeling of multi-post waveguide cavity useful for oscillator applications. One of the most common configurations used for cavity oscillator development at higher frequencies is that of a post-loaded cavity. A negative resistance device (e.g., Gunn or IMPATT diode) is used for power generation. A post is used for mounting the device as well as providing the d.c bias voltage. One side of the waveguide is generally terminated in a short circuit and power is taken out from the other side. In case of a Voltage Controlled Oscillator (VCO) an additional post is used for mounting the tuning device (mostly a varactor diode) as well as providing the bias voltage to the tuning device. The post dimensions are of extreme importance for determining the oscillation frequency and power output.

So it is of paramount importance to properly model the device mounts while designing such oscillators. A full wave computer-aided analysis has been carried out of such a structure following the method of Joshi & Cornick [1, 2], where a two post structure inside a waveguide with both ends perfectly matched has been considered. The analysis has been extended considering arbitrary terminations on both end of the waveguide. The arbitrary termination case is required as the load presented to the oscillator is often of complex nature, which in turn affects the oscillator performance. A second order correction term has been incorporated in the analysis for computing the effective post diameter, which gives much more accurate results at Ka-band. Parametric study of mount impedance and resonance frequency of the structure has been carried out with variation of short position and post diameter. Computed results for a Ka-band cavity with two staggered posts with one end shorted is shown in Fig. 1.

To facilitate quick design, the structure has also been simulated with a commercial 3D electromagnetic solver using Finite Element Method. A specific simulation process has been worked out to represent the structure accurately, which can provide useful design data. This computer-aided simulation technique also includes parametric search and optimization in the design.

A prototype cavity has been fabricated and is under testing for characterization.

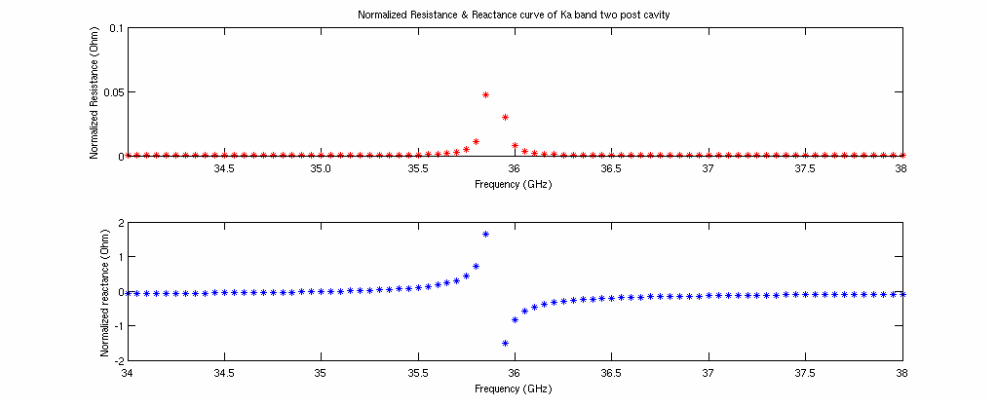

Figure 1

REFERENCES

1. Joshi, J. S. and J. A. F. Cornick, "Analysis of waveguide post configurations: part 1 — gap immitance matrices," *IEEE Transactions on MTT*, Vol. 25, No. 3, 169–173, March 1977.
2. Joshi, J. S. and J. A. F. Cornick, "Analysis of waveguide post configurations: part 2 — dual gap cases," *IEEE Transactions on MTT*, Vol. 25, No. 3, 173–181, March 1977.

Modeling and Realization of a Ka Band GUNN Based Phase Locked Source

G. Arun Kumar[1], **A. Majumder**[1], **M. Kundu**[1], **S. Chatterjee**[1], **and S. Kar**[2]

[1]SAMEER Kolkata Centre
Plot-L2, Block-GP, Sector-V, Salt Lake, Kolkata, PIN-700091, India
[2]Institute of Radio Physics & Electronics, University College of Science & Technology
92, A.P.C Road, Calcutta 700009, India

Abstract— In this paper the modeling and realization technique of a Phase Locked source at Ka-band using a Gunn based Voltage Controlled oscillator (VCO) has been described. The approach followed is hybrid in nature, wherein an analogue frequency down conversion has been followed with digital phase frequency comparison and subsequent phase correction. The full system was modeled functionally using time domain impulse invariance analysis with the help of a commercial system simulator. Fig. 1 gives the block schematic of the system.

The total system uses a two loop approach to achieve the desired goal. The two loops are shown with dotted lines in the schematic. The main loop comprises of the Gunn VCO along with directional coupler, harmonic mixer, digital phase frequency detector and a 10 MHz temperature controlled crystal oscillator as reference. The auxiliary loop is a C-band synthesizer locked to the same reference as the main loop. The C-band signal acts as the LO (Local Oscillator) frequency of the harmonic mixer in the main loop.

The working of the system is as follows. A portion of the power coming out of the Ka-band Gunn VCO is coupled out and used for phase comparison in the main loop with the help of a 10 dB directional coupler. The Ka-band signal is down converted using a harmonic mixer (x8) where the LO is provided from the auxiliary loop locked to the same reference. The IF frequency is then amplified, and phase compared with the reference. A 3rd order loop filter has been implemented to achieve the lock and desired phase noise. A commercial synthesizer chip from Analog Devices has been used as the phase frequency detector. The design of the main loop ensures that under locked condition the IF is always at 548 MHz. The change of frequency is achieved by changing the frequency of the C-band signal.

Table 1 gives the phase noise achieved from the above scheme. It can be seen that excellent close in phase noise has been achieved from the scheme. There is a peaking of phase noise at an offset of 500 KHz which can be attributed to the loop bandwidth of the system. A different design of the loop filter is being implemented currently to address this issue and results will be provided in the final paper. The phase noise at 1 MHz offset represents the free running phase noise of the VCO.

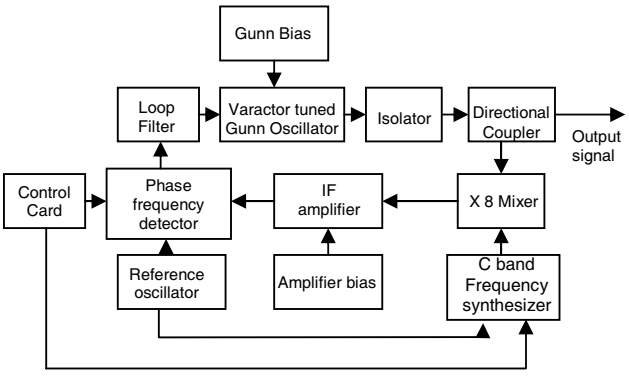

Figure 1: Block schematic of the system.

Table 1.

Carrier frequency (GHz)	Offset frequency (KHz)	Phase noise (dBc/Hz)
34.802	10	–94.62
	500	–90
	1000	–100.91

Computer-aided Design and Characterization of a Broad-band Millimeter-wave Source at 34 GHz

Subal Kar

Institute of Radio Physics and Electronics, University of Calcutta
92, A.P.C Road, Calcutta 700009, India

Abstract— Practical design of a novel coaxial-waveguide oscillator is done on the basis of computer-aided solution of analytical model equations. Theoretical and experimental characterization of the oscillator is carried out and the results compared. The oscillator designed with IMPATT diode (Hughes 47101H-0405) embedded in the coaxial-waveguide cavity is found to provide a broad bandwidth ($\sim 20\%$) and high power (~ 1 W) with the oscillation frequency centered at 34.25 GHz.

Broadband and high power oscillators useful for modern millimeter-wave communication systems can be designed with IMPATT diode mounted in a suitable cavity. The impedance matching of low impedance IMPATT diode with the high impedance of the circuit is a crucial problem in the design of such oscillators. In the oscillator we have designed, the waveguide characteristic impedance (377 O) is matched to the IMPATT diode impedance (5.2 O) first by a two step impedance transformer (5:1) and then with two spacer slabs (12:1) having coaxial holes in them, as shown in the figure below. The bias post (radius, $a = 0.7$ mm) acts as center conductor passing through the coaxial holes in the spacer slabs.

The oscillator is characterized theoretically on the basis of analytical modeling and the experimental results of the fabricated oscillator is compared with theoretical characterization to establish its broadband and high power properties.

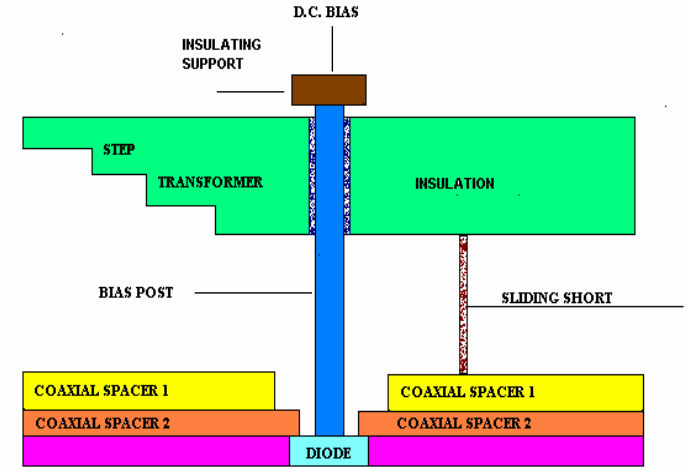

Linearized Distributed Amplifier by Self-adaptive Biasing Technique

K. W. Lau, K. Y. Chan, Q. Xue, and C. H. Chan

City University of Hong Kong
Tat Chee Avenue, Kowloon Tong, Hong Kong SAR, China

Abstract— Multi-band/multi-mode, reconfigurable, or simply wideband are the candidates for realizing seamless global coverage for the development of the future radios. Power amplifiers are the indispensable components in wireless communications systems, but they are inherently nonlinear. Spectral regrowth is a common problem resulting from high-efficiency amplification when the amplifier is operated close to the saturation region. Class A and Class AB operations are commonly used for the non-constant envelope modulation schemes with comparatively low distortion among other classes. However, the average power efficiency of this mode of operations is normally low. Therefore, efficiency enhancement and linearity improvement are two highly desirable objectives. Feedforward and digital predistortion are the common wideband linearization techniques, but they always require complicated and expensive circuitry, additional power consumption and a large area on the printed circuit broad. As a result, they are only favourable for the base station applications. For the handset, analog linearizing circuits are more preferable as they are always with the advantages of simple, low power consumption and low cost. Unfortunately, these techniques always focus on narrow band operation.

In this paper, a self-adaptive biasing technique is proposed for both efficiency enhancement and linearity improvement of the bipolar distributed amplifier. The proposed self-adaptive biasing network is to bias self-adaptive current to improve the average power efficiency and to perform dynamic sweet spots (IMD3 minima) for IMD3 elimination. Experimental results show more than 10dB suppression of the spectral regrowth over 0.9 GHz to 3.3 GHz and more than 30% reduction of DC power consumption at the 1 dB gain compression point.

A Study on Improvement of Transmission Characteristics near the Passband of BPFs Using Branch-stub Resonators

T. Yasuzumi[1], **T. Ohno**[2], **and O. Hashimoto**[1]

[1]Aoyama Gakuin University, Japan
[2]Kisarazu National College of Technology, Japan

Abstract— Realization of an attenuation pole is well known as an effective technique for improving transmission characteristics of a microwave filter. If an attenuation pole is formed near the passband, a sharp skirt characteristic will be obtained. For example, an elliptic function bandpass filter can realize a sharp characteristic by locating the attenuation poles extremely near the passband. However, the filter tends to increase the number of the component. Therefore, it is desirable for the attenuation poles to be controllable with a simple approach and a small number of parts. To achieve the requirements above, we focus on a branch-stub resonator.

In this paper, branch-stub resonators are designed by using a genetic algorithm. Through the designing the resonator, fundamental characteristics including the control of attenuation poles are examined. After that, BPFs using the branch-stub resonators are also designed and calculated. Fig. 1 shows a schematic circuit of a resonator using branch-stub, and the resonance characteristics of the resonator is shown in Fig. 2. As shown in Fig. 2, attenuation poles are realized at near the passband, as designed. Moreover, Figs. 3 and 4 show a schematic circuit and the characteristics of the filter using the branch-stub resonator shown in Fig. 1. As a result, it is confirmed that a very sharp skirt characteristic is achieved by locating the attenuation poles extremely near the passband.

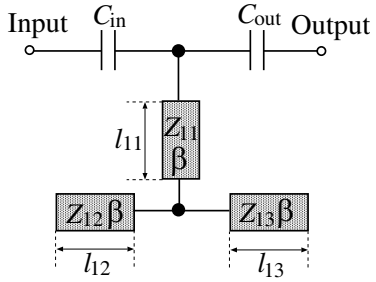

Figure 1: Branch-stub resonator.

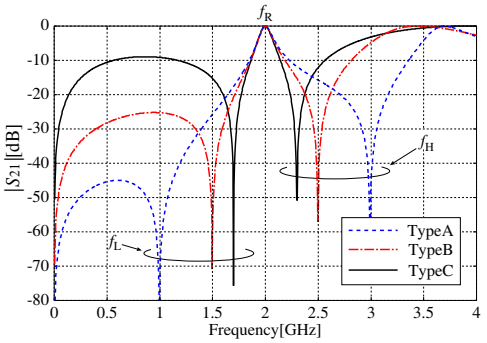

Figure 2: Calculated characteristics of the resonator shown in Fig. 1.

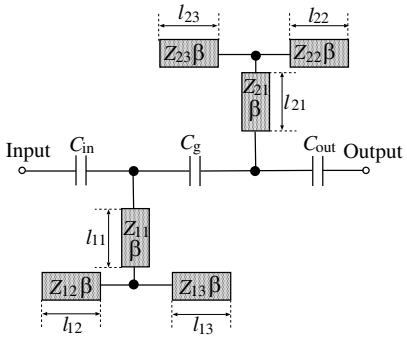

Figure 3: BPF using branch-stub resonators.

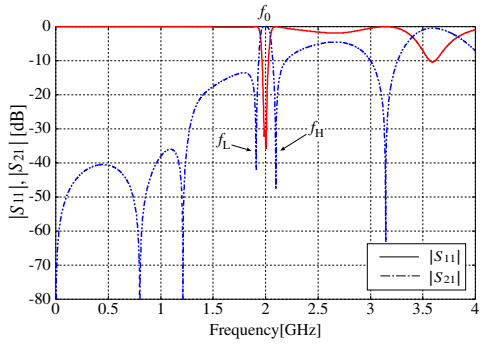

Figure 4: Transmission characteristic of the BPF shown in Fig. 3.

CAD of Broadband Mixer Design at Microwave and Millimeter Wave Frequencies

Arun Kumar
SAMEER Kolkata Centre, Plot - L2, Block - GP, Sector - V
Salt Lake, Kolkata, PIN - 700091, India

Abstract— This paper relates to a novel computer aided design technique of K-band (18–26.5 GHz) broadband mixer. The LO is at 35 GHz while the instantaneous IF bandwidth is 8.5 GHz. The mixer configuration (shown in Figure 1) that has been used for analysis is crossbar configuration to support broadband requirement. The diodes chosen for the mixer design are GaAs Schottky barrier beam lead diode with low parasitics to achieve broadband performance.

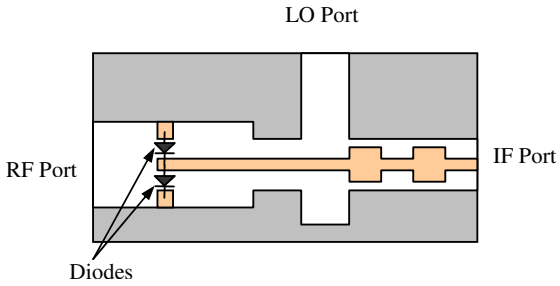

Figure 1: Crossbar mixer configuration.

We have carried out 3-D EM and circuit co-simulation with nonlinear analysis. First all the passive circuits have been modeled in 3-D EM simulator with either FDTD or FEM technique. Then those results from the EM simulation are used in circuit simulator. Nonlinear analysis of the mixer has been done with harmonic balance to get conversion loss and isolation between different ports (RF, LO and IF). The simulated results have been shown in Figures 2 and 3. Other parameters like VSWR at different ports, frequency spectrum as well as the diode current and voltage waveforms can also be found out through simulation. For accurate mixer simulation at microwave and millimeter wave frequencies one should have correct diode model to be incorporated in nonlinear circuit simulation. The accurate diode model can be extracted based on s-parameter and DC measurements of the diode mounted in test fixture.

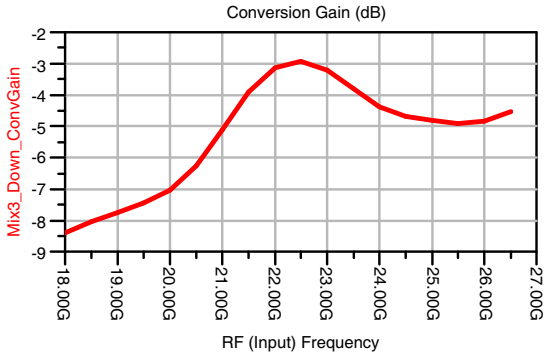

Figure 2: Conversion loss.

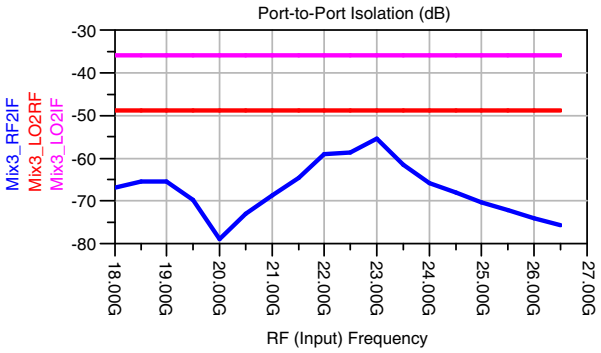

Figure 3: Isolation between ports.

RF-ID Tag Location Using RF-over-fibre Techniques

P. V. Brennan, **A. J. Seeds**, **and Y. Huang**
University College London, UK

Abstract— The proposed paper investigates techniques for the indoor location of a high density of people and/or objects based on the deployment of RF-ID tags, operating over a fibre-optic infrastructure with RF-over-fibre communications. The work is part of the wider EPSRC-funded TINA (The Intelligent Airport) program involving a consortium including UCL, the University of Cambridge, the University of Wales and several industry partners such as Motorola and Boeing, which is investigating the feasibility of a high speed fibre-optic infrastructure to carry the full range of airport services — data, video, security, PMR radio and RF-ID tag data.

The paper concentrates on the tag location element of the program, which aims to achieve accurate, frequently-updated indoor location from numerous (>1000 in a 10 m radius) RF-ID tags in an airport or other similar indoor environment. The associated infrastructure is to consist of a number of tag antenna units connected to a high-speed fibre network, with a central unit to perform identification and location of the various tags. A prototype demonstration unit is to be built in the 2.4 GHz or 5.8 GHz bands.

Various location strategies are under consideration, such as Time-of-Arrival (TOA), Time Difference of Arrival (TDOA), Angle of Arrival (AOA) and Signal Strength estimation. The TOA and TDOA techniques offer the best performance in terms of location accuracy and resistance to multipath effects, provided sufficient bandwidth is available, whereas the other techniques generally offer lower performance but with reduced bandwidth requirements and the likelihood of more economic implementation. In our paper these techniques and a number of combinations (e.g., TOA plus AOA) will be compared and contrasted in order to assess the optimal solution(s) for indoor RF-ID tag location applications.

There are a number of feasible communications protocols in this application, most obviously Direct Sequence Spread Spectrum (DSSS). Again, the proposed paper will review the key techniques, in particular concentrating on the use of an innovative chirped-FM approach, under development at UCL, which is likely to achieve high accuracy location with a convenient and economic Surface Acoustic Wave (SAW) device implementation.

Finally, several approaches to distribution of the signals via RF-over-fibre will be outlined and compared, including distribution at RF, IF and baseband (data), again to arrive at a solution best suited to this application. The paper will conclude with a detailed description of the demonstrator unit under development in this program, along with modelled and measured results indicating its projected performance.

A Cross-coupled Voltage-controlled Oscillator in 0.6 μm BiCMOS Process

T. Yang, **K. W. Lau**, **K. C. Wan**, **Q. Xue**, **and C. H. Chan**

City University of Hong Kong, Tat Chee Avenue, Kowloon Tong, Hong Kong SAR, China

Abstract— Radio frequency identification (RFID) is becoming an important technology for the applications in the supply chain management and the inventory control systems. Identification number transmitted from the RFID tag to the reader gives the information of the tagged item. To enhance the tracking range of the tags, the active type is preferable. It is known that size, cost and power consumption of the active tags are the key issues to realize this technology in industries.

Oscillator is one of the essential active components in wireless communications systems. Therefore, this paper is to present a voltage-controlled oscillator (VCO) integrated circuit design for RFID application. Utilizing the cross-coupled structure, a differential VCO is implemented in the 0.6 μm BiCMOS process. For the operation of RFID (ETSI: 865.6–867.6 MHz and FCC: 902–928 MHz), −10 dBm output power for each differential output and 90 dBc/Hz phase noise are achieved. Moreover, the VCO can operate from 540 MHz to 1300 MHz by biasing the varactor diodes from 0 V to 5.6 V. It can be concluded that a cross-coupled VCO is successfully implemented in 1.5 mm^2 chip area with 40 mW power consumption.

Design of New DGS Hairpin Microstrip Bandpass Filter Using Coupling Matrix Method

A. Boutejdar[1], **A. Elsherbini**[2], **A. Balalem**[1], **J. Machac**[3], **and A. Omar**[1]

[1]Microwave and Communication Engineering, University of Magdeburg, 39106 Magdeburg, Germany
[2]Department of Electrical and Electronic Engineering, Ain Shams University, Cairo, Egypt
[3]Faculty of Electrical Engineering, Czech Technical University, Technick 2, 16627 Prague 6, Czech Republic

Abstract— In this paper we present a novel compact Hairpin bandpass (BPF) microstrip filter employing two U-slots etched in the ground plane (DGS) and two 50 Ω feeds on the top. A new type of microstrip BPF based on coupled DGS resonators is designed using coupling matrix method. The new BPF is very compact, in addition, the filter has a very wide stopband with two transmission zeroes. A good agreement between the measured and simulated results is achieved.

Session 2P4
Microwave Imaging & Inverse Scattering Problem

The Use of Inhomogeneous Surface Impedance Modeling in the Shape Reconstruction

Mehmet Çayören, Özgür Özdemir, and İbrahim Akduman

Electrical and Electronics Engineering Faculty, Istanbul Technical University
Maslak 34469, Istanbul, Turkey

Abstract— During the last three decades shape reconstruction problems related to dielectric and perfectly conducting bodies has gained considerable attention of scientist from different areas. This is due to fact that the results of such problems have a large domain of applications including microwave remote sensing, optical system measurements, underwater acoustics or non-destructive testing etc. Such problems have been extensively investigated in the open literature and several methods based on different approaches such as physical optics theory, Newton-Kantorovich method, equivalent source technique, decomposition methods etc. have been developed [1, 2].

The main objective of the work is to give a new and simple one step method for the shape reconstruction of perfectly conducting bodies. For the sake of simplicity we present the method for the cylindrical bodies of arbitrary shape. The method requires only a single illumination at a fixed frequency of a plane wave. The scattered field is measured on a circular domain all around the object. The method presented here is based on the equivalent surface impedance modeling of the perfectly conducting object on a chosen circular reconstruction domain, i.e., it is assumed that the perfectly conducting object is equivalently represented by a circular object having variable surface impedance on its boundary. The equivalent surface impedance is determined directly from the standard impedance boundary condition which requires knowing the total field and its derivative on the boundary of the circle. The required field values can be calculated through the single layer potential approach [3]. If the equivalent circle is intersecting the unknown object, the surface impedance should vanish at those intersection points. This property can be used to reconstruct the unknown object. To this aim one chooses a number of concentric circles and calculates the surface impedances on each circle and observes the points where the impedance function tends to zero. The method does not require a forward solver and yields quite accurate reconstructions for objects of different sizes.

REFERENCES

1. Colton, D., H. Haddar, and M. Piana, "The linear sampling method in inverse scattering theory," *Inverse Problems*, 19, S105–S138, 2003.
2. Liu, C. Y. and Y. W. Kiang, "Inverse scattering for conductors by the equivalent source method," *IEEE Trans. Antennas and Propagat.*, Vol. 44, 310–316, March 1996.
3. Akduman, I. and R. Kress, "Direct and inverse scattering problems for inhomogeneous impedance cylinders of arbitrary shape," *Radio Science*, Vol. 38, No. 3, Art. No. 1055, 2003.

A Profile Inversion Scheme for the Reconstruction of Dielectric Layers Having Rough Interfaces

Çağla Taşdemir, **Evrim Tetik**, **and Ali Yapar**

Electrical and Electronics Engineering Faculty, Istanbul Technical University
Maslak 34469, Istanbul, Turkey

Abstract— Imaging of an inaccessible rough surface located over a perfectly conducting plane constitutes an important class of problems in inverse scattering theory due to large domain of applications such as microwave remote sensing, optical system measurements, underwater acoustics, non-destructive testing etc. This problem can also be considered as the reconstruction of a dielectric coating located on a perfectly conducting substrate. In these kind of problems one tries to recover the location and shape as well as surface characteristics of an unknown surface through scattered field measurements at a certain domain. The main aim of this paper is to give a new and simple method to determine the surface profile of a dielectric layer over a conducting plane. For the sake of simplicity we consider surfaces having a variation in one direction. The reconstruction is achieved via a single illumination by a plane wave at a fixed frequency and the reflected field measurements are performed on a line parallel to the surface. After separating the half-space above the dielectric layer into two parts by a planar surface, the scattered field in the upper region above this plane is expressed in terms of a Fourier transform whereas in the lower part between the layer and the plane a Taylor expansion is employed. Similar representations are applied for the scattered field in the dielectric layer below the interface. The use of the continuity conditions of the total field and its derivative on the unknown interface then allows the reduction of the inverse problem to the solution of a coupled system of two integral equations containing a spectral coefficient for the scattered field and the interface function as unknowns. The coupled system is solved iteratively starting from an initial guess of the surface function. For a given estimate of the surface profile, keeping the profile function fixed, one of the two equations is solved as a linear and ill-posed equation for the spectral coefficient of the scattered field through a Tikhonov regularization. Then one inserts the obtained spectral coefficient into the other equation and, keeping the spectral coefficient fixed, considers this equation as a nonlinear equation for the interface function and performs a linearization, i.e., one Newton step, for its solution. Since the solution is sensitive to errors in the data, a regularization in the least square sense is applied within this Newton step. The iterative scheme then consists in alternating these two steps until an appropriate stopping criterion is fulfilled. The method yields quite satisfactory reconstruction for layers having a rough surface with variation less than half-wavelength.

REFERENCES

1. Akduman, I., R. Kress, and A. Yapar, "Iterative reconstruction of dielectric rough surface profiles at fixed frequency," *Inverse Problems*, Vol. 22, 939–954, 2006.

A Fisher Information Based Gradient Scaling for Microwave Tomography

Andreas Fhager[1], **Mats Gustafsson**[2], **Sven Nordebo**[3], **and Mikael Persson**[1]
[1]Chalmers University of Technology, 412 96 Göteborg, Sweden
[2]Lund University, 221 00 Lund, Sweden
[3]Växjö University, 351 95 Växjö, Sweden

Abstract— As a means to analyze the information content in the measurement data for microwave tomography the Fisher information and the Cramér-Rao lower bound is utilized. These statistical techniques are often used in different areas of signal processing to analyze the information content of data. The Cramér-Rao lower bound can be used to determine at which accuracy an estimation problem can be solved, for exampel an inverse electromagnetic problem. Here this technique has been applied to the two-dimensional microwave tomography problem for the purpose of determining the accuracy in the reconstruction of the dielectric parameters. In lossy background media it has been found that the sensitivity to the dielectric data is continuously decreasing towards the center of the imaging domain.

Image reconstruction in microwave tomography is usually a very computationally intensive problem that is solved by an iterative optimization algorithm. We have developed an experimental prototype of a tomographic system for microwave imaging with a time-domain conjugate-gradient image reconstruction algorithm. The FDTD formulation is used to model the electromagnetic problem and for solving the forward scattering problem. The inverse problem is solved iteratively by minimizing a cost functional containing the difference between the measured scattered field and the corresponding simulated field. Gradients computed from solutions of the adjoint Maxwell equation are used in the minimization. Based on the Fisher information matrix a spatial scaling of the gradients have been deduced and implemented into the image reconstruction algorithm, with the purpose of compensating for the decreased sensitivity towards the center of the reconstruction domain. Both numerically simulated and experimental data have been used for image reconstruction. The reconstructions where the spatial gradient scaling has been utilized show an improved robustness and accuracy compared to when it is not used.

Electromagnetic Imaging of a Collection of Small Scatterers Using MUSIC

Xudong Chen
National University of Singapore, Singapore

Abstract— The multiple signal classification (MUSIC) method has been successfully applied to determine the location of point-likes scatterers in acoustic imaging. In electromagnetic imaging, most research work on MUSIC considers 2-dimensional case under the TM incidence. Recently, the application of MUSIC method to electromagnetic imaging is extended to the determination of a collection of small 3-dimensional scatters. However, the scatterers have to be separated far enough so that the multiple scattering can be ignored. This paper presents a MUSIC model that accounts for the multiple scattering between small scatterers. In addition, the locations of scatterers of special shape, i.e., disk or needle, can also be determined by the proposed MUSIC model. Finally, the entries of the polarization tensor are obtained by solving a linear equation system.

Imaging of Perfectly Conducting Objects Buried in a Dielectric Cylinder

Oğuz Semerci, Onur Mudanyalı, and Gül Seda Ünal
Electrical and Electronics Engineering Faculty, Istanbul Technical University
34469 Maslak, Istanbul, Turkey

Abstract— Reconstruction of the shape and the location of a perfectly conducting objects constitutes one of the basic and important class of problems in inverse scattering theory. Besides the remarkable theoretical aspects, the relevance of this kind of problems is due to fact that they have a large domain of applications including microwave remote sensing, optical system measurements, underwater acoustics or non-destructive testing, only to mention some examples. Accordingly, such problems have been extensively investigated in the open literature and several methods have been developed [1–2]. In all these works, the methods are developed for the objects located in an homogeneous space or buried in an unbounded media. On the other hand, the body can be located in a bounded medium such as a dielectric sphere or cylinder. Such problems are of importance especially in medical applications.

Within this framework, the aim of this paper is to provide a new, simple and fast method to reconstruct the unknown shape of a perfectly conducting object buried in a dielectric circular cylinder. The cylinder is located in an infinite homogeneous space and illuminated by a plane wave of fixed direction and frequency. The measurements are performed on a circular domain all around the cylinder. In the method presented here, the measured data is analytically continued to the surface of the cylinder by using series representation of the scattered field in terms of Hankel functions. For the scattered field inside the cylinder, a circle which is assumed to be the minimum circle covering the unknown object that separates the region into two parts is initially determined. In the outer part between the minimum circle and the boundary of the cylinder the scattered field is expressed as a series through the Bessel functions while it is represented in terms of Taylor series in the region between the unknown object and the minimum circle. The use of the boundary conditions reduces the problem to the solution of a nonlinear equation which can be treated by linearizing in the Newton sense. Since the problem is ill-posed, a regularization in the least square sense is also applied. The method we propose is able to provide satisfactory results when the size of the scatterer is comparable to the wavelength.

REFERENCES

1. Liu, C. Y. and Y. W. Kiang, "Inverse scattering for conductors by the equivalent source method," *IEEE Trans. Antennas and Propagat.*, Vol. 44, 310–316, March 1996.
2. Belkebir, K., R. E. Kleinmann, and C. Pichot, "Microwave imaging-location and shape reconstruction from multifrequency scattering data," *IEEE Trans. Microwave Theory and Tech.*, Vol. 45, 469–476, April 1997.

Reconstruction Scheme for Polygonal Cylindrical Targets with Curved Surfaces

Hiroshi Shirai and Yoshinori Hiramatsu

Department of Electrical, Electronic, and Communication Engineering
Faculty of Science and Engineering, Chuo University
Tokyo 112-8551, Japan

Abstract— Target reconstruction is one of the important research topics for various areas such as remote sensing and advanced radar technologies. Various methods, which are mainly based on the signal processing techniques or numerical methods, have been proposed previously for target imaging. Radar Cross Section (RCS) is one of the fundamental indexes to evaluate the equivalent size of the scatterer, and it is known that the RCS value changes according to the scatterer's shape and materials. Many authors have already been studied and shown that high frequency asymptotic techniques such as the Geometrical Theory of Diffraction (GTD) and the Equivalent Source Method (ESM) can be confidently used for analyzing the electromagnetic wave scattering, and for estimating the RCS of large polygonal scatterers.

We have already proposed a simple target reconstruction algorithm for closed polygonal cylindrical scatterers using high frequency techniques. This reconstruction algorithm is mainly based on our previous finding that for polygonal objects, the main contribution to the backscattering arises from the edge diffracted waves at the facets at the specular reflection direction, and each facet size can be estimated by the local RCS maxima and its lobe width. While we assume primarily that the targets are all polygonal and their constitutive facets are straight metal plates, we have extended our reconstruction algorithm, in this paper, to handle the case when the target's facets have curved surfaces. Half and quarter circular cylinders are used as canonical scattering objects, and their measured and numerically simulated monostatic RCS values have been studied extensively to find scattering pattern characteristic difference between flat and circularly curved surfaces. Thus estimated constitutive facets are connected in order, and this procedure will be continued until the distance between the first and the final edges would be minimized. Our algorithm has been tested for other targets, and it is found that it works well for predicting metal convex targets with flat and curved facets.

Inverse Problem of ECG for Different Equivalent Cardiac Sources

C. G. Xanthis, P. M. Bonovas, and G. A. Kyriacou
Mircowave Lab, Department of Electrical and Computer Engineering
Democritus University of Thrace, Xanthi 67100, Greece

Abstract— The objective of electrocardiography in general is the qualitative and quantitative representation of the heart's electrical activity exploiting the information provided by the potentials recorded at the body surface. The inverse electrocardiography (ECG) in particular, refers to a pre-determined modeling of the cardiac activity by a variety of equivalent electric sources as a single or double moving/rotating electric dipole, multiple fixed location dipoles, the epicardial potential distribution and the activation of isochrones on the heart surface, e.g., [1]. The aim of the inverse problem of electrocardiography is to reconstruct the heart activity from a given set of body surface potentials. The solution of this inverse problem is generally based on a "volume conductor model" representing the whole body, which enables the solution of the forward problem. Preferably this model should retain high spatial resolution around the heart. The assumed equivalent electric source for heart activity is modeled and the generalized Poisson equation (forward problem) is solved to obtain a "calculated data set" for the body surface potentials. In turn an inverse problem solution algorithm like Newton's, Newton-Raphson etc. can be employed for the minimization of a cost function, usually in the least squares sense. Moreover, like most inverse problems this is a non-linear one. So, the initially assumed equivalent electric source parameters are iteratively updated until the differences between the measured and calculated data sets become comparable to an accepted error tolerance. The latter may be defined by the measurements errors and their noise as well as the computer modeling inaccuracies.

Another common characteristic of these inverse problems is their ill-posed nature, where this difficulty becomes worst when the number of unknown parameters is increased. In order to confront this problem, our previous work was based on the modeling of the hearts activity by a central cardiac electric dipole, which was allowed only to rotate about a fixed origin (3 variables), similar to a classical work [2]. For this purpose an anatomically realistic three-dimensional volume conductor model of the human body was constructed based on a classical anatomic atlas [3]. This was excited by an assumed (initial guess) dipole located at the center of the heart. In turn a Least squares optimization scheme was employed, aiming at the matching of the potential distribution calculated on the torso surface to the corresponding distribution measured with the aid of multiple electrodes. The nonlinearity was confronted by the implementation of the Levenberg — Marquardt strategy. The efficiency of the method stemmed from the employment of arbitrary shaped hexahedral elements within the finite element method for the minimization of the required computational resources while the model realistically reflected the body internal structure. Finally, this algorithm was successfully tested using measured data available online. Successful results of this work along with dipole images for the whole cardiac temporal period were presented in our previous work [5].

In the current study, the same algorithm for the solution of the inverse ECG problem along with the same volume conductor model is tested for three different equivalent electric sources. Firstly, a single cardiac dipole is allowed to move and/or rotate, namely having six degrees of freedom: 3 dipole moments and 3 coordinates of dipole origin. Compared to our previous work, a remarkable decrease in the mean square error was observed. The use of two dipoles constitutes the second step toward the establishment of the algorithm. One dipole is allowed only to rotate about a fixed origin, located at the sinoatrial node of the heart. The second dipole is a moving dipole free to move and rotate in the heart area during the whole cardiac temporal period. Finally, in order to verify the validity of our algorithm, the use of multiple dipoles concludes our current work. Each one of these dipoles represents a certain anatomical region of the heart. Hence, these dipoles are fixed in location but their dipole moments are allowed to vary in direction and magnitude. For these three different equivalent electric sources, the algorithm was tested for both computer generated data and a real multichannel measured data set available on-line, [4]. Successful dipole images for the whole cardiac temporal period based on this data set will be presented at the conference. Furthermore, one of our primary aims is the establishment of our own multichannel-measurements instrument using 28–192 electrodes, based on commercially available data collection systems. The team is currently working toward this aim.

REFERENCES

1. Gulrajani, R. M., "The forward and inverse problems of electrocardiography," *IEEE Engineering in Medicine and Biology*, 84–101, September/October 1998.

2. Guard, R., B. McA. Sayers, and D. M. Morno, "Evaluation and analysis of the cardiac electrical multipole series based on a two-dimensional Fourier technique," *The Theoretical Basis of Electrocardiology*, edited by C. V. Nelson and D. B. Geselowitz, Chapter 10, 213–256, Clarendon Press, Oxford, 1976.
3. Eycleshymer, A. C. and D. M. Shoemaker, *A Cross Section Anatomy*, Appleton Century Crofts, New York, 1911.
4. MacLeod, R., S. Shome, L. Lorenzo, and B. Yilmaz, "ECG measurement and analysis," March 2005. http://www.cvrti.utah.edu/∼macleod/bioen/be6000/labnotes/ecg/data/
5. Xanthis, C., P. Bonovas, and G. Kyriacou, "Localization of an equivalent central cardiac electric dipole for electrocardiography applications," *Int. Conference ITAB 2006*, Ioannina, Greece, October 2006.

A Sensitivity Matrix Based Microwave Tomography Exploiting an Adjoint Network Theorem

D. G. Drogoudis[1], **G. A. Kyriacou**[1], **and J. N. Sahalos**[2]
[1]Mircowave Lab, Department of Electrical and Computer Engineering
Democritus University of Thrace, Xanthi 67100, Greece
[2]School of Sciences, Radiocommunications Lab, Department of Physics
Aristotle University of Thessaloniki, Thessaloniki 54124, Greece

Abstract— Microwave tomography is a novel technique with many applications in medical imaging and geophysical prospecting. This is based on the high contrast observed in relative dielectric permittivity and conductivity between physiological and malignant or abnormal tissues, e.g., Pething [1]. Likewise, the geophysical application are justified by the different σ and ε_r properties of different materials-minerals, e.g., Keller [2]. The degree (or contrast) of these changes is large enough to be tomographically reconstructed. Another important biomedical application of microwave tomography is in thermometry of the human body [3]. These examples demonstrate the significance of microwave tomography (MWT) for biomedical applications as an imaging modality for non-invasive assessment of functional and pathological conditions of tissues.

The basic objective of microwave imaging is the reconstruction of the spatial distributions of permittivity and conductivity of the body under investigation. The body is illuminated by electromagnetic waves from a number of different directions. The reconstruction of σ and ε_r is based on these scattered electromagnetic field measurements which are the result of the interaction of the incident wave and the inhomogeneous body.

For the solution of the forward scattering problem the Finite Element Method (FEM) will be used, exploiting the sparsity of the matrices that arise from the method for faster simulation time. As we have to deal with open geometry-problem, second order absorbing boundary conditions are applied on a fictitious circular surface that encloses the body under investigation.

For the solution of inverse problem the reconstruction algorithm will be based on an extension of the Modified Perturbation Method (MPM). In our previous work, [4], MPM was developed for inverse problems in the area of Electrical Impedance Tomography (EIT). Now the aim is to extend this technique in order to be applicable in Microwave Tomography problems. MPM is a robust iterative technique that is based in the closed form expressions for the calculation of the Jacobian matrix (sensitivity matrix). Within this effort the Jacobian matrix will be calculated using an Adjoint Network-Field approximation.

Finally the proposed method will be applied for the reconstruction of 2D scatterer's profiles. The so called "computer phantom" is assumed. Namely, first the forward problem was solved and the results are stored, labeled as "measurements". In turn the reconstruction algorithm starts from a homogeneous model and the desired complex permittivity profile is sought.

REFERENCES

1. Pethig, R., "Dielectric properties of biological materials," *IEEE Trans. Elect. Insulation*, Vol. E1-19, 17–10, Jan. 1984.
2. Keller, G. V., "Electrical properties of rocks and minerals," *Handbook of Physical Constemts*, editor S. P. Calrk, N. Y. Geological Society of America, 553–770, 1988.
3. *Non-invasive Thermometry of the Human Body*, edited by Michio Miyakawa and J. Ch. Bolomey, CRC Press, 257 pages, 1996.
4. Drogoudis, D. G., G. C. Trichopoulos, G. A. Kyriacou, and J. N. Sahalos, "A modified perturbation method for three-dimensional time harmonic impedance tomography," *PIERS-05*, Hangzhou, August 2005.

Estimation of Ground Permittivity from a GPR Echo of a Cylindric Conducting Pipe

Yiwei He[1] and Qinglian Guo[2]

[1]Osaka Electro-Communication University, 18-8 Hatus-cho, Neyagawa 572-8530, Japan
[2]Kanazawa Institute of Technology, 7-1 Ohgigaoka, Nonoichi 921-8501, Japan

Abstract— The dielectric constant of ground is important in the estimation of the depth of buried object as well as in various imaging processing such as migration and synthetic aperture. Because the dielectric constant is usually unknown, many estimation methods have been proposed by utilizing the electromagnetic coupling, propagation time between bore-holes, and GPR echo of a small scatter. These methods are effective in certain environment, and eche has its disadvantages. In this report, the estimation of ground permittivity is considered for the case that the buried object is a conducting cylindric pipe such as water or gas pipe. Because an GPR echo profile is characterized by the permittivity of the ground, the depth and the radius of buried cylindric pipe, a least squares method is utilized to estimate the electric permittivity of ground from the GPR echo profile. The existence of the ground surface is take into account by the propagation paths of lateral wave and evanescent wave (direct wave). The proposed method is validated by some numerical simulations.

Identification of Multiple Cylindrical Targets Located above Perfectly Conducting Flat Surface by Artificial Neural Networks

A. Kızılay[1,2] **and S. Makal**[1,2]

[1]Electrical-Electronics Faculty, Yıldız Technical University, Turkey
[2]Electronics and Communications Engineering Department
Yıldız Technical University, Turkey

Abstract— This paper evaluates the radar target identification performance of neural networks. A set of features are derived from scattered fields calculated by using the image technique formulation and Moment Method (MoM). An artificial neural network that utilizes the feature set is proposed for target identification. This work aims to find the radiuses of the targets and the distances between the targets located above perfectly conducting flat surface from the scattered field values.

Firstly, a cylindrical target is located at a distance from the perfectly conducting (PEC) flat surface. The method of images can be used to replace the infinite flat surface with images of the incident field and the cylinder. The scattered electric field can be rewritten in terms of the induced current on the cylinder and the image current. The Electric-Field Integral Equation (EFIE) is obtained by applying the boundary condition on the electric field. The moment method is used to solve the EFIE to obtain the induced current on the target. Then, the induced current is used to calculate the scattered E-field from a cylinder located above a ground plane. Secondly, two cylindrical targets are located at a distance from the PEC flat surface and there is a distance between the two targets. The total scattered E-field is calculated by using EFIE-MoM solution like the solution of the only one target on PEC flat surface. Lastly, frequency data points consist of the real and the imaginary parts of the scattered E-field are obtained by calculating fields at the frequencies between $1\,\mathrm{GHz} - 30\,\mathrm{GHz}$ and then transformed into the time domain using the inverse Fourier Transform. The data set including time and amplitude values of scattered E-field is obtained by using cylindrical targets having various radiuses and distances between each other. All the targets using for composing the database are at the same heights.

A portion of the database is used to train the network and the rest is used to test the performance of the neural network for target identification. The inputs of the network are the time and the amplitude values of scattered E-field transformed into the time domain. The outputs of the network are the radiuses and the distances between the two targets. In this work, a neural network solution is proposed for target identification which gives reasonably good results. It is shown that electric field features for a target can be extracted from its radar returns that are independent of such radar parameters as target range, loss, antenna gain, etc. These results are very useful in practical applications especially relating to target identification.

A Neural Network Model for Target Identification of Cylindrical Targets Located above Perfectly Conducting Flat Surface

A. Kızılay and S. Makal

Yıldız Technical University, Istanbul, Turkey

Abstract— An artificial neural network (ANN) is trained to achieve radar target identification. The features used by ANN are derived from scattered fields calculated by using the image technique formulation and Moment Method (MoM). A General Regression Artificial Neural Network (GRNN) that utilizes the feature set is proposed for target identification. This work aims to find the heights measured from the surface and the radiuses of the cylindrical targets.

The scattered electric field caused by a cylindrical target located at a distance from the perfectly conducting (PEC) infinite flat surface can be rewritten in terms of the induced current on the cylinder and the image current using the method of images. The Electric-Field Integral Equation (EFIE) is obtained by applying the boundary condition on the electric field. The moment method is used to solve the EFIE to obtain the induced current on the target. Then, the induced current is used to calculate the scattered E-field from a cylinder located above a ground plane. After calculating the scattered E-field, the inputs of the neural network is formed. The inputs of the GRNN are the frequency, the reel part of the scattered E-field and the imaginary part of the scattered E-field. The outputs are the radius and the height of the target used for evaluating the test performance of GRNN. Ten targets are used to forming the database. Nine of them are used to train the network and one of them is used to test the performance of the neural network. Namely, the purpose of this paper is to find the radius and the height of a target which is not in the database.

In this work, a neural network solution has been developed for target identification which gives reasonably good results. It is shown that electric field features for a target can be extracted from its radar returns that are independent of such radar parameters as target range, loss, antenna gain, etc. These results are very useful in practical applications especially relating to target identification.

Shape Reconstruction of 3D PEC Objects via a PO Distributional Approach: Numerical Results

Raffaele Solimene, **Giovanni Spina**, **Aniello Buonanno**, **and Rocco Pierri**
Dipartimento di Ingegneria dell'Informazione, Seconda Università di Napoli
Via Roma 29, I-81031 Aversa, Italy

Abstract— We deal with the electromagnetic inverse scattering problem to reconstruct the shape of perfect electric conducting (PEC) objects from the knowledge of the field that they scatter once a known electromagnetic radiation impinges on them.

As it is well known, such a problem is non-linear and ill-posed. To escape from the non-linearity we restrict ourselves to consider "smooth objects" for which the physical optics approximation can be employed. This approximation for the scattering phenomenon, in conjunction with the fact that we represent the unknown of the problem, that is the shape of the objects, as the support of a delta-distribution, allows to formulate the problem as the inversion of a linear integral operator acting on a distributinal set. In order to obtain a stable reconstruction (with respect to the noise) the inversion of the above said operator is performed by means of the Tikhonov regularized inversion scheme. In particular, a criterion for the choice of the regularizing parameter is given.

We remark that the problem to hand has been already tackled within the framework of a two-dimensional and scalar geometry for the case of cylindrical objects [1] and for the case of a three-dimensinal geometry for point-like objects (i.e., objects which are small in size as compared to the wavelength) [2]. Here, we extend such an analysis for the case of extended objects in a three-dimensional geometry. In this case the problem amounts to inverting a linear integral operator having a dyadic kernel.

We consider the objects to be embedded in free-space and residing within a known investigation domain. A multi-static/multi-frequency reflection-mode is exploited. More in detail, the scattered field is collected over a portion of a spherical domain (concentric to the investigation domain) from the same side where the incident field impinges. In particular, the observation domain is in far zone and as incident field we consider plane waves having fixed angle of incidence and varying frequency. Also the diversity in polarization is exploited.

Numerical reconstructions are shown. They are obtained by inverting the scattered field data provided by the FEM based code HFSS/Ansoft. As the data are generated indipendently on the model adopted to develop the inversion scheme the so-called inverse crime is avoided.

Numerical reconstructions show that the proposed inversion scheme is able to localize the scatterers and to reconstruct the "illuminated" part of their shapes as long as the objects are not too far from to verify the physial optics approximatiom. Furthermore, the polarization diversity proves to be useful in reconstructing different parts of the objects' shapes.

REFERENCES

1. Pierri, R., A. Liseno, R. Solimene, and F. Soldovieri, "Beyond physical optics SVD shape reconstruction of metallic cylinders," *IEEE Ant. and Propag.*, Vol. 54, 655–665, 2006.
2. Solimene, R., A. Buonanno, and R. Pierri, "Linear 3D imaging of small PEC spheres," *PIERS*, Prague, Czech Republic, 27–30 August, 2007 .

Session 3A1
Electromagnetic Simulation and Applications

A Dynamic Simulation Approach for Electrostatic Force Microscopy on Inhomogeneous Sample Material

M. Greiff, U. B. Bala, and W. Mathis

Leibniz University of Hanover, Germany

Abstract— For the time and cost efficient development of electrostatic force microscopes accurate simulation tools are necessary. This paper is dedicated to a high quality simulation approach for electrostatic force microscopes.

From a physical point of view the electrostatic force microscope (EFM) can be separated into a mechanical and an electrical part [1]. Since the governing equations for both parts are different, they must be modelled separately. However, a simulation model has to take into account the coupling between them. In this work this is achieved by passing the electrostatic forces from the electrical to the mechanical part and vice versa, passing the deformations from the mechanical to the electrical part (Fig. 1). This coupling process has to be carried out iteratively. The paper at hand focuses on the electrostatic part. An accurate simulation model is developed and applied to the EFM. Typically the cantilever of an EFM is of length several hundreds of micrometers while the tip is only at a nanometer scale. These kind of multi-scale and open boundary problems can conveniently be treated by using the boundary element method (BEM). However, the inclusion of nonlinear material is not possible in BEM. Therefore the finite element method (FEM) is used in the region near the tip [2]. In order to keep computational cost low, linear ansatz functions are used in the main part of the FEM region. Unfortunately the linear FEM lacks accuracy very close to the tip where the solution is not linear. Since the tip is the most important interaction zone between sample and probe, accurate field results are very important there. Therefore the linear FEM is augmented by using singular ansatz functions close to the tip [3]. The calculated electric field can be seen in Fig. 2. Since the accuracy of the electric fields obtained by using FEM is better at some distance to the boundary, the forces are obtained by integrating the Maxwell stress tensor over a surface integral enclosing the part of the boundary under investigation [4]. The resulting forces are shown in Fig. 3.

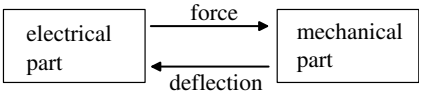

Figure 1: Electro-mechanical coupling.

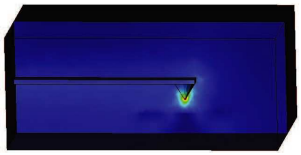

Figure 2: Electric field.

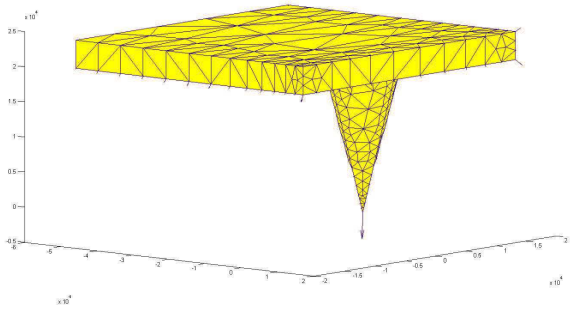

Figure 3: Forces on cantilever.

REFERENCES

1. Morita, S., R. Wiesendanger, and E. Meyer, *Noncontract Atomic Force Microscopy*, Springer, 2002.

2. Stephan, E. P., "Coupling of boundary element methods and finite element methods," *Encyclopedia of Computational Mechanics*, Vol. 03, Chapter 13, 375–412, 2004.
3. Strang, G. and G. J. Fix, *An Analysis of the Finite Element Method*, Prentice Hall, 1973.
4. Hui, C. Y., J. L. Yeh, and N. C. Tien, "Calculation of electrostatic forces and torques in MEMS using path-independent integrals," *J. Micromech. Microeng.*, Vol. 10, 477–482, 2000.

Controlled Approximation of the Coefficient Matrix of the Finite Network Method

A. Eppler, **A. Farschtschi**, **and M. Pfefferkorn**
Chemnitz University of Technology, Germany

Abstract— A method is presented for electrostatic field calculations in unlimited three-dimensional space with boundary conditions on the surface of electrodes. The method is based on surface discretization of electrodes and charge loading on electrode patches. The realization of boundary conditions yields a system of equations to calculate the charges. The structure of the referring coefficient matrix is analyzed and afterwards one algorithm is applied to compute a controlled element-wise approximation of this matrix in order to save time while not losing accuracy for the solution.

Adaptive Meshing for Volterra Integral Equation

A. Al-Jarro, P. Sewell, T. M. Benson, and A. Vukovic
George Green Institute for Electromagnetics Research, The University of Nottingham
University Park, Nottingham, NG7 2RD, UK

Abstract— Modelling the physics of time varying electromagnetic phenomena by means of a Volterra Time Domain Integral Equation (TDIE) [1–5] has previously led to the development of numerical algorithms with significant computational advantages [3, 4, 6]. These investigations have been based on approximating the problem using a structured Cartesian discretisation of the problem, which offers the greatest computational simplicity through its uniformity and symmetry. However, a structured discretisation scheme has limitations when defining complex structures containing a diverse range of feature sizes or boundaries that are curved or non-tangential to the coordinate axes. Hence the need for a numerical tool that can provide a more accurate and flexible numerical approximation of the solution. A novel 1D spatial TDIE algorithm capable of running on 2D (space-time) triangular meshes is presented here for the first time.

In the unstructured TDIE approach, structures are subdivided into an adequate number of small elements whose electric field relationships are approximated using appropriate interpolating basis functions [7]. Here we choose the simplest geometric shape, the 2D linear triangle element, to approximate arbitrary 2D (space-time) problems as shown in the example given in Figure 1(a). A significant advantage of triangular elements lies in the fact that the contribution of each element is calculated and added in a global assembly independently from its neighbours. Therefore, a high density of elements may be utilised in regions where field variation is abrupt, while a smaller number may be assigned to regions with relatively small field variation. Hence the specific triangular pattern being defined takes into account field distribution, which offers significant scope for adaptive schemes.

In TDIE calculations the nodal values are determined in an evolutionary manner with precedence given to nodal values that come first in time, therefore satisfying causality condition imposed by the TDIE formulation. It is also noted that the domain of integration only encompasses the discontinuity, i.e., the region whose properties differ from the background medium. Hence, it is only necessary to refine those specified areas in order to achieve solution convergence. This feature will be shown to demonstrate an accuracy advantage with a minimal computational effort and with no restriction on maintaining a uniform time step-size. As an illustrative, Figure 1 considers a Gaussian pulse that strikes a slab created at $t = 0.5\,\text{fs}$ by switching the material permittivity from $\varepsilon_b = 1.0$ to $\varepsilon_1 = 1.21$ for $(0.27\,\mu\text{m} \leq z \leq 0.36\,\mu\text{m})$. The initial field and the transmitted and reflected signals are shown in Figure 1(b), where field is plotted against the propagation z-axis at $t = 1.6\,\text{fs}$.

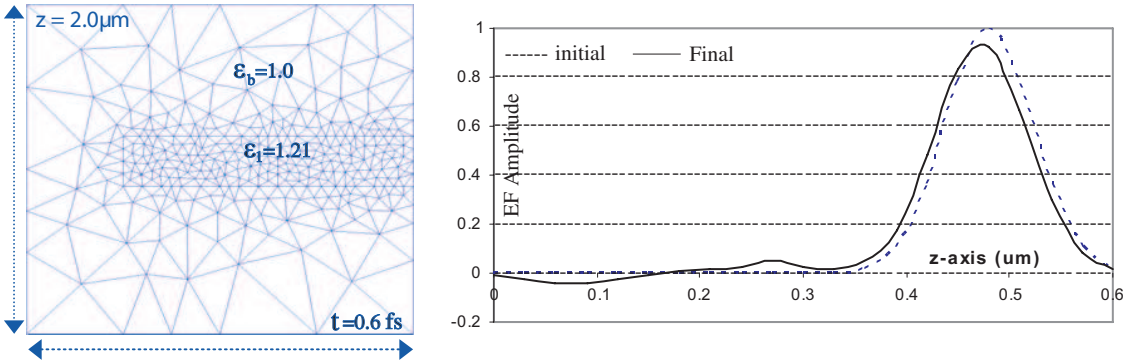

(a) (b)

Figure 1: 2D triangular mesh for a slab with $\varepsilon_1 = 1.21$ created within a background medium $\varepsilon_b = 1.0$ at $t = 0.5\,\text{fs}$ for $(0.27\,\mu\text{m} \leq z \leq 0.36\,\mu\text{m})$ in 1(a) and the corresponding initial and final transmitted and reflected signals at $t = 1.6\,\text{fs}$ in 1(b).

REFERENCES

1. Nerukh, G., "Evolutionary approach in transient electrodynamics problems," JRS 30, 481–491, 1995.
2. Nerukh, A. G., I. V. Scherbatko, and M. Marciniak, "Electromagnetics of modulated media with applications to photonics," *Nat. Inst. Telecommun.*, Warsaw, Poland, 2001.
3. Fedotov, F., A. Nerukh, T. Benson, and P. Sewell, *IEEE J. Lightwave Technology*, Vol. LT-21, 305–314, 2003.
4. Al-Jarro, A., P. Sewell, T. M. Benson, and A. Nerukh, "Effective and flexible analysis for propagation in time varying waveguides," *Optical and Quantum Electronics*, Vol. 36, 133–144, 2004.
5. Al-Jarro, A., P. Sewell, and T. M. Benson, "Time domain integral equation; 3D Model," *Symposium of Integrated Photonics Research*, San Francisco, June 30–July 2, 2004.
6. Benson, T. M., A. Al-Jarro, P. Sewell, V. Janyani, J. D. Paul, and A. Vukovic, "Simulation of nonlinear integrated photonics devices: A comparison of TLM and numerical time domain integral equation approach," *Proc. EUROEM Conference*, *Abstract UWB* 14-2, 174, Magdeburg July 2004, Extended version to appear in *Ultra-Wideband, Short-Pulse Electromagnetics 7 Book*, ed. F. Sabath, 2007.
7. Harrington, R. F., *Field Computations by Moment Methods*, New York, Macmillan, 1968.

SIRENA an External Electromagnetic Simulator for Radio Electric Systems in the Close Environment of an Airport Using Asymptotic Methods

H. J. Mametsa[1], **A. Bergès**[1], **M. Crokaert**[2], **N. Douchin**[3], **and P. Pitot**[3]

[1]ONERA, 2 av. E. Belin 31055 Toulouse Cedex 04, France
[2]Airbus France, 316 route de Bayonne 31060 Toulouse, France
[3]OKTAL Synthetic Environment, 2 rue Boudeville 31100 Toulouse, France

Abstract— The objective of the SIRENA project is to provide a set of simulation tools enabling one to compute the high frequencies ElectroMagnetic (EM) radiation environment of current and future airport vicinity for different EM assessments (radio links availability, ECM analysis, etc.).

The simulation will deal with all external sources such as MLS (Microwave Landing System), ILS (Instrument Landing System), VOR-DME (VHF Omnidirectional Radio beacon, Distance Measurement Equipment), GPS (Global Positioning System), GSM (Global System for Mobile communications), TN (Telecommunications Network), beacons, radars, and TV emitters. These elements are implemented in a geometrical and physical 3D realistic environment of geographical area of interest and they constitute the input data of EM simulations.

The outcome of the research will assess interactions of all external EM sources with environment (masking, multiple reflections, etc.), interactions of all these sources with aircraft structures and interactions between emitting and receiving antennas of aircraft during approach or on the airfield. Thus, a realistic 3D model of the airport environment, a particularly accurate 3D design of aircraft and airport buildings, a realistic model of antennas sources in the environment and on the aircraft and an efficient processing of EM propagation in 3D space have been developed.

SIRENA project starts from the generic FERMAT software, formerly developed under an agreement of partnership between the Electromagnetism and Radar Department of ONERA and OKTAL SE company within the framework of projects dedicated to EM modelling. It has an ambition to calculate scattered EM fields at high frequencies (i.e., size of objects is supposed large compared to wavelength), in a virtual 3D, geometrical and physical complex environment including natural and man made objects. FERMAT associates various techniques and tools and mainly:

- An optimised technique of geometrical Shooting and Bouncing Rays (SBR), to calculate the intersections between the rays from the transmitter towards the database and back to a receiving point.
- EM models of propagation, reflection, diffraction and an operating strategy (thanks to SBR) which make possible unified calculation for the near or far EM scattered fields from the scenes.

In the framework of the SIRENA project, various applications have been treated, particularly concerning:

- prediction of performance for an installation of new radioelectric equipment on an airport site.
- comparison of simulated performances of given equipments according to their location.
- prediction of induced disturbances, by the addition of new built structures (buildings, vehicles or large aircrafts), close to the site of existing equipments.
- providing recommendations for EMC standards by accurate simulation of perturbing electromagnetic effects.
- to have available tools to analyse EMC disturbance phenomena on airport zones.

SIRENA project proved the feasibility of various components necessary to achieve EM simulations in the close environment of an airport.

Magnetic Separation of Paramagnetic Particles Produced by Electrochemical Process with Magnetic Sphere

Ikko Ihara[1] **and Tsuneo Watanabe**[2]

[1]Kobe University, Japan
[2]Tokyo Metropolitan University, Japan

Abstract— The paramagnetic flocks produced by electrochemical process with iron electrodes have the excellent feature from the view of wastewater treatment.The produced iron hydroxide flock has the excellent agglomeration ability due to its positively charged colloidal flocks for collecting negatively charged contaminations in waste water. The HGMS (high gradient magnetic separation) is very useful method to separate contaminations from waste water without producing secondary sludge. In generally, the HGMS needs to prepare the slim magnetized wire for paramagnetic flocks due to its week magnetization. The slim wire is not so good substances since its troublesome pre-preparation processes and cost for its recycling use. The authors tried to use spherical magnetized steel ball as a practical usable filter element and obtained promising results. This paper reports the magnetic separation efficiencies with spherical magnetized steel ball with 2 mm and 4 mm in diameters and conventional slim wire with 0.2 mm in diameter under the strong superconducting magnetic field from 5T to 10T for paramagnetic iron hydroxide flocks. This paper also describes the promising results of 2 mm diameter magnetized steel ball.

Numerical Analysis of Cylindrical Cavities Used for Microwave Heating, Employing the Mode Matching Technique

A. P. Orfanidis[1], **G. A. Kyriacou**[1], **and J. N. Sahalos**[2]

[1]Democritus University of Thrace, Xanthi, Greece
[2]Aristotle University of Thessaloniki, Thessaloniki, Greece

Abstract— The application of high power microwaves for thermal processing of dielectric materials, has received a great attention in the past. The benefits of using microwaves instead of conventional heating mechanisms are mainly due to the fact that microwave energy can penetrate the material achieving rapid internal heating. The main disadvantages are non-uniform heating and thermal runaway [1].

As rectangular cross-section cavities are mainly used, the amplitude field distribution depends on the cavity dimensions and the modes excited in the cavity. Even for a high order modes cavity there is a great fluctuation of the field distribution, resulting in non uniform heating of the material under process. Many techniques have been proposed to overcome this problem, such as the frequency variation and the field disturbance using a metallic blade. Frequency variation can be used only in relatively low power or small size devices, since high power microwave generators cannot alter their frequency. Moreover, the use of a metallic blade in a high power microwave cavity will produce high voltage arcs with unpredictable results.

This paper proposes the use of a cylindrical cavity, which can produce a more uniform field distribution. The exact analysis of the cavity as well as the feeding mechanism will be performed using a closed-form mode matching technique. Since all the involved coupling integrals are evaluated analytically, this results in a very fast and compact technique without numerical instabilities. The dimensions of the cavity and the feeding source section will be designed aiming at the higher possible uniformity of the field amplitude. The feeding structure will be a rectangular waveguide, while its position will be optimized for the proper excitation of all necessary modes in the cavity. The material to be heated will be inserted to the cavity through a moving belt, since the devise will be used for industrialized applications. For this purpose, two openings will be included at the cavity, while $\lambda/4$ chokes will prevent microwave leakage [2].

REFERENCES

1. Kriegsmann, G. A., "Cavity effects and hot spot formulation in microwave heated ceramic fibers," *Microwave Processing of Materials V*, MRS, Vol. 430, 181–186, 1996.
2. Robinson, M. P., J. D. Turner, D. W. P. Thomas, J. F. Dawson, M. D. Ganley, A. C. Marvin, S. J. Porter, T. M. Benson, and C. Christopoulos, "Shielding effectiveness of a rectangular enclosure with a rectangular aperture," *Electronics Letters*, Vol. 32, 1559–1560, 1996.

Driving Characteristics for Hybrid Electric Drive with Super-capacitor as Energy Storage Unit

D. Cundev and P. Mindl

Department of Electric Drives and Traction, Faculty of Electrical Engineering
Czech Technical University, Prague, Czech Republic

Abstract— This paper deals with calculation of the driving characteristics of the hybrid electric drive which uses super-capacitor as energy storage unit. Results has been obtained thought simulation of the driving regime of the experimental working stand for electric and hybrid car drive research, which was developed in the research Centre Josef Bozek at the Technical University in Prague. Computer program and algorithm for simulation of the drive regime is explained. Results of the simulation define the driving characteristics of the entire working stand.

Steady-state Analysis of Salient Poles Synchronous Motor with Damper Based on Determination of the Magnetic Field Distribution

D. Cundev and Z. Cerovsky
Department of Electric Drives and Traction, Faculty of Electrical Engineering
Czech Technical University, Prague, Czech Republic

Abstract— This paper deals with steady-state analysis of the magnetic field by using Finite Element Method (FEM) in salient poles synchronous motor with damper (SPSMD). The knowledge of electromechanical characteristics is very important in performance analysis of electrical machines, in general. In this paper it presents a methodology for numerical calculation of electromechanical quantities, starting with the determination of the magnetic field distribution and numerical computation of the electromechanical characteristics of SPSMD by using FEM.

On the Influence of Slot Width of Field Shapers in Electromagnetic Metal Forming of Aluminum Sheets

A. Farschtschi[1], **T. Richter**[1], **and H.-J. Roscher**[2]

[1]Chemnitz University of Technology, Germany
[2]Fraunhofer Institute IWU, Germany

Abstract— In industry there is currently a strong desire to use significantly more aluminum. There are some obstacles in forming of aluminum by stamping methods, e.g., tearing and spring-back due to the elastic modulus of aluminum (compared to steel). Electromagnetic metal forming (EMF) works by the magnetic induction effect and causes much higher accelerations and velocities in sheet forming compared to stamping processes. That's why EMF as a method of high velocity forming can overcome these obstacles.

The apparatus of sheet forming consists of a flat spiral and a capacitor bank. A current pulse from the capacitor bank is passed through the coil and field between the coil and the workpiece. This field induces eddy currents in the workpiece and causes repulsion forces on the workpiece. One variation of forming is a hybrid method where the final forming after stamping is done by EMF. This method includes a field former device between the coil and workpiece (see Figure 1).

To understand the work principle of the former simulations of the electromagnetic process are-made by ANSYS. ANSYS is a commercial Finite-Element-Analysis program widely used in structural and multiphysics analysis. Due to the complexity of a fully 3-dimensional simulation only electromagnetic simulations are made neglecting structural dynamic effects.

Figure 1 shows the geometry of EMF simulated by ANSYS. A 7-winding flat spiral coil is connected to a capacitor bank and is positioned below the base of the field former. The head of the former contains a slot. The workpiece is an aluminum sheet of 1.2 mm thickness positioned parallel to the head of the former at a distance of 2 mm. Figure 2 sows a typical discretisation of the former and the workpiece. The border of the former and the thickness of the workpiece were discretised with an element width comparable to the skin depth of the frequency of the transient or even smaller.

A time dependent analysis was requested with varying a slot width (2, 4, 6 and 8 mm). Figure 3 shows the transient of the discharging current of the capacitor bank. To guarantee numerical stability at tolerable run times the transient was simulated by the implicit Euler method.The slot of the former enforces eddy currents at the wedge-faces of the slot resulting in a vertical magnetic field within the slot. The components of the total force can be separated into two parts:

- Since the workpiece overhangs the border of the head of the former stray fields induce eddy currents at the border of the workpiece. The force on these eddy currents will depend on the shape of the precasted workpiece.
- The main aim of this work is the examination of forces generated by eddy currents around the slot. As Figure 4 shows even the separation of these forces from the total force shows a strong linear dependency of these forces on the the slot width.

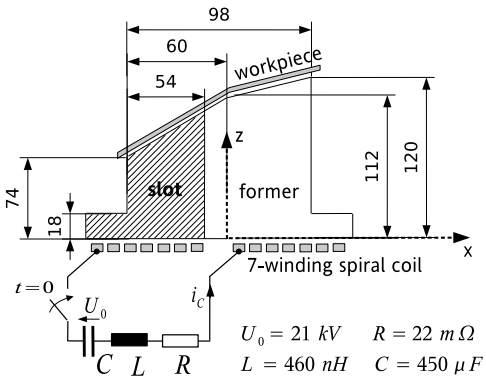

Figure 1: Sample geometry (lengths in mm).

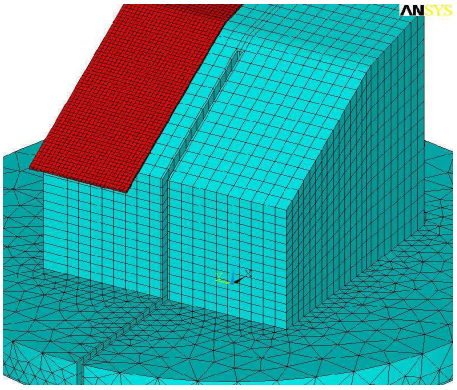

Figure 2: Typical discretisation of former (cyan) and a part of the workpiece (red) in ANSYS.

An increasing slot width results in a higher pressure on the aluminum sheet and a more non-uniform pressure distribution around the slot (see Figure 5). Above facts imply that the design of the former will be a compromise between the uniformity of pressure distribution and a maximum amount of total force.

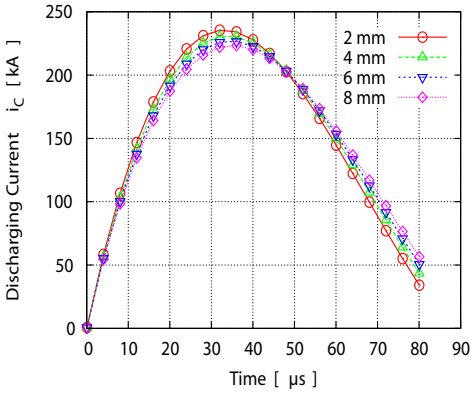

Figure 3: Current transients of the capacitor bank.

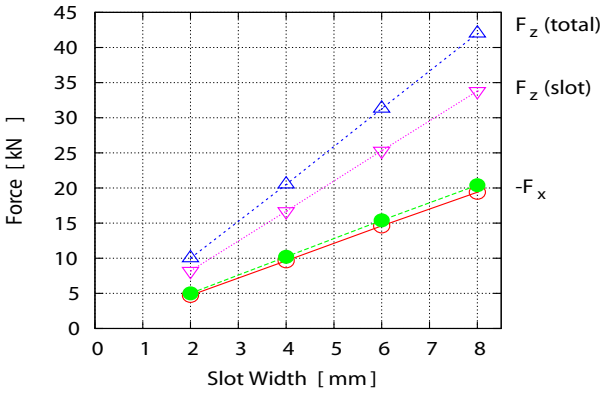

Figure 4: x and z components of forces on workpiece at 36 µs. The force components across the slot were separated from the total components and show a strong linear dependency on slot width.

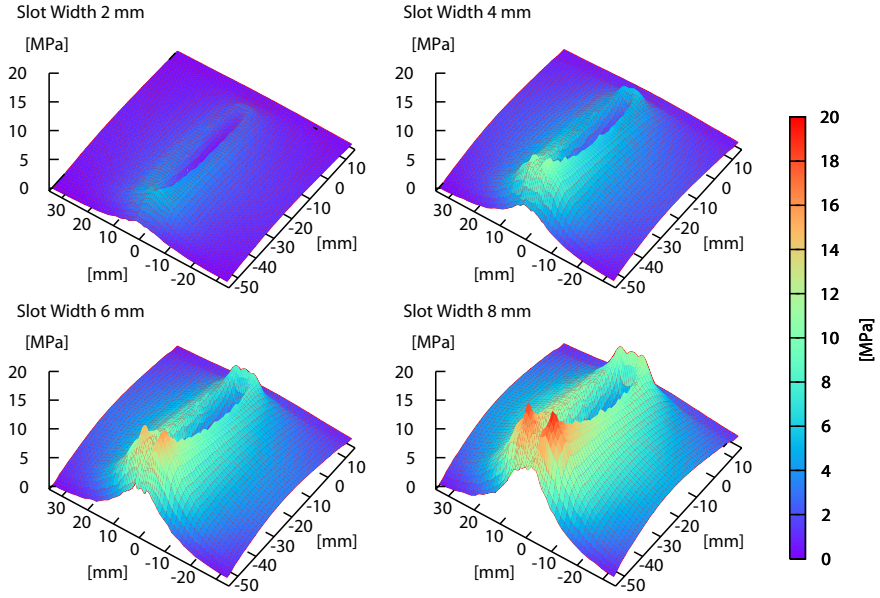

Figure 5: Distribution of z component of pressure across the slot at 36 µs.

Amplification of Acoustic-electromagnetic Waves in GaN Films

A. García-B.[1], **V. Grimalsky**[2], **A. Silva**[1], **P. Rivera**[1], **A. Morales**[3], **and F. Marroquín**[1]

[1]Department of Mecatronics, University Polytechnics of Pachuca (UPP)
Carretera Cd. Sahagun, Pachuca Km. 20, Z.P. 43830, Hidalgo, México
[2]Autonomous State University of Morelos, CIICAp
Av. Universidad No. 1001, Z.P. 62209, Cuernavaca Mor., México
[3]Centro Nacional de Microelectrónica (CNM), Campus UAB
Bellaterra 08193, Barcelona, Spain

Abstract— In this work, theoretical results on amplification of acoustic-electromagnetic waves due to piezoelectric effect and deformation potential mechanism are presented. The results are very interesting at 10 and 15 GHz because these have application in communication systems like filters and delay lines. The numerical simulations have shown the possibility of a strong amplification due to mechanism of resonant excitation and using the negative differential conductivity.

Another important result is the following: the study comparative between two mechanisms due to piezoelectric effect and deformation potential to excitation of hyper sound waves, the results show that to high frequencies (30 GHz) the excitation due to potential deformation is more important.

We had used the simplest models of crystals with piezoelectric effect, deformation potential. For the case of piezoelectric effect, we consider the substrate with big value of electric mechanic coefficient of piezoelectric effect.

Session 3A2a
Subwavelength Resolution and Near-field Effects of Wave Multiple Scattering by Dielectric and Magnetic Materials

Sub-wavelength Focusing with Far-field Time Reversal

G. Lerosey, **J. de Rosny**, **A. Tourin**, **and M. Fink**

Laboratoire Ondes et Acoustique, E.S.P.C.I., Universite Paris 7,
C.N.R.S, UMR 7587, 10, rue Vauquelin, 75005, Paris, France

Abstract— We have time-reversed the field produced by a small antenna placed inside a random distribution of scatterers. The scatterers leads to re-generate by time-reversal not only the propagating but also the evanescent components of the initially emitted wave. Consequently, in such a case, the focal spot size can be smaller than half a wavelength, namely the "classical" diffraction limit. Focal spots as small as $\lambda/30$ have been observed. One example of application in the telecommunication field will presented which shows enhancement of the information transmission rate by a factor 3.

Recently, experimental demonstrations of phase conjugation and broadband time-reversal (TR) were reported for microwaves [1–3]. In our microwave time-reversal experiments [2, 3], a Time Reversal Mirror (TRM) operating at a central frequency of 2.45 GHz with a bandwidth of 250 MHz is used. The experiments are performed inside a 1-m^3 reverberant chamber. The sketch of an electromagnetic time-reversal experiment is as follows: in a first step, the nth antenna of a 8-antenna array emits a 10-ns long RF pulse. The elements of the array are quarter-wavelength antennas. The time-dependent signals are recorded at the antennas of the Time Reversal Mirror. Second each signal is flipped in time, and re-emitted by each antenna of the TRM. Then the 8 signals received by the 8-antenna array are recorded. The maximum amplitude is observed at the nth antenna. Thanks to the reflections off the metallic walls, the focusing on the array is isotropic and the focal spot size roughly equals half-a-wavelength [3]. Consequently when the antennas are closer than $\lambda/2$, not only nth received a strong RF TR pulse but all the antennas of the array.

Very recently, we have replaced the 8 quarter-wavelength antennas by 8 micro-structured antennas. One micro-structured antenna consists of a short wire antenna surrounded by a random distribution of thin copper wires. Contrary to the case of the quarter wavelength antennas, when a wave generated by the nth micro-structured antenna is time-reversed, only this antenna of the array is excited, even when the other antennas are closer than half a wavelength. Experimentally a focal spot size as small as $\lambda/30$ has been observed.

A model is proposed in order to interpret this result. The evanescent waves produced by a source are usually lost during the propagation between the source and the TRM (here the TRM is assumed to be in the far-field). After time-reversal, these evanescent waves are missing at the focus and the focal spot size is equal to half a wavelength. But when the random distribution of thin copper wires is located in the near-field of the small antenna, the evanescent waves produced by the nth antenna are converted into propagative ones. During the second step of the TR, due to reciprocity of the evanescent waves [4], the time-reversed propagative wave field is back-converted into evanescent waves on the same micro-structure and a focal spot with sub-wavelength width can be obtained.

One potential area of application is wireless communications. As a demonstration, we have shown that 3 different information fluxes can be independently sent to 3 micro-structured antennas that are only $\lambda/30$ distant.

ACKNOWLEDGMENT

This work has been partially funded by Agence Nationale pour la Recherche under grant ANR-05-BLAN-0054-01.

REFERENCES

1. Henty, B. E. and D. D. Stancil, *Phys. Rev. Lett.*, Vol. 93, 243904, 2004.
2. Lerosey, G., J. de Rosny, A. Tourin, A. Derode, and M. Fink, *Phys. Rev. Lett.*, Vol. 92, 193904, 2004.
3. Lerosey, G., J. de Rosny, A. Tourin, A. Derode, and M. Fink, *App. Phys. Lett.*, Vol. 15, 154101, 2006.
4. Carminati, R., J. J. Saenz, J.-J. Greffet, and M. Nieto-Vesperinas, *Phys. Rev. A*, Vol. 62, 012712, 2000.

Energy Emission from Evanescent Wave and Interference of Opposite Wave Streams: Near Field Coherent Scattering by Random Medium

Yu. N. Barabanenkov[1] and M. Yu. Barabanenkov[2]

[1]Institute of Radioengineering and Electronics, Russian Academy of Sciences
Mohovaya 11, 103907 Moscow, GSP–3, Russia
[2]Institute of Microelectronics Technology and High Purity Materials, Russian Academy of Sciences
142432 Chernogolovka, Moscow Region, Russia

Abstract— In 1968, Veselago [1] predicted that a planar slab of left-handed materials (LHM), which posses both negative permittivity and negative permeability, could refocus the electromagnetic waves from a point source. Pendry [2] extended Veselago's analysis and further predicted that evanescent waves, which carry subwavelength structural information of the object, can be amplified inside the LHM slab. Therefore the LHM slab can be used as a superlens to achieve a subwavelength resolution. However, several recent analysis showed that the achievable subwavelength resolution is limited by the absorption and thickness of the LHM slab [3] and the slab surface plasmon modes [4]. There is also a limitation of subwavelength resolution caused by signal-to-noise ratio at information extraction from evanescent waves with the aid of a detection process where the evanescent waves have to couple on to propagating waves [3].

In this report we suppose that the above coupling an evanescent wave to propagating waves is performed at the evanescent wave scattering by a dielectric structure. We derive [5] a general and effective rule to estimate an upper limit of energy emission from an evanescent wave at scattering by a given dielectric material, in particular, a 3D random medium. Besides, the proposed analytical technique gives a better inside into the origin of energy emission effect from an evanescent wave considered in [6, 7].

The central point of the derivation is using a system of linear differential equations of the fist order for angular spectrum amplitudes of local electromagnetic waves going (propagating or decaying) forward and backward with respect to an embedding parameter into a 3D inhomogeneous dielectric medium. An original representation for the total energy flux along the embedding parameter is obtained as a pseudo-trace of the density matrix of angular spectrum amplitudes. The obtained representation reveals that energy emission from an evanescent wave explicitly relates with the interference between evanescent waves going (decaying) in opposite directions. This key result enables one to write the coefficient of energy emission from an evanescent wave at scattering by a dielectric structure in terms of interference of the evanescent wave incident onto dielectric medium with an evanescent component in its reflection from the medium. In particular, the evanescent wave coherent reflection by a 3D random medium slab can be evaluated with an appropriate Dyson equation for the ensemble-averaged angular spectrum amplitudes.

REFERENCES

1. Veselago, V. G., *Sov. Phys. Usp.*, Vol. 10, 509, 1968.
2. Pendry, J. B., *Phys. Rev. Lett.*, Vol. 85, 3966, 2000.
3. Garcia, N. and M. Nieto-Vesperinas, *Phys. Rev. Lett.*, Vol. 88, 207403, 2002.
4. Smith, D. R., D. Schurig, M. Rosenbluth, S. Schultz, S. A. Ramakrishna, and J. B. Pendry, *Appl. Phys. Lett.*, Vol. 82, 1506, 2003.
5. Barabanenkov, M. Y., Y. N. Barabanenkov, Y. V. Gulyaev, and S. A. Nikitov, *Phus. Lett. A*, Vol. 364, 421, 2007.
6. Gulyaev, Y. V., Y. N. Barabanenkov, M. Y. Barabanenkov, and S. A. Nikitov, *Phys. Lett. A*, Vol. 335, 471–472, 2005.
7. Gulyaev, Y. V., Y. N. Barabanenkov, M. Y. Barabanenkov, and S. A. Nikitov, *Phys. Rev. E*, Vol. 72, 026602-1-026602-12, 2005.

The Characteristic Properties of Description of the Near Fields in the Wicinity of Wood Resonance

V. L. Kuznetsov

Department of Applied Mathematics, Moscow State Technical University of Civil Aviation (MSTUCA)
20, Krondshtadskiy blv., Moscow 125993, Russia

Abstract— The interaction of radiation with periodic structures is very interesting because the problems like this meet often in different applications. The most interesting aspect of this problem is the detection of the near fields' role in the condition of Wood anomalies. The one of the most promising approaches to this problem, from our point of view, is imbedding method, where as an imbedding parameter we choose depth of flat layer with periodic structure. Calculation of reflection and transparence coefficients of elementary layer with asymptotical small width adding to periodic structure takes an important place in this method. The infinitesimal of the thickness of elementary layer allows in any cases to use Born approximation by calculation transmitted and reflection fields in the conditions of finite dielectric permittivity. On attempted to describe effects in the areas of Wood anomalies this approximation causes the appearance of singularity in the coefficients of the imbedding equation. Description of this event is the most interesting in the problems like the problem about distortion of the hyper short impulse propagating in photonic crystal.

In the report considers another approach to the calculation problem of electrodynamics parameters of elementary layer which is clear from Born approximation's limitation. It's shown that limiting transition in deduction of differentiation imbedding equations cause partially information loss about any properties of reflection near Wood resonance, which is substantial in use numerical methods. There are presented finite increments equations which allow correct describe the wave interaction with the periodical structure in the vicinity of Wood resonance.

Near Field Effect in Microwave Radiation of Periodically Heated Plane-like Thermal Source

Yu. N. Barabanenkov[1] and M. Yu. Barabanenkov[2]

[1]Institute of Radioengineering and Electronics, Russian Academy of Sciences
Mohovaya 11, 103907 Moscow, GSP-3, Russia
[2]Institute of Microelectronics Technology and High Purity Materials
Russian Academy of Sciences, 142432 Chernogolovka, Moscow Region, Russia

Abstract— In 1953, Rytov [1] has predicted theoretically the near-field (quasistationary) component in thermal radiation of absorbing dielectric media. Carminati and Greffet [2] extended Rytov's analysis and showed that a long-range spatial coherence may exist in near-field of light thermally emitted into free space by an opaque materials supporting resonant surface waves, such as surface-plasmon or surface phonon polaritons. Gaikovich et al. [3] discovered experimentally a near-field effect in thermal radio emission of an absorbing dielectric medium, having shown in fact that the effective depth of the receiver emission formation appears to be less than the skin-layer depth and depends on the size of the receiver antenna and its height above the surface. Coello et al. [4] investigated experimentally a local control of evanescent microwaves using a scanning near-field microwave microscope (SNMM). It is interesting to note that in the SNMM a signal probe — small metallic sphere is used that acted as a scatterer of the evanescent field, leading to homogeneous (propagating) waves which can be easily detected and evaluated with the aid of the general analysis of energy emission effect from evanescent wave at scattering by dielectric structures [5, 6]. Here we would like to show that the SNMM mentioned can be used with some modification of signal probe also for local control of evanescent microwaves in thermal radiation from periodically heated plane-like thermal source and consider a specific near-field coherent effect related to spatial variation of source temperature.

Actually we consider an evanescent wave created by a plane-like source of thermal radiation, in the form of thin slab with thickness tending to zero and conductivity tending to infinity, such that their product becomes constant. The slab temperature is supposed to be periodically varying along the x-axis on the slab and has the form of series in a 1D diffraction grating spectral orders. This diffraction grating is placed in the near field zone of the slab, consisting the cylindrical rulings which are parallel to the y-axis and placed periodically along the x-axis. The diffraction grating is used as a signal probe in the SNMM and the signal energy is evaluated according to general theory [5, 6] of energy emission from evanescent wave. We show analytically that the intensity of energy emission from evanescent waves of thermal radiation through the diffraction grating should have an interference pattern at diffraction grating moving parallel to heated slab. In this case the diffraction contrast of the pattern is defined by temperature variation along the heated slab and the grating height above the slab.

REFERENCES

1. Rytov, S. M., *Theory of Electrical Fluctuations and Heat Emission*, Akademii Nauk SSSR, Moscow, 1953.
2. Carminati, R. and J. J. Greffet, *Phys. Rev. Lett.*, Vol. 82, 1660, 1999.
3. Gaikovich, K. P., A. N. Reznik, V. L. Vaks, and N. V. Yurasova, *Phys. Rev. Lett.*, Vol. 88, 104302, 2002.
4. Coello, V., R. Villagomez, R. Cortes, and R. Lopez, *Revista Mexicana de Fisica*, Vol. 51, 426, 2005.
5. Gulyaev, Y. V., Y. N. Barabanenkov, M. Y. Barabanenkov, and S. A. Nikitov, *Phys. Lett. A*, Vol. 335, 471–472, 2005.
6. Gulyaev, Y. V., Y. N. Barabanenkov, M. Y. Barabanenkov, and S. A. Nikitov, *Phys. Rev. E*, Vol. 72, 026602-1-026602-12, 2005.

Scattering Properties of a Cylinders Fabricated from Left-Handed Material

V. Kuzmiak[1] and A. A. Maradudin[2]

[1]Institute of Photonics and Electronics, Czech Academy of Sciences, Prague 8, Czech Republic
[2]Department of Physics and Astronomy, University of California, Irvine, California 92697-4574, USA

Abstract— We investigate scattering properties of electromagnetic (EM) waves by a cylinder fabricated from a left-handed (LH) material represented by a system of combined split-ring resonators (SRR) and thin metal wires that is characterized by an effective frequency-dependent permittivity and permeability. We study separately the effects of the specific forms of the effective permittivity and permeability on the existence of both bulk and surface polaritons, and compare the results to those obtained for a cylinder fabricated from LHM. We examine the scattering properties of such a cylinder by evaluating the total scattering width, which for an infinitely long cylinder is defined as the scattering cross section per unit length. We find that in the case where the magnetic field is perpendicular to the plane of the SRR, the scattering width as a function of the frequency of the incident wave reveals Mie resonances for both E- and H-polarized waves. These peaks occur in the frequency range where the effective refractive index is negative, and they arise from modes that propagate with a negative group velocity. This behavior is consistent with the results of transfer-matrix calculations and transmittance experiments on two-dimensional left-handed metamaterials, which show that the medium becomes transparent to the EM radiation in this frequency range. In discussion we put our results into the context of recent activities linked to the existence of surface polaritons that can be classified by distinct families that correspond to surface polaritons in the large-radius limit and whispering gallery modes that are specific to left-handed materials.

Operation of Evanescent Wave Intensity Using Metamaterials of Negative Permittivity and Permeability

Yu. N. Barabanenkov[1], **M. Yu. Barabanenkov**[2], **and S. A. Nikitov**[1]

[1]Institute of Radioengineering and Electronics, Russian Academy of Sciences
Mohovaya 11, 103907 Moscow, GSP-3, Russia
[2]Institute of Microelectronics Technology and High Purity Materials, Russian Academy of Sciences
142432 Chernogolovka, Moscow Region, Russia

Abstract— As it was shown by Pendry [1] extending Veselago's analysis [2], a planar slab of material, for which both the dielectric permittivity ε and magnetic permeability μ have the values of $\varepsilon = -1$ and $\mu = -1$, can amplify at transmission the electromagnetic evanescent waves. On the other hand, the authors [3–5] have studied the energy emission effect from electromagnetic evanescent wave at scattering by a dielectric structure and elucidated this effect in terms of interference of the evanescent wave incident onto a dielectric structure with an evanescent component in its reflection from the structure.

In this report we bring together the mentioned effects of evanescent wave amplifying and energy emission from evanescent wave at evanescent wave scattering by an inhomogeneous metamaterial. Actually this means operation of evanescent wave intensity using a medium with negative and inhomogeneous dielectric permittivity and magnetic permeability. Physically we consider an evanescent wave scattering by a metamaterial slab, with dielectric permittivity $\varepsilon = -1 + \delta\varepsilon(x, y)$ where $\delta\varepsilon(x, z)$ is a 2D deviation and magnetic permeability $\mu = -1$. Mathematically we generalize the invariant imbedding method [6] and transfer relation approach [7] on the case of metamaterials. Besides, the proposed analytical technique gives a better inside into boundary problem associated with wave scattering by medium inhomogeneous in dielectric and magnetic properties simultaneously.

The central point of our consideration is an integral equation for the Green function of the scattering problem with TE polarization when the electric field vector is parallel to the y axis. This equation has two integral terms, with volume integral (volume effective scattering potential) and surface integral (surface effective scattering potentials). According to references [3–5], the volume scattering potential describes the energy emission from evanescent wave at scattering by the dielectric permittivity inhomogeneities $\delta\varepsilon(x, z)$. But the surface scattering potential describes, as appeared, the evanescent wave amplifying by metamaterial, in accordance with effect of the surface polaritons in a left-handed material slab [8]. We see, that there is a concurrence between two opposite processes: the evanescent wave intensity decreasing because the energy emission from this one at volume scattering and the evanescent wave amplifying because effect of surface scattering potential in the left-handed material slab. We study this concurrence phenomenon with the help of Riccati equation for the slab reflection coefficient and associated equation for the slab transmission coefficient, which are obtained in the framework of invariant imbedding method.

REFERENCES

1. Pendry, J. B., *Phys. Rev. Lett.*, Vol. 85, 3966, 2000.
2. Veselago, V. G., *Sov. Phys. Usp.*, Vol. 10, 509, 1968.
3. Gulyaev, Y. V., Y. N. Barabanenkov, M. Y. Barabanenkov, and S. A. Nikitov, *Phys. Lett. A*, Vol. 335, 471, 2005; *Phys. Rev. E*, Vol. 72, 026602, 2005.
4. Gulyaev, Y. V., Y. N. Barabanenkov, M. Y. Barabanenkov, and S. A. Nikitov, *Phys. Rev. E*, Vol. 72, 026602, 2005.
5. Barabanenkov, M. Y., Y. N. Barabanenkov, Y. V. Gulyaev, and S. A. Nikitov, *Phys. Lett. A*, Vol. 364, 421, 2007.
6. Klytskin, V. I., *The Imbedding Method in the Theory of Wave Propagation*, Nauka, Moscow, 1980.
7. Barabanenkov, Yu. N., V. L. Kouznetsov, and M. Yu. Barabanenkov, *Progress in Electromagnetic Research, PIER*, ed. Kong, J. A., Vol. 24, 39–75, EMW, Cambridge, England, 1999.
8. Ruppin, R., *J. Phys.: Condens. Matter*, Vol. 13, 1811, 2001.

Session 3A2b
Printed Antenna and RFID Sensor Elements

About Feasibility of Reducing Dimensions of Sectioned Microstrip Antennas

B. A. Mishoostin, **V. G. Slyozkin**, **and M. S. Sinkovsky**
Sevastopol National Technical University, Studgorodok, Sevastopol 99052, Ukraine

Abstract— Well-known microstrip antennas called as "patch" antennas (PA) have the radiating structure formed by a flat conductive patch (section) on a dielectric base and located above the conducting screen. Minimum dimensions of a MSA are limited by the condition of ensuring certain excitation phases of the section edges, as well as by the antenna-to-feeder matching condition.

In our previous works [1, 2] we had proposed various alternatives of sectioned microstrip (patch) antennas (SPA) and considered various calculation methods, electrical characteristics and feasibility to create SPA having two, three and four sections.

The simplest SPA has two sections separated with a small gap. Coaxial feeder running along one of the sections connects the edge of this section to the screen with its outer conductor and terminates at the center of the structure. Since the cable inner conductor excites the second section, the sections prove to be excited at any frequency so that the pattern maximum is directed perpendiculary to the radiating structure. So, the main factor limiting minimum dimensions of the SPA is its feeder matching conditions.

The purpose of this report is to determine feasibility of reducing dimensions of the SPA by means of such complication of the shape of the radiating structure that would not cause the construction to become more complex. As before, antenna can be made mainly using printed-circuit technology.

Input impedance of each section of the considered SPA near operating frequency has the frequency dependance similar to that of a parallel oscillating circuit. Near a resonant frequency there are two frequencies at which active component of the impedance of one section equals to the half of the feeder wave impedance. At any of these frequencies SPA can be matched with the feeder by using series reactance having opposite sign and required value.

Dimensions of the SPA can be reduced additionally (or operating frequency can be lowered without increasing overall dimensions) by raising the parallel circuit inductivity. To do this physically it is sufficient to make two small-width rectangular cutouts parallel to the cable in one section, and two cutouts symmetrically to the first two in another section. Cutouts are to begin at the section edges, progress to their centers and must terminate before of the gap between the sections.

Experimental model without cutouts was designed to have 430 MHz operating frequency and had the structure of 120 mm radius or near 0.17λ, where λ is wavelength. Relative matching band for level VSWR equals to 2.0 was about 1.5%. After making cutouts of 40 mm in length and 3 mm in width, operating frequency came down to 350 MHz, and relative band became equal to 0.43%.

So, it is not difficult to reduce dimensions of a SMA by about 20% even without optimizing parameters of the radiating structure. Of course, this results in shortened operating frequency band, but in those cases where antenna dimensions are of critical importance and the operating frequency bandwidth is insignificant, the proposed solution can be of particular interest.

REFERENCES

1. Mishoostin, B. A. and V. G. Slyozkin, "The sectioned microstrip antennas," *4th Int. Conf. on Antenna Theory and Techniques ICATT-2003*, *Proceedings*, Vol. 1., 501–503, Sevastopol, Ukraine, 8–11 Sept., 2003.
2. Mishoostin, B. A., V. G. Slyozkin, and M. S. Sinkovsky, "About new trends in development of microstrip antennas based on sectioned structures," *European Conference on Antennas and Propagation EuCAP-2006*, Proceedings on CD, Nice, France, 6–10 November, 2006,

Performance of a Folded Dipole with a Closed Loop for RFID Applications

Sung-Lin Chen and Ken-Huang Lin

Department of Electrical Engineering, National Sun Yat-Sen University, Taiwan

Abstract— Radio frequency identification is a rapidly developing technology for automatic identification of objects in the supply chain. In an RFID system, a tag antenna acts as a power receiver that transforms the electromagnetic wave into electrical energy for the chip. For the purpose of energy conversion, the tag chip includes a charge capacitor that causes the tag chip to have a large reactive impedance, making the antenna more difficult to match with the tag chip than with a general radio frequency system of 50 Ω characteristic impedance. The electromagnetic power from the antenna is maximally delivered to the tag chip when the antenna has a conjugate impedance of the chip. A successful antenna design is determined by conjugate impedance match between both components. In this paper, we present a folded dipole antenna with a closed loop near the tag chip. The required input resistance (R_i) and reactance (X_i) can be achieved separately by choosing appropriate geometric parameters. The closed loop makes impedance matching design more easily especially when a small resistance part of the antenna impedance is required. In RFID applications, this allows the antenna to match to the tag chips that usually have small resistance and large reactance. In addition, the closed loop serves as short circuit to DC current, so it can eliminate electrostatic discharge (ESD) from damaging the tag chip. The closed loop inductance and the chip capacitance form a resonant circuit that can be used with near field characteristics of the interested frequency band. Finally, we also give the detailed design parameters of a real case with TI UHF Strap. The design method presented here can also be applied to various impedances of the commercial tag chips which operate at other frequency bands, such as 2.45 GHz and 5.8 GHz.

Radiation Characteristics of Optimized Ultra Wideband Printed Dipoles for Different Impulse Excitations

P. Cerny and M. Mazanek

Department of Electromagnetic Filed, Czech Technical University in Prague
Czech Republic

Abstract— In case of particular ultra wideband applications (i.e., radar, positioning, etc.), it is crucial to know the transient responses of antennas. This paper picks up the threads of the previous work, where the optimization process searches for the dipole shape, which accomplishes two required parameters — good matching and minimal distortion. The particle swarm optimization method was used in the process of dipole shape optimization.

The dipole structure is excited by the second derivative of the Gaussian impulse. Because of derivative radiation characteristics of dipoles, the distortion of radiated impulses is evaluated as fidelity using convolution function (with the third derivative of the Gaussian impulses). The differential feeding port used for excitation of optimized dipole shape is non-physical port and was used only for the simplification of the optimized structure and acceleration of the optimization process. The optimized and serrated dipole shape is smoothed.

Two very different feeding circuits were used for dipoles feeding. For the feeding of the optimized dipole structure, the $50\,\Omega$ microstrip line was used. In the first case, a feeding planar balun transformer progressively transforms from the impedance $50\,\Omega$ of the microstrip line to impedance $100\,\Omega$ of the parallel plate line. This parallel plate line is directly connected to the feeding gap between dipole parts. The second solution is based on feeding of the monopole directly by the $50\,\Omega$ microstrip feeding line. The monopole element and the planar ground plane are situated on the same microwave substrate, but on the different sides. The feeding parts of dipole and monopole were tuned step-by-step in order to minimize the reflection coefficient in the required frequency band.

The main part of the paper presents the transient radiation characteristics of optimized dipoles with common dipole element shape, such as the ideal dipole, dipole with balun transformer and monopole with planar ground plane. The comparison of radiation characteristics is focused on the distortion of radiated impulses for different impulse excitation, such as Gaussian impulse, the first derivative of Gaussian impulse and the second derivative of Gaussian impulse.

Collinear and Coparallel Principles in Antenna Design

M. Polivka and A. Holub
Department of Electromagnetic Field, Czech Technical University in Prague, Czech Republic

Abstract— The paper first summarizes collinear principle (CoP) used for the design of linear, coaxial and microstrip line types of collinear array (CoAr), see Fig. 1. Physical nature of CoP is explained via description of surface current density of various types of CoArs starting from original wire design introduced by Franklin in 1924 [1] that had $\lambda/4$ U-shaped sections to provide 180° phase shift to maintain in-phase feeding of straight $\lambda/2$ parts of wire, going through coaxial collinear (COCO) arrays [2] as far as to CoArs implemented in microstrip line technology [4, 5]. Linear versions of CoAr have nearly omnidirectional radiation pattern due to more or less longitudinal axis symmetry of surface current as a source quantity.

Further CoP implemented by authors in microstrip patch technology in linear [5] and planar versions of collinear microstrip patch antenna (CoMPA) is mentioned. Antenna properties exhibiting directive type of radiation pattern due to the presence of ground plane as integral part of patch antennas are discussed. Detailed operational principle based on explanation of current distribution of excited TM_{0x} modes is provided.

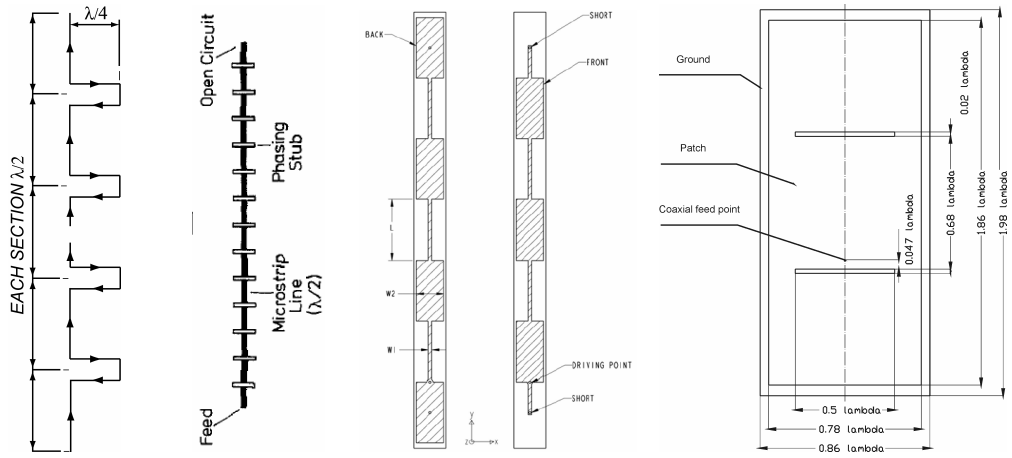

Figure 1: Geometry of several collinear arrays, (a) original Franklin dipole [1], (b) microstrip line with a flat O shaped sections [3], (c) thin/thick section microstrip line [4], (d) collinear microstrip patch antenna [5].

As a new contribution of this paper collinear antenna based on sequential arrangement of basic F-type antenna elements is presented. Again operational principle, corresponding radiation pattern properties as well as particular implementation with coaxial-microstrip feeding structure of 2.44 GHz antenna prototype will be presented.

REFERENCES

1. Franklin, C. S., Brit. Patent 242342-1924, 1924.
2. Judazs, T. J. and B. B. Balsley, "Improved and theoretical and experimental models for the coaxial collinear antenna," *IEEE Trans. Antennas and Propagat.*, Vol. 37, 289–296, 1989.
3. Solbach, K., "Microstrip-Franklin antenna," *IEEE Trans. Antennas and Propagat.*, Vol. 30, No. 4, 773–775, 1982.
4. Bancroft, R. and B. Bateman, "An omnidirectional planar microstrip antenna," *IEEE Trans. Antennas and Propagat.*, Vol. 52, No. 11, 3151–3153, 2004.
5. Polívka, M., A. Holub, and M. Mazánek, "Collinear microstrip patch antenna," *Radioengineering*, Vol. 14, No. 4, 2005.

Session 3A3
Circuits and Devices, CAD 1

An Expression for the Intrinsic Coupling Unbalance of a Symmetrical 4 Port Directional Coupler in Terms of the Cross Ratio of Its 4 Eigenadmittances or 4 Eigenimpedances

G. P. Riblet
Microwave Development Laboratories, Inc.
Needham, MA 02494-14834, USA

Abstract— It is a well known theorem that if suitable matching networks are connected in each of the 4 ports of a lossless reciprocal 4 port device so that each of the ports of the overall device is matched ($S_{11} = S_{22} = S_{33} = S_{44} = 0$), then the overall 4 port is a directional coupler. That is in each case the coupling is zero to one of the three output ports. An important unknown quantity is the coupling unbalance between the remaining two output ports that results from this process. This quantity will be referred to here as the intrinsic coupling unbalance of the original unmatched 4 port. It is shown in this paper that for the most common case of a symmetrical lossless reciprocal 4 port, the intrinsic coupling unbalance (as a power ratio) is given by the cross-ratio of the unmatched circuit's 4 eigenadmittances or 4 eigenimpedances.

Compact CPW Bandpass Filter Based on Three-line CPW Structure and Lumped-element K-inverter

Yo-Shen Lin and Tsung-Ping Kao

Department of Electrical Engineering, National Central University, Chungli 320, Taiwan

Abstract— In this work, a compact coplanar-waveguide (CPW) bandpass filter is proposed, using the 3-line parallel-coupled CPW along with metal strip inductors between the CPW coupled-lines as the lumped-element K-inverter. The proposed filter structure is equivalent to a quarter-wavelength resonator filter. As a result, the filter size may be reduced by about 40% and no spurious passbands at even harmonics will be observed. Due to the symmetry of proposed filter, no bondwires or airbridges are required, which simplifies the fabrication process. In addition, by introducing the capacitive cross-coupled effect, two transmission zeros at the upper and lower stopbands may be created. Suitable equivalent-circuit model is also established as effective design tool. Specifically, a 2nd-order CPW bandpass filters as shown in Fig. 1 is implemented on an Al_2O_3 substrate ($\varepsilon_r = 9.8$, $\tan\delta = 0.002$, and thickness = 325 μm). The measured insertion loss is 2 dB at $f_0 = 31.52$ GHz, with a 3 dB bandwidth of 23.8% and two transmission zeros.

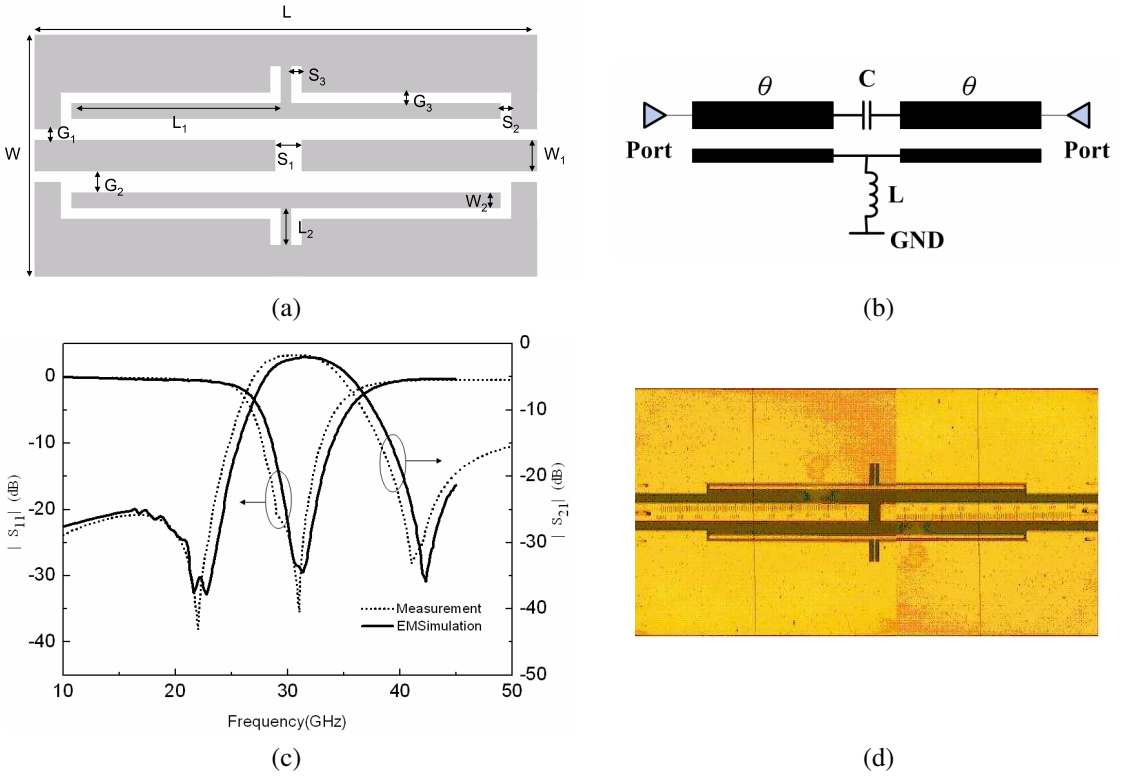

Figure 1: (a) Layout of proposed CPW bandpass filter structure, (b) circuit model, (c) measured and simulated results, (d) filter photograph.

The Duplexer for the Urban Cable Television 40 GHz Band Bi-directional Transmission System

Y. Utsumi[1], **T. Kamei**[1], **N. Thanh**[1], **and H. Suzuki**[2]

[1]National Defense Academy, Japan
[2]Keycom Corporation, Japan

Abstract— Urban cable television in Japan has begun to increase transmission capacity in parallel with the trend toward digital broadcasting. This development will require large-capacity bi-directional transmission technology for the interval from the cable company's head end to apartment complexes and other sites. The device that will play an important role in such a bi-directional transmission system for urban cable television is a transmit/receive duplexer. In this paper, we report on the design and construction of a prototype band pass filter using inductive-strips (E-plane planar circuits) based on electromagnetic-field simulations. We also report on the construction and characteristics of a prototype duplexer consisting of two band pass filtersone each for the uplink and downlinkand a Y-shaped branch circuit.

The downlink from the cable-TV head end to subscribers uses the 40.65–41.5 GHz band while the uplink from subscribers to the head end uses the 42.0–42.15 GHz band. Within these bands, the system is suppose to transmit cable-TV signals in the 42.090–42.135 GHz slot (bandwidth: 45 MHz) on the uplink and in the 40.77–41.47 GHz slot (bandwidth: 700 MHz) on the downlink.

Figure 1(a) shows a cross sectional view of an E-plane planar circuit and Fig. 1(b) shows inductive strips for an n-step band pass filter made up of E-plane planar circuits. Filter characteristics are achieved by a structure that divides the waveguide at the center of the H plane and inserts the conducting strip shown in (b) into the divided waveguide. The strength of inductive coupling changes according to the width (W_j) of an inserted inductive-strip, and resonator length l determines the center frequency of the filter. Band pass filter characteristics can be determined by adjusting the strength k_{ij} of coupling between resonators by inductive-strip width W_j.

For the uplink, we constructed a 3-step maximally flat filter and obtained a center frequency of 42.1125 GHz, a 3-dB bandwidth of 196 MHz (design value: 200 MHz), and an insertion loss of 2.80 dB. This corresponds to an unloaded Q value of $Q_0 = 2000$. For the downlink, we constructed a 5-step Tchebycheff filter and obtained a center frequency of 41.12 GHz, a 3 dB bandwidth of 900 MHz (design value: 1 GHz), an insertion loss of 1.32 dB, and an in-band ripple of about 1 dB (design value: 0.5 dB). This corresponds to an unloaded Q value of $Q_0 = 1500$.

Figure 2 shows an external view of our prototype duplexer consisting of transmit/receiving filters using E-plane planar circuits and a Y-branch circuit. The insertion loss of the Y-branch

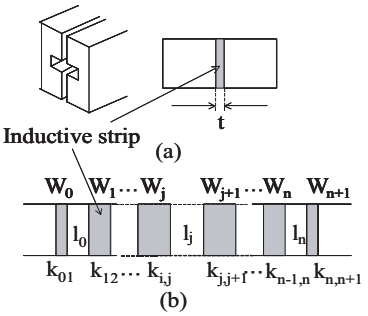

Figure 1: The structure of E-plane planar circuit band pass filter with inductive strips. (a) cross sectional view. (b) inductive strips for n-step band pass filter.

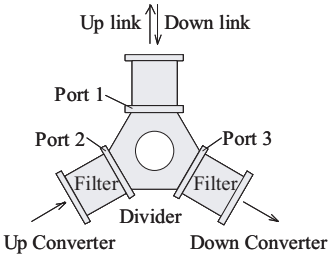

Figure 2: External view of the prototype duplexer.

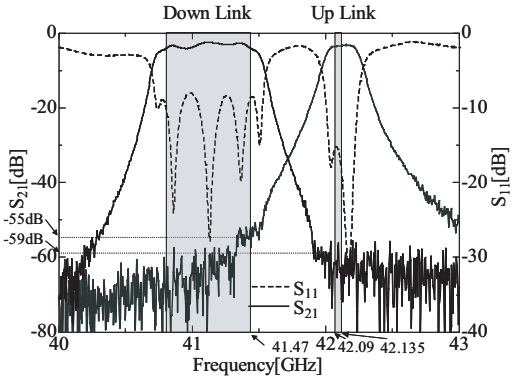

Figure 3: The frequency characteristics of the prototype duplexer.

circuit used here is about 0.3 dB. Port 1 of the branch circuit is used as a high-frequency-signal input/output port. The uplink filter connects to Port 2 and the downlink filter to Port 3.

Figure 3 shows overall frequency characteristics of the prototype duplexer. The solid line represents S_{21} transmission characteristics and the broken line S_{11} reflectivity characteristics. These results show a bandwidth of 195 MHz and an insertion loss of about 3.1 dB for the uplink filter and a bandwidth of 763 MHz and an insertion loss of about 1.7 dB for the downlink filter. It was found that an out-of-band attenuation for the uplink filter (the attenuation from the flat section at the upper frequency limit used in the downlink) of 53 dB at 41.47 GHz could be achieved, as could an out-of-band attenuation for the downlink filter (the attenuation from the flat section at the lower frequency limit used in the uplink) of 56 dB at 42.09 GHz.

Coupled-resonator Design of Microstrip Shorted-stub Bandpass Filters with Quarter-wave Resonators

Shih-Cheng Lin and Chun Hsiung Chen
Department of Electrical Engineering and Graduate Institute of Communication Engineering
National Taiwan University, Taipei 106, Taiwan

Abstract— Bandpass filters based on half-wavelength ($\lambda/2$) open stubs or quarter-wavelength ($\lambda/4$) shorted stubs are quite attractive owing to the relatively wide realizable bandwidth and low insertion loss around the passband. Usually, these filters are good candidates for wideband applications. Although the dual-behavior resonator (DBR) filter is possible to be designed with narrow bandwidth, the design formulas for obtaining the required specifications are not intuitive for the designers and the DBR filter also suffers from the drawback of no DC block. The traditional n-pole $\lambda/4$ stub filter provides the bandpass response according to the designed characteristic admittances of the stubs and the characteristic admittances of the connecting lines. However, if one would like to design a $\lambda/4$ shorted-stub filter with a narrow bandwidth, the admittances of the shorted stubs become too high to be realized due to fabrication restriction. Hence, it is essential to develop a convenient and easy approach for designing the shorted-stub filters with narrow bandwidth.

In this study, an alternative coupled method, different from the conventional approach, for controlling the bandwidth of microstrip shorted-stub bandpass filters is proposed. Among the proposed filter, two adjacent quarter-wavelength shorted-stub resonators are coupled together by directly connecting a $\lambda/4$ transmission line to the resonators, with its connecting position being adjustable. By properly moving the connecting position, one may adjust the coupling coefficient between two stub resonators so that the bandwidth of developed filter may easily be controlled. More precisely, the $\lambda/4$ connecting line is regarded as an admittance inverter with inverter value proportional to its line characteristic impedance while the tapped stub-resonator is principally composed of short-circuited stub and open-ended stub with stepped impedance. Therefore, the required line impedance can be obtained by considering the susceptance slope of connected $\lambda/4$ resonator. Very simple mathematical relationship between the required connecting-line admittance and coupling coefficient is derived in accordance with the transmission-line equivalent circuit. As a result, the design curve of coupling coefficient versus connecting position is illustrated for design convenience. To this end, the design procedure based on the mostly popular coupled-resonator approach can be achieved.

With the controllable coupling coefficient, one may implement the filter with narrow or moderate bandwidth without being restricted by the unhandy admittances. Based on the proposed coupled scheme, the filters with narrow/moderate bandwidth may be designed and implemented. Specifically, a two-pole microstrip filter with the bandwidth of 13% impractical in conventional stub filters is successfully fabricated. In addition, another four-pole filter possessing the bandwidth of 40% is also designed and implemented. Good agreement between measured and simulated results is observed.

Planar Filters Using High-Q Slotted Cylindrical Ring Resonators

Dariush Mirshekar-Syahkal and Y. C. Mark Lim
Department of Electronic Systems Engineering, University of Essex, Colchester CO4 3SQ, UK

Abstract— The slotted or split cylindrical ring (SCR) resonator has been used in pulsed electron paramagnetic resonance measurement, electrostatic resonance spectroscopy, magnetron design and heavy-ion particle accelerators. The SCR resonator is relatively small, but when properly designed, it can offer a high Q at the lower end of microwave frequencies. Therefore, it is attractive for development of compact filters for mobile communications.

In [1], we have reported a numerical technique for the analysis of the SCR resonator and for computing the coupling between two longitudinally (uniaxially) coupled SCR resonators. Using the technique, we designed and demonstrated a longitudinal fourth-order filter using SCR resonators [1].

We have extended the work with the objective of achieving filters using SCR resonators located in one plane. The planar structure can offer easy realisation of cross-couplings amongst nonadjacent resonators, thus allowing one to realise real or imaginary transmission zeros. Realisation of such zeros is important in many present mobile communications applications where the filter requires a steep skirt or a flat group delay.

This paper commences with a brief introduction to the SCR resonator and highlights those parameters which significantly influence its resonant frequency and Q-factor. It then proceeds to the numerical analysis of single and coupled SC resonators in planar arrangement. From the analysis, the resonant frequency and the Q-factor of a typical resonator, and the coupling coefficients between two of these resonators are obtained. Since the resonators are in the same plane, the quasistatic numerical technique proposed in [1] cannot be adopted for the analysis of the planar coupled SCR resonators. Instead, the transmission line matrix (TLM) technique is used to compute the couplings. The theoretical results are verified experimentally. One important point emerged from the analysis is the variation of the coupling coefficient with the relative slot positions of the resonators. This effect, which can be significant, may be used to fine tune a coupling in practice. The results of the analysis are used to develop a compact fourth-order Chebyshev filter with a centre frequency at 1.75 GHz and 0.1 dB ripple. The measurement revealed that the fabricated filter, which is approximately $10\,\text{cm} \times 2\,\text{cm} \times 2\,\text{cm}$, has a low insertion loss of 1.23 dB at the centre frequency. The insertion loss can be reduced further by silver plating the aluminium resonators used in the filter.

REFERENCES

1. Mostafavi, R. F., Y. C. M. Lim, and D. Mirshekar-Syahkal, "Small filters based on slotted cylindrical ring resonators," *IEEE Trans. Microwave Theory Tech.*, Vol. 49, 2369–2375, Dec. 2001.

Wiener-Hopf Analysis of the Open Rectangular Asymmetrical Groove Guide

İ. H. Tayyar[1], **A. Büyükaksoy**[1], **A. Işıkyer**[1], **and G. Uzgören**[2]

[1]Gebze Institute of Technology, Çyırova Campus, 41400, Gebze, Kocaeli, Turkey
[2]Istanbul Kültür University, Ataköy Campus, 34156, Istanbul, Turkey

Abstract— Because of its many advantages such as low-loss and high power capacities at millimeter wavelengths, the rectangular groove guide has been extensively studied both analytically and experimentally. In almost all investigations, the groove guide is assumed to be symmetrical which simplifies considerably the analysis. The aim of the present work is to provide a rigorousWiener-Hopf analysis to the asymmetrical groove waveguide depicted in Fig. 1, in the case where the grooves are filled with different dielectric materials. The formulation of the problem in terms of Fourier integrals leads to a matrix modified Wiener-Hopf equation. Although, no general methods exists to perform the Wiener-Hopf factorization of an arbitrary kernel matrix, the simultaneous modified Wiener-Hopf equations encountered in this work are uncoupled by using the anaytical properties of the functions that occur and by introducing some infinite sums over certain poles with unknown expansion coefficients. The solution involves two infinite sets of unknown coefficients satisfying two infinite systems of linear algebraic equations which are solved numerically. Some graphical results showing the effects of the depts of the grooves and the material parameters on the reflection and transmission coefficients are presented.

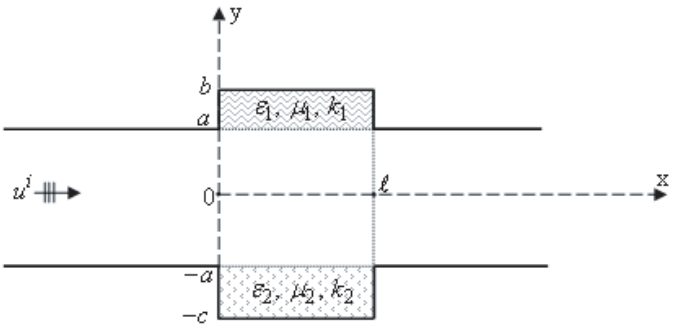

Figure 1: Dielectric filled asymmetrical groove guide.

Wide-band Coaxial-to-coplanar Transition

Y. Utsumi, T. Kamei, N. Q. Dinh, and N. Thanh
Department of Communications Engineering, National Defense Academy
1-10-20 Hashirimizu, Yokosuka, Kanagawa, 239-8686, Japan

Abstract— Targeting the transition from a coaxial waveguide to a coplanar waveguide (CPW), a microwave and millimeter-wave wide-band coaxial-to-coplanar transition is proposed. This design connects the coaxial center conductor to the CPW center conductor in a perpendicular manner to directly couple, on the same plane, the radial high-frequency electric field in the coax to the gap between the CPW's center conductor and ground plane. The characteristics of the proposed transition were compared with those of the conventional transition by experiment and electromagnetic field simulations, and it was found that the proposed method is independent of CPW shape and that it exhibits good matching characteristics in comparison to the conventional method especially in high-frequency bands above 15 GHz.

Figures 1 and 2 show the structures of conventional coaxial-to-coplanar transition and proposed coaxial-to-coplanar transition, respectively. In these figures, both side's transitions are connected by a 50 Ω CPW (length l) for measuring the transmission performance, S_{21}. In Fig. 1, two center conductors connect on the same plane, but here, the two-dimensional radial high-frequency electric field of the coax couples with the high-frequency electric field in the CPW's gap S. In Fig. 2, in contrast, the center conductors of the two lines connect at a right angle suggesting that the radial high-frequency electric field of the coax can directly couple with the high-frequency electric field in gap S of the CPW in a uniform manner and on the same plane without being dependent on the values of W and S.

In the following experiments, we connected each of the transition structures to both ends of 50 Ω CPW with line length $l = 25.4$ mm, the substrate's thickness, $h = 350$ μm, the conductor's thickness $t = 9$ μm and the relative dielectric constant of the substrate, $\varepsilon_r = 3$.

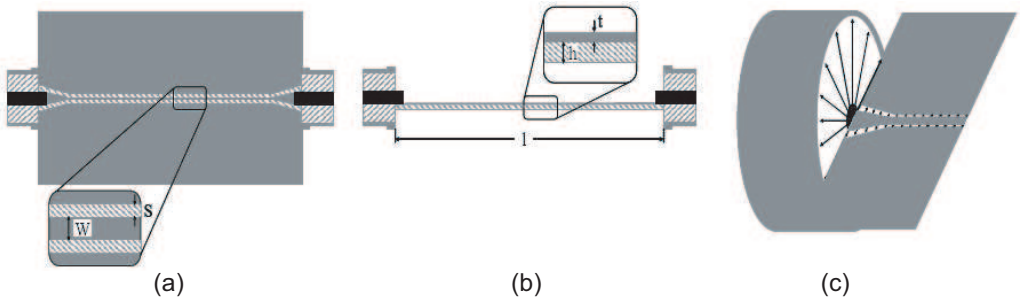

Figure 1: Structure of conventional Coaxial-to-Coplanar Transition. (a) Top plan view. (b) Sectional view. (c) Enlarged view.

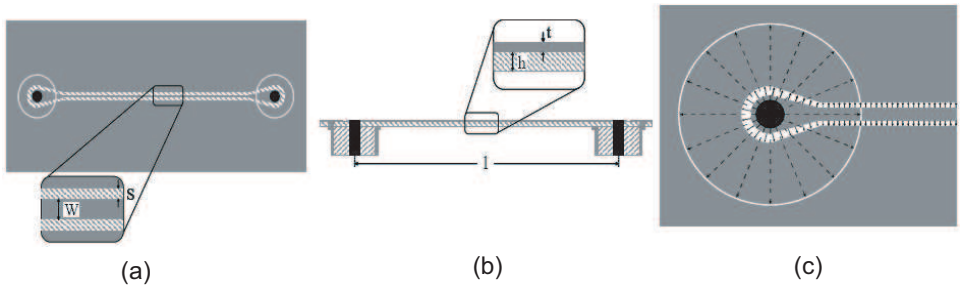

Figure 2: Structure of proposed Coaxial-to-Coplanar Transition. (a) Top plan view. (b) Sectional view. (c) Enlarged view.

For the Fig. 1 transition, Fig. 3 shows experimental results for the three W and S combinations, ($W = 300$ μm, $S = 30$ μm), ($W = 600$ μm, $S = 48$ μm), ($W = 900$ μm, $S = 65$ μm), and

simulation results for the ($W = 300\,\mu m$, $S = 30\,\mu m$). It can be seen that experimental and simulation values agree well and that a standing wave forms due to mismatch in the two transitions connected to both ends of the CPW. Also, for high-frequency bands in excess of 15 GHz when using the conventional method shown in Fig. 1, S_{21} values differ greatly depending on the values of W and S even if Zc of $50\,\Omega$ in the CPW is maintained. That is to say, S_{21} values deteriorate the smaller the values of W and S become.

Figure 4 shows S_{21} for the proposed method shown in Fig. 2 for the above three combinations of W and S. These results show that the mismatch at the two transitions connected to both ends of the CPW has been reduced. Also, for high-frequency bands up to 27 GHz, S_{21} values are nearly the same for the various combinations of W and S provided that $50\,\Omega$ is maintained for Zc of the CPW. The reason for this is thought to be as follows. As shown in Fig. 2, the radial high-frequency electric field of the coaxial wave guide's basic mode can be made to uniformly couple on the same plane with the 2D-like high-frequency electric field in the CPW's S section, this regardless of the values of W and S. In any case, there is very little generation of higher-order modes. Simulation results for the ($W = 300\,\mu m$, $S = 30\,\mu m$) combination are also shown here together with experimental results, and it can be seen that they agree.

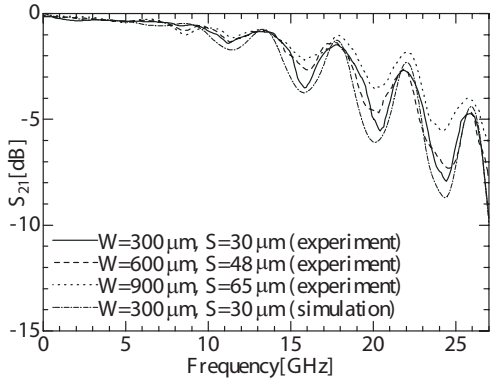

Figure 3: Frequency performances of S_{21} of conventional Coaxial-to-Coplanar Transitions.

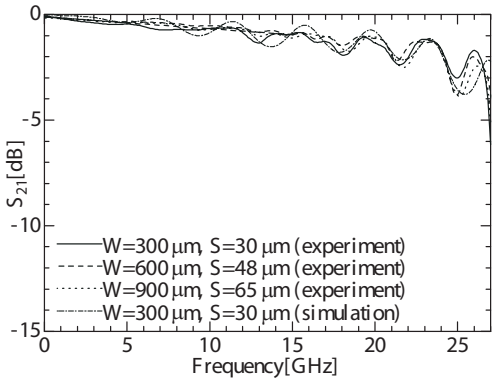

Figure 4: Frequency performances of S_{21} of conventional Coaxial-to-Coplanar Transitions.

Coupling of Fourier Series and Orthogonality of Functions in Computing Currents Induced in a Cable Enclosed in an Electromagnetic Enclosure

Habib Rahman
Department of Electrical Engineering, Saint Louis University
3450 Lindell Boulevard, Saint Louis, MO 63011, USA

Abstract— The boundary-value problem of determining currents induced on a cable enclosed in an electromagnetic cavity has found increasing applications to a variety of areas of practical interests. Electromagnetic sources exterior to cavity excite the cable which, in turn, excites the cavity interior. The analysis of cavities is associated with the dyadic Green's function which is most appropriately considered as an operator to generate the field from a given source function. Extensive expositions of such a function pertaining to cavities are available [1]. The dyadic Green's function for a problem of this nature can be solved numerically by the method of moments. But the dilemma of large computation time and complexity involved in case of dyadic Green's function approach warrants further work in this area. In this paper, an analytically simple, computationally stable and efficient approach that makes use of the Fourier series and the orthogonal functions is presented.

The formulation of this problem makes use of the Fourier series to approximate waveform of unknown current excited on the conducting cable. Of course, the infinite Fourier cosine series has to be truncated on order to obtain an analytically feasible solution. The choice of such a series is made by observing the orthogonal behavior of each mode existing inside the cavity interior. The field distribution in the cavity is determined by using the orthogonality properties. Once the field has been determined as a function of orthogonal modes, a matrix equation for the unknown Fourier coefficients is obtained by enforcing appropriate boundary conditions on the surface of the cable. The triply infinite sum representing the cavity environment is reduced into a doubly infinite one by using the Fourier series representation and orthogonality. This makes the solution much easier to handle as compared with the Green's function approach.

This method of analysis is efficient and versatile in its applications. The tedious task ordering modes that exist within the cavity has been eliminated by this method. This formulation can easily handle a load conditions. It has been shown that physically reasonable solution can be obtained for a variety of problems involving cables inside the cavity. However, it is worthwhile to mention that a comparison between the theory and the experiment must await the availability of experimental results.

REFERENCES

1. Tai, C. T. and P. Rosenfeld, "Different representations of dyadic Green's functions for a rectangular cavity," *IEEE Trans. Microwave Theory Tech.*, Vol. MTT-24, 597–601, September 1976.

A FEM Functional for Lossy Gyrotropic Phase Shift and Control Components

A. M. T. Abuelma'atti and A. A. P. Gibson
Microwave and Communication Systems Research Group, School of Electrical & Electronic Engineering
University of Manchester, Manchester, M60 1QD, England, UK

Abstract— A four transverse field formulation for a lossless Hermitian tensor material was introduced previously for an arbitrary direction of applied bias field. This method is extended here to include loss, which is critical in modeling experimental devices and which causes variational functionals for gyrotropic waveguides to become non-Hermitian. The functional is developed from Maxwell's equations before demonstrating its stationary properties at the boundary value problem solution. Using the finite element method, the functional is implemented and then validated against various waveguide structures. For the first time, the $\mathbf{E_t} - \mathbf{H_t}$ formulation has been explicitly applied to lossy gyrotropic waveguide cross-sections. This method has important implications for the study and design of future phase shift and control components used in sub-millimeter wave and terahertz systems.

Analysis of Non Uniform Transmission Lines Using the Direct Numerical Resolution of Hill's Equation

M. Boussalem, **H. Gaha**, **F. Choubani**, **J. David**, **and R. Crampagne**

Laboratoire d'électronique de l'école nationale supérieur d'électronique, électrotechniques, informatique, hydraulique et télécommunications-6'Telcom, école supérieure de communication de Tunis
ENSEEIHT 2, rue Charles Camichel, BP 7122-F 31071 Toulouse Cedex 7, France

Abstract— The Analysis of non uniform transmission lines was largely investigated in the literature [1, 2]. The issue of our paper is to expose clearly an original method to analyse the non uniform transmission lines with any non uniform profile. This Analysis is based on the numerical solving of the Hill's equation [3], which is a second degree differential equation.

Our methodology consists to modelize a non uniform structure by determining the explicit expression describing accurately its behavior and deducing its repartition matrix S.

The first step is to write the propagation equations adequately to the non uniform profile. In the second step, we apply on these equations a mathematical procedure to transform them in the form of a traditional Hill's equation without a first derivative term [3]. This latter is solved in a third step using the Floquet theorem [4], and one general and one particular solutions are given. Finely, we use these solution's values to calculate directly the different elements of the repartition matrix S of the lines.

A program was implemented with Matlab calculator and the code was written to obtain an efficient tool to analyse such non uniform lines. More investigations will be carried to validate this analytic development by experimental prototypes.

REFERENCES

1. Khalaj-Amirhosseini, M., "Analysis of coupled or single nonuniform transmission lines using step-by-step numerical integration," *Progress In Electromagnetics Research*, PIER 58, 187–198, 2006.
2. Khalaj-Amirhosseini, M., "Analysis of coupled or single nonuniform transmission lines using Taylors series expansion," *Progress In Electromagnetics Research*, PIER 60, 107–117, 2006.
3. Hill, G. W., *One the Share of Motion of the Lunar Perigee*, Cambridge the USA, 1877, reprinted in acta Mathematica, flight 8, 1–36, 1886.
4. Rossetto, B., "Détermination des exposants de Floquet de l'équation de HILL d'ordre n," Thèse d'état, Toulon, 1983.

Session 3A4
Electromagnetic Modeling and Inversion and Applications

Circuit Model of Two Bent Traces in Arbitrary Directions on a PCB

S. W. Park[1], **F. Xiao**[1], **D. C. Park**[2], **and Y. Kami**[1]

[1]The University of Electro-Communications, Japan
[2]Chungnam National University, Korea

Abstract— The demand of high density and high-speed operation of modern integrated circuit has been making layouts of trace lines more various and complex. Therefore, the problems of electromagnetic interference (EMI) become crucial and the crosstalk is one of the electromagnetic compatibility (EMC) problems that we have to solve.

A set of parallel lines is a typical model for crosstalk problem and can be easily analyzed using the conventional telegrapher's equations. Analyzing crosstalk of various and complex layouts of trace lines using only this telegrapher's equations, the approach using the per unit length parameters on a cross-section of parallel lines model, is almost incompetent.

When a transmission line is excited by external electromagnetic fields, a current induced in the line. The phenomenon can be expressed in modified telegrapher's equations. i.e., telegrapher's equations having forcing terms consisting of a distributed voltage and current sources along the line, which can be obtained from Maxwell's equations. When electromagnetic fields generated by currents flowing in a transmission line affect nearby lines, the similar phenomenon would be occurred, which is regarded as crosstalk. Thus, to analyze the crosstalk between lines in complex structure, the conventional telegrapher's equations in the concept of circuit theory are modified adding the concept of field theory [1].

To calculate theoretically the coupling of lines in inhomogeneous media such as printed circuit board (PCB), the accurate estimation of electromagnetic field in this model is needed. The electromagnetic fields are obtained based on a quasi-dynamic model that obtains an electric field by considering image charges [2].

By using the above approach, various layouts of lines including bent and straight traces on a PCB have been analyzed. To verify the proposed approach, the experiments are conducted for some models. Both ends of a modeled trace are joint connectors in the fabricated PCBs. The effect caused by the currents flowing in the inner conductors of the connectors has been also taken into account in our proposed approach.

REFERENCES

1. Park, S. W., F. Xiao, D. C. Park, and Y. Kami, "Crosstalk analysis for two bent lines using circuit model," *IEICE Trans. Commun.*, Vol. E90-B, No. 2, 323–330, Feb. 2007.
2. Chow, Y. L., J. J. Yang, D. G. Fang, and G. E. Howard, "A closed-form spatial Green's function for the thick microstrip substrate," *IEEE Trans. Microwave Theory Tech.*, Vol. 39, 588–592, Mar. 1991.

Physically Based Prediction of Multi-antenna Signal Properties for Propagation through and over Vegetation

Dmitry Chizhik
Alcatel-Lucent, Room R121, 791 Holmdel-Keyport Rd, PO Box 400, Holmdel, NJ 07733-0400, USA

Abstract— Engineering and performance prediction of wireless communication systems requires accurate modeling of propagation effects both for the desired as well as for the interfering signals. Specification of the frequency selective spatial channel requires knowledge of path loss, angular spectra, and delay profiles. Most prediction methods may be divided into either empirical methods or numerical methods. Numerical methods, such as the parabolic equation method, as well as the ray tracing methods can predict the field properties in detail, but require detailed knowledge of the fine scale of the obstacles which is either difficult or impossible to get. Empirical methods rely primarily on parametric representation of past data sets. Path loss is represented in these models in terms of a slope/intercept dependence on range. Terrain features such as hills are usually either ignored or represented as knife edges. Quantities such as angle spread and delay spread are either not predicted at all or predicted based on separate measurement campaigns, often in very different environments.

Tamir [1, 2] has analyzed propagation in the presence of vegetation by representing the vegetation as an effective medium described as a homogeneous dielectric slab for both terminals below clutter [1] and one terminal above clutter and one below [2]. The latter case is of interest in this work as well. Considering frequencies below 200 MHz, the dominant propagation mechanism from the mobile immersed in clutter to a base above clutter was reported to be that of refraction at the canopy-air interface [2]. Tamir [1, 2] has also pointed out that such effective medium representation is only valid for wavelengths larger than expected spacing between scatterers. Analysis of shorter wavelength propagation requires consideration of multiple scattering from trunks, branches and leaves. This approach provides prediction of path loss but produces no explanation of the angle and delay spread observed in measurements.

In this work an approach to field prediction over clutter is proposed, combining both statistical and deterministic methods for field prediction, allowing computation of such field quantities as path loss and angular spread. Scattering around the mobile is modeled statistically, explicitly allowing for the reported wide angular spread at the mobile. The vegetation is represented as a diffuse scattering and absorbing medium. Representing the tree canopy as a statistically homogeneous layer where the wave suffers diffuse scattering leads to the following picture: the field seen at the base is due to a "hot spot" on top of the trees, corresponding to the location right above the terminal. This results in a random field on the surface of the vegetation canopy above the mobile, with the spatial coherence scale on the order of a half wavelength. It is argued that the dominant mechanism for coupling mobile signal near ground level to the signal propagating over clutter is not that of coherent refraction adequate at lower frequencies but rather a result of multiple diffuse scattering. Propagation in free space over the tree canopy is treated deterministically by representing the canopy as a dielectric slab. In the case of flat terrain with uniform height clutter, simple closed form expressions for path loss and angular spectrum are derived from first principles. The approach may be extended to treat variable terrain as well as to predict power delay profiles.

REFERENCES

1. Tamir, T., "On radio-wave propagation in forest environments," *IEEE Transactions on Antennas and Propagation*, Vol. 15, No. 6, 806–817, Nov. 1967.
2. Tamir, T., "Radio wave propagation along mixed paths in forest environments," *IEEE Transactions on Antennas and Propagation*, Vol. 25, No. 4, 471–477, Jul. 1977.
3. Bertoni, H. L., *Radio Propagation for Modern Wireless Systems*, Prentice Hall, 2000.

Development of 60 GHz Band Fabry-Perot Resonator

K. Shibahara, T. Suzuki, S. Theerawisitpong, Y. Takahashi, and Y. Watanabe

Nippon Institute of Technology, Japan

Abstract— As 60 GHz band is going to be mandated to public use, the dielectric measurement of various materials and ambient atmosphere at this band will be more addressed and the demand for resonators for such purposes will grow larger. This research aims at developing 60GHz band specific Fabry-Perot resonator. The basic mirror structure is a semi-confocal [1], consisting a movable curved mirror and a plane mirror, on the latter of which two input and output coupling holes with the diameter of one-third of the wavelength are juxtaposed according to the simulation analysis [2]. The waveguide type is WR-15. The main common settings are listed in Table 1. The design is made by two appro aches.

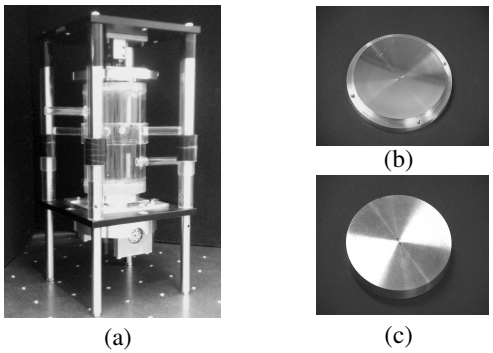

Figure 1: Phase 1 product, (a) Fabry-Perot resonator, (b) sphere mirror, (c) plane mirror.

Mirror structure	Semi-Confocal
Upper Mirror	Spherical Mirror(R305)
	Φ65 Al-Cu alloy (2000series)
Downside Mirror	Plane Mirror
	Φ65 Al-Cu alloy (2000series)
Mirror Distance	L=150±5[mm]
Wave guide	Band type WR-15 E-Bend
Coupling	2Port(transmission type)
	Hole size:D = 1mm

Table 1: Resonator design parameters.

(1) The product of the first design with a gas cell installed in the cavity is shown in Fig. 1. In the plane mirror, the cylindrical coupling holes are drilled, and the rear side is carved out so as to conform to a flange in which two waveguides are screwed on. When the flange/waveguides is fit into the rear of the plane plate, there remains unavoidably minute gap between them so that a silver epoxy conductive adhesive is coated in between. Although the resultant Q-characteristics shown in Fig. 2 indicates not so much high values as expected, in pure O2 absorption measurement shown in Fig. 3, the cavity generates moderately stable outcome at lower frequency region at where the d esign aimed.

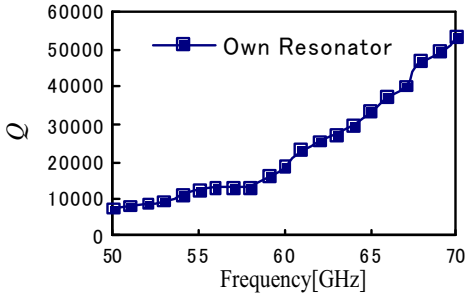

Figure 2: Resonator's Q filled with N_2.

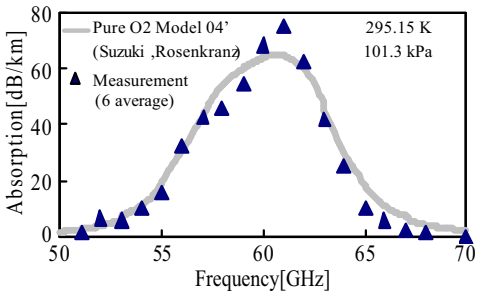

Figure 3: Pure O_2 absorption characteristics.

(2) In the second phase undertaking at present, the design focuses on the improvement at the connection between the holes and the waveguides. In the first design, in addition to the input/output coupling between the surface holes, the fitting structure causes mutual coupling between the two waveguides inside the plane plate. In the new design as shown in Fig. 4, a independent through hole is made so that the mutual coupling inside the plate is prevented. The resultant characteristics are to be presented.

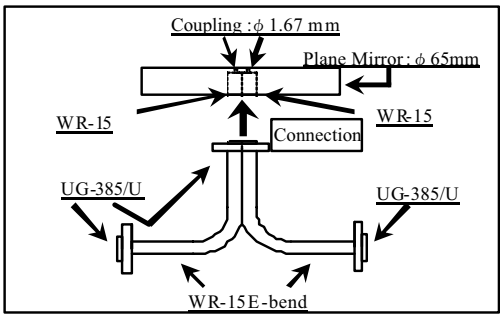

Figure 4: Coupling of phase 2model.

REFERENCES

1. Alder, J. F. and J. G. Baker, "Quantitative millimetre wavelength spectrometry," *Royal Society of Chemistry*, 23, 2002.
2. Sasanuma, H., et al., "Design and fabrication of 110 GHz band Fabry-Perot resonator for Gas absorption measurement," *Proc. IEICE Gen. Conf. '02 Proceedings of the commun IEICE General Conference*, 298, 2002

Synthetic Image Generation of Line Targets and Submerged Features for Shallow Waters with Gravity and Capillary Waves Using a Monte Carlo and Analytical Radiative Transfer Model

Charles R. Bostater, Jr.
Florida Institute of Technology, USA

Abstract— Comparisons are presented which demonstrate the utility of utilizing airborne hyperspectral images, high spatial resolution photgrammetric images and advanced radiative transfer model synthetic images. Results show the value of each of the above, including airborne remote sensing data types for use in helping to detect man-made line targets and natural bottom features in harbors, waterways and coastal marine inlets. Methods are presented to demonstrate how sensor and model calibration is central to producing high quality data and images for coastal mapping and detection applications. The models utilized are a three dimensional radiative transfer model and an iterative plane parallel radiative transfer model. Both models are run on parallel computer architectures that allow the generation of "synthetic water surface images". Model results are presented and compared to actual imagery of line targets submerged within a shallow water environment. The line targets are retrieved from the models and compared to simulations with and without gravity and capillary waves at the air-sea interface. Our initial results demonstrate the use of a novel approach for comparing simulated images to actual images of a shallow water environment for mapping and identification of submerged features in a water body, as well as a conceptual model for understanding the residuals between simulated and observed imagery.

Linear 3D Imaging of Small PEC Spheres

Raffaele Solimene, Aniello Buonanno, and Rocco Pierri

Dipartimento di Ingegneria dell'Informazione, Seconda Università di Napoli
Via Roma 29, I-81031 Aversa, Italy

Abstract— The inverse problem of the determination the number and the locations of "*small*" perfect electric conducting (PEC) spheres from the knowledge of the electric scattered field is considered. By *small spheres* we mean that their radia are much smaller than the wavelength so that the Rayleigh approximation can be adopted to describe the scattering phenomenon [1]. We consider a far zone *reflection-mode* configuration, that is the scattered field is collected in far-zone from the same side the incident field impinges. The latter is provided by plane waves whose angle of incidence and/or frequency is varying. Thus, the cases of a *multi-frequency/single-view, single-frequency/multi-view*, and *multi-frequency/multi-view* configurations are all addressed.

We present a linear-like inversion algorithm obtained in the following way. First, the mutual scattering between the different scatterers is neglected. As the scatterer centre positions are the argument of the pertinent Green's fucntion, the latter are not linearly linked yet to the scattered field. Second, the positions of the scatterers are represented as the supports of 3D Dirac-δ functions. This allows to establish a linear integral relationship between the scattered field and the unknowns now given by the δ-functions. The inversion is then carried out by means of a truncated-singular value decomposition (TSVD) scheme. Third, a thresholding procedure, aiming at curtailing spurious artifacts appearing in the reconstructions due to the spatial filtering introduced by the regularization and to the noise, follows.

The aim we purse is threefold.

First, we analize the perfomences of the inversion scheme in terms of the resolution achievable in the reconstructions and their dependece on the adopted configuration.

Second, we study how to set the threshold in order to remove the spurious artifacts. In particular, emphasis is put into determining the threshold which allows to obtain a given probability of false alarm (i.e., the probability that artifacts due to the noise are mistaken as actual scatterers in the reconstructions) when the data are corrupted by a known white Gaussian random process.

Finally, the linear inversion scheme is checked against the mutual scattering which becomes not negligible when the scatterers are closer (in terms of the wavelength) and/or their number increases. More in detail, the role of the multiple interactions on the linear reconstructions and its dependence on the adopted configuration, that is the angular and the frequency diversities, is highlighted.

Numerical simulations are presented to validate the analysis.

As a concluding remark we outline that the inverse problem of concern herein is relevant in different applicative contexts such as nondestructive testing (NDT), ground penetrating radar (GPR), remote sensing, to quote only a few of examples. Furthermore, it is an extention to a full 3D geometry of a previous work conducted within a 2D geometry [2].

REFERENCES

1. Kleinman, R. E., "The Rayleigh region," *Proceedings of the IEEE*, Vol. 53, Issue 8, 848–856, Aug. 1965.
2. Pierri, R., R. Solimene, A. Liseno, and J. Romano, "Linear distribution imaging of thin metallic cylinders under mutual scattering," *IEEE Transactions of Antennas and Propagation*, Vol. 53, No. 9, September 2005.

The GPR Image by Using the GL Metro Carlo EM Inversion

Lee Xie, **Jianhua Li**, **and Ganquan Xie**

GL Geophysical Laboratory, USA

Abstract— The Ground Penetration Radar (GPR) image technique plays important role in the mine, oil, and earthquake geophysical exploration and engineering geophysics. In this paper, we present the Ground Penetration Radar Imaging by using the GL Metro Carlo EM inversion. We propose a weight for the GL Metro GPR image. The Metro Carlo inversion has merits over than the traditional inversion. There is no any big matrix needs to solve and no artificial boundary needs for te infinite domain. There is no any boundary error refection to contaminate the image. We use the GL Metro Carlo EM inversion method to reconstruct the resistivity and dielectric parameter from the GPR data. The synthetic data simulations show that the GL Metro Carlo inversion GPR image software is high resolution and stable and available for any frequency band and wide type GPR.

MUSIC-type Imaging of Dielectric Spheres from Single-Frequency, Asymptotic and Exact Array Data

S. Gdoura[1], **D. Lesselier**[1], **G. Perrusson**[1], **and P. C. Chaumet**[2]

[1]Département de Recherche en Électromagnétisme, Laboratoire des Signaux et Systèmes
CNRS-SUPÉLEC-UPS 11, 91192 Gif-sur-Yvette cedex, France
[2]Institut Fresnel, Université Aix-Marseille III, 13397 Marseille cedex 20, France

Abstract— MUSIC-type, non-iterative, single-frequency imaging of dielectric spheres of unknown number, location, size and dielectric permittivity embedded in air in a fixed cubical search box is investigated herein. Data of the imaging procedure consist of a finite number of discrete samples of the scattered electric fields. They are collected by a planar squared array which is made of a small number of ideal, point-like dipoles located (each half-a-wavelength) on one side of the search box when the spheres are either illuminated by the same array (operated in a transmit-receive mode) or by another one with similar features located on another side. The transmit array is operated at one polarization only (the electric dipoles it is made of are orientated perpendicularly to its surface) and one electric field component only is inverted, orthogonal to the array surface as well.

In brief, one collects the MultiStatic Response (MSR) matrix of the sought scatterers for a prescribed set of illuminations and observations — times its conjugate-transpose, let us remind that is the time-reversal matrix calculated at the frequency of operation. MUSIC (MUltiple SIgnal Classification) methodology then enables us to work in fruitful fashion with the eigenvalue structure of the MSR matrix, this structure being indeed rigorously explained within the framework of an asymptotic formulation of the wavefield vs. average size of the scatterers; more accurately said at the present stage, one is dealing with the leading-order terms of asymptotic expressions involving the (static) electric and magnetic polarization dyads associated to the scatterers. Here, one follows [1].

Yet the MSR matrix remains a intrinsic feature of the scattering phenomenon. It should possibly be inverted for characteristic features of the scatterers, even if the scatterers are not conveniently electrically small (the case of strongly-scattering extended objects) or not that far in terms of their average size (the case of coupled scatterers not close enough to be seen as one single object) from one another. However, the form provided by the asymptotic analysis might differ from the one truly observed. Correspondingly, images provided by the MUSIC procedure might differ as well.

In the present contribution, referring to a preliminary study by [2], and using the same MUSIC code as therein, one will summarize the results of a systematic and thorough study carried out from both asymptotic electric fields and electric fields computed by a numerical code without approximations [3].

The presentation will be illustrated by the cases of either one or two spheres, with various dielectric contrasts, volumes, and locations, for the two array configurations already specified in the above. In addition to comparison of asymptotic and exact scattered fields, pertinent distributions of eigenvalues, (the singular value decomposition being performed in numerical fashion by standard application of a SVD subroutine onto theMSR matrices) and illustrative maps of MUSIC cost functionals (theoretically peaked at the centers of the spheres) will be exhibited in order to appreciate, in particular by keeping us free of the inverse crime, the pros and cons of the proposed imaging procedure.

REFERENCES

1. Ammari, H., E. Iakovleva, D. Lesselier, and G. Perrusson, "MUSIC-type electromagnetic imaging of a collection of small three-dimensional bounded inclusions," *SIAM J. Scientific Computing*, 2007, to appear.
2. Iakovleva, E. and D. Lesselier, "On the MUSIC-type electromagnetic imaging of a small collection of 3-D dielectric spheres from its multi-static response matrix using exact and asymptotic numerical data," *ACES Proc.*, Verona, March 2007, to appear.
3. Chaumet, P., A. Sentenac, and A. Rahmani, "Coupled dipole method for scatterers with large permittivity," *Physical Rev. E*, Vol. 70, 03606, 2004.

Propagation Characteristics of a Nonlinear TM Surface Wave in a Parallel Plate Superconductor/Antiferromagnet Waveguide

Chien-Jang Wu
Department of Applied Physics, National University of Kaohsiung, Kaohsiung 811, Taiwan

Abstract— A sinusoidal field solution for a nonlinear transverse magnetic (TM) surface wave in a symmetric planar waveguide made of a superconducting film sandwiched by two antiferromagnets is derived. Based on this solution we have investigated the propagation characteristics in the infrared frequency region. Propagation characteristics such as the attenuation constant and the phase constant are numerically analyzed as a function of the frequency, the temperature, and the thickness of superconductor as well. In the temperature-dependent attenuation constant it is found that there exists a characteristic temperature at which the attenuation constant attains a maximum. This characteristic temperature is seen to decrease with increasing the frequency. In addition, it is seen that both the attenuation constant and the phase constant decrease with increasing the thickness of superconducting film. Finally, numerical result in the total power flow reveals that there exists a threshold value in propagation constant. Electromagnetic wave is expected to propagate when the propagation constant is greater than this threshold value.

A New GL Method for Solving Differential Equation in Electromagnetic and Phys-Chemical and Financial Mathematics

Jianhua Li, **Ganquan Xie**, **and Lee Xie**
GL Geophysical Laboratory, USA

Abstract— In this paper, we propose a new GL method for solving the ordinary and the partial differential equation. These equations govern the electromagnetic field etc. macro and micro physical, chemical, financial sciences and engineering. The differential equation is held on an infinite domain which includes a finite inhomogeneous domain. The inhomogeneous domain is divided into finite sub domains. We present the solution of the differential equation as an explicit recursive sum of the integrals in the inhomogeneous sub domains. The analytical solution of the equation in the infinite homogeneous domain is called as an initial global field. The global field is updated by local scattering field successively subdomain by subdomain. Once all subdomains are scattered and the updating process is finished in all the sub domains, the solution of the equation is obtained. We call our method as Global and Local field method, in short GL method. It is different from FEM method, the GL method directly assemble inverse matrix and solution. There is no big matrix equation needs to solve in the GL method. There is no needed artificial boundary and no absorption boundary condition for infinite domain in the GL method. We proved several theorems and proposed a triangle formula of the Green's functions that is the theoretical base of our GL method. The numerical discretization of the GL method is presented. We proved that the numerical solution of the 1-D GL method convergence to the exact solution when the size of the sub domain is going to zero. The error estimation of the GL method for solving 1-D wave equation is presented. The simulations show that the GL method is accurate, fast, and stable for solving elliptic, parabolic, and hyperbolic equations. The GL method has advantages and wide applications in the 3D electromagnetic (EM) field, 3D elastic and plastic etc seismic field, acoustic field, flow field, and quantum field. The GL method software for the above 3D EM etc field are developed.

Uniform Equiconvergence of the Spectral Expansion Corresponding to a Nonself-adjoint Sturm-Liouville Operator for a Two-layer Medium with the Fourier Integral on the Entire Real Line

E. G. Saltykov
Lomonosov Moscow State University, Moscow, Russia

Abstract— In the present paper, we study a nonself-adjoint Sturm-Liouville operator

$$Lu = -\frac{\partial^2 u}{\partial z^2} - k^2(z), \tag{1}$$

defined on the entire real line $R^1 = (-\infty, \infty)$.

We set $k(z) = k_1$ if $z < 0, k(z) = k_2$ if $z > 0$, where k_i are complex constants, $Rek_i \geq 0,\ k_i^2 = \varepsilon_i + j\sigma_i,\ \varepsilon_i \in R^1, \sigma_i \geq 0$ or $\sigma_i \leq 0,\ (i = 1, 2)$, and j is the imaginary unit.

Let a function $f(x)$ and its first derivative $f'(x)$ are absolutely integrable over R^1.

If for this function to specify its Fourier transform

$$\hat{f}_i(\mu) = \int_{-\infty}^{\infty} f(z')u_i(z, \mu)dz',\ (i = 1, 2),$$

the spectral expansion of this function has the form

$$\sigma_\Lambda(z, f) = \sum_{i=1,2} \int_0^\Lambda \hat{f}_i(\mu)u_i(z, \mu)dp_i(\mu). \tag{2}$$

This expansion is characterized by the spectral measure, which is a diagonal matrix function with nonzero entries $p_i(\mu)$, and the fundamental functions $u_i(z, \mu)$.

The function $u_0 = \psi_0$ and $u_2 = \psi_2$ are bounded on the entire real line z solutions of ordinary Sturm-Liouville equations with complex coefficients

$$\begin{aligned} -d^2u_i/dz^2 - k^2(z)u_i &= (\mu^2 - k_i^2)u_i, \quad \mu \in R^1,\ (i = 1, 2). \\ dp_i(\mu) &= d\mu/\left(a_i^i(\mu)b_i^i(\mu) \cdot 2\pi\right),\ (i = 1, 2). \end{aligned} \tag{3}$$

The coefficients a_i^i and b_i^i are defined by the relations

$$\begin{aligned} b_0^0(\mu)\varphi_0(z, \mu) + a_0^0(\mu)\varphi_0(z, -\mu) &= \psi_0(z, \mu), \\ b_2^2(\mu)\psi_2(z, \mu) + a_2^2(\mu)\psi_2(z, -\mu) &= \varphi_2(z, \mu). \end{aligned}$$

The functions ψ_2 and φ_0 are unbounded on the entire real line z solutions of Equations (3).

The representation (2) holds for $Imk^2(z) \gtrless 0$.

Passing to the limit in (2) as $\sigma_i \to 0 (i = 1, 2)$ we arrive at the case $k^2(z) \in R^1, \varepsilon_i \leq 0$.

If $\sigma_i = \varepsilon \to 0\pm, (i = 1, 2), \varepsilon_i > 0$ then we obtain the limit case $k^2(z) \in R^1, \varepsilon_l > 0$.

Theorem. If a function $f(x)$ and its first derivative $f'(x)$ are absolutely integrable over R^1, $\sigma_\Lambda(z, f)$ is the spectral expansion of a function $f(z)$ associated with the Sturm-Liouville operator (1), $S_\Lambda(z, f)$ is the Fourier expansion of $f(z)$ i.e.,

$$S_\Lambda(z, f) = \frac{1}{\pi} \int_{-\infty}^{\infty} \frac{\sin \Lambda(z - z')}{(z - z')} f(z')dz',$$

then the equation

$$\lim_{\Lambda \to \infty} |\sigma_\Lambda(z, f) - S_\Lambda(z, f)| = 0.$$

is valid uniformly with respect to z on the entire real line z.

The spectral excpansion (2) of this function is convergent to $f(z)$ as $\Lambda \to \infty$.

If $k^2(z) \in R^1$ the spectral expansion of a function $f(z)$ (2) corresponds to the formula (6) of the article [1] for the potential $-k^2$ satisfying to the Kato condition.

The spectral expansion on the entire real line of Green's function for a two-layer medium in the fundamental functions of a nonself-adjoint Sturm-Liouville operator was considered in [2, 3].

REFERENCES

1. Il'in, V. A., "Uniform equiconvergence of the spectral expansion corresponding to a self-adjoint extension of the Schrödinger operator with a uniformly locally integrable potential with the Fourier integral on the entire axis R," *Differents. Uravn.*, Vol. 31, No. 12, 1957–1967, 1995.
2. Saltykov, E. G., "The spectral expansion on the entire real line of Green's function for a two-layer medium in the eigenfunctions of a nonself-adjoint Sturm-Liouville operator," *Differents. Uravn.*, Vol. 38, No. 5, 687–691, 2002.
3. Dmitriev, V. I. and E. G. Saltykov, "The new representation of Green's function of Sommerfeld's problem for a conductive homogeneous half-space," *Uspekhi Mat. Nauk*, Vol. 49, No. 4(298), 79–80, 1994.

Session 3AP
Poster Session 2

A New Non-paraxial Time-domain Method for Modeling Ultra Short Optical Pulses

Husain M. Masoudi[1, 2]

[1]Department of Electrical Engineering, King Fahd University of Petroleum and Minerals
Dhahran 31261, Saudi Arabia
[2]Electrical and Computer Engineering Department, Emerging Communications Technology Institute
University of Toronto, 10 King's College Rd. M5S 3G4, Ontario, Canada

Abstract— A new non-paraxial technique to model ultra short optical pulses has been proposed, implemented and verified. The technique uses rational complex coefficient approximation of Pade approximant $\sqrt{1+X} \approx \prod_{i=1}^{p} \left[\left(1+a_i^p X\right) / \left(1+b_i^p X\right)\right]$ to overcome the paraxial limitation. The aim of this technique is to model efficiently very short pulses in long optical structures. The implementation and the verification of the technique show excellent results in terms of accuracy, efficiency and stability where the traditional paraxial Time-Domain Beam Propagation Method failed to achieve [1]. The method is based on the idea of the paraxial TD-BPM, in which the wave equation is written as a one-way wave propagation equation along the direction of z while retaining the time variation as another axis down with the other transverse spatial dimensions that can be represented as

$$\frac{\partial^2 E}{\partial z^2} - 2jk\frac{\partial E}{\partial z} + \nabla_\perp^2 E + \left(n^2 k_o^2 - k^2\right) E - \frac{n^2}{c_o^2}\frac{\partial^2 E}{\partial \tau^2} - 2j\frac{n^2}{c_o} k_o \left(\frac{1}{c_o} - \frac{1}{v_g}\right)\frac{\partial E}{\partial \tau} = 0$$

where v_g is the pulse group velocity. This arrangement has the advantage of allowing the time window to follow the evolution of the pulse and hence minimizes the required computer resources. After factorizing the above equation into a forward and a backward operators, the one way wave equation can be written as [2]

$$E(z) = \exp\left(jk_o n_o z\right) \times \exp\left(-jk_o n_o \sqrt{1+Xz}\right) E(0)$$

We apply this technique to model ultra short optical pulse propagation using Finite Difference approach.

The figure shows a comparison between the present technique and the parabolic method for different initial ultra short pulse widths. The figure shows the divergence of the parabolic method

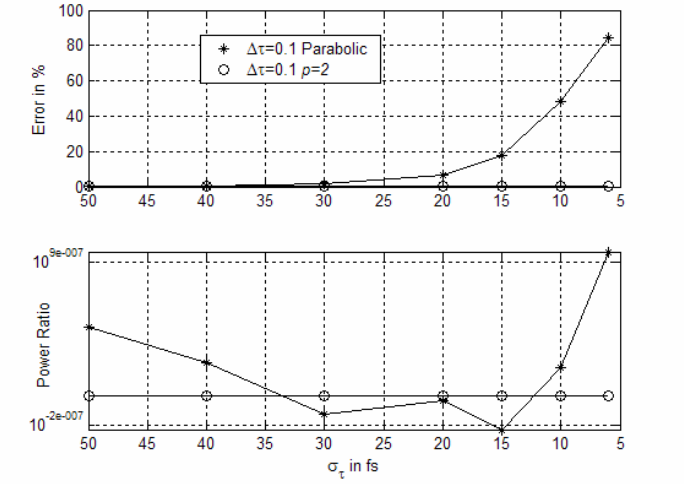

Figure 1: Comparison between the new technique and the parabolic Time Domain BPM for different initial ultra short pulse width. (Upper) The percentage maximum field error (Lower) The power ratio of the pulsed beam.

for ultra short pulse widths, where the error here is mostly associated with the paraxial approximation although very small time step was used. On the other hand, the present technique shows an outstanding performance even for ultra small optical pulse widths. Again from the figure one also notices the strong stability of the present technique compared with the parabolic counterpart.

ACKNOWLEDGMENT

This work was supported by King Fahd University of Petroleum and Minerals KFUPM, Dhahran, Saudi Arabia and also by King Abdul-Aziz City for Science and Technology KACST, Riyadh, Saudi Arabia. Thanks are also due to the University of Toronto, Canada for hosting my sabbatical leave with special appreciation to Prof. J. Setwart Aitchison.

REFERENCES

1. Masoudi, H. M., M. A. AlSunaidi, and J. M. Arnold, "Efficient time-domain beam propagation method for modelling integrated optical devices," *J. of Lightwave Technology*, Vol. 19, No. 5, 759–771, May 2001.
2. Masoudi, H. M., "A stable time-domain beam propagation method for modelling ultra short optical pulses," to appear in *IEEE Phtonics Technology Letters*, 2007.

A Novel Approach to Model Linear and Nonlinear Dispersion with ADE-FDTD

M. Ammann[1], **S. Schild**[1], **N. Chavannes**[2], **and N. Kuster**[1]

[1]Foundation for Research on Information Technologies in Society (IT'IS), ETHZ, Switzerland
[2]Schmid & Partner Engineering AG, 8004 Zurich, Switzerland

Abstract— Emerging applications in photonics in general and of metamaterials in particular involve media with frequency and intensity dependent polarisations. A novel finite-difference time-domain (FDTD) algorithm for arbitrary dispersive media (ADM) allows to model materials with linear multipole Drude- and Lorentz dispersion as well as Kerr-Effect and Raman-Scattering. The ADM algorithm is faster than any previously reported solution (e.g., [1]) while providing full modularity allowing to model every combination of the mentioned phenomena. Moreover, it has proven stability conditions for every effect as well as the used fixed-point iteration.

Methodology

Consider the FDTD expression of Ampere's law

$$\nabla \wedge \mathbf{H}^{\mathbf{n+\frac{1}{2}}} = \epsilon_0 \epsilon_\infty \frac{\mathbf{E^{n+1}} - \mathbf{E^n}}{\mathbf{\Delta t}} + \frac{\mathbf{P_{tot}^{n+1}} - \mathbf{P_{tot}^n}}{\mathbf{\Delta t}} + \sigma \frac{\mathbf{E^{n+1}} + \mathbf{E^n}}{\mathbf{2}} \tag{1}$$

where in the presence of Drude- and Lorentz-Poles, Kerr-Effect and Raman-Scattering the finite-difference formulation of the total polarisation $\mathbf{P_{tot}}$ is given by

$$\mathbf{P_{tot}^{n+1}} - \mathbf{P_{tot}^n} = \sum_{\mathbf{l,d=1}}^{\mathbf{L,D}} \left(\mathbf{P_{l,d}^{n+1}} - \mathbf{P_{l,d}^n} \right) + \epsilon_0 \left(\mathbf{R^{n+1}E^{n+1}} - \mathbf{R^nE^n} \right) + \alpha \left(|\mathbf{E^{n+1}}|^2 \mathbf{E^{n+1}} - |\mathbf{E^n}|^2 \mathbf{E^n} \right). \tag{2}$$

The last term, being the contribution from the Kerr-effect, renders the finite-difference fomulation of Ampere's Law non-linear in $\mathbf{E^{n+1}}$. To avoid the costly matrix inversion in each Newtoniteration and to preserve modularity, the new variable

$$I^n \doteq |\mathbf{E^n}|^2 \tag{3}$$

is introduced to gain linearity in $\mathbf{E^{n+1}}$. It is shown that the update equation of I^n is badly conditioned for the Newton-method but can be solved efficiently through a fixed-point iteration with guaranteed convergence. Despite the fixed-point iteration converging slower than the Newton-iteration, the new formulation is by orders of magnitude faster as far less computations per iteration are required.

Results

The algorithm is integrated into the EM simulation patform SEMCAD X. The modularity allows to use conventional solvers including hardware accelration solutions to solve for the linear part of the update equations and to add the nonlinear contributions where necessary.

The *ADM* algorithm is shown to be significantly faster than the approach presented in [1] while its modularity and speed have proven to allow efficient integration into existing FDTD software. The algorithm was implemented and tested in full 3D including simulations of metamaterials with nonlinear dispersion, successfully simulating effects such as EM-cloaking and gap-solitons.

REFERENCES

1. Greene, J. H. and A. Taflove, "General vector auxiliary differential equation finite-difference time-domain method for nonlinear optics," *Opt. Express*, Vol. 14, No. 18, 8305–8310, 2006.

Interference Calculation for ATSC System against Interference from ISDB-T System Using Computational Simulation

Sung Woong Choi[1], **Tae Jin Jung**[2], **Wang Rok Oh**[3], **and Heon Jin Hong**[1]

[1]Radio & Broadcasting Technology Lab., ETRI, Korea
[2]Department of Electronic & Computer Engineering, Chonnam National University, Korea
[3]Division of Electrical & Computer Engineering, Chungnam National University, Korea

Abstract— Until now, it is general that the field test data are used for setting up the PR between the broadcasting systems. But it needs much time and cost order collect and analyze the field test data. Therefore, by drawing method for setting up the PR based on the computational simulation, it it easy to calculate the PR about the corresponding system.

In this paper, we proposed the method for calculating the PR of the ATSC broadcasting system from the ISDT-T broadcasting system through the computational experiment. For this, the transmitter/receiver of the ATSC system and transmitter of the ISDB-T system were modeled. By integrating those, the computational simulator for setting up the PR of the ATSC system from the ISDB-T system was implemented. The ATSC TV signal was regarded as the desired one and the ISDB-T TV signal was regarded as the interfering one. In order to simplify the simulation complexity, it modeled sending/receiving signals of the IF band instead of those of the RF band. It is assumed the channel modeling one considered received signal and there's no AWGN noise.

Feasibility of Defect Detection in Concrete Structures via Ultrasonic Investigation

A. Musolino, **M. Raugi**, **M. Tucci**, **and F. Turcu**
Dipartimento di Sistemi Elettrici e Automazione, Via Diotisalvi, Pisa 2 56126, Italy

Abstract— In this paper we investigate the feasibility of a diagnostic method for the Non Destructive Test (NDT) of concrete structure based on the ultrasonic wave propagation.

The techniques based on ultrasounds have been introduced in the non destructive analysis in different engineering fields. In particular, in the case of plants with systems of pipes, ultrasonic waves, guided by the walls of the pipes themselves, have been used. The presence of a defect in the structure produces a reflected wave that can be detected by properly positioned sensors. The analysis of the waveforms of the sensor allows the localisation of the defect.

The diagnostic system MsM 2020 is available at the Department of Electrical System and Automation of the University of Pisa. It is based on a magnetostrictive transducer and has been used to generate the propagation of elastic waves in guiding tubular structures in order to perform the inspection if metallic pipes. The system is also able to stimulate planar structures when a properly designed set of transducer is used.

In order to asses the validity of the method we performed a number of numerical analysis on a sample structure shown in Fig. 1. The transducer is able to impose an assigned displacement along the x-direction to a rectangular portion of the surface of the slab. The waveform of this imposed displacement is shown in Fig. 2.

The displacements the points belonging to the face of the slab where the transducer is located are shown at different instant in the Figs. 3–5. Fig. 6 shows the waveform in the point A and B as indicated in Fig. 1.

The obtained results show the feasibility of the proposed method also in the examined example where the dimensions of the defect are smaller than the wavelength. The maps of the displacements show that the defect acts as a secondary source that superimposes his effects to those of the transducer used to excite the structure. The analysis of the waves that originate from this secondary source may be used to determine the position of the source itself.

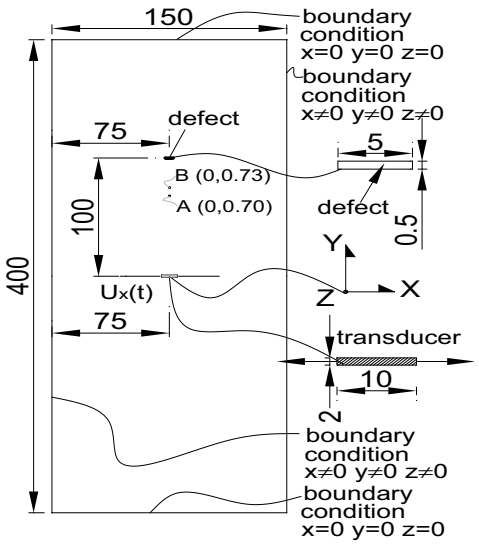

Figure 1: Sample geometry.

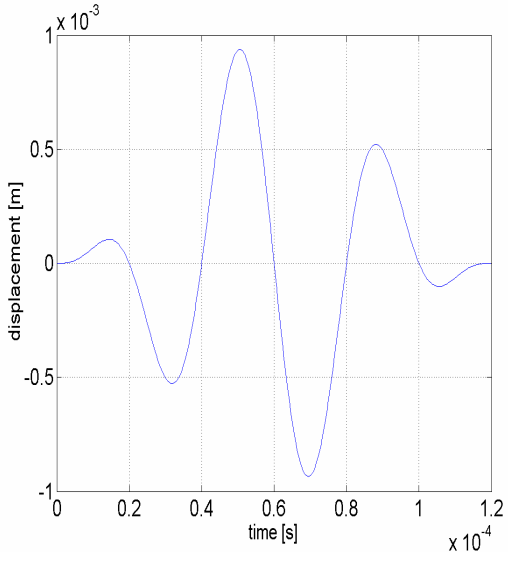

Figure 2: Displacement imposed by the transducer.

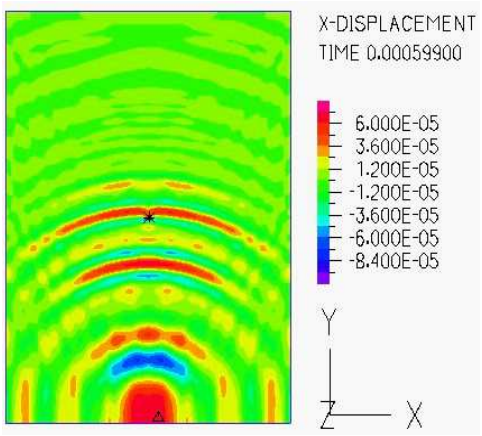

Figure 3: X-displacement at 0.6 ms.

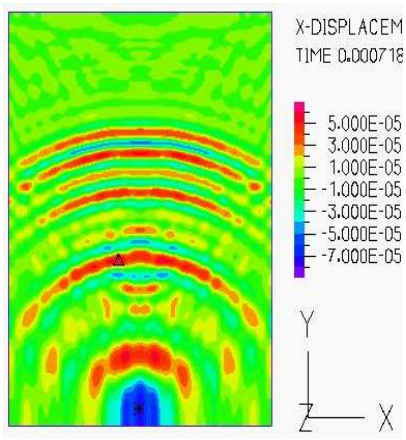

Figure 4: X-displacement at 0.72 ms.

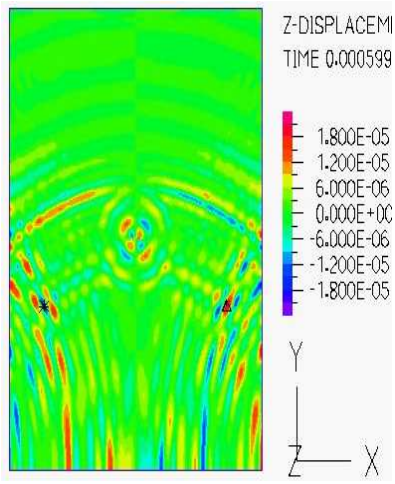

Figure 5: Z-displacement at 0.6 ms.

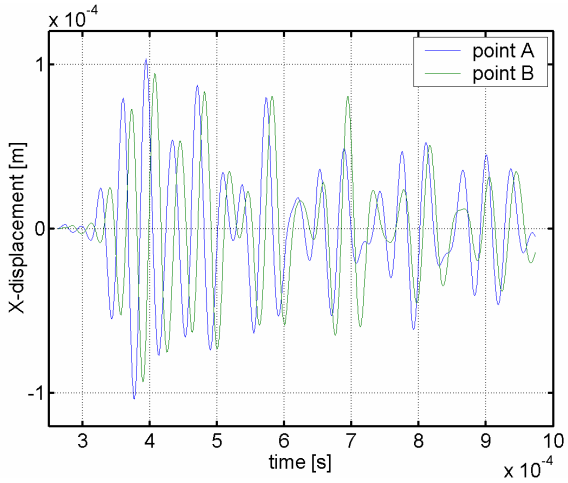

Figure 6: X displacement at point A and B.

Localisation of Defects in Concrete Structures via the Cross Power Spectrum Phase

A. Musolino[1], **M. Raugi**[1], **F. Turcu**[1], **R. Parisi**[2], **A. Uncini**[2], **A. Cirillo**[2]

[1]Dipartimento di Sistemi Eletrici e Automazione, Università di Pisa, Via Diotisalvi, Pisa 2 56126, Italy
[2]INFOCOM Department, University of Rome "La Sapienza", Via Eudossiana 18, Rome 00184, Italy

Abstract— The ultrasonic test of masonry is a technique of current use that allows the inspection of large non accessible portions of buildings. The physical principle is based on the propagation of elastic waves in a guiding structure that is constituted by the volume under inspection. In a homogeneous indefinite medium the elastic waves propagate outward from the source. The ultrasonic waveforms commonly used in the tests are characterized by a frequency range bounded below by 20 kHz. The upper limit depends on the dimension of the masonry components that have to be smaller of the wavelength corresponding to the highest frequency. The use of frequencies greater than 1 MHz is quite rare. Since gaseous media do not transmit such waves, they are used to identify micro-cracks that are able to reflect the wave's front if their dimensions are comparable with the wavelength; the higher are the frequencies the smaller are the defects that can be detected. The frequency cannot be arbitrarily increased as the ultrasonic signal is highly attenuated when its wavelength is comparable with the dimensions of the masonry components because of the presence of a huge number of reflections caused by the masonry components. Essentially the propagation medium cannot be considered as homogeneous and as a consequence the discrimination between defects and masonry component based on the wave front reflection is no longer possible.

While the reflection due to the masonry component can be avoided by using properly chosen (low enough) frequencies, the reflection due to the boundaries of the structure are always present. These reflections interfere with those produced by internal defects and make it the recognition of the components due to the defect a very difficult task. In this situation the use of multiple sensors might help in effectively localizing the internal defects.

Array processing has become a very popular discipline in many fields. Its success is motivated by the fact that combined use of spatial and temporal information allows to overcome the limitations of many practical information processing systems. Array processing techniques are typically employed to localize the sources emitting the observed signals. Typical applications can be found in radars, communications and acoustic signal processing.

In the problem under consideration, an array of sensors is deployed on the surface of the structure under exam to sense the ultrasonic field originated by the transducers. The ultrasonic field in the masonry structure is due to the superposition of waves emitted by transducers and those reflected by boundaries and internal defects. In particular, defects can be treated as *secondary sources*, whose position can be estimated by proper processing of acquired signals.

A number of techniques are available. In particular, source localization can be performed by a two step strategy. In the first step a set of relative time differences of arrival (TDOA) between pairs of sensor signals are estimated. Usually the well-known generalized crosscorrelation (GCC) is employed [1]. In the second step the source position is estimated by exploiting the derived TDOAs according to some specified strategy (e.g., by geometrical triangulation). The presence of reflections yields multiple peaks in the GCC function; proper strategies should be then devised in order to discriminate among peaks due to primary and secondary sources [2]. In particular the GCC function (or its frequency counterpart, called Cross Power Spectrum, CPS) can be exploited to derive an acoustic 3D map of the concrete structure [3]. In practice, a 3D grid is considered which contains the structure. A weighting function derived from the CPS is computed for each node of the grid in order to estimate the probability that a source (primary or secondary) is located in it. Since the positions of primary sources (the transducers) are known, this method allows to detect and localize the internal defects of the structure.

In particular in this work a novel weighting function has been introduced, in order to improve the robustness of the localization task. The proposed approach is based on selection of the most significant peaks each GCC, whose position is exploited to build a weighting functional based on the superposition of gaussian distributions. The proposed algorithm has been tested on simulated data. Preliminary results confirm the superiority of the proposed solution with respect to existing approaches in terms of localization accuracy.

REFERENCES

1. Knapp, C. H. and G. C. Carter, "The generalized correlation method for estimation of time delay," *IEEE Trans. on Acoust., Speech and Signal Processing*, Vol. 24, No. 4, Aug. 1976.
2. Parisi, R., A. Cirillo, M. Panella, and A. Uncini, "Source localization in reverberant environments by consistent peak selection," accepted for publication at *2007 IEEE Int. Conf. on Acoustics, Speech and Signal Processing*, Honolulu, Hawaii, USA, April 15–20, 2007.
3. Mungamuru, B. and P. Aarabi, "Enhanced sound localization," *IEEE Transactions on Systems, Man and Cybernetics*, Part B, Vol. 34, Issue 3, 1526–1540, June 2004.

Microwave Phase Interferometry for Nondestructive Testing in Industry

Ondrej Zak, **Jan Vrba**, **and Marika Pourova**
Department of Electromagnetic Field, FEE, CTU in Prague, Czech Republic

Abstract— In the paper contactless method for measurement of properties of constructional and machine material is dealt. It discuss phase microwave interferometry. We can determine e.g., moisture of material constructional and inner structure of material etc. via this method. Method is realized in a frequency range from 1 GHz to 8 GHz.

At present monitoring is currently implemented by a variety of sensors, such as network of optical targets installed over the structure, strain gauges to measure deformations, collimation nets to measure displacements, inclinometers to measure rotations. Such sensors are accurate and reliable, but require contact with the structure to be surveyed, and information is local to the specific point of the sensor position. In a number of situations, moreover, placing of sensors on the structure is not possible or is too time consuming. Calibers are used in measurement of definite dimensions, which are very expensive.

Therefore the method of microwave phase interferometry is developed. This method is contactless method for measurement i.e., moisture masonry, warping object or finding inner inhomogeneous in various build of material. We can minimize the costs of place and time for compile of measured date.

This method is used for detecting defects of optic transparent materials. But wavelength of light is manifold smaller than wavelength in microwave spectrum that is why we can't inquired into material helped by optic, which they are not optic transparent.

Principle of method is to measure face of equiphase surface unknown microwave field, so that unknown field interfere with reference field and we carry out scalar measurement of electrical field strength in single points of interferential field. When we use for measurement matrix decoder, we can carry out measurement in short interval. We can determine phase inquiry field from measured values of electrical strength field in single points, so that we change phase of reference field known for style. Then we calculate phase from measured values helped by known algorithms. Algorithms used for evaluation are implied from optic spectrum.

A Signal Explanation for the Electromagnetic Induction Law

S. L. Vesely[1] and A. A. Vesely[2]

[1]I.T.B. - C.N.R., via Fratelli Cervi 93, Segrate (MI) I-20090, Italy
[2]via L. Anelli 13, Milano 20122, Italy

Abstract— Today people consider the law of electromagnetic induction a consequence of the Lorentz force, the basic force in electrodynamics. As electromagnetism has merged with the latter theory, it does not seem reasonable to look for explanations that do not refer to electrodynamics.

Indeed, one reason to look for an alternative explanation is that, according to the equation, the microscopic Lorentz force that a magnet exercises on an elementary charge depends further only on their relative motion, and therefore the equation means as well that electricity can be transduced directly and independently of the system size into a mechanical effect. Though this is quite true of all electric motors, nevertheless the macroscopic approach to electromagnetic induction sticks to statistical mechanics, and explains the transient via lack of coherence between microscopic features or energy dissipation and associated heat.

Since the transitory aspect of the electric response is difficult to handle adhering to dynamic principles only, an explanation is called for as to why dissipation may occur. It can be understood that some form of friction stops the effect, once generated, from perpetuating. But if replacing the magnet with another electric winding has the same effect, it cannot be easily seen why it is generated with those characteristics both on switching on and on switching off the current. In fact J. Clerk Maxwell himself based his mechanical explanation of electromagnetic induction on idle wheels.

But as it is not truly necessary to provide a mechanics based approach for electricity, he finally summed up the effect called "electromagnetic induction" in one of a system of four fundamental equations, linking the variation of induction by the magnet to the electric current in a way that mathematically couples the equations. That development had a consistent mathematical meaning. However it was not also deemed a physical explanation.

Today to the plain description of facts, people prefer to confer reality on electric and magnetic fields, mathematical solutions to the whole equation system. Therefore the fields are considered as physical quantities, which means in the end that there is a prescribed method to measure **E** and **B** (in a vacuum). The operational interpretation, being an alternative interpretation of the system of equations, in particular does not explain electromagnetic induction.

Now Maxwell's electromagnetic induction equation exactly parallels the observed fact, which shows that the (relative) movement of a magnet through an electric coil is seen at the coil terminals as an electric transient, and that one can obtain the same kind of electric signal by substituting a linked inductor coil for the magnet.

Perhaps we will be able to understand the transient response of an electric winding on a purely electrical basis, i.e., starting from the analogous effect for a condenser. When a Leyden jar is electrically charged, touching it, there can be a number of shocks until discharge is reached. In this case it is as if the jar is not suddenly discharged, while transient electricity manifests itself. In the same way, when the electromagnetic induction transient ceases, simply no more signal is detected. Vice versa the signal is detected only when some coupling is mismatched. In fact a tuned resonance coupling within a system does not by itself entail any energy transfer, but an external load does.

According to the interpretation that we wish to suggest here, the descriptive induction equation written by Maxwell just tells that, under conditions of perfectly tuned resonance, that is, under steady conditions, there is no signal that a coupling may be present within an electric system. But the signal manifests as soon as resonance is spoiled. As is known, maximum transfer to a receiver occurs under matched conditions. It could be said that the principle of conservation of energy expresses the same concept. But we do not think so, because our explanation does not concern useful power transfer in electro-mechanics, but only the linear case contemplated by the induction equation.

Analytical Solutions to the Applicators for Microwave Textile Drying by Means of Zigzag Method

M. Pourová and J. Vrba

Department of Electromagnetic Field, Faculty of Electrical Engineering, Czech Technical University
Technická 2, 166 27 Prague 6, Czech Republic

Abstract— In this contribution we would like to describe the analytical method for solving microwave applicators for drying of textile materials, which is based on the solving transfer characteristics of waveguide with discontinuities.

We have designed two types of applicators, which we use for testing. The first applicator is derived from the Fabry-Perrot resonator, which is open type resonator. Whole system works at frequency 2.45 GHz and uses magnetron, which generates power 700 W. This machine is intended for the drying at factory production of fabrics. The second one is waveguide type applicator, which is waveguide with a longitudinal slot in wider side of waveguide. This slot is situated in the middle of this side, because maximum of electric field strength is here. Waveguide proportions were designed so that only dominant mode TE_{10} could propagate inside the waveguide at the working frequency 2.45 GHz.

We analyzed drying system with the analytical method. This method is based on the solving transfer characteristics of waveguide with discontinuities. We can describe the wet textile as discontinuity by means of three quantities: the size of reflection coefficient $|\rho|$, its phase angle φ and phase angle ψ of transmission coefficient τ. The size of the transmission coefficient is defined by known relation $\tau\tau^* = 1 - |\rho|^2$ which results from the principle of conservation of energy.

We created diagram of EM waves inside this structure and reached the resulting expression, which is used for calculation of electric field strength in the plane of drying textile. This quantity depends on electrical characteristics of wet textile such as permittivity and loss factor. Measurements of these dielectric properties for the coburg is complicated and this method makes it possible to solve our problem with dielectric parameters. We can also describe the absorbed power in the textile in dependence on the dielectric properties.

The results of this method are very good corresponding with simulations and experimental measurements.

Broadband Leaky-wave Antenna Fed with Composite Right/Left Handed Transmission Line

Y. Miyama[1], **T. Nishikawa**[1], **K. Wakino**[1], **Y.-D. Lin**[2], **and T. Kitazawa**[1]

[1]Department of Electrical & Electronic Engineering, Ritsumeikan University, Japan
[2]Institute of Communication Engineering, National Chial Tung University, Taiwan, R. O. C.

Abstract— The broadband planar leaky-wave antenna fed with the composite right/left handed (CRLH) transmission line is presented. Tapered planar leaky-wave antenna element is designed based on the EM simulation for the broadband applications. The balanced feeding lines with 180-degree phase difference required for the selective excitation of odd leaky mode to the strip conductor is realized by inserting the section of CRLH in one branch of the feeding transmission lines. CRLH section is designed by using FEM simulator and composed with commodity chip capacitor and inductor in the market. Leaky-wave antenna system consisted of the tapered antenna element and CRLH feeder is designed and fabricated on commercially available high frequency substrate. Measured return loss is less than −9.5 dB over the wide frequency range more than 3.1 GHz. The measured radiation patterns show the familiar feature of the leaky-wave antennas.

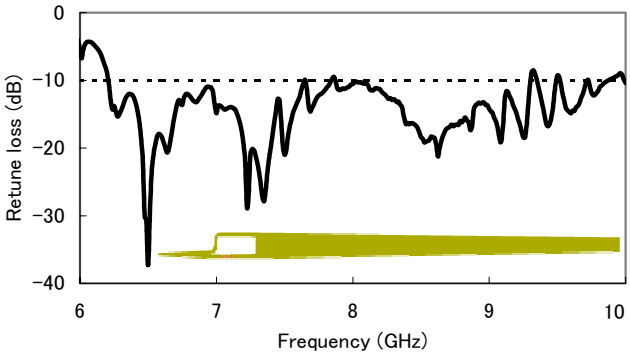

Figure 1: Measured retune loss frequency characteristics of leaky-wave antenna system.

Modeling and Simulation of UWB Signal for Indoor Radio Channels

Je-Sung Ahn[1], **Seo Yu Jung**[1], **Deock-Ho Ha**[1], **Young-Hwan Lee**[2], **and Dong-Won Jang**[2]

[1]Department of Telecommunication Engineering, Pukyong National University, Busan, Korea
[2]Technical Regulation Research Team, ETRI, Daejeon, Korea

Abstract— In this paper, we describe the indoor radio channel characteristic of Ultra-wideband signals by computer simulation. To analyze the propagation characteristic of UWB radio signals, we used the parameter proposed by IEEE P802.15 WPANs in 2003. From the simulation analysis, it can be clearly seen that the UWB signals generated by insufficient time intervals should be encountered to intersymbol interference due to mean excess delay and RMS delay. In addition, it was found that the total usable number of receiver depends on the number of significant paths within 10 dB of peak, or depends on the number of significant paths capturing 85% higher level for the total energy.

Introduction: In this paper, we analyzed the propagation characteristic and implemented the channel simulator for the UWB system parameters. The impulse response, average power delay profile and the number of multipath components are studied. From these data, we studied and analyzed the radio propagation characteristic of UWB band representing path loss model. In general, many models are available in the literature for predictions and simulation of indoor channel. To investigate the radio channel characteristic, we used channel environments reported in IEEE 802.15-02/294SG3a and adopted their model parameters [1].

UWB Channel Model and Channel Simulator: To analyze the system performance of PHY, a multipath channel model is proposed by IEEE 802.15 Study Group 3a High Rate WPAN [2]. Based on the clustering phenomenon observed in several channel measurements, they proposed UWB channel model derived from the Saleh-Valenzuela model with a couple of slight modification [3]. In this paper, we implemented a channel simulator using by this model to analyze the propagation characteristic of UWB indoor radio channel. Tab1e 1 shows the characteristic of channel parameters. Figure 1 shows the flowchart of the simulation procedure.

Model parameters	CM1	CM2	CM3	CM4
Λ (1/nsec)	0.0233	0.4	0.0667	0.0667
λ (1/nsec)	3.5	1	3	3
Γ	7.1	5.2	14.00	24.00
γ	4.3	6.7	7.9	12
σ_1 (dB)	3.3941	3.3941	3.3941	3.3941
σ_2 (dB)	3.3941	3.3941	3.3941	3.3941
σ_x (dB)	3.3941	3.3941	3.3941	3.3941

Table 1: Parameter characteristic for CM1-CM4.

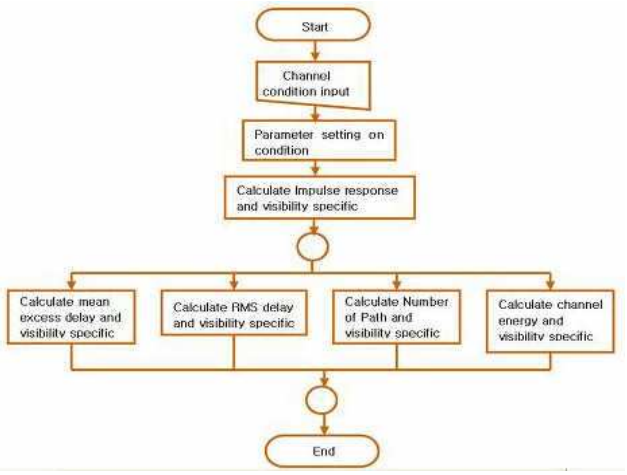

Figure 1: Flowchart of the UWB channel simulator.

Simulation Results: Figure 2 shows the mean excess delay for each channel. The red line in the Figure 2 indicates the average value for each channel model. The average time which signal arrives to the transmitter from receiver is 5.0 nsec for CM1, 9.9 nsec for CM2, 15.9 nsec for CM3, 30.1 nsec for CM4, respectively. This means that the UWB time signal having insufficient time intervals can be affected by intersymbol interference, because the 500 MHz frequency bandwidth indicates 2 nsec time spread. The summery of simulation results are represented in Table 2.

Concluding Remarks: From this study, it can be clearly seen that the UWB signals generated by insufficient time intervals should be encountered to intersymbol interference due to mean excess delay and RMS delay. In addition, it was found that the total usable number of receiver depends on the number of significant paths within 10 dB of peak, or depends on the number of

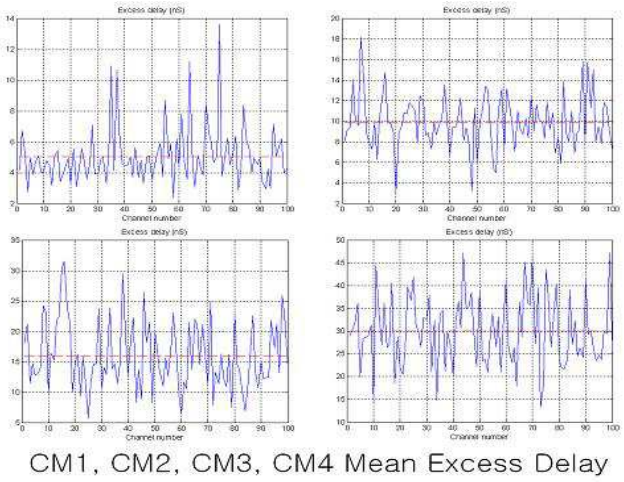

Figure 2: Mean excess delay for each CM1-CM4.

Channel Characteristics	CM1	CM2	CM3	CM4
Mean excess delay (nsec)	5.0	9.9	15.9	30.1
RMS delay (nsec)	5	8	15	25
NP(10dB)	12.5	15.3	24.9	41.2
NP(85%)	20.8	33.9	64.7	123.3
Channel energy mean(dB)	-0.4	-0.5	0.0	0.3
Channel energy std.(dB)	2.9	3.1	3.1	2.7

Table 2: Results of channel characteristic.

significant paths capturing 85% higher level for the total energy. Therefore, we recommend that the UWB system such as DS-CDMA, MB-OFDM must be designed by considering the complex of receiver in NLOS or LOS environments. And also, the UWB channel simulator developed in this research can be used in analyzing the channel interference.

REFERENCES

1. Pendergrass, M., "Empirically based statistical ultra-wideband channel model," *IEEE P802.15- 02/240-SG3a.*
2. Foerster, J. and Q. Li, "Channel modeling contribution from Intel," *IEEE P802.15-02/490r-SG3a*, February 2003.
3. Saleh, A. and R. Valenzuela, "A statistical model for indoor multipath propagation," *IEEE Journal of SAC.*, Vol. SAC-5, No. 2, 128–137, February 1987.
4. FCC, "Revision of part 15 of the commission's rules regarding ultra-wideband transmission systems," First Report and Order, ET Docket 98–153, Feb. 2002.

Modal Analysis of Miniature Microstrip Patch Antennas Based on Fractal Geometry

P. Hazdra and M. Mazanek
Department of Electromagnetic Field, FEE, Czech Technical University in Prague
Technicka 2, Prague 166 27, Czech Republic

Abstract— The paper deal with the fractal microstrip patch antennas with specific properties based on rearrangement of current densities on their surface by means of special fractal geometrical modifications. Description of physical behavior via surface current distribution and radiation properties are summarized. Different modal analysis approaches (cavity model and the Theory of characteristic modes) have been used for the simulations.

Meandering of surface current paths associated with the operational modes is effective way for lowering resonance frequency or decreasing antenna dimension when the resonant frequency is maintained. Plenty of configurations have been proposed based on introducing slot and notch types of perturbation elements (PE) that force the surface currents to flow around PEs. These configurations have a general drawback in increasing of cross-polar level and decreasing impedance bandwidth due to the resonance behaviour of highly geometrically modified patches. Advantage of further presented set of fractally modified patches with fixed outer sizes is relatively small cross-polar level compared to the patches designed by standard techniques using slot and notche types of PEs.

Among others, study of so-called Inverted Koch Square Patch with indentation angle 85° and of iteration order 3, is presented. It has been found that a special current distribution of fundamental mode causes significant lowering of resonant frequency compared to canonical structures. To gain deeper insight into properties of the proposed structures, well-known cavity model and the theory of characteristic modes (TCM), which both allows perform modal analysis of structures independent of its feed configuration, have been used. The patch shape is generated by the L-System fractal generator.

Algorithm for Noise Reduction in Output Signal of Race-track Core Fluxgate

M. Butta[1], **P. Ripka**[1], **and J. Kubík**[1,2]

[1]Department of Measurement, Czech Technical University, Technická 2, Praha 166 27, Czech Republic
[2]Tyndall National Institute/MAI, Lee Maltings, Prospect Row, Cork, Ireland

Abstract— We present a novel algorithm for noise reduction in fluxgate sensors [1].

Noise measurements have been performed on the output signal of the race-track core PCB fluxgate sensor [2] inserted into a six-layer magnetic shielding. The output signal has been conditioned using a low noise amplifier Stanford Research SR560, then sampled with high speed digitizer NI 5911. Proper amplifying gain and high resolution (18 bits) of the digitizer gave as a result the possibility to properly measure the even harmonics, even if buried in higher amplitude signal at odd harmonics. This method, based on the sampling of the signal, allowed us to measure all the even harmonics simultaneously. Similar measurement with conventional lock-in amplifier would be of excessive complexity. The resulting noise on all even harmonics was then subjedcted to statistical analysis: a strict correlation between them is clearly shown from their variations in time [3]. The algorithm for noise reduction is proposed based on this key feature of the noise. While the sensitivity at the even harmonics is rather different, the noise is quite similar both in average rms value and varying part, which has been shown to be strictly correlated. The proposed algorithm is based on the proper linear combination of even harmonics in order to obtain suppression of the noise, even with the drawback of a reduction in sensitivity. Detailed analysis is finally shown for the achievement of optimum t performance for both noise reduction and sensitivity.

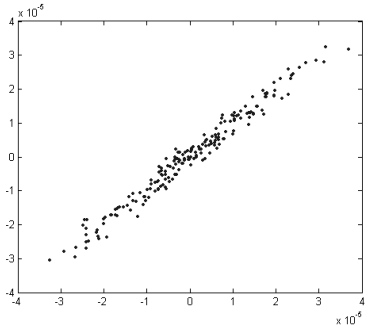

Figure 1: Correlation between 2nd and 4th harmonic.

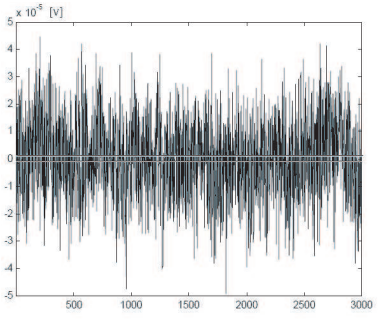

Figure 2: Noise at 2nd Harmonic vs period.

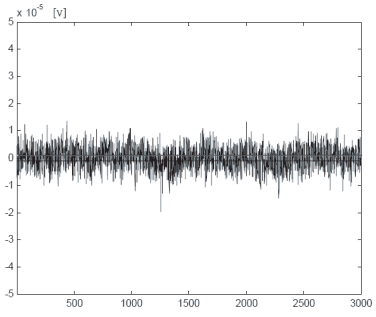

Figure 3: Noise at output signal of the algorithm vs period.

REFERENCES

1. *Magnetic Sensors and Magnetometers*, Pavel Ripka (ed.), 78–79, Artech House, 2001.
2. Kubík J., L. Pavel, and P. Ripka, "PCB racetrack fluxgate sensor with improved temperature stability," *Sensors and Actuators A*, Vol. 130, 184–188, 2006.
3. Butta, M., "An innovative algorithm for noise reduction in a fluxgate output signal," MSc Thesis work in Electrical Engineering, Politecnico di Milano, 2005.

Polarization-dependent Diffraction of Cholesteric Liquid Crystal Grating with Silver Nanoparticles

I.-Min Jiang[1], **Ming-Shan Tsai**[2], **Wen-Chi Hung**[3], **and Wood-Hi Cheng**[3]

[1]Department of Physics, National Sun Yat-sen University, Kaohsiung 804, Taiwan, R. O. C.
[2]Department of Applied Physics, National Chiayi University, Chiayi 600, Taiwan, R. O. C.
[3]Institute of Electro-Optical Engineering, National Sun Yat-sen University
Kaohsiung 804, Taiwan, R. O. C.

Abstract— The polarization-dependent diffraction of cholesteric liquid crystal (CLC) grating was demonstrated in this study. One of ITO glass plates of the CLC grating cell was covered by silver nanoparticles. The CLC grating was probed by the polarized monochromatic beam, and the wavelength was scanned from 450 nm to 700 nm. While the polarization angle of the incident beam was rotated from 0 to 90, the blue-shift phenomenon was observed in the diffraction spectrum. The novel blue-shift phenomenon could cause by the periodic variation of the localized surface plasmon excitation emerged from silver nonoparticles in the CLC grating. The polarization dependent property enables a flexible modulation in the diffraction efficiency that offers potential applications in the switch devices.

ACKNOWLEDGMENT

This research was under the grant NSC96-2816-M-110-001.

A Useful Approximation to Add up Contributions in Ray Based EM Propagation Algorithms

Marco Allegretti, Luca Coppo, and Giovanni Perona

Electronic Department, Politecnico di Torino
C.so Duca degli Abruzzi 24, Torino 10129, Italy

Abstract— In last years ICTs required a huge development of wireless communication channels. The growth of wireless devices distribution induces channels to carry a large amount of data, so leading transmission frequency to increase. At the same time respecting environmental shock criteria requires the transmission power to be as low as possible. In such context, an optimized wireless network plan is the best way to lower transmission power and optimize radio coverages.

Electromagnetic (EM) propagation simulation represents a good way to predict the distribution of the electric field avoiding in-place field measures. Automated wireless network design routines can include simulation results as a feedback to improve network parameters until project constraints have been satisfied. Despite modern electronic calculators have reached very high levels of computation strength, EM propagation simulation requires punctual evaluation of the field yielding simulation algorithms more complex. Hypothesis of high frequency (short wavelength) allow simulation routines to use simplified deterministic ray-based propagation models such as Ray-Tracing and Ray-Launching algorithms.

In ray-based algorithms the punctual value of the electric field is function of contributes of each ray reaching the specified point. Considering a perfect system geometry, the electric field may be evaluated as a magnitude and phase sum of all the contributions given by incident rays. This solution cannot be applied in real environments, where high frequency ($> 2\,\mathrm{GHz}$) wavelength and tolerances on geometry measurements keep the same order of magnitude, making the degree of accuracy of the simulation decrease.

For such reasons, the most meaningful value to estimate is *expected value* of electrical field strength which provides a good estimation of the real field with an higher level of significance. Due to the uncertainty on the environment geometry model, it can be assumed that the phase between rays incident in one point of the space is a random variable equally distributed in the $[0, 2\pi)$ interval. The expected value of the electric field can be calculated with the solution of the integral:

$$\frac{1}{2\pi}\int_0^{2\pi}\sqrt{h^2+k^2-2kh\cos\theta}\,d\theta$$

In the case of only two incident rays, where h and k are the magnitudes and θ is the phase difference related to the contributes of the two incident rays. Unfortunately this integral has no explicit solution and it can be evaluated only with numerical approximations.

One of the most employed methods to approximate this kind of integral is the *Montecarlo* algorithm which estimates the integral value as a mean of N values ($N >> 1$) of the integrand function evaluated with a random value of θ. This method is not suitable because a good approximation requires a very large N, so increasing the complexity of the algorithm.

Other less expensive methods, like *Simpson* formula or *spline-based* approximation, can be used too and they are more resource saving if compared to *Montecarlo* algorithm, but since the improvement of such algorithm is a crucial task to make the simulation as fast as possible another solution was adopted.

The suggested solution for this integral is a different kind of approximation and is useful only for this case. The approximation is based on the periodic form of the function to be integrated: it denotes a similarity with a *cosine* shape. Obviously the only cosine is not enough to represent the function, therefore an error function is needed to correctly perform the approximation. It is not necessary to find an optimal approximation of the error function, since it's fundamental just its integral value. A deep analysis on the integral of the error function has given a simple form to represent with good approximation its value.

The final form (not in minimal terms) of the integral approximation is:

$$|h-k|+\frac{2}{\pi}(h+k-|h-k|)+\min(h,k)\frac{k_1}{k_2\frac{\max(h,k)}{\min(h,k)}-k_3}$$

where k_1, k_2, k_3 are free coefficients calculated to fit the approximation with the real integral.

Validation and Calibration of a 3D Ray Tracing Propagation Model for Urban Environment at UMTS Frequencies

Marco Allegretti, **Claudio Lucianaz**, **Riccardo Notarpietro**, **and Giovanni Perona**
Electronic Department, Politecnico di Torino
C.so Duca degli Abruzzi 24, Torino 10129, Italy

Abstract— This work depicts results from outdoor UHF measurement campaigns carried out in dense urban environment. The analysis focuses on the 2 GHz frequency band chosen for the UMTS standard. The optimization of urban micro-cells requires accurate propagation models, but urban structures can present important changes from a region to another which make unuseful even the most complex models. Old cities are characterized by an irregular layer defined by narrow streets and unequal building, while modern towns have a squared structure with parallel and orthogonal streets. Turin city (Italy) presents a combination of both structures.

In order to characterize the EM propagation in such environments a measurement campaign was carried on. The chosen area is a square 3×3 Km centered around the "Politecnico di Torino" university building: the size of the area was chosen in order to include at least one UMTS urban microcell that usually is less than 1 Km in radius. The transmitter was installed on the roof of the university building and measurements were carried out following two different approaches:

1. Omnidirectional measurements with a moving van in order to determine the field coverage around the transmitter. The receiving antenna was mounted on the roof of a van at an height of about 3 meters and inside it was set up an automated measurements chain. The chain was made of a discone antenna, a Spectrum Analyzer controlled via GPIB interface, a PC used as automated logger and a GPS receiver to acquire the exact position for every measurement point. Routes were planned in order to investigate both LOS and non-LOS zone.
2. Directional measurements in order to characterize building scattering. The aim is to point out and to distinguish the presence, at the receiver, of the various terms due to direct, reflected and building scattered field. The study of such phenomena allowed the construction of fine models that discriminate the effects introduced by the different building architectures and streets' shape.

Measurements highlighted canyoning phenomena that establish in dense urban area, were buildings play a very important role as scatterers. The study of the interactions between an electromagnetic wave and buildings, in further analysis could be integrated with the statistical effects on the signal fluctuations (for example due to traffic).

Measurements were then compared with the predictions obtained by a deterministic EM propagation software based on Ray Tracing and a good agreement was found. The same measurements were at last used to calibrate the software prediction model with good final results.

Surface Wave Propagation above a One-dimensional Rough Sea Surface at Grazing Angles

Y. Brelet, **N. Déchamps**, **C. Bourlier**, **and J. Saillard**
IREENA, Université de Nantes, Polytech'Nantes, Rue Christian Pauc
La Chantrerie, BP 50609, 44306 Nantes Cedex 3, France

Abstract— The scattering of electromagnetic waves from a finitely conducting one-dimensional random rough surface at grazing angles is investigated, what, one of many practical interests, concerns wave propagation over a sea surface from a coastal radar (Fig. 1).

Study is firstly done using the conventional small perturbation method (SPM), by mean of the "extinction theorem" [1]. This theory applies to rough surface with small Root-Mean-Square (RMS) heights compare to the incident wavelength. The fields are calculated *on* the surface and the scattered fields in the half-space (vacuum) above the surface. In this paper, the authors present the computation of this asymptotic method with an exact one. The latter is a recent fast rigorous numerical method, Forward-Backward Novel-Spectral-Acceleration (FBNSA) approach [2], with complexity of order $\mathcal{O}(N)$, based on the Method of Moments, and adequate for such a scattering problem since the number of unknowns is of order of 6000 for an incidence angle of 85°.

It is then put forward that the small perturbation method is applicable for moderate angles of incidence (smaller than 80°). On the other hand, it tends to fail for grazing angles in TM polarization, whereas it does not in horizontal polarization (H or TE polarization).

These observations lead to use the extended small perturbative method [3, 4] based on the Green formalism, to take into account complex propagation occuring in TM case, that classical perturbation theory does not include. This extended method is derived in a similar manner of the Zenneck-Sommerfeld solution [5], when the source and/or observation points are located near the surface. The asymptotic theory of Fuks et al. and Ishimaru et al., quoted above, needs to be numerically tested, and possibly improved. This theory was derived for the coherent and incoherent scattered fields. The authors propose the derivation of the exact fields *on* the rough surface and scattered fields in the upper-half space with both analytical and rigorous methods mentionned above.

Therefore, the aim of the final paper is to present comparisons of the fields *on* the surface and in the upper-half space, derived from the extended SPM theory, with the fast rigorous FB-NSA, to verify if the Zenneck surface wave may occur at the V polarization for a rough surface, when the radar is closed to the surface with frequency ranges $f \in [1; 500]$ MHz.

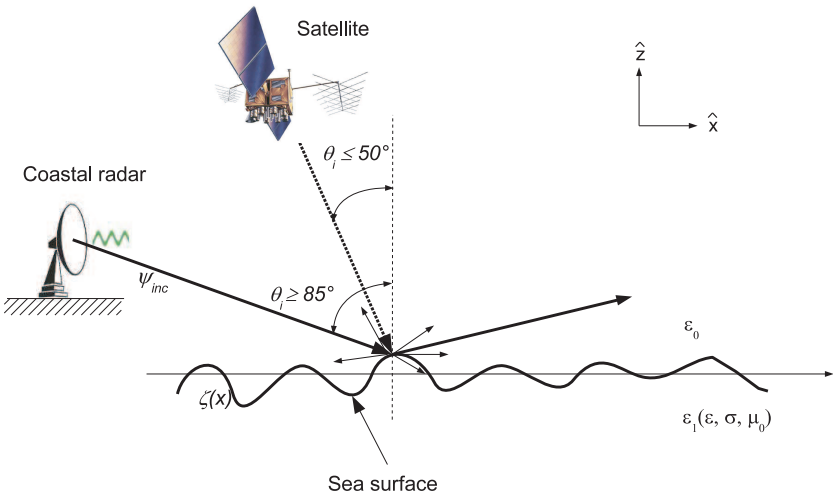

Figure 1: Incident field from a coastal radar onto a conducting medium with real permittivity ϵ, conductivity σ and permeability μ_0. Conducting medium is bounded by rough surface given by the height $z = \zeta(x)$.

REFERENCES

1. Pattanayak, D. N. and E. Wolf, "General form and a new interpretation of the Ewald-Oseen extinction theorem," *Opt. Commun.*, Vol. 6, 217–220, 1972.
2. Chou, H.-T., "A novel acceleration algorithm for the computation of scattering from rough surfaces with the forward-backward method," *Radio Science*, Vol. 33, No. 5, 1277–1287, Sept. 1998.
3. Bass, F. G. and I. M. Fuks, "Wave scattering from statistically rough surfaces," *Pergamon*, Oxford, 1979.
4. Ishimaru, A., J. D. Rockway, Y. Kuga, and S.-W. Lee, "Sommerfeld and Zenneck wave propagation for a finitely conducting one-dimensional rough surface," *IEEE Transactions on Antennas and Propagation*, Vol. 48, No. 9, 1475–1484, 2000.
5. Sommerfeld, A. N., "Propagation of waves in wireless telegraphy," *Ann. Phys.*, Leipzig, Vol. 81, 665–737, 1919.

Simulations of Magnetically Tunable Ferrite/Dielectric/Wire Negative Index Composites

F. J. Rachford[1], **D. N. Armstead**[2], **Vincent Harris**[3], **and Carmine Vittoria**[3]

[1]Naval Research Laboratory, 4555 Overlook Ave SW, Washington, DC 20375, USA
[2]The College of Wooster, Department of Physics, 308 E. University St., Woster, Ohio 44691, USA
[3]Electrical and Computer Engineering Department, Northeastern University, 440 Dana Research Center 360 Huntington Ave., Boston, MA 02115-5000, USA

Abstract— We have performed extensive finite difference time domain (FDTD) simulations to design ferrite based negative index of refraction (NIM) composites. Our simulations center on the use of Barium M type ferrite with in-plane anisotropy to provide the magnetically tunable permeability. A wire grid is employed to provide negative permittivity. The ferrite and wire grid interact to provide both **negative** and **positive** index of refraction transmission peaks in the vicinity of the BaM resonance with several GHz tunable index at Q-band frequencies. We find that the wires and the ferrite must be spatially separated by a low loss dielectric (Mylar). The ferrite and dielectric lamina are paired with combined thickness equal to the square wire grid lattice distance. We assume the presence of a in plane orienting magnetic field. Working with thin planar oriented ferrite lamina implies that the composites will have a negative index in only one direction of propagation. Notwithstanding the extreme anisotropy in the index of refraction of the composite, negative refraction is seen at the composite air interface allowing the construction of a focusing concave lens with magnetically tunable focal length.

Theoretical and Real Absorption of High-frequency Electromagnetic Energy in Mouse Animal Model

J. Barcal[1], **V. Žalud**[1], **F. Vožeh**[1], **and J. Vrba**[2]

[1]Department of Pathophysiology, Faculty of Medicine Pilsen
Charles University in Prague, Czech Republic
[2]Department of Electromagnetic Field, Faculty of Electrical Engineering
Czech Technical University in Prague, Czech Republic

Abstract— High frequency electromagnetic field (HF EMF) became a common part of our environment because it is produced by many artificial sources as radars, transmitters and especially cellular (mobile) phones. Considering a possible harmful effect of it the term "electromagnetic smog" is often used for this situation. Among the sources mentioned, first of all the number of mobile phones is rapidly rising (10 million devices was in the Czech Republic in 2005!) and during a call the source of radiation is close to the head. That is why there is a question of possible negative effects of HF EMF on a human body, especially on the brain. HF EMF can influence tissues by both thermal and nonthermal effects. While the thermal effect is relatively well known, the nonthermal effects are still discussed and remain unclear. In the presenting study we demonstrate a possible methods for theoretical and real measurement of HF EMF absorption using 900 MHz generator.

Experimental animals were exposed to HF EMF with frequency of 900 MHz. Output power of the HF EMFgenerator after amplifying was aproximately 10 W. Mice were placed into a plastic box just before the orifice of the waveguide. Control mice were kept in analogous conditions without the HF EMF. In the first phase model experiments which are able to detect SAR (**S**pecific **A**bsorption **R**ate) were performed. This value shows a absorption dose of radiation in the animal tissue. 10 W output power is radiated as equal quanta from the area cca 600 cm^2 of waveguide. In the distance 0.3 m from the orifice is practically impossible to measure SAR directly and only an estimate (from the gradient of field) suggest the whole-body exposure which correspond to the triple power of classical GSM.

In the second part a computerized modeling of electromagnetic field absorption in the animal body was created. To estimate SAR in experimental animals we have done basic 3D calculation of electromagnetic energy distribution in a simplified dielectric model of an adult mouse. The model consists of a homogenous lossy dielectric material mimicking muscle tissue and has shape of a cylinder (radius 3 cm and high 9 cm terminated to cone) with dielectric properties $e_r = 54$, conductivity $s = 0.8\,S/m$, density $r = 1000\,kg/m^3$. The calculations were done with the aid of 3D electromagnetic field simulator SEMCAD which used FDTD (**F**inite **D**ifferent **T**ime **D**omain). The method is based on the fact that original continuous function is replaced by the set of discrete function's values. Maxwell's equations are discretized using a 2nd order finite-difference approximation both in space and in time in an equidistantly spaced mesh. Several simulations for different positions of mice were done. Input power during simulations was normalized to 1 W.

Calculations of SAR performed in connection with the simulation of absorption electromagnetic energy by experimental animals using the arteficial dielectric model showed the dependence of the absorption on the real topical position of the mouse against the waveguide and was in the range of 0.05 to 1.44 mW/g.

The complex knowledge resulting from these experiments is not only a contribution to the store of basic neuropathophysiological information but will be also useful for clinical neuropathology with possible consequences for the public health prevention.

ACKNOWLEDGMENT

This work was supported by the Research Program Project No. MSM 021620816.

Microwave Applicator for Treatment of Atherosclerosis

Kateřina Novotná and Jan Vrba

Department of Electromagnetic Field, Czech Technical University in Prague
Technická 2, 166 27 Prague 6, Czech Republic

Abstract— One of prospective domains of microwave thermotherapy is microwave angioplastic for treatment of atherosclerosis. Due to dysfunction of endothelium a sedimentation of cholesterol on a blood vessel wall can happen. This evokes its sequential closing. Basic principle of microwave angioplastic is, that heating gained by microwave energy irradiated into artery by microwave applicator, enables safe clear out of atherosclerotic plates in the wall of vessel.

Methods: This paper describes the design of special applicator for microwave angioplastic. As the most acceptable structure to create intracavitary applicator, coaxial quarter wave monopole, was chosen. The applicator in our model was inserted into vein with blood and surrounded by phantom of muscular tissue. First goal was to obtain good impedance matching between generator and microwave applicator. Then we studied the distribution of absorbed power (SAR) along the applicator. For the applicator working at 2,45 GHz there was maximum of SAR at point of termination of outer conductor.

Results: The function of the microwave applicator was experimentally evaluated by measurement of reflection coefficient. This tested applicator had good impedance matching, less than −20 dB. Then the distribution of the temperature along the applicator was measured with IR camera. Described applicator was placed in to the phantom of muscular tissue and exposed by 50 W during 1 minute. The temperature grew to 47°C (Fig. 1).

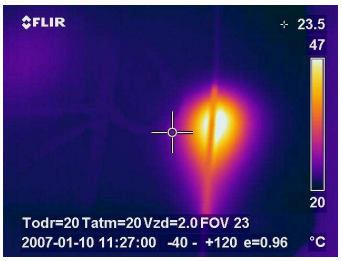

Figure 1: The distribution of the temperature along the applicator.

Conclusion: This paper describes only technical solution to design the intracavitary applicator for microwave angioplastic. Into the future we plan the cooperation with medical doctors, who will provide us the medical information. Main goal of this project is to determine the optimal temperature for different stadium of this illness.

ACKNOWLEDGMENT

The described research has been financed by the Czech Grant Agency under the grant No. 102/05/0989, and by the Czech Ministry of Education in the frame of the research plan No. MSM 6840770012.

REFERENCES

1. Novotná, K., "Intracavitary applicator for microwave angioplastic (in Czech)," Diploma thesis, Prague, 2007.
2. Vrba, J., "Medical application of microwave thermotherapy (in Czech)," Publishing by ČVUT, Prague, 2003.

A Fat Dipole Antenna for Spark Switched LC Oscillator

Sang Heun Lee[1], **Young Joong Yoon**[1], **Hoon Heo**[2], **Woosang Lee**[3], **and Dowon Choi**[3]

[1]Yonsei University, Korea
[2]Pohang Accelerator Laboratory, Korea
[3]Agency for Defense Development, Korea

Abstract— Spark switched LC oscillator (LCO) is used to generate damped sinusoidal signal which has wideband width. Specially, some high power wideband systems use LCO because spark switched LCO using gas or insulating oil can radiate high power microwave without self-breakdown. Recently, there are many researches of the equivalent circuit modeling and the various characteristics of LCO, such as high repetition rate, fast recovery time, low spark gap loss and so on. On the other hand, the fat dipole antenna which is attached to LCO is not significantly mentioned. Although the length of dipole affects operating frequency and field strength, a dipole antenna is just regarded as 50 Ω or 100 Ω load in the equivalent circuit model of LCO [1, 2]. In many case, dipole length is not considered to determine the operating frequency [1, 2].

Therefore, received field of LCO is analyzed according to the variation of a dipole length which is shown in Fig. 1. The operating frequency is 430 MHz when x is 0 mm and it gradually lower until 300 MHz when x is 150 mm. This experimental result and analysis will be useful to design of LCO which uses a fat dipole because the variation of the dipole length changes the operating frequency of LCO.

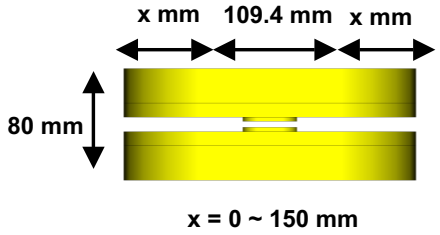

Figure 1: The designed LCO and dipole.

REFERENCES

1. Rinehart, L. F., J. F. Aurand, J. M. Lundstrom, C. A. Frost, M. T. Buttram, P. E. Patterson, and W. R. Crowe, "Development of UHF spark-switched L-C oscillators," *Pulsed Power Conference*, 1993. *Digest of Technical Papers. Ninth IEEE International*, Vol. 2, 534–537, 21–23 June, 1993.
2. Moran, S. L., "High repetition rate LC oscillator," *IEEE Transaction on Electron Devices*, Vol. 26, Issue 10, 1524–1527, 1979.

Frequency Responses of Reconfigurable Frequency Selective Surfaces Using Square Aperture with Loading

Kihun Chang and Young Joong Yoon

Yonsei University, Korea

Abstract— In this paper, frequency responses of reconfigurable frequency selective surface (RFSS) with squared aperture with loading are introduced. The electromagnetic properties of the frequency selective surface (FSS) can be changed by applying a dc bias to the substrate. The proposed structure can be designed to switch between a reflector and a transparent surface at resonance, while the reported structures provides the FSS tuned to higher or lower frequencies.

We discuss square aperture with loading, which can be treated as one prototype of frequency selective surfaces. Secondly we discuss the transmission and reflection curves in RFSS slabs, which are composed of substrate with a symmetric FSS unit cell and PIN diodes. Equivalent circuit in the structure is investigated by analyzing transmission and reflection spectra. Measurements on RFSS are compared with numerical calculation, based on the scattering matrix formalism. The origin of experimentally observed frequency responses will be scrutinized.

ACKNOWLEDGMENT

This research was supported by the MIC (Ministry of Information and Communication), Korea, under the ITRC (Information Technology Research Center) support program supervised by the IITA (Institute of Information Technology Assessment) (IITA-2005-C1090-0502-0012).

REFERENCES

1. Munk, B. A., *Frequency Selective Surfaces: Theory and Design*, Wiley, New York, 2000.
2. Bossard, J. A., D. H. Werner, T. S. Mayer, and R. P. Drupp, "A novel design methodology for reconfigurable frequency selective surfaces using genetic algorithms," *IEEE Transaction on Antennas and Propagation*, Vol. 53, No. 4, 1390–1400, April 2005.

2D Quasistatic TLM Field Solver for High Speed PCB Design

Caner Altınbaşak[1] and Lale Tükenmez Ergene[2]

[1]The Scientific & Technological Research Council of Turkey (TUBITAK), Marmara Research Center
Institute of Informatics, Kocaeli, Turkey
[2]Istanbul Technical University, Institute of Informatics, Istanbul, Turkey

Abstract— Modern computer communication busses like PCI-Express or Fibre Channel have rise and fall times nearly 100 ps. Nowadays, increasing speed in computer technology creates new challenges for designers, and the tools they use to design, verify and debug the systems. Generally designers follow general high speed design rules, built up a prototype, make measurements and redesign if necessary.

But short on the shelf cycles of the commercial market forces the industry to speed up design process. Redesigning may cost much and cause the product to be delayed for the production for months. Nowadays field solvers play a crucial role in high speed interconnect design.

In this work, a traditional differential mode serial communication line is chosen for the analysis. 2D Quasistatic TLM algorithm is developed to solve electromagnetic field distribution within PCB stack up. The verification of the results is achieved by using a commercial tool (SI8000 Quick Solver from Polar Instruments) which uses boundary elements method.

Transmission Line Modeling provides a conceptual model which produces a time domain numerical technique for solving networks and fields [1]. To calculate the field distribution in quasistatic state, we will assume sinusoidal source or harmonic fields.

Each node is connected to other four nodes and the circuit (or field) equations must be used to calculate the E value of the neighboring node. There is no time-stepping in this procedure. Field values are extracted directly. Each node builds up five equations: four for neighboring nodes, one for the stub node. The known values are the field values at the surface of the conductors. Height of the PCB is divided into 50 nodes. Width is divided into 100. There is one equation for each node. So the matrix size is 5000×5000. However, as each line has only four elements, using sparse matrix techniques our memory requirement reduces to 20.000 elements, not $5000 \times 5000 = 25.000.000$ elements. A very sparse band matrix with three bands is constructed using these equations. Field value of each node is extracted by solving this matrix. Problem setup consists a broadside coupled stripline PCB. In the first experiment both IO lines are fed with sinusoidal signals in even mode. Then the same procedure is applied for the odd mode.

ACKNOWLEDGMENT

The authors would like to thank to TUBITAK for the support with grant No. 105E067.

REFERENCES

1. Johns, P. B., "The art of modelling," *IEE Transactions on Electronics and Power*, No. 8, 565–569, 25, 1979.
2. Lindenmeier, S. and P. Russer, "Design of planar circuit structures with an efficient magnetostatic-field solver," *IEEE Transactions on Microwave Theory and Techniques*, Vol. 45, No. 12, December 1997.
3. Christopoulos, C., *The Transmission-line Modelling Method*, IEEE Press, 1995.

An Hybrid Steepest Descent Fast Multipole Method for the Scattering of Electromagnetic Waves by Dielectric Rough Surfaces

Cihan Tuzcu[1], **Lale Tükenmez Ergene**[1], **and Yasemin Altuncu**[2]

[1]Institute of Informatics, Istanbul Technical University, Istanbul, Turkey
[2]Electrical and Electronics Engineering Faculty, Istanbul Technical University
Istanbul, Turkey

Abstract— Analysis of electromagnetic scattering by rough surfaces constitutes an important and interesting class of problems in electromagnetic theory due to its potential applications in modeling of ground wave propagation, remote sensing of geophysical terrains such as snow, soil and vegetation etc. Surface based integral equation methods have been widely used in the solution of such problems. One of the main problems is the application of the integral equation methods is that it requires heavy computational work and one has to develop new approaches with reduced computational cost. Steepest Descent Fast Multipole Method is one of the effective methods in this direction and it has been applied to several complex problems. The computational cost can be also reduced by direct methods with high performance and massively parallel codes.

The main objective of this paper is to give a hybrid method which combines the Steepest Descent Fast Multipole Method and Buried Object Approach [1] for the scattering of electromagnetic waves from the dielectric rough surfaces. In the Buried Object Approach the irregularities of the rough surface are assumed to be as buried objects in a two half-space media with planar interface which allows us to formulate the problem as a scattering problem related to cylindrical bodies of arbitrary cross sections. Through the Green's function of the two half spaces medium where the irregularities are buried, the problem is reduced to the solution of a Fredholm integral equation which is solved via an application of Method of Moments (MoM) by reducing it to a linear system of equations. The computational cost of the present method is directly proportional to the number of irregularities of the surface and their sizes. As a result the method is very effective for surfaces having a localized roughness, arbitrary rms height and slope. In the calculation of the Green's function we adopt the Steepest Descent Fast Multipole Method to the present problem [2].The method permits us to obtain both the near and far field expressions of the scattered wave in the half-spaces above and below the surface. We have shown that the results of the method match with those obtained through the existing ones.

ACKNOWLEDGMENT

The authors would like to thank to TUBITAK for the support with grant no. 105E067.

REFERENCES

1. Altuncu, Y., A. Yapar, and I. Akduman, "On the scattering of electromagnetic waves by bodies buried in a half-space with locally rough interface," *IEEE Transactions on Geoscience and Remote Sensing*, Vol. 44, No. 6, 1435–1443, Jun. 2006.
2. Hu, B. and W. C. Chew, "Fast inhomogeneous plane wave algorithm for electromagnetic solutions in layered medium structures: two-dimensional case," *Radio Science*, Vol. 35, 31–43, Jan. 2000.

Electromagnetic Fundamentals Revisited: An Overview

Subal Kar[1] **and M. Nakajima**[2]

[1]University of Calcutta, India
[2]University of Kyoto, Japan

Abstract— Does the electromagnetic field propagate as a consequence of time differentiation of physical quantity? Faraday's experiment says so. If this conventional notion is followed, then we have the paradox associated with radiation of e.m energy from a dipole antenna in terms of Poynting vector (usually done on the basis of current element concept!).

However, if we assume that the electric field should me moved first (i.e., charge is the fundamental entity giving rise to the field) in order to excite e.m waves then it may be shown that propagation of e.m wave may take place as a consequence of time integration of physical quantity. On the basis of this concept a sampled-field analysis technique introduced is capable of explaining e.m phenomena from a more fundamental view point. We have established that a generalized plane wave solution is possible for e.m field, irrespective of the field being static or dynamic. Following this approach, we could resolve the paradox of antenna radiation problem need to be addressed on the basis of Poynting vector.

Electromagnetic radiation from antenna is conventionally derived from current flowing through the conductor. However, if e.m radiation from, say, a dipole antenna is to be treated in terms of Poynting vector then as $E_t = 0$ on the conductor surface, the normal component $\vec{E}x\vec{H}$, representing e.m power from the antenna, is zero — thus no radiation can emerge out of the conductor surface of dipole antenna (!) and hence the paradox.

In our model, we consider a plane e.m. wave: $\vec{E}^i = \bar{\vec{E}}^i e^{-j\vec{k}_i\cdot\vec{r}}$, $\vec{H}^i = (k^i/\omega\mu)\cdot\vec{E}^i$ is incident on a plane conductor whose surface lies on the z and x coordinates, the normal of the plane being oriented in the y direction. For the case of TE wave with $\bar{\vec{E}}^i = \hat{x}\bar{E}_x$, we can derive the Poynting vector over the surface of the plane conductor as:

$$\begin{aligned}\frac{1}{2}\mathrm{Re}(\vec{E}x\vec{H}^*) &= \frac{1}{2}\mathrm{Re}(\bar{\vec{E}}^i x\bar{\vec{H}}^{i*}) + \frac{1}{2}\mathrm{Re}(\bar{\vec{E}}^r x\bar{\vec{H}}^{r*}) + \frac{1}{2}\mathrm{Re}(\bar{\vec{E}}^i x\bar{\vec{H}}^{r*} + \bar{\vec{E}}^r x\bar{\vec{H}}^{i*})\cos 2k_y y \\ &= \hat{z}2Re(\bar{E}_x\bar{H}_y^*)\sin^2 k_y y \end{aligned} \quad (1)$$

where the superscripts i and r represent the incident and reflected terms, respectively.

On the basis of this equation the Poynting vector may be interpreted in two ways:

1) Analytical view: The first two terms in the first row on right hand side of Eq. (1) expresses the Poynting vectors for the incident and reflected waves. In this view, the interference term (i.e., the third term on right hand side in the same row) must be taken into account. However, the interference term vanishes, if it is integrated throughout the space over the conductor, on account of the orthogonality of plane waves.
2) Synthetic view: The three terms can be summed up to be a single term, as is written in the last row. This represents energy flow in parallel with the surface of the plane conductor. In the direction normal to the surface, there are energy flows back and forth which produces a standing wave represented by $\sin^2 k_y y$. Standing wave normal to the plane conductor conveys no net energy in the direction normal to the conductor surface.

Solution to the Antenna problem: With the aid of this model, the paradox of the radiation from half wave antenna may be resolved as follows.

The conventional mode of calculation of the Poynting vector may belong to the synthetic view. In this sense, the calculated Poynting vector did not give us the incident and reflected powers to and from the antenna respectively, so that there is no net power flow into or out of the antenna.

However, according to the analytical point of view, which is based on our analysis, the incident and reflected Poynting vectors are separated. We are then led to the interpretation that the incident wave starts from the signal source and excite current in the antenna conductor. While the radiated wave is being caused by the reflected wave. Along the antenna conductor, these two waves are superposed and the resultant Poynting vector becomes parallel to the conductor surface. In the usual observation procedure, these two waves cannot be distinguished. If a sensor such as a direction coupler is created, the exciting wave and emitted wave can be observed separately.

Calculation of GTD/UTD Reflection Points over Parametric Surfaces Using the Particle Swarm Optimizacion

A. Rubio, **O. Gutierrez**, **F. Saez de Adana**, **and M. F. Cátedra**
Departamento de Ciencias de la Computación, Universidad de Alcalá
28806, Alcalá de Henares, Spain

Abstract— A new method to find reflection points on parametric surfaces is presented in this communication. The technique uses the Particle Swarm Optimization to perform the minimization of the path associates with the computation of the reflection points. The points are referred to the parametric coordinates of the surface and a cost function, based on the Snell's Law and the Fermat's Principle, is applied to find the best position. The technique is applied to the computation of the reflection points of the Uniform Theory of Diffraction (GTD/UTD) and it is an alternative to another minimization methods like the Conjugate Gradient, and can be applied to cases where not good convergence is present.

In complex environments, the principal difficulty of the GTD/UTD is the ray-tracing calculation, especially when complex structures with arbitrary shape are analyzed. One of the tasks in the raytracing process is to determine where the rays are reflected or diffracted. These critical points can be calculated using analytical and close expressions when the scene is modeled by flat surfaces. However, for arbitrary curved surfaces, modeled by parametric surfaces, minimization techniques, such as the Conjugate Gradient, must be used. This method obtains good results for convex surfaces, where no local minimums are present. On the other hand, convergence problems can appear for concave surfaces. An alternative technique, based on the Particle Swamp Optimization (PSO), is presented in this communication. The PSO avoids the local minimum, therefore both convex or concave surfaces can be analyzed with the same accuracy.

PSO is an optimizer based on an evolutionary model used to solve engineering problems. It is based in the behavior of a swarm of bees in the search of the biggest flowers concentration. The algorithm defines a number of particles or agents into the solution space as starting solution. After that, each particle moves, randomly, over the space, and in each iteration every particle records its best position (pbest). Also the best position of all the particles is stored (gbest). The application of this algorithm to the computation of the reflection points consists in using a cost function which takes into account the two conditions that the reflection ray must accomplish: the Fermat's principle which says that the distance of the reflected path between the transmitter and the receiver must be minimum and the Snell's law.

Some results have been obtained which prove the accuracy of the method and its advantages with respect to other approaches.

Dielectric Properties of Ore Minerals in Microwave Range

V. V. Tikhonov[1], **D. A. Boyarskii**[1], **and O. N. Polyakova**[2]

[1]Earths Exploration from Space Department, Space Research Institute Russian Academy of Sciences
Profsojuznaya, 84/32, Moscow 117997, Russia
[2]Department of Physics, Moscow State Pedagogical University
M. Pirogovskaya, 29, Moscow 119992, GSP-2, Russia

Abstract— Dielectric characteristics of many natural minerals are poorly investigated. The lack of such data poses a problem for modeling the interaction of electromagnetic radiation with many media, such as ground, soils and rocks. This results in significant difficulties in the interpretation of radiometry, radar, subsurface sensing and dielectric spectroscopy data.

Microwave dielectric properties of ore minerals still remain virtually uninvestigated due to considerable technical problems. No data on dielectric properties of such minerals are reported in the literature.

A technique to define dielectric properties of ore minerals is discussed. Using this technique, dielectric characteristics of some minerals in a range of 77–300 GHz are obtained.

The real and imaginary parts of complex dielectric constant of a substance cannot be measured directly and can be derived only from measurements of other parameters (for instance, reflection and transmittance coefficients) through application of a corresponding theory.

Spectral measurements of reflection and transmittance coefficients of plane-parallel samples of the minerals were conducted at a test board at normal radiation incidence. Measurements of reflection and transmittance coefficients were carried out using a carcinotron spectrometer. The spectrometer had a generating unit (with highly-stabilized electronic feed), a receiver unit (optophone and synchronous detector), and also a measuring quasi-optical line.

The real and imaginary parts of complex dielectric constant of a mineral were determined by solving a system of equations for reflection and transmittance coefficients of the multi-layer absorbing film placed between two dielectric media. This system of equations did not allow for an analytical solution and demanded numerical solution using corresponding algorithms and computer software. The problem was solved by minimization of the criterion function. The criterion function was square standard deviation of the theoretical dependence of absorption in a layer from the experimental one in the wave interval where dielectric constant could be considered constant. An algorithm using Rosenbrock method was developed for minimization of the criterion function. This method is a typical method of search with restrictions where minimization directions are completely defined on the basis of consecutive calculations of the criterion function.

In the work, the results of spectral measurements of reflection and transmittance coefficients of plane-parallel samples of some ore minerals (magnetite, chalcopyrite, sphalerite, etc.), in microwave range are presented. On the basis of these dependences, values of real and imaginary parts of dielectric permittivities of the studied minerals in a range of 77–300 GHz are calculated. The results of the calculations are approximated by smooth functions of radiation frequency. The obtained formulas can be used to calculate complex dielectric constant or complex refraction coefficient of ore minerals in a range of 77–300 GHz.

Patch Antenna at Frequency $f = 2.35\,\mathrm{GHz}$ for Telecommunications Applications

K. ELkinani[1], **S. Bri**[1], **A. Nakheli**[1], **O. Benzaim**[2], **and A. Mamouni**[2]

[1]Equipe Hyperfréquences et Matériaux, ESTM, B. P. 3103, Meknès, Maroc
[2]Institut d'Electronique, de la Microélectronique et de Nanotechnologie, UMR CNRS 8520
IEMN, Cité Scientifique, Avenue Poincaré, B. P. 60069 59652, Villeneuve d'Ascq Cedex, France

Abstract— This paper analyzes the effects of electromagnetic radiation from a cellular phone on the head. Various antenna designs were created and analyzed. Special consideration was taken to create an antenna with high efficiency and optimum radiation characteristics in frequency $f = 2.35\,\mathrm{GHz}$. The antenna was placed next to human head materials and specific absorption rates were calculated. Tests were performed at various distances from the material for analysis and evaluation of the fields. Simulations on the antenna were done on Ansofts Ensemble software. The application of the antenna next to the head and the creation of the head model itself were done on Ansofts High Frequency Structure Simulator (HFSS). The antenna was built and tested on a network analyzer to obtain near field. Mathematical models were used in all designs.

REFERENCES

1. Abd-Alhameed, R. A., K. Khalil, P. S. Excell, and C. H. See, "Simulation and measurement of broadband microstrip patch antenna for 3G wireless communications," The Institute of Electrical Engineers, Printed end Published by the IEE, Michael Faraday House, Six Hiil Wav, Steveneage SG 1 2AY, 2003.
2. Covert, L. and J. Lin, "Simulation and measurement of a heatsink antenna: A dual-function structure," *IEEE Transactions on Antennas and Propagation*, Vol. 54, No. 4, April 2006.
3. Ollikainen, J., O. Kivekäs, A. Toropainen, and P. Vainikainen, "Internal dual band patch antenna for mobile phones," *2000 European Space Agency (ESA), Proceedings of the AP2000 Millennium Conference on Antennas & Propagation*, Davos, Switzerland, 9–14 April, 2000.

Electroplating Uniformity Estimation Using Electromagnetic Analysis

Han Kim
SAMSUNG Electro-Mechanics, Korea

Abstract— As integrated circuit miniaturizes, the manufacturing process of package substrates have become more fastidious to be handled. In particular, the electroplating uniformity control is more difficult because of its inaccuracy estimation.

In generally, the simulation approach for electroplating of package substrate is based on an electrochemical theory. There are some calculation methods and commercial simulation tools using electrochemical analysis for the estimation of electroplating uniformity. However, the typical electrochemical analysis is inadequate for the estimation of electroplating uniformity at PCB (printed circuit board) because it is not included the analysis of bus lines at PCB panel.

In this paper we propose a novel simulation approach using electromagnetic analysis for the estimation of electroplating uniformity. This approach is based on the calculation of current distribution at PCB panel. The current distribution is calculated by using modified material properties at the electroplating bath and the plating uniformity can be represented by using this current distribution.

To verify this proposed approach, we calculated electroplating uniformity at PCB panel by using commercial electromagnetic analysis program and our program for estimation of electroplating uniformity. Both simulation results are comparable with measurement one as shown in Fig. 2–4. The improvement of the electroplating uniformity can be achieved by using this proposed method.

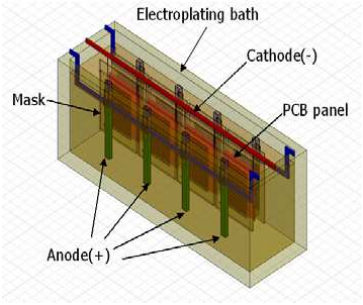

Figure 1: Electroplating bath.

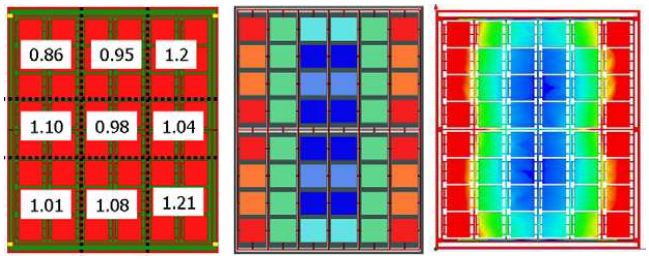

(a) (b) (c)

Figure 2: Electroplating uniformity (a) measurement result (b) simulation(commercial program) (c) simulation (our program).

REFERENCES

1. Kim, H. and C.-H. Ahn, "Fast inductance extraction of microstrip lines using adaptive PEEC grid," *Microwave Conference, APMC 2002*, Vol. 1, 81–84, Nov. 2002.

Progress of Mobile Natural Gas Pipeline Leak Detector Based on Near-infrared Diode Laser Absorption Spectroscopy

Lei Wang, **Xiaoming Gao**, **Tu Tan**, **Baixiang Li**, **and Weijun Zhang**
Laboratory of Environmental Spectroscopy, Anhui Institute of Optics & Fine Mechanic
Chinese Academy of Sciences, Hefei 230031, China

Abstract— Natural gas is a cleanly energy source, which has very high benefit at environmental protection and improving people health as a substitute of coal. China government will encourage the using of natural gas, decrease the dependence on coal and petroleum, but the distribution of china natural gas is unbalanced. To solve the problem, china government has built a natural gas pipeline from west to east in china, and will build five transverse and two longitudinal main natural gas nets covering whole china. For these long transport pipelines, the leakage of the natural gas is unavoidable. Detecting leakage sources is a very laborious task.

We have developed a portable natural gas pipeline leak remote detector based on near infrared diode laser absorption spectroscopy. Based on the groundwork, we are developing a mobile natural gas pipeline leak remote detector. The reflected scattering laser was collected by a ϕ114 lens to focus on a detector, the ratio between first and second harmonic was recorded. A bag filled 0.3% methane mixture gas was set at far away 7 m from the detector. The detector was mounted on a simulated mobile platform. Rotating the platform, the different scanning angle speeds corresponded to different transfer speeds. The laser was scanned across the gas bag come-to-go. The recorded signals at different transfer speeds were showed in Figure 1. We can know that the signals at lower moving speed had small fluctuation, at high moving speed, the fluctuation is large. The fluctuation will be decreased by setting the parameters of the system. In the system, we will realize automatic storage of pipeline leak information using a GPS (Global Positioning Systems) and a CCD camera. The saved information will include methane concentration, the leak position, leak scene and distance from the detector.

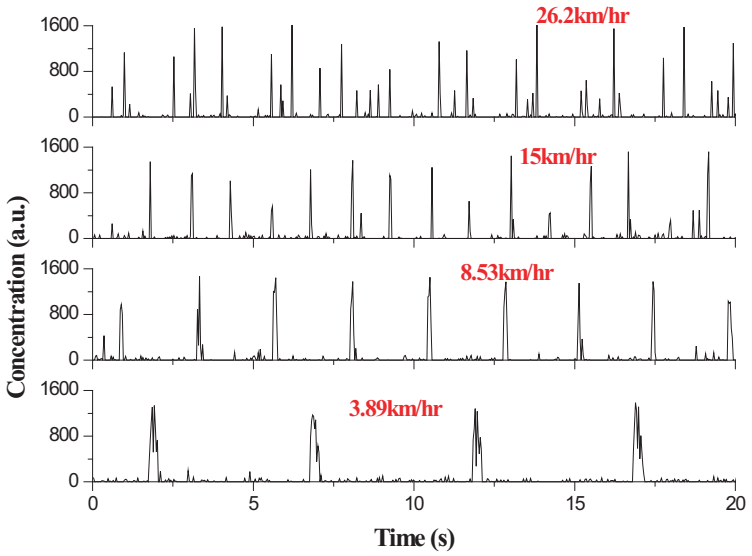

Figure 1: Measured methane concentration at different transfer speed.

Incoherent Broadband Cavity-enhanced Absorption Spectroscopy Based on Light-emitting Diodes

Tao Wu[1], **Weijun Zhang**[1], **Weidong Chen**[2], **Weixiong Zhao**[1], **and Xiaoming Gao**[1]

[1]Anhui Institute of Optics & Fine Mechanics, Chinese Academy Sciences, Hefei 230031, China
[2]MREID, Université du Littoral, 145 Av. Maurice Schumann, Dunkerque 59140, France

Abstract— A compact incoherent broadband cavity-enhanced absorption spectroscopy (IBBCEAS) system has been established at visible wavelengths using a high powered blue light emitting diode (LED). The LED light was coupled into a 92.5 cm long high finesse cavity that composing of two 30 mm diameter spherical mirrors (1.0 m radius of curvature) with reflectivity of ~ 0.993. The light leaked out of the cavity was collected by a compact CCD spectrometer (HR 2000). The IBBCEAS spectrum of NO_2 has been recorded at 455 µm.

The reflectivity of the mirrors was measured as a function of wavelength using standard concentrations of NO_2 and further confirmed by absorption of O_2-O_2 collisional pair. The minimum detectable concentration of NO_2 is estimated to be 7 ppbv for a 60 s averaging period in the system.

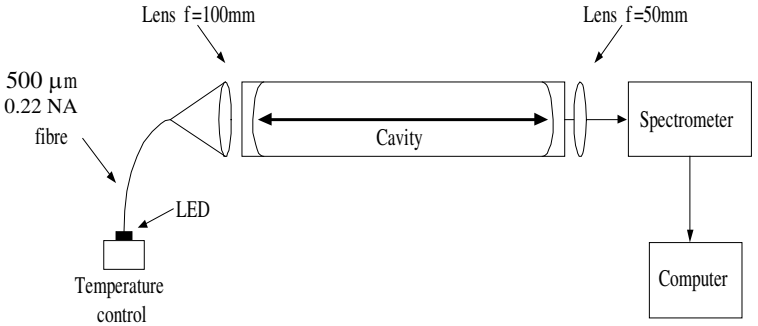

Figure 1: Experimental set-up for incoherent broadband cavity-enhanced absorption instrument.

REFERENCES

1. Langridge, J. M., S. M. Ball, and R. L. Jones, *Analyst*, Vol. 131, 916–922, 2006.

Session 3P1a
Advances in Reverberation Chambers: Modelling and Applications

Numerical Simulation of a Reverberation Chamber with a Stochastic Collocation Method

F. Diouf[1], **P. Bonnet**[1], **F. Paladian**[1], **M. Fogli**[2], **and C. Chauvière**[3]

[1]LaSMEA, Université Blaise Pascal, 24 Avenue des Landais 63177 Aubière, France
[2]LaMI, Université Blaise Pascal, 24 Avenue des Landais 63177 Aubière, France
[3]Laboratoire de Mathématiques, Université Blaise Pascal, 24 Avenue des Landais 63177 Aubière, France

Abstract— The numerical modeling of Reverberation Chambers (RC) by frequential [1] or temporal [2] methods is meeting growing interests. If one observes suitable comparisons between theory and experimentation, these results nevertheless are obtained at high computing expenses. Alternatively, it is possible to consider the cavity without stirrer by introducing randomness in the quality factor (Q). Thus, starting from measurements carried out in LaSMEA's RC, the first step of this study is to determine the probabilistic density function (pdf) of Q. When the density of modes inside the cavity is sufficient, we can show that the total quality factor follows a chi-2 distribution of order 6 (χ^2_6) with scale factor α_f. The estimation of a pdf requires a significant number of data which cannot be obtained by taking measurements on one point in LASMEA's RC which dimensions (a, b, d) are respectively 6.7 m, 8.4 m, 3.5 m. In order to avoid this drawback, experimental data are taken into 80 points of the working volume of the RC and for 51 steps of the stirrer i.e., 4080 electric field's modulus samples. Note that the pattern might have a spatial correlation even if the linear correlation coming from the stirrer is avoided by taking a limited number of steps. As is shown in Fig. 1, the experimental pdf seems to be very closed to the theoretical one.

The proposed approach is based on the hypothesis that the stirrer in the RC can be replaced by a randomly quality factor. Indeed, the boundary conditions change at each step of the stirrer; therefore, we suppose that each step corresponds to one value of the quality factor which depends on the wall conductivity value. In order to simulate realizations of this random variable, the mean, standard deviation and pdf of the conductivity σ have been obtained from the quality factor for each frequency: the electromagnetic field inside the working volume of the MSRC can be calculated by a FDTD software through Monte-Carlo simulations. If this rather popular method is easy to implement and allows one to re-use available deterministic codes, the convergence rate is yet typically very slow (proportional to $1/\sqrt{N}$ where N is the number of samples). Over the last few years, other approaches have been proposed, which in certain situations give a much faster convergence rate then Monte-Carlo (spectral Galerkin method, stochastic collocation method, ...) [3]. We have chosen to use the stochastic collocation method because it can be easily implemented and leads naturally to the statistical moments of the electromagnetic field (mean value, variance, ...). In addition, only a limited number of σ realizations need to be computed in order to get accurate results. For example, Fig. 2 shows that results obtained by our stochastic collocation method converge to the theoretical value at high frequencies i.e., the stirring is efficient.

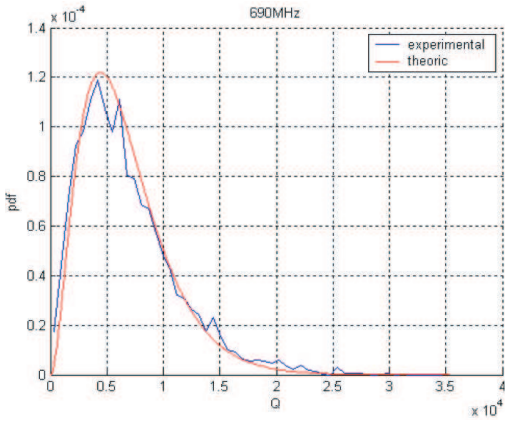

Figure 1: pdf of the total quality factor at 690 MHz in LASMEA's RC.

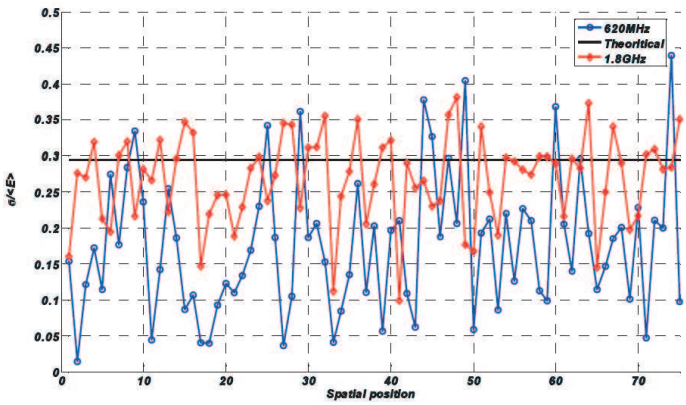

Figure 2: Ratio standard deviation over mean value of magnitude of the electric inside the MSRC.

REFERENCES

1. Bruns, C., "Three-dimensional simulation and experimental verification of a reverberation chamber," Ph.D. Thesis ETH Zurich, 2005.
2. Lalléchère, S., "Modélisations numériques temporelles des CRBM en compatibilité electromagnétique. Contribution aux schémas volumes finis," Thèse de Doctorat, Université Blaise Pascal, 2006.
3. Chauvière, C., J. S. Hesthaven, and L. Wilcox, "Efficient computation of RCS from scatterers of uncertain shapes," *IEEE Trans. Antennas Propagation*, 2006.

The Use of Reverberating Chambers as Modern Telecommunications Simulating Tool

Paolo Corona
University Parthenope, Naples, Italy

Abstract— The use of Reverberating Chambers (RC) in Electromagnetic Compatibility (EMC) has been well assessed in the last decades. Still some theoretical problems are open, as well as practical aspects in the lower frequency use. On the other hand the use is so satisfactory for so many reasons (speediness of measurements, low cost of the chamber itself, efficiency in terms of field to power ratio) that its diffusion appears now competitive and prevailing against other possible alternative, such as anechoic chambers or open air test sites.

In last decade some other use emerged to the consideration. It appeared that what was a limiting condition for basic EMC use, i.e., the presence of some direct coupling, could be a specific tool to test signal integrity in a multipath random environment. The first attempts can be tracked in some application for homing tests, in eighties (of last century), at Dahlgren (VA, U.S.) Navy Facility, and in the statistic analysis of off centered RC field at Parthenope (then Naval) University of Naples (Italy) in nineties (of last century).

At the present time, activity is in progress, at National Institute of Standards and Technology (U.S.), as well as at Parthenope University, but also in many other laboratories. The purpose is to use the plane wave non coherent (in space) spectrum that can be produced in the RC as frequency coherent "noisy" environment to interfere direct path, to use such environment to interfere with code modulated signals to affect Bit Error Rate (BER), and to use the RC to produce direction sensible environment to test smart antennas in wireless indoor connection.

Work is in progress in all the above, and appears able to cope with demanding test procedures for modern systems, such as indoor WiFi and urban wireless environment.

PEDs Emission Determination in a Reverberation Chamber

R. De Leo and V. Mariani Primiani

Dipartimento di Elettromagnetismo e Bioingegneria, Università Politecnica delle Marche
Via Brecce Bianche, Ancona 60131, Italy

Abstract— Portable Electronic Devices (PEDs) are nowadays available on the market and will be potentially used during aircraft flights. As a consequence a more extensive use of mobile phones, laptop, wireless systems, CD player, etc. is predictable (at least accidentally) in the next few years. Moreover, the bandwidth covered by existing PEDs available on the market is increasing year after year. The main intrinsic features of PEDs which have to be taken into account for the interference problem are the emitted power and the working frequency bandwidth. When PEDs works inside an aircraft, different phenomena occur that give rise to a coupling with antennas and/or electronic equipments through cables and apertures. For this potential coupling risk, the use of PEDs are forbidden during the take off and landing phases. To make sure that the use of PEDs is under control, it may be useful to install special detectors able to advise for the presence of working devices. A proper design of such detectors cannot leave the PED radiated emission characterization out of consideration. Beside the traditional anechoic chamber test facility, the radiated emission measurement can be carried out inside a reverberation chamber (RC). This situation is completely different from the traditional one, and appears much more meaningful for the type of problem that is being faced: since the orientation of the PED, during its illicit use, is random, also the field intensity at the detector position will be characterized by this random characteristic. Moreover, inside the aircraft the energy emitted by the PED suffers several reflections before reaching the detector. In this sense, the RC is the environment most suitable to reproduce this kind of propagation, because in a ideal chamber the field can be described as a proper summation of infinite plane waves coming from any direction, with any polarization and arbitrary phase. The reverberation chamber quickly provides the radiated power and statistics of the field without having to rotate the equipment. In this way the measurement procedure is easier. Recently, it has been also demonstrated the possibility to simulate absorption effects inside an aircraft using a properly loaded reverberation chamber. For these reasons, an RC has been used to determine the total radiated power of typical PEDs, according to the set-up of Fig. 1. The novelty of the proposed method essentially lies in the power determination, which is independent from the device observation direction. The electric field determination required the directivity knowledge, which is a deterministic quantity in free space, but assumes a statistic meaning inside an aircraft for the above mentioned considerations. To establish a threshold for a security detection system, the most probable directivity value can be adopted, fixing a distance for the detector. As an example in Fig. 2 the emission of a photo-camera is reported. The paper will present also a comparison with measurement in anechoic chamber, where a deterministic knowledge of the directivity is needed.

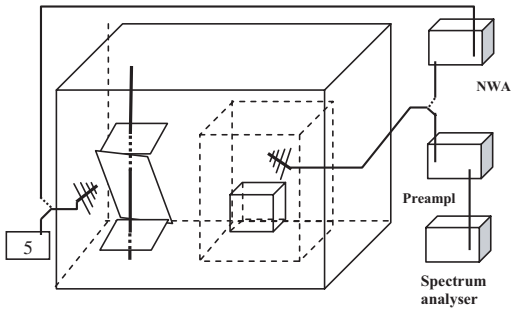

Figure 1: RC set-up.

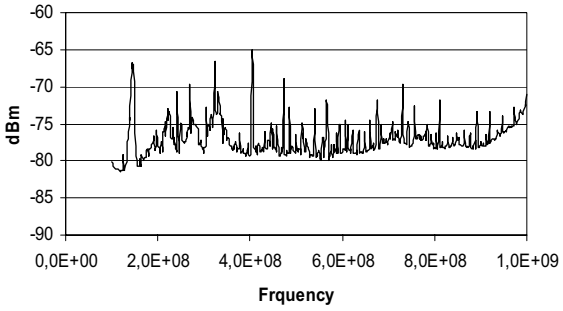

Figure 2: Photo-camera emissions.

On the Generation of Reference Currents by Means of a Reverberation Chamber

R. De Leo, V. Mariani Primiani, F. Moglie, and A. P. Pastore

Dipartimento di Elettromagnetismo e Bioingegneria, Università Politecnica delle Marche
Ancona 60131, Italy

Abstract— Reverberation chambers (RC) are nowadays widely used for EMC testing. Their electromagnetic use began thirty years ago, and a lot of improvement in the theoretical and experimental understanding about such a structure has been achieved up to now. The RC represents a valid alternative to traditional anechoic chamber (AC) and therefore they have been also standardised.

The reverberation chamber environment is characterised by an electromagnetic field which is statistically uniform, isotropic and depolarised. In this sense, in a well operating chamber the field statistics is well known and similarly also the current induced by this electromagnetic field on metal structures follows the same statistical properties. More precisely, considering a wire conductor, it acts as a receiving antenna and the current distribution along it can be accurately calculated from the knowledge of the chamber electric field. Therefore, placing a wire inside an RC the resulting induced current represents a reference current useful for calibration purposes. Starting from the Hill's plane wave integral representation, the RC field can be represented by a finite summation of proper plane waves, of amplitude Ei, coming from arbitrary directions and characterised by arbitrary phase and polarization

$$\bar{E}(\bar{r}) = \sum_{i=1}^{N} \bar{E}_i e^{j\phi_i} e^{j\bar{\beta}_i \cdot \bar{r}} \tag{1}$$

Assuming an equal amplitude Eo for each plane wave, the total chamber field, ensemble average over the stirrer rotation, is given by

$$\langle |E_{RC}| \rangle = \frac{15}{16} \sqrt{\frac{\pi}{3}} \sqrt{N} |E_o| \tag{2}$$

The previous expression allows to correlate the measured averaged field $\langle |E_{RC}| \rangle$ with the computed field in order to correctly estimate the amplitude of each plane wave necessary to simulate the chamber. The current induced along the wire by each plane wave is easily calculated by means of a home made FDTD code, and the application of the superposition effect allows to recover the total current distribution. Two applications are considered: the calibration of a current probe using the current induced on a 50 cm straight wire, (Fig. 1), and the determination of a

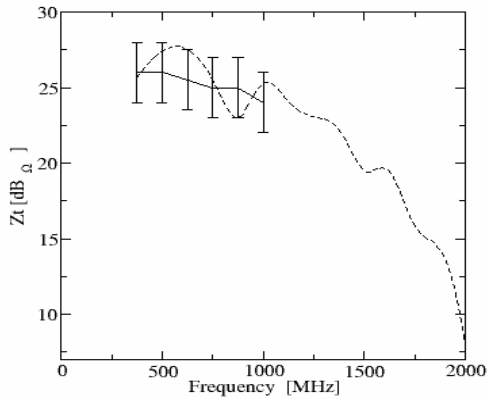

Figure 1: Transfer impedance of a F-61 current probe: RC calibration (dashed line), manufacturer data (cont. line with error bars).

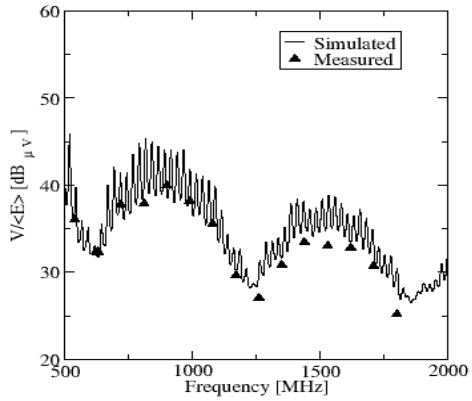

Figure 2: Field normalised voltage at the end of a RG-58 coaxial cable with a 1 nH/m shield mutual inductance.

cable shield transfer impedance using the current induced along the outer cable shield itself. In this second case, the shield current knowledge allows to calculate the signal induced in the cable internal circuit, whose cumulative effect is represented by the cable end voltage, Fig. 2. The comparison between the computed and measured voltage gives the shield transfer impedance.

Improvement of the Reverberation Chamber Performances below the Starting Frequency

S. Leman[1], **L. Koné**[1], **V. Deniau**[2], **S. Baranowski**[1], **and B. Démoulin**[1]

[1]Université des Sciences et technologies de Lille
Groupe TELICE de l'IEMN, Villeneuve d'Ascq, France
[2]Institut National sur la Recherche dans les Transports et leur Sécurité
Villeneuve d'Ascq, France

Abstract— Generally speaking, the usual frequency range in reverberation room measurements correspond to short wavelength in respect of the room dimensions. Then the field distribution in the room behaves like a random data when the stirrer is moving. Such behaviour is acquired above the starting frequency which is about five or six times the frequency of the first eigen mode of this rectangular shaped cavity.

To insure the random field distribution for a given frequency, field data checked when the stirrer is moving are compared with the well know Raleigh distribution which involve agreement or not following the location in respect of the starting frequency. Indeed, above this, agreement with the Raleigh distribution occurs always at any frequency, then below the starting frequency, the probability of agreement falls dramatically when the frequency is decreasing toward the first eigen mode.

The paper is aimed in proposing improvement of the reverberation room performances in terms of random field distribution in the gap within the first eigen mode to the starting frequency. We can imagine a wire running along the inner side of two or three contiguous walls of the rooms. This is like a transmission line where the length of the wire determine a resonance frequency which may be three or four time more smaller than the first eigen mode of the room. Thus just above the first eigen mode this line behaves as an over sized device in respect of the wavelength. Assuming that one termination of the line is opened and short circuited at the opposite, we can observe a sharp resonance amplitude which may be sufficient to change the field strength in the room whole space with a random fashion when the stirrer is moving.

First part of the paper will be to examine the field distribution in the room with and without the transmission line in order to observe the effect of the wire distance from the room's walls surfaces. This will be achieved with computation by means of the method of moments. Second part will be related with experiments carried out to observe change in the random behaviour of electromagnetic field in the room, especially with the agreement of statistical gauge for a large number of frequency samples within the gap above the first eigen mode. To conclude, this method will be extended to a combination of several lines with various lengths in order to realize a sort of mode stirring in switching the lines to the wall surfaces.

Scattering Cross Section Measurement in Reverberation Chamber

J. de Rosny and G. Lerosey
Laboratoire Ondes et Acoustique, E.S.P.C.I., Universite Paris 7
C.N.R.S, UMR 7587, 10, rue Vauquelin, 75005, Paris, France

Abstract— Reverberation chambers are now common test facilities used in electromagnetic compatibility. Objects loaded in the chambers, such as antennas, reflectors, can affect the measure because they absorb and scatter the diffuse field. Thus it is important to know the scattering and absorbing cross sections of these objects. Here we propose a new technique to measure the scattering cross sections averaged over all directions of incidence and both polarization in a reverberation chamber. It is based on stacking time-dependent fields generated by a repetitive pulsed source while the objects are moving. The fields recorded by wire antennas, are averaged over the object positions. The square of the averaged field is shown to decrease exponentially with the time spent by the wave in the chamber. The cross section is deduced from the exponential factor. The technique has been experimentally validated in a $1\,\mathrm{m}^3$ reverberation chamber at 2.45 GHz with metallic spheres of several radii. The experimental cross sections are found to be in agreement with the theoretical ones.

REFERENCES

1. Henty, B. E. and D. D. Stancil, *Phys. Rev. Lett.*, Vol. 93, 243904, 2004.
2. Lerosey, G., J. de Rosny, A. Tourin, A. Derode, and M. Fink, *Phys. Rev. Lett.*, Vol. 92, 193904, 2004.
3. Lerosey, G., J. de Rosny, A. Tourin, A. Derode, and M. Fink, *App. Phys. Lett.*, Vol. 15, 154101, 2006.
4. Carminati, R., J. J. Saenz, J.-J. Greffet, and M. Nieto-Vesperinas, *Phys. Rev. A*, Vol. 62, 012712, 2000.

Session 3P1b
Advanced Optimization Techniques in Electromagnetics

Antenna Rotation Aperture Synthesis for Short-range Personnel Scanning at mm-wavelengths

B. M. Lucotte and A. R. Harvey
Heriot-Watt University, UK

Abstract— Passive and semi-passive mm-wave imaging techniques are currently receiving considerable attention as personnel scanners due to their ability to detect concealed weapons through obscurants such as clothing. In comparison to conventional real-aperture imaging systems, synthetic aperture imaging enables images to be recorded with an infinite depth of field and using an essentially planar and sparse array. Synthetic aperture imaging systems have traditionally been considered for the recording of high spatial resolution images in a single snapshot. Snapshot operation necessarily requires a large number of antennas: this not only results in a high cost but also makes calibration highly problematic. It is highly desirable therefore to reduce the antenna count without adversely affecting the spatial resolution and radiometric sensitivity of the imager. We show that this can be achieved by introducing some degree of mechanical scanning between the source and the array in a similar *modus operandus* to the Earth Rotation Synthesis technique used in radio astronomy, but with the added complexity of near-field operation. Since the spatial frequencies are recorded in time-sequence the reduction in antenna count is achieved at the cost of a reduced imaging frame rate.

In this paper we adapt the fundamental imaging equations and image reconstruction algorithms for near-field synthetic aperture imaging, before considering the fundamental requirements of the array to adequately sample the image spatial frequencies. We then describe the necessary trade-off between the radiometric sensitivity and imaging frame rate for various array complexities. For instance, we devise a 15 GHz bandwidth imager operating at a centre frequency of 94 GHz (delay lines are employed to enable wide bandwidths and high sensitivity), recording an extended scene at a range of 2 m with a 30° Field of View (FoV) and achieving a noise level of 2 K and a Point Spread Function with a Full Width at Half Maximum of 7 mm. In comparison to a snapshot aperture synthesis radiometer, the time-sequential recording of n individual images enables the number of antennas to be reduced by a factor of approximately $\sqrt{n}$ without a reduction in image quality. Finally, various array designs including a rotationally scanned antenna array are presented. We show that a rotational scan provides better sampling of scene spatial frequencies and a more compact mechanical scanning system. The arrays presented here are based on Reuleux triangle arrays because they sample the Fourier components of the image more uniformly than other conventional arrays (T-shape, Y-shape and circular arrays). Small random perturbations were introduced in the arrays in order to break the symmetry patterns of their spatial frequency coverage, and were optimized with a Genetic Algorithm.

Non-conventional Optimization Techniques in Computational Electromagnetics

Zbyněk Raida

Department of Radio Electronics, Brno University of Technology
Purkyňova 118, 612 00 Brno, Czechia

Abstract— In case of a global optimization of complicated electromagnetic structures, CPU-time demanding numerical analysis has to be repeated for each frequency separately. The global optimiza-tion is therefore extremely time-consuming. And this is the motivation for the development of non-conventional optimization approaches providing very high efficiency and a satisfactory accuracy.

In the paper, novel optimization approaches for computational electromagnetics that have been deve-loped at the Dept. of Radio Electronics, Brno University of Technology, during the last decade, are reviewed. Abilities of the developed techniques are illustrated by several examples.

Hybrid global algorithms. Several global optimization techniques can be shown to exhibit comple-mentary properties (e.g., swarm intelligence algorithms and evolutionary ones). This is the reason for mutual combination of such techniques. Several ways of the hybridization are compared and the properties of several variants are analyzed. Methodological conclusions are formulated.

In case the global algorithms reveal the regions potentially containing the global optimum, highly effi-cient local optimization techniques can be applied to reach the optimum as accurately as possible and as quickly as possible. Quasi-Newton techniques are applied as the most efficient local optimizers.

Advanced neural networks. In order to make the evaluation of the cost function as efficient as pos-sible, wide-band numerical models of electromagnetic structures can be replaced by properly trained artificial neural networks. Both the feed-forward architecture and the recurrent one can be exploited. Using the neural network, the region containing the global optimum can be revealed more efficiently compared to the full-wave techniques.

Time-domain approaches. In case of wide-band electromagnetic structures, frequency-domain ap-proaches require a separate numerical analysis at each frequency of the investigated frequency band. In case of the time-domain analysis, the electromagnetic structure can be fully characterized within a single analysis when excited by an extremely narrow excitation pulse. Time-domain parameters of electromagnetic structures are therefore proposed, and the objective function is composed directly in the time domain in order to enhance the efficiency of the optimization procedure.

Experiments. The developed techniques have been applied to the design of multi-band antennas, electromagnetic bandgap structures, and metamateril applications. Selected structures have been fabricated and measured. The measured results have been confronted to numerical models.

The paper brings the overview of several techniques enhancing the efficiency of the glo-bal optimization of electromagnetic structures. Abilities of the proposed methods are illustrated by examples of practical electromagnetic devices. Several results are experimentally verified.

ACKNOWLEDGMENT

Research described in the paper has been financially supported by the Czech grant Agency under the grant No. 102/07/0688, and by the research program No. MSM0021630513.

Modified Standard Amplitude Distribution for the Generation of Low Sidelobe Patterns of Arrays for EMC Applications

R. Ramana Reddy and G. S. N. Raju

Department of Electronics and Communication Engineering, AU College of Engineering
Andhra University, Visakhapatnam 530 003, India

Abstract— Radiation pattern of an antenna is one of the important specifications for all applications. It is well known that a single radiator produces radiation patterns which contain relatively wide beam width. Moreover its directivity is also low. The applications like long distance communications, very high gains are desirable. Although it is possible for large antennas the size becomes prohibitive practically. In such cases an array in which a group of elements arranged either in linear form or in planar form is the best option. The design of such arrays depends on the geometrical configuration, spacing of the elements, amplitude distribution, phase distribution and type of element.

Although, the above factors form the basis design criteria to meet the requirements of directional patterns, the design of amplitude distribution keeping the remaining factors constant is of present interest for producing useful low sidelobe patterns for EMC applications.

Several standard distributions [1–3] are reported in the literature along with a few methods [4–9] of design. Each distribution and method reported yield patterns of different characteristics. They differ in sidelobe levels, beamwidths and also in overall characteristics.

However, in the present work some studies are carried out to produce low sidelobe patterns from the proposed new tapered amplitude distributions. The proposed amplitude distributions are basically raised cosine on pedestal type. The taper is modified by two independent parameters, one being the tapering coefficient and the other being raised power.

Using the proposed newly tapered amplitude distributions, the radiation patterns are numerically computed for large and small arrays. The distributions are basically continuous in nature and hence the patterns are evaluated for large and small line sources. These are extendable to discrete arrays. The results presented in this paper are useful for array designers to pickup the suitable distributions required for EMC and other applications.

REFERENCES

1. Ma, M. T., *Theory and Application of Antenna Arrays*, John Wiley & Sons Inc., New York, 1974.
2. Steinberg, B. D., *Principles of Aperture and Array System Design*, Wiley Interscience publications, 1976.
3. Taylor, T. T., "Design of line source antennas or narrow beamwidth and low sidelobes," *IRE Trans. Antennas Propagat.*, Vol. AP-3, 16–28, January 1955.
4. Woodward, P. M. and J. D. Lawson, "The theoretical precision with which an arbitrary radiation-pattern may be obtained from a source of a finite size," *J. IEE*, Vol. 95, Pt. III, No. 37, 363–370, September 1948.
5. Praba, K., "Optimal aperture for maximum edge-of-coverage (EOC) directivity," *IEEE Antennas and Propagation Magazine*, Vol. 36, No. 3, 72–74, June 1994.
6. Elliot, R. S., "Beamwidth and directivity of large scanning arrays," *Microwave Journal*, 74–82, January 1964.
7. Stegen, R. J., "Excitation coefficients and beamwidths of Tschebyscheff arrays," *Proc. IRE*, 1671–1674, November 1953.
8. Kumar, B. P. and G. R. Branner "Generalized analytical technique for the synthesis of unequally spaced arrays with liner, planar, cylindrical or spherical geometry," *IEEE Trans. on Antennas and Propagation*, Vol. 53, No. 2, 621–634, February 2005.
9. Wong, K.-L., F.-R. Hsiao, and T.-W. Chiou, "Omni-directional planer dipole array antenna," *IEEE Trans. on Antennas and Propagation*, Vol. 52, No. 2, 624–628, February 2004.

Session 3P2
Antenna and Array System 1

Printed Antennas Tuned by Transversely Magnetized Ferrite Operating at a Novel Resonant Mode

A. A. Mavridis[1], **G. A. Kyriacou**[1], **and J. N. Sahalos**[2]

[1]Microwaves Lab., Department of Electrical and Computer Engineering
Democritus University of Thrace, Greece
[2]Radiocommunications Lab., Department of Physics, Aristotle University of Thessaloniki, Greece

Abstract— There is an increasing research effort toward the analysis of circuits and patch antennas printed on magnetized ferrite substrates. Certain unique features of the latter like electronic tuning, beam steering, radar cross section reduction and possible surface wave power reduction, makes them very attractive in a variety of applications. These features are the direct result of the ability to dynamically control the ferrite permeability tensor from its DC-bias, which is in turn reduced to the control of the DC-current of a preferably miniaturized electromagnet.

The resonant frequency of circular and ring patch antennas printed on transversely magnetized ferrite substrate was analytically studied in our previous work [1, 2]. The analysis was performed using the perfect magnetic walls approximation and the ferrite losses were also taken into account. Closed form expressions were given for all the geometries studied. Those expressions proved to be satisfactorily accurate compared to numerical simulation results performed by commercially available software. Moreover, two additional geometries adopting a ferrite-inclusion into a dielectric substrate were proposed, in order to reduce the volume and the overall losses of the ferrite material.

A number of published works (e.g., Pozar [3]) show that in the case of patch antennas printed on magnetized ferrite substrates, there is a cutoff area where there is not any propagating mode in the substrate below the radiator. In this area the effective permeability tensor μ_{eff} of the ferrite is negative, so the corresponding wavenumber becomes imaginary leading to an evanescent mode. By including ferrite losses in our analysis and with the proper mathematical handling of the involved Bessel functions, the solution of the characteristic equation in the negative μ_{eff} area became possible revealing a novel single propagating mode. There is only one similar work published in the literature reporting on this mode as propagating in a grounded ferrite substrate [4]. Baccarelli et al. [4] have considered a lossy ferrite substrate biased with an H_{DC} parallel to the ground plane. Assuming propagation along the substrate, but in a direction transverse to the H_{DC}, they indeed found a single mode denoted as TE_{1+} in the region of negative μ_{eff}.

In the present work, the excitation of the mode in the negative μ_{eff} area is studied in a number of additional geometries. In all cases the DC magnetic field is considered perpendicular to the substrate plane. Moreover, the ferrite is considered saturated. The first geometry studied is the rectangular patch antenna printed on a ferrite substrate. The geometry of the rectangular patch antenna tuned by a ferrite post is analyzed next. The ferrite post shape is considered either cylindrical or rectangular and numerical results are presented for both cases. Results for all the above cases show that the investigated mode is excited even when small ferrite losses are considered. Besides the resonant frequency, a study of the input impedance versus feeding position is presented. This matter is of critical importance especially in the case of ferrite post tuned antennas where the coaxial probe is adopted. Ferrites are hard to drill, so it is very convenient if the feeding position lies in the dielectric part of the substrate. Finally, results for the electric and magnetic field under the patch are presented.

REFERENCES

1. Mavridis, A. A., G. A. Kyriacou, and J. N. Sahalos, "Resonant frequencies of circular and ring patch antennas printed on partially magnetized ferrite substrates", *PIERS 2004*, Pisa, Italy, March 28–31, 2004.
2. Mavridis, A. A., G. A. Kyriacou, and J. N. Sahalos, "On the design of patch antennas tuned by transversely magnetized lossy ferrite including a novel resonating mode", *Progress In Electromagnetics Research*, PIER 62, 165–192, 2006.
3. Pozar, D. M., "Radiation and scattering characteristics of microstrip antennas on normally biased ferrite substrates," *IEEE Trans. AP*, Vol. 40, No. 9, September 1992.
4. Baccarelli, P., C. Di' Nallo, F. Frezza, A. Galli, and P. Lampariello, "Anomalous propagation, loss and radiation effects in open waveguides with gyrotropic media," *IEEE MTT-S Digest*, Vol. 1, 283–286, 17–21 June, 1996.

Design and Implementation of Ultra Wideband Antenna for Improved Radiation

Sangbong Jeon, **Jaehyun Oh**, **and Chang-Hoi Ahn**

Yeungnam University, Korea

Abstract— Antennas used for the detection of buried object require very wideband characteristics especially when using input pulse. The standing wave by multiple reflections between the feed and the open ends of an antenna makes distortions of input pulse called "late-time ringing". The most widely used way to reduce the reflections is to attenuate the outward traveling current towards the ends of the structure by loading the antenna with tapered profile from the feed point to the ends of the antenna. For that resistive loading techniques are adopted, such as the well-known Wu-King profile [1]. However the disadvantage of resistive loading is that it also reduces the radiation efficiency.

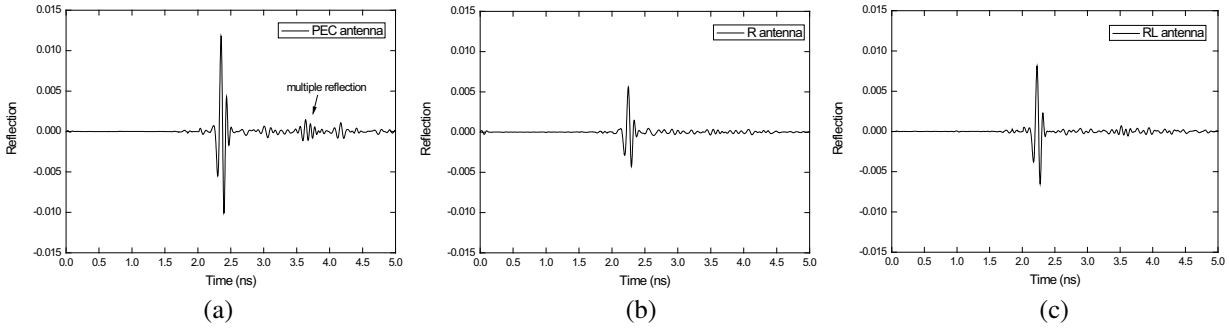

Figure 1: The reflection signal from target (a) PEC antenna, (b) R antenna (resistive loading only), (c) RL antenna (resistive and inductive loading).

In this paper we propose a resistive and inductive loading technique on the slotted arms of the antenna. The slotted arms have an inductance loading effect for high radiation efficiency of a double-sided feed line antenna. To analyze the performance in time domain, we measured reflected signal from a large PEC plane which is placed 10 cm in front of antennas by using a network analyzer (0.5 GHz–10.5 GHz). The PEC (Cupper printed) antenna has biggest reflection but it has multiple reflections at 3.5 ns in Fig. 1(a). The R (Graphite printed) antenna has smallest peak reflection, which means bad radiation efficiency. The reflection in the RL (Graphite printed with slot) antenna is higher than the R antenna but maintaining the ripples in similar level with the R antenna. The proposed antenna is implemented and shows good performance in reducing the late-time ringing and more efficient radiation.

REFERENCES

1. Wu, T. T. and R. W. P. King, "The cylindrical antenna with nonreflecting resistive loading," *IEEE Trans. Antennas Propag.*, Vol. AP-13, 369–373, 1965.

Design of a Small Aperture Coupled Patch Antenna on UC-PBG Structure

Abdelnasser A. Eldek
Department of Computer Engineering, Jackson State University
JSU Box 17098, Jackson, MS 39217-0198, USA

Abstract— The Electromagnetic band gap (EBG), often called Photonic Band Gap (PBG), are periodic structures in which optical waves are forbidden in certain frequency bands. Due to the superior performance of PBG assisted microwave devices, research on different PBG structures is accelerating exponentially. Researchers have investigated different kinds of PBG structures that may include via hole connections. However, the recently developed uniplanar compact photonic bandgaps (UC-PBG) are very useful for different applications. The passband characteristic of the UC-PBG is used as a slow-wave medium, which reduces the size of electronic circuits. The deep stopband is applied to suppress spurious transmission and leakage in guiding structures such as conductor backed coplanar waveguides (CB-CPW) and striplines. The use of PBG structures in antenna design provides better performance, which includes gain increasing, radiation efficiency improvement and size reduction.

This paper presents a small aperture coupled patch antenna design using Uniplanar Compact Photonic Band Gab (UC-PBG) structure. The geometry of the antenna is shown in Fig. 1, and the dimensions in mm are given in Table 1. The UC-PBG is utilized to decrease the operating frequency of the antenna, which implicitly means decreasing the size of the antenna. Numerical study of the parameters of the UC-PBG structure is performed and presented to understand the effect of each parameter on the return loss of the antenna, and also to improve the size reduction factor. The return loss and radiation patterns are computed and compared for the antennas with and without UC-PBG structure. An omni-directional pattern is obtained at lower operating frequency when using the UC-PBG. This study shows that a 45% size reduction is feasible by tuning the parameters of the UC-PBG.

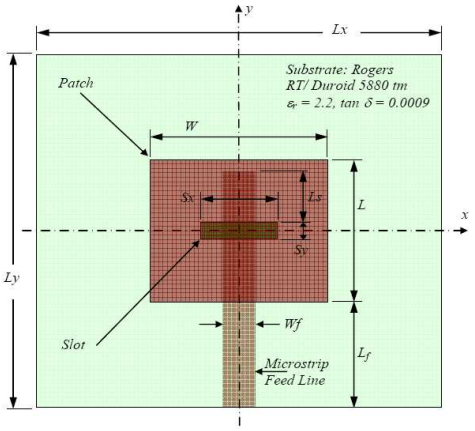

Figure 1: Antenna geometry.

The analysis and study in this paper is based on numerical simulations of the commercial computer software package, Ansoft HFSS. This work is supported by the High Performance Computational Design of Novel Materials (HPCDNM) Project funded by the U.S. Department of Defense through the U.S. Army Engineer Research and Development Center (Vicksburg, MS); Contract #W912HZ-06-C-0057.

Table 1: Antenna dimensions in mm.

W	13.2	L	10.1
Lf	$(Ly - L)/2$	Wf	1.556
s	0.3	ys	$L/4$

Ultra Wideband Microstrip-Fed Planar Tap Monopole Antenna

Abdelnasser A. Eldek
Department of Computer Engineering, Jackson State University
JSU Box 17098, Jackson, MS 39217-0198, USA

Abstract— In the last few years, planar tap monopole antennas have been adopted and studied extensively for UWB communications systems because of their many appealing features. These features include wide impedance bandwidth, simple structure, small size, low profile, and omni-directional radiation patterns. Number of wideband tap monopole configurations, such as rectangular, elliptical, pentagonal, and hexagonal has been proposed for UWB applications. Recently, ultra wideband planar tap monopole antennas were reported in the literature, with a bandwidth of (1:1.7), (1:2.25), (1:3.4), (1:3.5), (1:3.7), (1:3.7), and (1:7.9) for VSWR < 2, and an antenna size of 20, 23, 16, 26, 30 and 16 mm, respectively. In this paper, we present a modified printed tap monopole antenna for UWB applications. The presented antenna exhibits an ultra wide impedance bandwidth of (1:10), with a low VSWR level of less than 1.75, and a small size of 16 mm, which is less than or equal to the previously reported antennas. The VSWR, input impedance, radiation patterns and gain for the proposed antenna will be presented. The results in this paper are obtained from Ansoft HFSS simulations, which are based on the Finite Element Method (FEM). Verification of the final results is performed using a FDTD based code designed by the author.

The geometry and parameters of the proposed broadband tap monopole antenna are depicted in Fig. 1. The basic antenna structure consists of a rectangular patch with a narrow slit, a tapered transition, a feedline, and a truncated ground plane with a two-step staircase notch. The rectangular patch has a width P_1 and a height P_2. A narrow slit of width S_1 and depth S_2 is cut on the patch's right side and placed at a distance S3 away from the lower right corner of the patch. The slit is placed to create additional path for the surface current, which produces an additional resonance, and as a result, increases the bandwidth when the dimensions are properly chosen. Additionally, because this slot is very narrow it does not disturb the existing resonances of the tap monopole. The patch is connected to a feed line of width W_f and length L_f through a tapered transition, which is defined by the parameters T_1 to T_6, as shown in Fig. 1. The tapering produces a smooth transition, which reduces the reflections resulting from the sudden change from the feedline width to the patch width. On the other side of the substrate, a conducting ground plane of width $= W_s$ and length $= L_G$ is placed. The truncated ground plane is playing an important role in the broadband characteristics of this antenna, because it helps matching the patch with the feedline in a wide range of frequencies. This is because the truncation creates a capacitive load that neutralizes the inductive nature of the patch to produce nearly-pure resistive input impedance. To further enhance the matching, a two-step staircase notch is embedded in the truncated ground plane. The notch is defined by the parameters N_1 to N_4 as depicted in Fig. 1. In addition, two triangles of height $= N_5$ are added at the notch sides. The two-step staircase notch and the two triangles are used to control the impedance bandwidth and return loss level by modifying the capacitance between the patch and the ground plane.

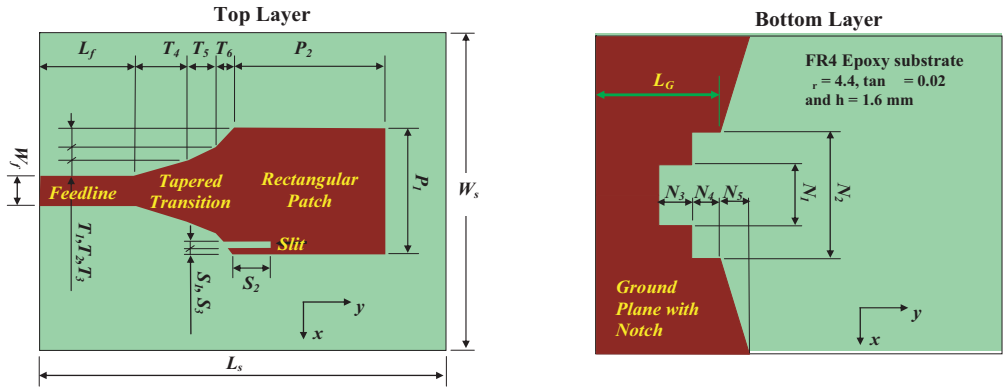

Figure 1: Antenna geometry and parameters.

Neural Network — Based Design of EBG Surfaces for Effective Polarization Diversity of Wireless Communications Antenna Systems

T. Ganatsos, K. Siakavara, and J. N. Sahalos

The Radiocommunications Lab, Department of Physics, School of Sciences
Aristotle University of Thessaloniki, Thessaloniki 54124, Greece

Abstract— The signal fading in the mobile radio environment causes severe reception problems. Various techniques as, space, polarization, frequency or time and field component diversity are employed to reduce this effect. The most commonly used ones are the space and polarization diversity, due to their benefits. All the aforementioned techniques must not be applied at the cost of a complex or bulky radiating system. From this side of view the polarization diversity offers great advantages, especially to mobile stations antennas. Simple and low profile antennas using Electromagnetic Band Gap (EBG) printed structures have been proposed for polarization diversity antenna systems. A properly designed EGB surface could reflect a x-polarized wave with $+90^\circ$ shift phase while a y-polarized wave with a -90° one. Due to this behaviour, even a single linear dipole antenna, positioned very close to this polarization dependent EBG (PDEBG) surface can effectively receive or transmit circularly polarized waves. The main problem of the entire mechanism is that the $\pm 90^\circ$ phase shifting does not generally occur at the same frequency.

In the present work a Neural Network (NN) procedure for the design of EBG structures with pre-specified attributes is presented. The procedure focuses to the determination, via the NN-based algorithm, of the appropriate structural parameter values of the EBG lattice, in order to reduce the difference between the frequencies $f^x_{90^\circ}$ and $f^y_{-90^\circ}$ at which the $\pm 90^\circ$ reflection phase for x- and y-polarized waves is observed.

A Multiple Layer Perceptron (MLP)-NN was composed. It was trained via the backpropagation algorithm and four cases, with respect to the Mean-Square Error (MSE) function of the output layer were studied. The procedure permits the calculation of the exact size of the printed elements if their spacing and the frequency of operation are given or the size and spacing of the printed elements if only the frequency is given.

An additional algorithm was composed, by which all the sets of the elements' dimensions L, W, and the inter-element distances g_x and g_y can be calculated for a desired value of the ratio $\left(f^x_{90^\circ} - f^y_{-90^\circ}\right)/\bar{f}$ (where $\bar{f}$ is the mean value of the frequencies $f^x_{90^\circ}$ and $f^y_{-90^\circ}$). This potential is useful in the design of the system. To ensure the validity of the procedure various PDEBG surfaces were structured via the results yielded by the network in the UMTS range and they were simulated via the HFSS software. The property of the PDEBG to give $f^x_{90^\circ} \simeq f^y_{-90^\circ}$ was checked in the entire range of UMTS. Furthermore results for a linear dipole positioned in various directions in front of the PDEBG were received. The reflection coefficient of the signal at the feeding input of the dipole and the polarization properties of the radiated field will be presented.

A Surfaguide Fed Plasma Antenna

G. Cerri, **R. De Leo**, **V. Mariani**, **and P. Russo**

Dipartimento di Elettromagnetismo e Bioingegneria, Università Politecnica delle Marche Ancona
via Brecce Bianche, I 60100 Ancona, Italy

Abstract— The plasma antenna considered in this paper is a standard glass fluorescent tube; the gas inside the dielectric cylinder is ionized by application of a strong electric field at microwave frequency at one termination of the tube.

The main task of this section is the description of the characteristics for a surfaguide device; this structure is able to excite a surface wave that propagated along the tube axis and provides the power required to ignite the plasma.

This is not the only way that can be used to energize the plasma, but it was chosen because of some advantages that can be favourably considered in designing plasma antennas.

The first advantage is related to the exciting frequency adopted as pump signal, $fp = 2450\,\mathrm{MHz}$. This frequency does not interfere with telecommunication systems, and at this frequency high power is available at low cost. Therefore the surfaguide is the most suitable device to propagate a power signal at this frequency, confining its electromagnetic field in a closed structure. Moreover the surfaguide is simple to realize, and matching stubs can be easily inserted in the design.

The surfaguide consists of two trunks of a standard waveguide WR340, two transitions , and a waveguide with a reduced height to increase the electric field strength. The guide is terminated by a moving short, whose length can be varied for matching.

Along the central axis of the reduced height guide two holes allow to insert the glass tube.

A commercial software was used to optimize the structure for plasma ignition, in the sense that all geometrical parameters were determined for the maximum field strength along the axis of the glass tube.

The experimental results are very satisfactory and will be presented at the Conference.

Multiple Signal Direction of Arrival (DoA) Estimation for a Switched-Beam System Using Neural Networks

K. A. Gotsis, E. G. Vaitsopoulos, K. Siakavara, and J. N. Sahalos

Radiocommunications Lab, Department of Physics, School of Sciences
Aristotle University of Thessaloniki, Thessaloniki 54124, Greece

Abstract— Direction of Arrival (DoA) estimation for signals impinging on an antenna array is a very important issue for wireless communications. In this paper, a new multiple signal DoA estimation method based on the neuro-computational methodologies is presented. Previous published works introduce the application of Neural Network (NN) techniques on the DoA estimation for adaptive array systems. In the present work the NN-DoA procedure was created for a switched-beam system. The radiating part of the system is a linear array of eight, $\lambda/2$ spaced, microstrip patches structured on a single layer dielectric substrate. The array is fed by a 8×8 Butler Matrix (BM) and the entire system operates at 2.4 GHz. The input ports of the BM are connected to a switching network that performs beam switching using SPDT (Single Pole Double Throw) switches.

The proposed technique is based on the application of strict power control at the mobile stations and on the a priori knowledge of the number of simultaneously incoming signals. Due to power control, all signals arrive at the base station receiver at the same power level. Therefore, the contribution of each signal to the total power measured at the output of the structure depends only on its angle of incidence. Consider a random set of N signals arriving from angles φ_i, $i = 1 \dots N$. These values would compose an angle vector $\boldsymbol{\varphi}_\mathbf{m} = (\varphi_1, \varphi_2, \dots, \varphi_N)$. If beam switching takes place, each one of the eight beams gives a total output power $\boldsymbol{\varphi}_{mn}$, $n = 1 \dots 8$ and these values construct a power vector $\mathbf{P_m} = (P_{m1}, P_{m2}, \dots, P_{m8})$. In this way a mapping between the vectors $\boldsymbol{\varphi}_\mathbf{m}$ and $\mathbf{P_m}$ is established. The target is to perform the reverse procedure, namely accomplish DoA estimation based on the output power. This target was obtained via a neuro-computational methodology. A Multilayer Perceptron (MLP) NN was composed by a) an input layer of eight nodes which is fed by the vector $\mathbf{P_m}$, b) an output layer of N nodes that gives the corresponding vector $\boldsymbol{\varphi}_\mathbf{m}$, from which the vector $\mathbf{P_m}$ came and c) one or two hidden layers. The number of hidden layers and the number of each layer's nodes depends on the number of the simultaneously impinging signals. The criterion of their choice is the better NN training convergence and the results' accuracy. The NN is trained via a collection of randomly created pairs ($\boldsymbol{\varphi}_\mathbf{m}$, $\mathbf{P_m}$), the number of which depends on the number of signals. Simulated results of DoA tests are extensively presented and show very accurate DoA estimation even for a big set of incoming signals. The simulations and the NN trainings are performed in MATLAB.

The synthesis, the requirements and the accuracy of the proposed method lend to the system some interesting advantages: a) The most widespread super resolution algorithms (MUSIC, ESPRIT, Matrix Pencil etc.) or other techniques using NN, need measurements at every antenna element and intensive signal processing in order to compute the signal autocorrelation matrix. In the described method only power measurements at a single output of the system is needed, saving cost, complexity and time. b) Due to the simplicity of the algorithm and the speed of NN, the described technique is proper for real time applications. c) It can be easily integrated into existing base stations, and finally d) contrary to the majority of DoA estimation techniques, it is very effective even for a number of signals greater than the number of the antenna elements.

Design of Dual-band Reconfigurable Smart Antenna

Hamid Torpi and Yasin Damgacı
Yıldız Technical University, Department of Electronics and Communication Engineering, Turkey

Abstract— This paper presents use of reconfigurable microstrip patch antenna elements in adaptive arrays. An adaptive antenna that can direct its main lobe to the desired signal and null the interference signal. Adaptive antenna systems are referred to smart antennas.

A dual-band antenna operates at two seperate frequency bands with the same radiation characteristics within these bands. In reconfigurable antennas, the switching between the frequency bands is achieved by changing the shape of the radiating element. The combination of both reconfigurability and adaptivity in a single array is investigated in this study.

Frequency bands are chosen as 2.4 GHz and 3.5 GHz which are used in WLAN and WiMAX applications. The single element is designed as inset-fed microstrip patch antenna using transmission line model. Firstly, design parameters calculated for 3.5 GHz and simulated. Secondly, U-like shaped patch is attached to 3.5 GHz antenna for 2.4 GHz and this new antenna is simulated. The switching between these patches is achieved by using metal strips corresponding to the ON state of ideal switch for dual-band operation. Lastly, reconfigurable antenna will be achieved by replacing metal strips to the RF-MEMS switches. For this task, RF-MEMS capacitive series switch is modeled and simulated.

On the second phase of this work the designed reconfigurable antenna is used as a single element in smart antenna. Smart antennas uses adaptive signal processing algorithms. In adaptive beamforming, the goal is to adapt the beam by adjusting the gain and phase on each antenna element such that a desirable pattern is formed. LMS algorithm is used for this purpose. Calculated gains and phases are used as excitation for reconfigurable antennas for each frequency. Simulations are performed using Ansoft Designer. Different array configuration simulation results will be presented.

A New MIMO Spatial Correlation Approximation of Large Angular Spread

Po-Chuan Hsieh and Fu-Chiarng Chen
Department of Communication Engineering, National Chiao Tung University
1001 Tahsueh Road, Hsinchu 300, Taiwan

Abstract— MIMO systems offer an effective solution scheme to achieve the goal of maximal spectral efficiency and the essential increase in channel capacity that can be reached with several antennas at both transmitter and receiver ends. Incorporating MIMO technology into small wireless devices means multiple antennas are set into the limited spacing of small portable devices. Therefore, antenna spatial correlation, which takes antenna spacing, angle-of-arrival (AoA) distributions and antenna mutual coupling into account, is the design criterion of whether the physical antenna design can result in the performance of low signal correlation.

We propose a new approximate AoA distribution formula to express the antenna spatial correlation under the condition of large AoA angular spread. Consider two antenna elements are separated from a distance apart, and the antenna spatial correlation can be determined as in [1]. Uniform AoA distribution is the most common AoA distribution of scattering rich environments when we analyze the parameter of any undetermined channel model. For the uniform distribution, all the possible AoAs share the same possibilities of incidence. If the range of the uniform distribution is equal to 2π, the spatial correlation has a closed-form solution which is well-known as the Bessel function [2]; however, for the case where the AoA range is smaller than 2π, the spatial correlation does not have any closed form formula, and thus the time-consuming numerical integration is needed when substituting the AoA distribution into correlation formulation. Therefore, we propose a new approximate AoA distribution for the uniform distribution of any AoA range without numerical integration. This approximate AoA distribution uses the combination of many Gaussian AoA distributions, thought of as the best description of small angular spread AoA distribution, to fit a given large angular spread uniform distribution. The computational speed of the approximate type will outperform that of the time-consuming numerical integration by 17 times, and only negligible deviation is caused at larger antenna element spacing. Furthermore, since the AoAs vary with different geographic scenarios, this approximation strategy can help extend its application to approximate any large-angular-spread AoA distribution, as long as we properly give different weighting probabilities at specific AoA incidence.

We also investigate how mutual coupling affects the spatial correlation of uniform AoA distribution with the approximate form we suggest earlier. 1 GHz dipole pair case is discussed for simplicity using high frequency electromagnetic software Zeland IE3D®. The envelope spatial correlation (power correlation) with mutual coupling can be represented as in [3]. Incorporating the approximate correlation without mutual coupling into envelope spatial correlation suggested in [3], we may further analyze which factors bring impact on antenna spatial correlation from a mathematical perspective.

The new approximation correlation formulation which takes mutual coupling effect into consideration can speed up the judgement of channel conditions of two MIMO antennas, and therefore is beneficial for judging the performance of the MIMO antenna design before physical realization.

REFERENCES

1. Buehrer, R. M., "The impact of angular energy distribution on spatial correlation," *IEEE Vehicular Technology Conference*, Vol. 2, 24–28, 2002.
2. Vaughan, R. G. and J. B. Anderson, "Antenna diversity in mobile communications," *IEEE Transactions on Vehicular Technology*, Vol. VT-36, No. 4, 1987.
3. Li, X. and Z. Nie, "Effect of mutual coupling on performance of MIMO wireless channels," *ICMMT 4th International Conference*, 18–21, 2004.

Session 3P3
Extended/Unconventionl Electromagnetic Theory, EHD (Elecrohydrodynamics)/EMHD (Electromagnetohydrodynamics), and Electrobiology

Inversion Reconstruction of Signals Measured by the NMR Techniques

Pavel Fiala[1], **Eva Kroutilova**[1], **Miloslav Steinbauer**[1], **Michal Hadinec**[1], **and Karel Bartušek**[2]

[1]Brno University of Technology, Czech Republic
[2]Academy of science of the Czech Republic, Czech Republic

Abstract— This article deals with the reverse reconstruction results obtained from the numerical simulation of MR signals by various techniques, which will be usable for the experimental results verification. We solved the effect of changes of magnetic fields in MR tomography. The paper will describe the magnetic resonance imaging method applicable mainly in MRI and MRS in vivo studies.

Geometrical model: Fig. 1 describes the sample geometry for the numerical modelling. On both sides, the sample is surrounded by the referential medium. During the real experiment, the reference is represented by water, which is ideal for obtaining the MR signal. As shown in Fig. 1, in the model there are defined four volumes with different susceptibilities. The materials are defined by their permeabilites: material No. 1 — the medium outside the cube (air), $\chi = 0$, material No. 2 — the cube walls (sodium glass), $\chi = -11,67 \cdot 10^{-6}$, material No. 3 is the sample material (sodium glass), $\chi = -11,67 \cdot 10^{-6}$, quartz glass, $\chi = -8,79 \cdot 10^{-6}$, the simax glass (commercial name), $\chi = -8,82 \cdot 10^{-6}$, material No. 4 is the medium inside the cube (water with nickel sulfate solution $NiSO_4$, $\chi = -12,44 \cdot 10^{-6}$). The permeability rate was set with the help of the relation $\mu = 1 + \chi$. For the sample geometry according to Fig. 1, the geometrical model was built in the system. In the model there was applied the discretization mesh with 133584 nodes and 126450 elements, type Solid96 (Ansys). The boundary conditions (1.2) were selected for the induction value of the static elementary field to be $B_0 = 4,7000\,\mathrm{T}$ in the direction of the z coordinate (the cube axis) — corresponds with the real experiment carried out using the MR tomograph at the Institute of Scientific Instruments, ASCR Brno.

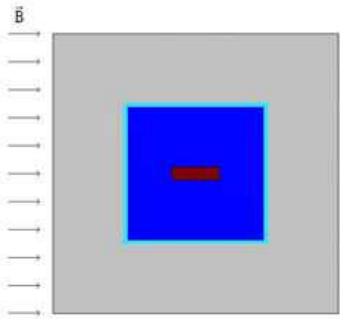

Figure 1: The geometrical model in the system.

Experimental verification: The experimental measuring was realized using the MR tomograph at the Institute of Scientific Instruments, ASCR Brno. The tomograph elementary field $B_0 = 4,7000\,\mathrm{T}$ is generated by the superconductive solenoidal horizontal magnet produced by the Magnex Scientific company. The corresponding resonance frequency for the 1H cores is 200 MHz.

The comparison of results: Numerical modelling and measuring: The numerical modelling and analysis of the task have verified the experimental results and, owing to the modificability of the numerical model, we have managed to advance further in the experimental qualitative NMR image processing realized at the ISI ASCR.

REFERENCES

1. Fiala, P., E. Kroutilová, and T. Bachorec, Modelování elektromagnetických polí počítačová cvicění vyd. Brno: VUT v Brně FEKT, Úolní 53, 602 00, s. 1–69 , Brno, 2005.
2. Steinbauer, M., Měrěni magnetické susceptibility technikami tomografie magnetické rezonance. vyd. Brno: VUT v Brně FEKT, Úolní 53, 602 00, Brno, 2006.
3. *Ansys User's Manual*, Svanson Analysys System, Inc., Huston, USA, 1994–2006.

The Effect of Non-homogeneous Parts into Materials

Pavel Fiala[1], **Eva Kroutilova**[1], **Miloslav Steinbauer**[1], **Michal Hadinec**[1], **and Karel Bartusek**[2]

[1]Brno University of Technology, Czech Republic
[2]Academy of Sciences of the Czech Republic, Czech Republic

Abstract— This article deals with the verification of experimental results obtained by numerical simulation. We solved the effect of changes in the homogeneity of magnetic fields evoked by different samples from conductive and/or magnetic materials and the different types of inhomogeneity in the MR tomograph. Moreover, the paper will describe the suitable magnetic resonance techniques.

Numerical Model: The numerical modelling was realized using the finite element method together with the Ansys system. As the boundary condition, there was set the scalar magnetic potential φm by solving Laplace's equation

$$\Delta\varphi_m = \mathrm{div}\mu\,(-\mathrm{grad}\varphi_\mathrm{m}) = 0 \tag{1}$$

together with the Dirichlet boundary condition

$$\varphi_m = konest. \quad \text{na oblastech } \Gamma 1 \text{ a } \Gamma 2 \tag{2}$$

and the Neumann boundary condition

$$\mathbf{u}_n \cdot \mathrm{grad}\varphi_m = 0 \quad \text{na oblastech } \Gamma 3 \text{ a } \Gamma 4. \tag{3}$$

The continuity of tangential elements of the magnetic field intensity on the interface of the sample region is formulated by the expression

$$\mathbf{u}_n \times \mathrm{grad}\varphi_m = 0 \tag{4}$$

The description of the quasi-stationary model MKP is based on the reduced Maxwell's equations

$$\mathrm{rot}\mathbf{H} = \mathbf{J} \tag{5}$$

$$\mathrm{div}\mathbf{B} = 0 \tag{6}$$

where $\mathbf{H}$ is the magnetic field intensity vector, $\mathbf{B}$ is the magnetic field induction vector, $\mathbf{J}$ is the current density vector. For the case of the static magnetic irrotational field, the Equation (5) is reduced to the Expression (7).

$$\mathrm{rot}\mathbf{H} = 0 \tag{7}$$

Material relations are represented by the equation

$$\mathbf{B} = \mu_0\mu_r\mathbf{H} \tag{8}$$

where μ_0 is the permeability of vacuum, $\mu_r(B)$ is the relative permeability of ferromagnetic material. The closed area Ω, which will be applied for solving the Equations (6) and (7), is divided into the region of the sample Ω_1 and the region of the medium Ω_2. For these, there holds $\Omega = \Omega_1 \cup \Omega_2$. For the magnetic field intensity H in area there holds the relation (7). The magnetic field distribution from the winding is expressed with the help of the Biot-Savart law, which is formulated as

$$\mathbf{T} = \frac{1}{4\pi}\int_\Omega \frac{\mathbf{J}\times\mathbf{R}}{|\mathbf{R}|^3}d\Omega \tag{9}$$

where $\mathbf{R}$ is the distance between a point in which the magnetic field intensity $\mathbf{T}$ is looked for and a point where the current density $\mathbf{J}$ is assumed. The magnetic field intensity $\mathbf{H}$ in the area can be expressed as

$$\mathbf{H} = \mathbf{T} - \mathrm{grad}\phi_\mathrm{m} \tag{10}$$

where $\mathbf{T}$ is the preceding or estimated magnetic field intensity, ϕ_m is the magnetic scalar potential. The boundary conditions are written as

$$\mathbf{u}_n \cdot \mu\,(\mathrm{T} - \mathrm{grad}\phi_\mathrm{m}) = 0 \quad \text{na oblastech } \Gamma 3 \text{ a } \Gamma 4. \tag{11}$$

where un is the normal vector, ΓFe-0 is the interface between the areas ΩFe and $\Omega 0 \cup \Omega W$. The area Ω0 is the region of air in the model, the area ΩW is the region with the winding. The continuity of tangential elements of the magnetic field intensity on the interface of the area with ferromagnetic material is expressed

$$\mathbf{u}_n \times (\mathrm{T} - \mathrm{grad}\phi_\mathrm{m}) = 0 \tag{12}$$

By applying the relation (10) in the relation (11) we get the expression

$$\mathrm{div}\mu_0\mu_r\mathbf{T} - \mathrm{div}\mu_0\mu_r\mathrm{grad}\phi_m = 0 \tag{13}$$

The equation can be discretized by means of approximating the scalar magnetic potential

$$\varphi_m = \sum_{j=1}^{NN} \varphi_j W_j(x,y,z) \quad \text{pro} \quad \forall(x,y,z) \subset \Omega \tag{14}$$

where φ_j is the value of the scalar magnetic potential in the j-th node, Wj the approximation function, NN the number of nodes of the discretization mesh. By applying the approximation (14) in the relation (13) and minimizing the residues according to the Galerkin method, we get the semidiscrete solution

$$\sum_{j=1}^{NN} \varphi_j \int_\Omega \mu \mathrm{grad}W_i \cdot \mathrm{grad}W_j d\Omega = 0, \quad i = 1, \ldots NN \tag{15}$$

The system of equations can be written briefly as

$$[k_{ij}] \cdot [\varphi_i]^T = 0, \quad i,j \in \{1, \ldots NN\} \tag{16}$$

The system can be divided into

$$\mathbf{K} \begin{bmatrix} \mathbf{U}_I \\ \mathbf{U}_D \end{bmatrix} = \begin{bmatrix} 0 \\ 0 \end{bmatrix} \tag{17}$$

where $\mathbf{U}_I = [\varphi_1, \ldots \varphi_{N1}]^T$ is the vector of unknown internal nodes of the area including the points on the areas Γ3 and Γ4. $\mathbf{U}_D = [\varphi_1, \ldots \varphi_{ND}]^T$ is the vector of known potentials on the areas Γ1 and Γ2 (the Dirichlet boundary conditions). NI in the index marks the number of internal nodes of the discretization mesh, ND is the number of the mesh boundary nodes. Then, the system can be written further in 4 submatrixes

$$\begin{bmatrix} \mathbf{k}_{11} & \mathbf{k}_{12} \\ \mathbf{k}_{21} & \mathbf{k}_{22} \end{bmatrix} \begin{bmatrix} \mathbf{U}_I \\ \mathbf{U}_D \end{bmatrix} = \begin{bmatrix} 0 \\ 0 \end{bmatrix} \tag{18}$$

and this yields the system with the introduced boundary conditions, which is solved in the MKP as

$$\mathbf{k}_{11}\mathbf{U}_I + \mathbf{k}_{12}\mathbf{U}_D = 0. \tag{19}$$

The coefficients k_{ij} of the submatrix $\mathbf{k}$ are non-zero only when the element of mesh contains both the i and the j nodes. The contribution of the element e to the coefficient k_{ij} is

$$k_{ij}^e = \int_{\Omega^e} \mu^e \mathrm{grad}W_i^e \cdot \mathrm{grad}W_j^e d\Omega, \quad e = 1, \ldots NE, \tag{20}$$

where Ωe is the area of the discretization mesh element, μ^e is the permeability of the selected element medium, NE is the number of the discretization mesh elements. The matrix $\mathbf{k}$ elements are then the sums of contributions of the individual elements.

$$k_{ij} = \sum_{e=1}^{NE} k_{ij}^e \tag{21}$$

The system of Equations (16) can be solved with the help of standard algorithms. The scalar magnetic potential value is then used for evaluating the magnetic field intensity according to (10).

Geometrical Model: Figure 1 describes the sample geometry for the numerical modelling. On both sides, the sample is surrounded by the referential medium. During the real experiment, the reference is represented by water, which is ideal for obtaining the MR signal. As shown in Fig. 1, in the model there are defined four volumes with different susceptibilities. The materials are defined by their permeabilites : material No. 1 — the medium outside the cube (air), $\chi = 0$, material No. 2 — the inhomogeneous sample, (clay), material No. 3 — the material of inhomogeneities inside the sample. The permeability rate was set with the help of the relation $\mu = 1 + \chi$.

For the sample geometry according to Fig. 1, the geometrical model () was built in the system. In the model there was applied the mesh of elements, type Solid96 (Ansys). The boundary conditions (2) were selected for the induction value of the static elementary field to be $B_0 = 4{,}7000\,\mathrm{T}$ in the direction of the z coordinate (the cube axis) — corresponds with the real experiment carried out using the MR tomograph at the Institute of Scientific Instruments, ASCR Brno.

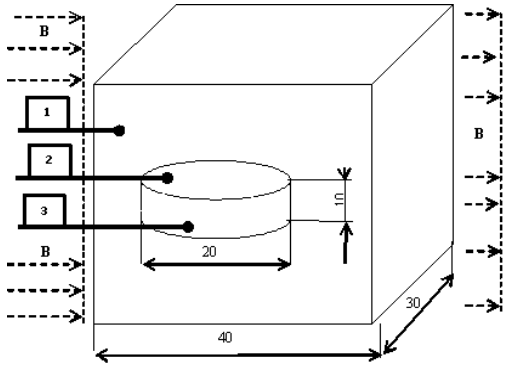

Figure 1: The sample geometry for numerical modeling.

Experimental Verification: The experimental measuring was realized using the MR tomograph at the Institute of Scientific Instruments, ASCR Brno. The tomograph elementary field B_0= 4,7000 T is generated by the superconductive solenoidal horizontal magnet produced by the Magnex Scientific company. The corresponding resonance frequency for the 1H cores is 200 MHz.

The Comparison of Results: Numerical Modelling and Measuring The numerical modelling and analysis of the task have verified the experimental results and, owing to the modificability of the numerical model, we have managed to advance further in the experimental qualitative NMR image processing realized at the ISI ASCR.

REFERENCES

1. *Ansys User's Manual*, Svanson Analysys System, Inc., Huston, USA, 1994–2006.
2. Fiala, P., E. Kroutilová, and T. Bachorec, Modelování elektromagnetických polí počítačová cvicění vyd. Brno: VUT v Brně FEKT, Úolní 53, 602 00, s.1–69, Brno, 2005.
3. Steinbauer, M., Měrěni magnetické susceptibility technikami tomografie magnetické rezonance. vyd. Brno: VUT v Brně FEKT, Úolní 53, 602 00, Brno, 2006.

Magnetic Field Approximation in MR Tomography

Michal Hadinec[1], **Pavel Fiala**[1], **Eva Kroutilová**[1], **Miloslav Steinbauer**[1], **and Karel Bartušek**[2]

[1]Institute of Scientific Instruments of the ASCR, v.v.i
Královopolská 147, 612 64, Brno, Czech Republic
[2]Department of Theoretical and Experimental Electrical Engineering
Faculty of Electrical Engineering and Communication, Brno University of Technology
Kolejní 2906/4, 612 00, Brno, Czech Republic

Abstract— In this paper I would like to describe a measurement method, which can be used for creating map of magnetic field in magnetic resonance tomography. Magnetic resonance tomography is an imaging technique used primary in medical setting to produce high quality images of the human body. Magnetic resonance imagining is based on the principles of nuclear magnetic resonance (NMR) and at the present time it is the most developed imagining technique at biomedical imagining. Lately, medical science lays stress on the measuring of exactly defined parts of human body, especially human brain.

If we want to obtain the best quality images we have to pay attention to homogeneity of magnetic fields, which are used to scan desired samples inside the tomograph, and also how to reduce inhomogeneity, which can cause misleading information at the final images of samples. Generally, inhomogeneity of magnetic fields at magnetic resonance imagining cause contour distortion of images. To eliminate these inhomogeneity correctly, we need to know the map of the magnetic field and we also need to have the exact information about parameters of the magnetic field.

Aproximation: This paper presents the experimental method, which can easily create the map of electromagnetic induction at any defined area inside the tomograph. This method uses mathematical theory of Legendre polynoms

$$\begin{aligned} P_n(z) &= \frac{1\cdot 3\cdot 5\cdot \ldots \cdot (2n-1)}{n!} * \\ &\quad * \left[z^n - \frac{n(n-1)}{2(2n-1)} z^{n-2} + \frac{n(n-1)(n-2)(n-3)}{2\cdot 4(2n-1)(2n-3)} z^{n-4} - \ldots \right] \qquad (1) \\ P_{n+1}(z) &= \left[(2n+1)\cdot z\cdot P_n(z) - n\cdot P_{n-1}(z) \right] / (n-1) \qquad (2) \end{aligned}$$

which are used for approximation of magnetic field, if we know coefficients of Legendre polynoms. The values of magnetic induction are approximated according to this formula

$$B_a(r,\theta,\varphi) = \sum_{k=0}^{N_K} \cdot \sum_{m=0}^{m=k} \cdot r^k \cdot P_{m,k}(\cos\theta) \cdot \left[A_{m,k} \cos m\cdot\varphi + B_{m,k} \sin m\cdot\varphi \right] \qquad (3)$$

The coefficients of Legendre polynoms, which are computed from measured values of magnetic field at exactly defined discrete points are used for computing map of magnetic field at any point

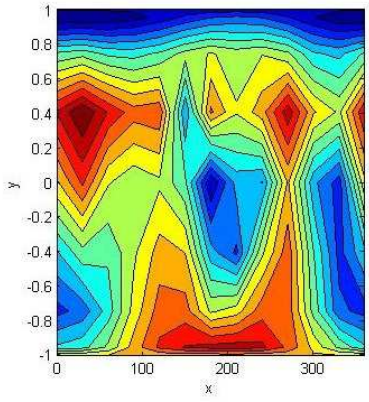

Figure 1: Contour map of the field.

of defined area. To do this, we use for example Least mean square method as follows

$$\Psi = \min \sum_{i=1}^{N_m} (B_{im} - B_{ia})^2 \tag{4}$$

At the ideal case, there should be no difference between measured data and approximated data. This problem is described at the end of this article and there is also an experimental verification of this method.

Experimental Results: As a development system was used Matlab, which provides great potentialities not only for mathematical operations with measured data, but also for modeling and creating magnetic field maps as we can see on the picture, which presents map of the magnetic field on the surface of sphere.

REFERENCES

1. Fiala, P., E. Kroutilová, and T. Bachorec, Modelování elektromagnetických polí počítačová cvicění vyd. Brno: VUT v Brně FEKT, Úolní 53, 602 00, Brno, 2005.
2. Haacke, E. M., R. W. Brown, M. R. Thomson, and R. Venkatesan, *Magnetic Resonance Imaging — Physical Principles and Sequence Design*, John Wiley & Sons, 2001. ISBN 0-471-48921-2.
3. Stratton, J. A., Teorie Elektromagnetického Pole, SNTL, Praha, 1961.

Progress in Gain Performance of Parametrically Amplifying Travelling-wave Antennas (PATA): PATA Analogous to Travelling-wave Tube Amplification and Negative Resistivity of Esaki Diodes

H. Kikuchi[1], **S. Tsuruoka**[2], **and T. Obata**[3]

[1]Institute for Environmental Electromagnetics, 3-8-18, Komagome, Toshima-ku, Tokyo 170, Japan
[2]Takuwa Corporation, 1-4-15, Uchi-Kanda, Chiyoda-ku, Tokyo 101, Japan
[3]Gunma National College of Technology, 580, Toriba-machi, Maebashi 371-0845, Japan

Abstract— Parametrically amplifying travelling-wave antennas (PATA) invented by one of the present authors are somewhat analogous to travelling-wave tubes and Esaki diodes in function and characteristics, though there are essential differences. PATA correspond to amplification of travelling wave tubes and the incident waves along the line play a role of electron beams. There are, however, essential differences between them. The role of electron beams in travelling wave tubes is an amplification only when an external microwave is passing through a helical circuit. In contrast, there are twofold roles of an incident wave in PATA. One is to induce a current wave along the line. The other is to amplify its induced current wave at the same time. Further, there is a difference that the coupling of electron beams to a helical circuit is capacitive for travelling-wave tubes but the coupling of incident waves to the line is inductive for PATA. While PATA is expressed by an equivalent active distributed parameter line whose shunt conductance G is negative in the transition region, the resistance in an equivalent lumped circuit of Esaki diodes is also negative. In this respect, there is some correspondence or analogy between them, though those negative effects are different. The negative shunt conductance of PATA leads to new results that the attenuation constant of the inrent wave decreases with increasing frequency and the wave-mode becomes a fast wave, while the negative resistance of Esaki diodes causes current decrease with voltage increase as a result of quantummeechanical tunnel: effects. Whole setup of PATA is composed of a bare copper (or aluminum) wire (tube) or its array (1 m long with (outer) diameter 2.75 cm) connected with a guide-horn above a certain semiconducting or lossy dielectric (foam polyethylene) base-plate (wire or tube centre is 2.7∼8 cm high) whose bottom side is grounded. When the incident plane-like wave at a certain range of frequencies is coming through the interval between the line and the base-plate, the induced line wave becomes a fast surface wave, causing a strong coupling with the incident sky wave, thus the energy transfer to the induced line wave occurring and amplifying it. According to experiments at a range of 2∼5 GHz, the incident sky wave dominates near the input side but the induced surface wave tends to be dominant, guide-wavelength increasing as long as 2∼4 λ (λ: wavelength in free space) and thus increasing the amplification ratio as high as 0.26∼0.4 dB/cm as approaching the output end.

Debye Shielding in Chasmas

D. K. Callebaut[1] **and H. Kikuchi**[2]

[1]University of Antwerp, Belgium
[2]Institute for Environmental Electromagnetics, Japan

Abstract— Chasmas are a generalization of plasmas, i.e., the condition of quasi-neutrality is dropped. That means that in chasmas the quasi-neutrality may be (strongly) violated over distances many times the Debye length which requires special circumstances (double layers, electric fields, ...). The question arises what the meaning is of a shielding length in chasmas. It was demonstrated that the so-called chasma (angular) frequency has an expression similar to the plasma frequency:

$$\omega_c^2 = \frac{|n_- - n_+|e^2}{\varepsilon m_-},$$

with an obvious notation. However, this chasma frequency plays a role as well in the equilibrium (or steady state) as in the stability. For the 'Debye length in chasmas' we obtained

$$\lambda_c^2 = \frac{\varepsilon k_B T}{(n_+ + n_-)e^2},$$

supposing the temperature of electrons and ions is the same and for ions that are only once ionized. This means that the chasma shielding length is much the same as the Debye length and that $\lambda_c\omega_p \sim \lambda_D\omega_p \sim k_B T$ while $\lambda_c\omega_c$ make a rather different combination involving the degree of non-quasi-neutrality

$$\frac{n_- - n_+}{n_- + n_+},$$

and the thermal energy per particle. Moreover, several subtleties occur.

REFERENCES

1. Callebaut, D. K., G. K. Karugila, and A. H. Khater, "Chasma perturbations," *Proc. PIERS 2005*, 720–723, Hangzhou, China, August 22–26, 2005.
2. Callebaut, D. K. and A. H. Khater, "Chasma including magnetic effects," *Proc. PIERS 2006*, 404–411, Cambridge, USA, March 26–29, 2006.

Optimization of EMI Power Filters

J. Sedláček, Z.Szabó, and M. Hadinec

Department of Theoretical and Experimental Electrical Engineering
Faculty of Electrotechnical Engineering and Communication, Brno University of Technology
Kolejni 2906/4, Brno 612 00, Czech Republic

Abstract— Electromagnetic interference (EMI) can be reduced to acceptable level using EMI filter circuits. Unfortunately, many known methods of filter design and optimization cannot be applied directly to power electronics, which has it own peculiarities. In comparison to EMI data communication filters EMI power filters operate typically under mismatched impedance conditions. One from important manner of a filter design and optimization process there is a filter modeling. The paper deals with methods of filter design and optimization which are useful in area of EMI power filter synthesis. Different types of EMI power filters and using of their equivalent models here are discussed. Synthesis and optimization methodology for different kinds of EMI power filters with required insertion loss in wide frequency range are discussed in some practical examples.

Material Influence on Field Homogeneity in MR Tomograph

K. Bartušek[1,2], **M. Steinbauer**[2], **P. Fiala**[2], **and M. Hadinec**[2]

[1]Institute of Scientific Instruments of the ASCR, v.v.i
Královopolská 147, Brno 612 64, Czech Republic
[2]Department of Theoretical and Experimental Electrical Engineering
Faculty of Electrical Engineering and Communication
Brno University of Technology, Kolejní 2906/4, Brno 612 00, Czech Republic

Abstract— Materials with different electrical conductivity and/or magnetic susceptibility can cause deformation of magnetic field in MR tomograph, resulting in errors in obtained image. Using simulation and experimental verification we can solve the effect of changes in homogeneity of static and HF magnetic fields caused by specimen made from conductive and/or magnetic material in MR tomograph.

Paper describes theoretical base and experimental measurement of the magnetic resonance imaging method for susceptibility measurement. The method uses deformation of magnetic induction field in specimen vicinity. For MR purposes it is necessary to immerse specimen into reference medium with measurable MR signal. Measured data obtained by means of the method using MRI will be shown. Shape of magnetic field changed by specimen impact (reaction field) we measure by means of Gradient Echo (GE) measuring method.

Numerical simulation of both (magnetic and electric conductivity) of material is presented.

ACKNOWLEDGMENT

This work is supported by GAAV ČR GAAV B208130603.

Design, Simulation and Realization the Specfic Source of Light

Eva Kroutilova, **Miloslav Steinbauer**, **and Zoltán Szabó**
Department of Theoretical and Experimental Electrical Engineering
Faculty of Electrical Engineering and Communication, Brno University of Technology
Kolejni 2906/4, Brno 612 00, Czech Republic

Abstract— This paper presents information about design of special light sources, which is intended for photosynthesis process research. Required properties were continuous spectral characteristic with respect to photosynthetically active wavelength area, possibility of luminous flux regulation and practically zero thermal effect to illuminated object. Owing to new high-performance LED this type of light source was selected. Design of light source consisting of high efficient white LED's, as well as experimental results, are presented.

The Light Source for Biological Application: On luminous characteristics sources were laying following requirements

- the continuity into the whole visible area
- the shape of the spectrum charakteristic should be very similar as the daylight
- the source should the light into the IR area as least as it is possible
- the specific size of the lighting surface
- very high and homogenous intensity of the light on the complete surface

Verification the Homogenity by the MATLAB Simulation: MATLAB simulation was designed for first verification of the lighting systems design. The main advantages of the MATLAB simulation are the simplicity of the submission for the initial figures and the high speed of the calculations for the simple assignments. This modeling is suitable for the verification of the results, which are received from other type of the modeling method.

Verification of the Design via Experiments: The results of the verification of the design via experiments. There are differences between the values obtained by modeling and experimental measurement, ranging to the 20%, depending on the distance. When the light is into the requested distance, the differences are also lower. Experimental measurements were used as second verification.

Conclusion: All requirements were executed. Increasing intensity of the light will be possible, as soon as will produce the LED diodes with higher powers.

REFERENCES

1. Plch, J., J. Mohelníková, and P. Suchánk, Osvětlení neosvětlitelnych prostor, ERA, 2004.

Preemphasis Coreection of Gradient Magnetic Field in MR Thomograph

Eva Gescheidtova, **Radek Kubasek**, **and Zoltan Szabo**
Faculty of Electrical Engineering and Communication, Brno University of Technology
Kolejni 2906/4, Brno 612 00, Czech Republic

Abstract— The magnetic resonance (MR) imaging techniques of tomography and spectroscopy are exploited in many applications. For the MR instruments to function properly it is necessary to maintain a high quality of homogeneity of the fundamental magnetic field. The pre-emphasis compensation of the generated gradient field increases the homogenity of the generated magnetic field and reduces the minimum switching times of the gradients. This enables measuring the MR images of incisions in the human body, the relaxation properties of nuclei, self-diffusion processes, flows of liquids and movements of solids faster and more accurately.

ACKNOWLEDGMENT

This work was supported within the framework of the research plans MSM 0021630516, GA102/07 /0389 and project B208130603 of the Grant Agency of the Academy of Sciences of the Czech Republic.

REFERENCES

1. Vlaardingerbroek, M., *Magnetic Resonance Imaging*, Springer-Verlag, 2000.
2. Kubásek, R., E. Gescheidtová, and K. Bartušek, "Measurements of time characteristics of the gradient magnetic field," *27th Annual International Conference of the IEEE Engineering in Medicine and Biology Society*, 1–4, Shanghai, 2005.
3. Rajmic, P., "Statistical properties of wavelet spectrum thresholding rules," *48th International Scientific Colloquium*, 87–88, Ilmenau, 2003.
4. Gescheidtová, E., R. Kubásek, Z. Smékal, and K. Bartušek, "Automatic adjustment of time-variant thresholds when filtering signals in MR tomography," *Lecture Notes in Computer Science (IF 0,513)*, 384–391, 2005.

Optimization Method of EMI Power Filters

J. Sedláček, M. Hadinec, and Zoltan Szabó
BUT FEKT Brno, Czech Republic

Abstract— Electromagnetic interference (EMI) can be reduced to acceptable level using EMI filter circuits. Unfortunately, many known methods of filter design and optimization cannot be applied directly to power electronics, which has it own peculiarities. In comparison to EMI data communication filters EMI power filters operate typically under mismatched impedance conditions. One from important manner of a filter design and optimization process there is a filter modeling. The paper deals with methods of filter design and optimization which are useful in area of EMI power filter synthesis. Different types of EMI power filters and using of their equivalent models here are discussed. Synthesis and optimization methodology for different kinds of EMI power filters with required insertion loss in wide frequency range are discussed in some practical examples.

T_1 Relaxation Time of the Xenon 129 Influenced by Magnetic Susceptibility of the Laboratory Glasses

K. Bartušek[1,2], **J. Rychnovský**[1,2], **and P. Fiala**[1]

[1]Institute of Scientific Instruments of the ASCR, v.v.i
Královopolská 147, Brno 612 64, Czech Republic
[2]Department of Theoretical and Experimental Electrical Engineering
Faculty of Electrical Engineering and Communication, Brno University of Technology
Kolejni 2906/4, Brno 612 00, Czech Republic

Abstract— Every substance has its own susceptibility, which can affect homogenous magnetic field in magnetic resonance measuring. The method of the magnetic susceptibility measurement is based on presumption of constant magnetic flux in working space of superconducting magnet. Inserted sample causes local deformation of homogenous magnetic field in working space and reduce T_1 and T_2 relaxation times of measured materials or gasses by this deformation. Described method was numerically in Ansys modeled and experimentally on 200 MHz MR tomography in ISI AS Brno verified. Reference substance was water filled into a cell. Gradient echo method was used to acquire MR image with contrast corresponding to the magnetic induction changes in measured volume of sample vicinity. Cylindrical samples — Simax, Schott and Si glasses and Si glass covered with Teflon layer were in Delrin case inserted. The Delrin case was filled to 300 kPa with natural xenon and inserted into the 200 MHz NMR system to thermal polarization. By the laboratory glasses magnetic susceptibilities measurement, we obtained glasses walls influence to thermally polarized ^{129}Xe T_1 relaxation times. The longest T_1 relaxation time was measured with Schott glass, the shortest with Si glass. The samples with Simax and Si glass with Teflon coat had comparable T_1 relaxation times.

ACKNOWLEDGMENT

This work is supported by GAAV ČR IAA1065303 and by GAČR 102/07/0389.

Experiments of Accuracy Air Ion Field Measurement

K. Bartušek[1], P. Fiala[2], T. Jirků[2], and E. Kadlecová[2]

[1]Institute of Scientific Instruments Academy of Sciences of the Czech Republic
Královopolská 147, 612 64 Brno, Czech Republic
[2]Department of Theoretical and Experimental Electrical Engineering, University of Technology Brno
Kolejni, 4, 612 00 Brno, Czech Republic

Abstract— An analysis of the electric state of air shows the presence of various ion sorts. The therapeutic effect of negative high-mobility ions of proper concentration is known. This positive effect was observed in caves that are used for speleotherapy. This article presents the capability of methods for measuring ion concentration and for ion spectral analysis. Here are new gerdien tube design steps based on numerical analysis and its experimental verification. Article describe of any experiments with different air ion generator.

Introduction

Air ion concentration and composition belong to the frequently monitored parameters of the atmosphere [5]. Their influence on living organisms has been the subject of intensive studies. Earlier research has demonstrated the positive influence of light negative ions and air cleanness on human health. The Department of the Theoretical and Experimental Electrical Engineering of Brno University of Technology and the Institute of Scientific Instruments of the Academy of Sciences of the Czech Republic are involved in the research of ion field in office and living spaces. The objective is to increase the concentration of light air ions in these spaces. Another task is to set up a simulated therapy room, with conditions similar to speleotherapy caves. It sets the requirements for accurate measurement of ion field with good repeatability. The article deals with the design of gerdien tube and peripheral measuring devices. An optimal design is important for eliminating the inaccuracy of ion concentration measurement.

REFERENCES

1. Bartušek, K., Mc̄ření speleoterapeutických parametrú jeskyní pro lékaŕské úc̄ely. Interní text UPT AVČR, 1997.
2. Buřival, Z., Vliv prostorového náboje v atmosféře na znečištční vzduchu v technologických provozech. Knižnice odborných a vc̆deckých spisú VUT Brno.
3. Spurný, Z., Atmosferická ionizace, Praha, Academia, 1985.
4. Puškeilerová, L., Nové poznatky o mc̆ření volných záporných iontú v laboratorním prostředí. Přísp̄vek k VŠTČFEI, Brno, 2000.

The Calculation of the V-shape Microstrip Line Impedance by the Conformal Mapping Method

Václav Šádek, Pavel Fiala, and Michal Hadinec
Faculty of Electrical Engineering and Communication, Brno University of Technology
Kolejni 2906/4, 612 00 Brno, Czech Republic

Abstract— The common microstrip line has one disadvantage — a lot of electromagnetic field is spread outside the dielectric substrate. This field moves $\sqrt{\varepsilon_r}$ times faster than field under the microstrip inside the dielectric substrate. This deformation of the field (HEM wave) complicates the application of the microstrip line on frequencies over c. 20 GHz.

Described complication can be eliminated in the structure, which cumulates major portion of power density of the EM field in dielectric substrate to the detriment of free space above the strip.

The sequence of three conformal mappings (used also in [1, 2]) faces to the formula for the characteristic wave impedance of the V-shape microstrip line

$$Z_0 = \frac{30 \cdot \pi^2}{\sqrt{\varepsilon_{r,\,ef}}\,\operatorname{arctanh}\sqrt{\frac{2\beta}{\alpha+\beta}}}. \tag{1}$$

where

$$\alpha = \sqrt{\left(\frac{h}{\sin\varphi}\right)^{\frac{\pi}{\varphi}} + \left(\frac{b}{\tan\varphi}\right)^{\frac{\pi}{\varphi}}} \quad \text{and} \quad \beta = \sqrt{\left(\frac{h}{\sin\varphi}\right)^{\frac{\pi}{\varphi}} - \left(\frac{b}{\sin\varphi}\right)^{\frac{\pi}{\varphi}}} \tag{2}$$

The effective relative permittivity is given as

$$\varepsilon_{r,\,ef} = \varepsilon_r - (\varepsilon_r - 1)\frac{\operatorname{arctanh}\sqrt{2 + 2\frac{\alpha}{\beta}}}{\operatorname{arctanh}\sqrt{\frac{2\beta}{\alpha+\beta}}}. \tag{3}$$

The result (1) was compared to numerical solution in *sc-toolbox* in *MATLAB*^{TM} [3]. The conformal mapping is not absolutely exact; there is an approximation in the method, which causes the error. This error depends on h/b ratio and in a mild way also on the angle φ and the result (1) is always bigger than numerical result. The worst case is for small h/b ratio (for $h/b = 1.5$ is error approximately 15%), for higher ratios increase (for $h/b = 5$ is only 10% and for $h/b = 50$ less then 5%). The error of calculated effective relative permittivity is hard to determine, but influence of this error would be very small, because of square root in (1).

There is a wide space for next work on this thema. First of them is a suppression of the error, next different variants of the dielectric substrate (multiple layers, segments, gaps...). Also different numerical models should be calculated for better verification of results. Also experimental results will be heplful for next work.

REFERENCES

1. Šádek, V, "Analysis of the two-wire transmission line by a conformal mapping method," *Proc. of Radioelektronika 2002*, Bratislava, Slovakia, 2002.
2. Hlávka, J., J. Klátil, and S. Kubík, *Komplexní proměnná v elektrotechnice* (Complex Variable in Electro technique), SNTL, Praha, Czech, 1990.
3. Driscoll, T. A., *SC-Tolbox, for MATLAB*, http://www.math.edu/ driscoll/SC/.

Session 3P4
Optics Devices, Nano Technology and Simulation

Analytic-numerical Approach to Solving Highly Irregular Problems in Special Fiber Optics

Hung-Chia Huang

SOFT (Special Optical Fiber Technology) R&D Center
Shanghai University, Shanghai 201800, China

Abstract— An analytic-numerical framework is structured on the ground of the author's initial analytic theory of *variably* coupled modes, implying the necessary and sufficient condition "fast spun and slow variation", for a variably spun birefringent optical fiber which behaves like a quarter waveplate in bulk optics. Extensive computer plots based on this framework reveal the very intricate properties of such waveplate fiber in an easy-to-understand way without recourse to complicated all-analytic mathematics. If a fiber is too short to satisfy the "slow variation" requirement, the waveplate behavior becomes oscillatory, hence unstable, while for a longer fiber a desirable, i.e., smooth therefore stable, waveplate behavior can be achieved when the "slow variation" requirement is met. This is verified by computer plots for characteristics of a waveplate fiber with a length in centimeter to decimeter range.

The approach adopted in the author's previous works on waveplate fiber was essentially analytical with numerical calculations as an auxiliary means. At the time when the author initially started his research in this area, numerical computations for solutions of simultaneous differential equations with *non-constant* coefficients was prohibitively time-consuming. With incredibly fast advances of computer technology in the past decade, numerical computation has become an extremely powerful yet indispensable means in the research of fiber optics. It is now feasible to substantially expand the scope of the author's original theoretical framework of waveplate fiber by including numerical solutions of variably coupled modes. Indeed, without extensive numerical computation that has produced a series of plots showing the polarization behaviors of waveplate fiber with various structural parameters, the results presented in the current paper would not have been possible. Detailed description of the computer plots as verified by experimental results will be given in the oral presentation.

REFERENCES

1. Huang, H.-C., *Microwave Approach to Highly Irregular Fiber Optics*, 307, Wiley InterScience, 1998.
2. Huang, H.-C., "Asymptotic approach to solving highly irregular problems in special fiber optics," *Surv. Math. Ind.*, Vol. 10, 1–21, 2001.

Light Propagation in a Random Waveguide System and the Memory Kernel

Akira Komiyama

Osaka Electro-Communication University, Hatsu-cho Neyagawa-shi 572-8530, Japan

Abstract— Propagation properties of light in a one-dimensional waveguide system with random geometrical imperfections have been discussed as a model of an image fiber which is used to transmit directly an optical image. Equations describing the behaviour of light can be derived theoretically from the perturbation solution of the coupled mode equations [1, 2], which are given by

$$\frac{dc_n^c}{dz} = \left(-\frac{\alpha}{2} - j\beta\right) c_n^c - j\kappa \sum_m c_m^c \tag{1}$$

$$\frac{dP_{nn}}{dz} = \kappa \sum_{l\neq n} Q_{ln} + \alpha \left|c_n^c\right|^2 \tag{2}$$

$$\frac{dQ_{mn}}{dz} = -\alpha Q_{mn} + (-1)^{m-n}\kappa \left(\sum_{l\neq m} Q_{ln} - \sum_{l\neq n} Q_{ml}\right) \tag{3}$$

c_n^c is the coherent part of the mode amplitude in the nth core and P_{nn} is the average power of the incoherent part of the mode amplitude ($P_{nn} = \langle|c_n^{ic}|^2\rangle$). α is the damping factor and κ is the mode coupling coefficint. By eliminating Q_{mn} we can obtain the integro-differential equations,

$$\frac{dP_{nn}}{dz} = 2\kappa^2 \sum_l \int_0^z K_l(z-\xi)\left(P_{n+l+1\,n+l+1}(\xi) - P_{n+l\,n+l}(\xi)\right) d\xi + \alpha \left|c_n^c\right|^2 \tag{4}$$

where K_l is the memory kernel,

$$K_l(z) = \left(M_l(z) = M_{l+1}(z)\right) e^{-\alpha z} \tag{5}$$

M_l is dependent only on a single variable κz, which can be obtained from the initial value problem,

$$\begin{aligned} q_{n+1\,n}(0) &= \delta_{n\,m},\ q_{n+2n}(0) = 0, \ldots \\ \frac{dq_{n+1\,n}}{dz} &= \kappa\left(q_{n+1\,n-1} - q_{n+2\,n}\right) \\ \frac{dq_{n+2\,n}}{dz} &= \kappa\left(q_{n+1\,n} - q_{n+2\,n+1}\right) + \kappa\left(q_{n+3n} - q_{n+2\,n-1}\right) \end{aligned} \tag{6}$$

In this paper, the dependence of the asymptotic behaviour of the solution to the integrodifferential Equations (4) on the damping factor will be clarified.

REFERENCES

1. Komiyama, A., *Proceedings of 2004 URSI EMT-S*, 260–262, 2004.
2. Komiyama, A., *Abstracts of PIERS 2006*, 274, Cambridge, 2006.

Experimental Results of a Wave Guide Using a Photorefractive Material SBN:Ce

Francisco Marroquín Gtz[1, 2], **Nikolai Korneev**[2], **A. Apolinar Iribe**[3], **and A. García B.**

[1]Universidad Politécnica de Pachuca (UPP), Departamento de Mecatrónica
Carretera Cd. Sahagun-Pachuca, Hidalgo, Km. 20, C. P. 43830, México
[2]Instituto Nacional de Astrofísica, Óptica y Electrónica (INAOE)
Apdo. Postal 51 y 516, C. P. 72000, Puebla, México
[3]Universidad de Sonora (UNISON), Apdo. Postal 1626, C. P. 83000, Hermosillo, Sonora, México

Abstract— The photorefractive effect is a physical phenomenon whereby the local index of refraction is modified by spatial variations of the light intensity. It is strongly observed when coherent rays interfere with each other in a photorefractive material which forms a spatially varying pattern of illumination. In this investigation, we report experimental results obtained when the light taken place by laser of He-Ne by an arrangement of photo induced waveguides in a Strontium Barium Niobate (SBN), which it has a large Electro-optic coefficient delivering a fast response time and high two wavelength mixing gain. The results reveal the important role that carrier out the phenomenon of transverse modulation instability in the control of light. The possible applications can be scientific and technological, the optic wave guides as well we know they transport the light in a transparent medium, in this case SBN:Ce, in a controlled way, so also it is possible the fabrication of devices for optic communication systems as; the sources of light, modulators and multiplexers devices and in active optic fibers used as medium of transmission of information to long distance.

How Much Can You Twist a Microstructured Optical Fibre?

A. Nicolet[1], **F. Zolla**[2], **and Y. Ould Agha**[2]

[1]Institut Fresnel, UMR CNRS 6133, Université Paul Cézanne, Marseille, France
[2]Institut Fresnel, UMR CNRS 6133, Université de Provence, Marseille, France

Abstract— The purpose of this paper is to investigate the effect of a twist on the losses of leaky modes in microstructured optical fibres (MOF). Classical optical fibres are most usually axisymmetric and therefore insensitive to a global rotation and even to a local rotation (torsion). This is not the case for MOF and the question may be raised of the behavior of a mode when the fibre is twisted, e.g., how varies the imaginary part of the propagation constant that gives the losses of the leaky modes?

In order to model twisted fibres, an helicoidal system of co-ordinates [1, 2] is introduced to define the structure and to set up the problem (every cross section suffers a rotation of an angle αz where z is the co-ordinate along the axis of the fibre and α is a constant). These co-ordinates, albeit non-orthogonal, preserve the translational invariance in a way that allows a two-dimensional finite element model similar to the one of classical straight waveguides. The Perfectly Matched Layer (PML) technique is used to compute the leaky modes in the fibres and is extremely accurate: [3] even when the imaginary part is several orders of magnitude smaller than the real part, it is computed with a very good precision without requiring a specially fine mesh. Helicoidal co-ordinates and PML are unified under the point of view of geometrical transformations which allows the design of "twisted PML" that provides the right tool to determine the leaky modes in the twisted structures.

Results of Fig. 1 show that the effect of the twist is much more important (in terms of relative variation) on the imaginary part than on the real part of the propagation constant.

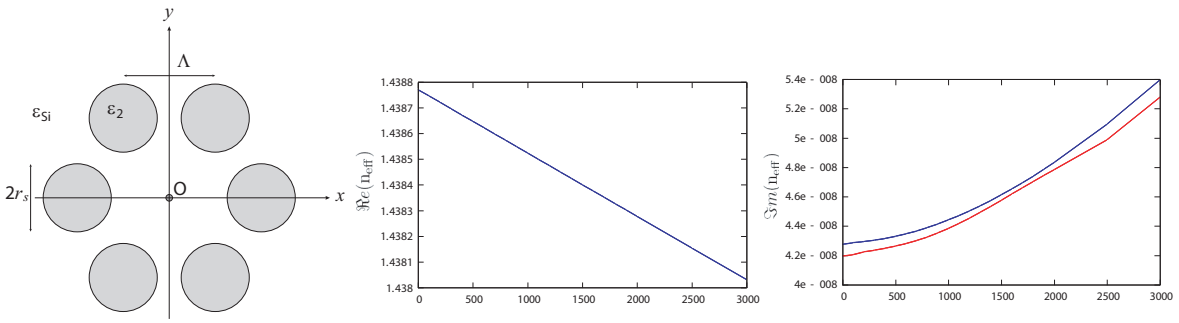

Figure 1: Cross section of a twisted six hole MOF structure with $\Lambda = 6.75\,\mu\text{m}$, $r_s = 2.5\,\mu\text{m}$, $\varepsilon_2 = 1$, and $\varepsilon_{\text{Si}} = 2.085$(left), real part of the effective index $n_{\text{eff}} = \beta/k_0$ for the fundamental mode (for $\lambda_0 = 2\pi/k_0 = 1.55\,\mu\text{m}$) versus the parameter of torsion $\alpha\,(\text{m}^{-1})$ — the maximum torsion corresponds to $\alpha = 3000\,\text{m}^{-1}$ so that the torsion length is $2\pi/\alpha = 2090\,\mu\text{m}$ — (center), imaginary part of the effective index $n_{\text{eff}} = \beta/k_0$ for the fundamental mode versus the parameter of torsion $\alpha\,(\text{m}^{-1})$, the blue (resp. red) curve corresponds to a mesh with 9102 (resp. 4032) elements (right).

REFERENCES

1. Zolla, F., G. Renversez, A. Nicolet, B. Khulmey, S. Guenneau, and D. Felbacq, *Foundations of Photonic Crystal Fibres*, Imperial College Press, London, 2005.
2. Nicolet, A., A. B. Movchan, S. Guenneau, and F. Zolla, "Asymptotic modelling of weakly twisted electrostatic problems," *C. R. Mecanique*, Vol. 334, No. 2, 91–97, 2006.
3. Ould Agha, Y., F. Zolla, A. Nicolet, and S. Guenneau, "On the use of PML for the computation of leaky modes: an application to gradient index MOF," *International Journal for Computation and Mathematics in Electrical and Electronic Engineering COMPEL*, Vol. 27, No. 1, Jan. 2008, to appear.

Far-field Method for the Characterization of Three-dimensional Fields

Oscar Rodriguez, **David Lara**, **and Chris Dainty**
National University of Ireland, Galway, Ireland

Abstract— In the focal region of a high numerical aperture (N.A.) lens, for certain polarisation states of the incident light, the field distribution can have a longitudinal component with amplitude comparable to the transverse components [1]. In conventional polarisation microscopy the longitudinal component of the illumination is usually ignored and only the information contained in the transverse components of the field is analysed [2, 3]. One attempt to retrieve the information contained in the longitudinal component was done with the Z-polarized confocal microscope (ZPCM) introduced by Huse et al. in 2001 [4]. However, the ZPCM uses only one configuration for the illumination and focuses its analysis on the longitudinal component of the illumination and scattered fields, ignoring the information contained in the transversal components.

To the best of our knowledge, the first attempt to analyse the three components of the electromagnetic field was done by Ellis and Dogariu [5]. Their method is based on the use of a near-field probe making it suitable only for applications where the distance between the probe and the sample can be controlled with sufficient precision.

We propose a far-field method for the analysis of the interaction of a sample with a three-dimensional field in the focus of a high N.A. lens. This makes our method suitable even in applications where the position of the sample cannot be controlled with high precision. To assess the performance of our method we have performed numerical simulations using the FDTD method with CPML absorbing boundary conditions and the scattered field formulation for the incident field.

REFERENCES

1. Richards, B. and E. Wolf, "Electromagnetic diffraction in optical systems II. Structure of the image field in an aplanatic system," *Proceedings of the Royal Society of London A*, Vol. 253, No. 1274, 358–379, 1959.
2. Wilson, T., R. Juskaitis, and P. Higdon, "The imaging of dielectric point scatterers in conventional and confocal polarization microscopes," *Optics Communications*, Vol. 141, 298–313, 1997.
3. Török, P., P. D. Higdon, and T. Wilson, "On the general properties of polarised light conventional and confocal microscopes," *Optics Communications*, Vol. 148, 300–315, 1998.
4. Huse, N., A. Schonle, and S. W. Hell, "Z-polarized confocal microscopy," *Journal of Biomedical Optics*, Vol. 6, No. 4, 480–484, 2001.
5. Ellis, J. and A. Dogariu, "Optical polarimetry of random fields," *Physical Review Letters*, Vol. 95, No. 20, 203905 (1–4), 2005.

Generation of High-brightness Radiation in the Region of UV and X-Ray Wavelengths — Tutorial Review

Toshiyuki Shiozawa

Department of Electronics and Information Engineering, Chubu University, Japan

Abstract— In recent years, synchrotron radiation (SR) and free-electron lasers (FELs) have been playing an important role for the radiation sources in the region of ultraviolet (UV) and X-ray wavelengths. The present paper briefly reviews the basic principles of synchrotron radiation and free-electron lasers, from the viewpoint of classical electrodynamics [1]. The operation principle of the free-electron laser can be explained purely classically, as opposed to the conventional laser whose operation principle is based upon quantum electrodynamics. In particular, special attention is paid to research efforts for the UV and X-ray free-electron lasers.

The electromagnetic waves emitted by synchrotron radiation cover a broad continuous spectrum extending from the far infrared (FIR) through the visible to the ultraviolet (UV) and X-ray wavelengths. On the other hand, free-electron lasers can generate coherent radiation with much higher brightness in the same spectral range, as compared with synchrotron radiation. In recent years, research efforts to realize the X-ray free-electron laser have been made in major research facilities in the world such as SLAC [2] (the United States), DESY [3] (Germany), and Spring-8 [4] (Japan). With its short and coherent pulses with enormous peak power, the X-ray free-electron laser will open a whole new field of scientific research, such as new medical and life sciences, solid-state physics, and fabrication of nano-scale structures.

REFERENCES

1. Shiozawa, T., *Classical Relativistic Electrodynamics — Theory of Light Emission and Application to Free-electron Lasers*, Springer, Berlin, 2004.
2. www.slac.stanford.edu
3. www.desy.de
4. www.spring8.or.jp

Three-dimensional Numerical Analysis of an Optical Near Field from a Nano-aperture of a Metallic Layer

Hiroki Ito[1], **Shinya Kagawa**[1], **Yiwei He**[2], **and Toshitaka Kojima**[1]

[1]Graduate School, Kansai University
3-3-35, Yamate-cho, Suita-shi, Osaka 564-8086, Japan
[2]Faculty of Engineering, Osaka Electro-Communication University
18-8 Hatsu-cho, Neyagawa-shi, Osaka 572-8530, Japan

Abstract— Recently, a density growth is demanded in optical storage technologies. But, it is said that the upper limit of recording density by the current optical recording system is several tens of gigabits per inch square due to the optical diffraction limit even in the case of using a short wavelength. Then, as a technology that enables us to break down the optical diffraction limit, the optical near field technology has gotten a lot of attention. The utilization of the optical near field technology will enable us to perform a terabyte class storage system much beyond the conventional optical system dominated by the diffraction limit.

In this paper, we try to carry out three-dimensional numerical analysis of electric field distributions near a metallic nano-aperture by using the finite difference time domain (FDTD) method. In the present analysis, the FDTD method combined with the motion equation of electron [1] is applied to a metallic medium because its permittivity can become negative at the optical wavelength range. In order to examine how the near field intensity depends on the structure of apertures, we demonstrate numerical simulation of the near field distributions in various configurations of apertures. The results indicate that the bow-tie aperture can generate much stronger near field than other types of aperture.

REFERENCES

1. Kagawa, S., Y. He, and T. Kojima, "Numerical analysis of an optical near field from an aperture in a metallic layer-application of the FDTD method combined with the motion equation of electron," *Progress In Electromagnetics Research Symposium 2006-Tokyo*, 232, Aug. 2006.

Three-dimensional Numerical Analysis of Light-beam Scattering from DWDD Disk Model with Rear Process

Akira Yokoyama, **Yoshiaki Irifune**, **and Toshitaka Kojima**

Graduate School of Electronics, Kansai University, Japan
3-3-35 Yamate-cho, Suita-shi, Osaka 564-8680, Japan

Abstract— We have developed numerical simulation techniques for the light-beam scattering and the detected signal characteristics from various types of optical disks as the digital versatile disk (DVD) and magneto optical (MO) disk so far. In our previous paper, we have demonstrated that the finite difference time domain (FDTD) method can be a powerful tool for the numerical simulation of light-beam diffraction from conventional MO disk structures [1].

Recently, various technologies of higher density version that exceed optical resolution are proposed for MO disk, and have been put to practical use. In those technologies, the domain wall displacement detection (DWDD) is one of excellent readout methods, which utilizes the characteristic of magnetic film called wall-displacement phenomenon by temperature gradient [2, 3]. This method has no limit of resolution in principle. However, it has a problem such that ghost signals are caused by so-called rear process (RP) due to continuously recorded marks. [4]

In the present paper, we try to apply the three-dimensional FDTD method to the analysis of the light-beam scattering and the characteristic of detected signal from DWDD disk model with RP and examine the influences of RP on the signal detection characteristics.

REFERENCES

1. Kojima, T., T. Sasai, I. Kobayashi, and Y. He, "$(FD)^2TD$ analysis of light-beam scattering from MO disks with land/groove recording structures," *IEICE Trans. Electron*, Vol. 85-C, No. 10, 1776–1783, Oct. 2002
2. Kai, S., A. Fukumoto, K. Aratani, S. Yoshimura, K. Tsutsumi, and M. Arai, "Over 15-GB capacity domain wall displacement detection magneto optical recording using a digital versatile disc dimensional optical head," *Jpn. Appl. Phys.*, Vol. 39, No. 4A, 1757–1761, Apr. 2000.
3. Irifune, Y., M. Miyake, and T. Kojima,"Three-dimensional numerical analysis of light-beam scattering from DWDD disk model," *Proc. of Progress In Electromagnetics Reserch Symposium 2006-Tokyo*, 219, Aug. 2006.
4. Atsushi, O., K. Kentarou, K. Tadashi, Fujiwara Yuuji, S. Shigeru, and K. Masahiko, "Wall structure and energy on DWDD," *Trans. Magn. Soc. Jpn.*, Vol. 4, No. 4-2, 152–155, Nov. 2004.

A Higher-order Accurate FDTD Solution to Scalar SHG Problems

M. A. Alsunaidi[1] and F. S. Al-Hajiri[2]

[1]King Fahd University of Petroleum & Minerals, Saudi Arabia
[2]King Faisal University, Saudi Arabia

Abstract— Higher order FDTD schemes allow the modeling of electromagnetic wave interaction in structures that have very long electrical lengths without jeopardizing the limit on phase error accumulation set by standard 2nd order methods. These higher order schemes become even more attractive in problems involving nonlinear interactions. For example, in a second harmonic generation (SHG) problem, the energy coupling between the propagating input optical beam and the generated beam is a strong function of the phase shift between the two waves. Failing to accurately estimate the phase of the waves at any given distance along the propagation direction results in errors in the calculation of both coherence length and coupled energy. Several researchers have attempted the FDTD solution of wave propagation in both linear as well as nonlinear optical structures using higher order methods to overcome the limitations of 2nd order explicit schemes. In this paper, the FDTD-SHG solution reported in [1] is revisited. The second order accurate approximations of the spatial derivatives are replaced by 4th order accurate schemes. Such a scheme has not been yet discussed in literature in the context of the nonlinear wave equation representing SHG.

To study the effectiveness of the proposed 4th order method, a symmetric AlGaAs-based dielectric slab waveguide is considered. It consists of a 0.44-μm thick guiding layer sandwiched between two 3-μm thick AlAs layers. The excitation field is a CW signal at a fundamental wavelength of $\lambda_f = 1.064\,\mu$m. The transverse profile of the excitation corresponds to the first guided mode at the given operating frequency. For the sake of comparison, both 2nd and 4th order schemes were considered. No matching technique is used such that the level of coupling between the input and the generated waves depends entirely on the phase shift between them. This phase shift is defined by the effective refractive indices of the two coexisting guided modes. The coherence length is given by $L_C = \lambda_f/2(n_s - n_f)$, where n is the effective refractive index. Because of the nature of the problem, propagation occurs in only one direction. Several numerical experiments have shown that negligible gain in accuracy is achieved by applying the 4th order scheme to the transverse direction. By applying the 4th order scheme to the spatial derivatives in the propagation direction only, an overall increase of 11% in computation time is expected, but no additional memory resources are necessary. As shown in Figures 1 and 2, this additional computation time is insignificant if compared to the savings made by relaxing the spatial step and hence the time step. For the same error tolerance, the 4th order scheme uses spatial steps with more than double the size required by the 2nd order scheme. In the figures, the grid factor is defined as the ratio of the wavelength to the spatial step size.

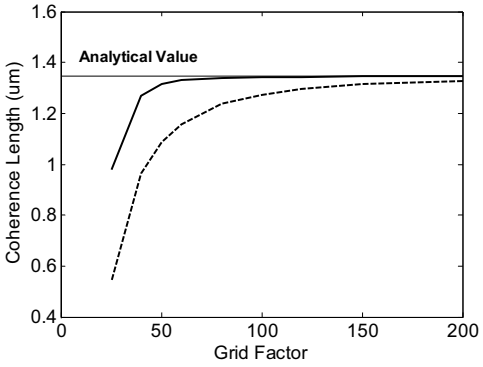

Figure 1: Coherence length vs. Grid factor using 4th order (solid) and 2nd order (dashed) FDTD.

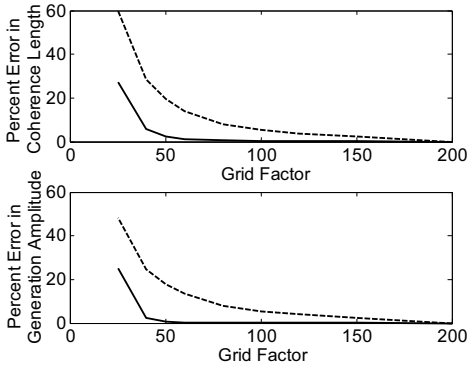

Figure 2: Error analysis for 4th order (solid) and 2nd order (dashed) FDTD

ACKNOWLEDGMENT

The authors would like to acknowledge the support of King Fahd University of Petroleum and Minerals.

REFERENCES

1. Alsunaidi, M. A., H. M. Masoudi, and J. M. Arnold, "A time-domain algorithm for second harmonic generation in nonlinear optical structures," *IEEE Photonics Tech. Lett.*, Vol. 12, 395–397, 2000.

Full-wave Solution of the Second Harmonic Generation Problem Using a Nonlinear FDTD Algorithm

H. M. Al-Mudhaffar, **M. A. Alsunaidi**, **and H. M. Masoudi**
King Fahd University of Petroleum & Minerals, Saudi Arabia

Abstract— A vectorial time-domain simulator of integrated optical structures containing second order nonlinearities is presented. This model is an extension of the scalar nonlinear FDTD solution algorithm reported in [1]. The simulation algorithm is based on the direct solution of nonlinear Maxwell's equations representing the propagating fields and is solved using the FDTD method. The model is derived by explicitly expressing the nonlinear polarization, $P^{NL} = 2\varepsilon[d]E \cdot E$, in the electric field equation. The dot product in the nonlinear polarization spans all field components at the fundamental as well as the second harmonic frequencies. If we assume an isotropic second order nonlinearity with $d_{14} = d_{25} = d_{36}$, the following equations apply for the generated second harmonic field in 2D.

$$\varepsilon_y \frac{\partial E_y^s}{\partial t} = \left(\frac{\partial H_x^s}{\partial z} - \frac{\partial H_z^s}{\partial x} \right) - 2\varepsilon_0 d_{14} \frac{\partial}{\partial t} \left(E_x^f E_z^f \right), \quad \mu \frac{\partial H_x^s}{\partial t} = \frac{\partial E_y^s}{\partial z} \quad \text{and} \quad \mu \frac{\partial H_z^s}{\partial t} = \frac{\partial E_y^s}{\partial x}$$

A symmetric AlGaAs-based dielectric slab waveguide is considered to test the proposed FDTD algorithm. It consists of a 0.44-μm thick guiding layer sandwiched between two 3-μm thick AlAs layers. The arrangement of the field components for both the fundamental and second harmonic are made according to the standard Yee cell. The excitation field is a CW TM signal at a fundamental wavelength of $\lambda_f = 1.064\,\mu\text{m}$ and an amplitude of $5.0\,\text{A}/\mu\text{m}$. The transverse profile of the excitation corresponds to the first TM guided mode at the given operating frequency. For the sake of illustration, two matching scenarios are considered. First, no matching technique is used such that the level of coupling between the input and the generated waves depends entirely on the phase shift between them. This phase shift is defined by the effective indices of the two coexisting guided modes. Second, the effective refractive index of the first odd guided mode of the TE field at $\lambda_s = 0.533\,\mu\text{m}$ is perfectly matched to the first even guided mode of the TM input field by numerically changing the value of the refractive index of the guiding layer at λ_s. The results for both scenarios are shown in Figure 1. As expected, energy exchange between the fundamental field and the second harmonic field takes place periodically during every coherence length if no matching technique is implemented. If, however, the two waves are perfectly matched, the energy exchange will be continuous, resulting in a coherent build-up of the second harmonic energy. The transverse profiles for the fundamental TM mode and the second harmonic TE mode is shown in Figure 2. The simulation varifies the coupling of second harmonic energy on the first odd TE mode.

The developed model can be utilized to efficiently analyze and study different optical structures. The extension of the model for applications involving pulsed excitations and different device nonlinearities is a future work. It should find application in a wide range of device structures and in the analysis of short-pulse propagation in second order nonlinear devices.

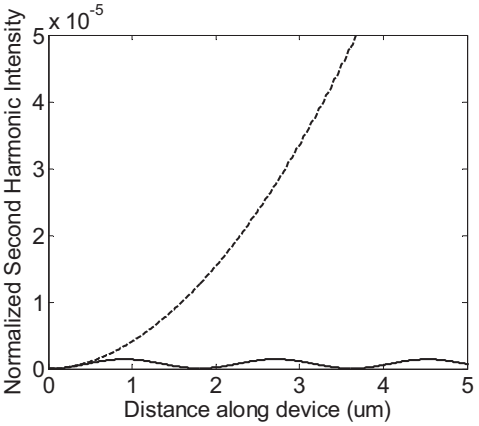

Figure 1: SHG along the nonlinear waveguide (solid: no matching, dashed: perfect match).

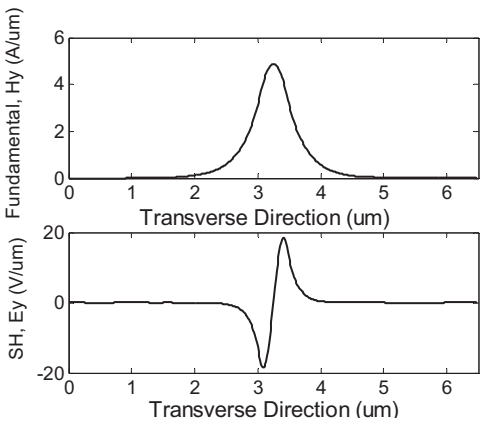

Figure 2: TM input (fundamental) and generated TE second harmonic profiles.

ACKNOWLEDGMENT

The authors would like to acknowledge the support of King Fahd University of Petroleum & Minerals.

REFERENCES

1. Alsunaidi, M. A., H. M. Masoudi, and J. M. Arnold, "A time-domain algorithm for second harmonic generation in nonlinear optical structures," *IEEE Photonics Tech. Lett.*, Vol. 12, 395–397, 2000.

Spectral Monte-Carlo Simulations of Photon Penetration in Biotissue in Visible and Near Infrared

M. Hülsbusch, **D. Hölscher**, **and V. Blažek**
Institute of High Frequency Technology, RWTH Aachen University, Aachen, Germany

Abstract— For design and optimization of optoelectronic sensor concepts the photon-tissue interaction has to be evaluated. The Monte Carlo method is a well suited tool for this task. This paper discusses different virtual skin models and the optical properties of biotissue in the visible and near infrared spectrum. Based on these fundamentals a simulation tool is presented, which is capable of handling arbitrary complex simulation scenarios. Apart from the assessment and quantification of penetration depth of different sensor concepts also dynamical simulations are presented, which allow simulations of blood volume pulses. These simulations permit the evaluation of the DC and also the AC component of the detector signal.

Session 4A1
Circuits and Devices, CAD 2

New Planar Technologies for Millimeter Waves

G. Di Massa and I. Venneri

Microwave Lab, Dipartimento di Elettronica, Informatica e Sistemistica
Università della Calabria, Rende (Cs) 87036, Italy

Abstract— Printed circuit technology has been successfully applied to high frequency circuits because of the reduced costs and the capability to easily integrate passive and active devices. Recently, several attempt have been done to bring PCB technology to millimetre wave applications and entire millimetre wave systems have been integrated using PCB like process called System On a Package (SOP). The major difficulties encountered are essentially due to the electrical characteristics of the materials commonly used at the higher frequencies and in particular to the losses into the dielectric substrates mainly due to the water absorption. Recently several dielectrics that can be used as a basis of a PCB process have been synthesized. In this paper we present the application of two dielectrics to millimetre wave circuits: Liquid Crystal Polymer (LCP) and Benzocyclobutene (BCB or Cyclotene).

LCP has low losses and low water absorption LCP laminates are extremely flexible and are particularly suited fo the realization of conformal arrays and MEMS. Recently it has been shown that LCP maintain its good electrical characteristics at millimetre wave frequencies. Measurements in the range between 30 GHz and 110 GHz have shown that the dielectric constant is 3,16±0,05 with a variation of less than 4.3% over the entire frequency range and the loss tangent is between 0.003 and 0.005.

BCB, or Cyclotene, is an organic resin with low loss, low dielectric constant and an excellent stability of the electrical properties on a wide frequency range. The producer (Dow Chemical) claims that measurements show a dielectric constant of 2.56 with a variation of less than 1% over a range of frequencies that goes from 400 GHz up to 1500 GHz. Tangent loss is between 0.0025 and 0.01 in the same range. BCB deposition has been successfully used to set up the MCM-D (Multichip Module Deposited) technique of integration for millimetre wave systems.

LCP laminates are already available on the market, as example Rogers sells LCP foils with a thickness from 25 µm to 100 µm and with a copper foil 18 µm thick. If commercial laminate are used the process is limited to spin-coating the photo-resist and to laser patterning the circuits. However, as frequency goes up tracks width may become comparable to the copper thickness of commercially available laminates. For this case the controlled deposition of the conductor layer on a foil of dielectric will be adopted. LCP will be also used to realize low cost membrane circuits. Cavities will be etched into thick copper foil on which a foil of LCP will be pressed. In this way areas of suspended LCP foil will be created on which copper or gold can be deposited to create the circuit.

BCB has been used up to know directly spinning it on a Si wafer and then depositing the conductor. In a different approach a cavity is etched into the Si wafer and the is filled with BCB to create an area available for the circuitry. The entire process to create BCB based millimetre circuit has been developed in all the phases: spinning, baking, and curing in a controlled atmosphere. A copper foil is deposed to create low cost millimetre wave radiators.

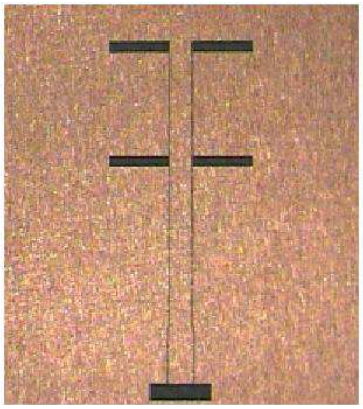

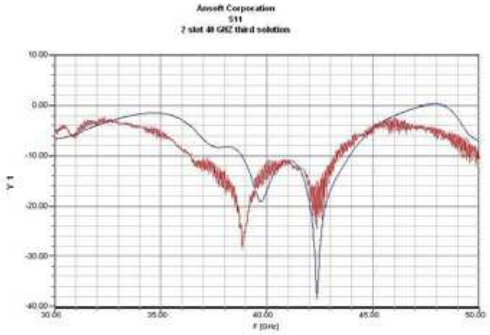

In this paper technological problems and solutions are addressed. New millimetre antennas and circuits in the frequency band 30–110 GHz are presented. In the figure an example of LCP antenna is presented. A two slot array has been realized. The slot has a length of 5.5 mm and a width 0.49 mm, the distance between the slots is 4.7 mm, the feeding slot lines have a width of 0.05 mm and are distant 0.99 mm. The measure has been done with a probing station that consists of two optical breadboards on which are placed two micropositioners which controls the probes movements. Between the boards is placed an adjusting platform on which is fixed a chuck to guest the device under test. With such arrangement the antenna is placed above the conductors that can be shielded with anechoic materials. The system includes a microscope with a camera to inspect the circuits and correctly places the high frequency probes. In the figure are reported the input scattering coefficients simulated (black line) and measured (red line).

Modeling and Analysis of Crosstalk between Differential Lines in High-speed Interconnects

F. Xiao and Y. Kami

University of Electro-Communications, Japan

Abstract— As clock frequency reaches the gigahertz band and signal transmission rate reaches the gigabit range, signal integrity issues, such as crosstalk between signals, are becoming serious problems in the interconnection of signals. Comparing with the single-ended signaling, differential traces are highly resistant to common-mode noise from other signals or external fields, reduce the common-mode radiation levels, and improve the signal integrity as well as the dynamic range [1–3]. Compared to single-ended signaling, differential signaling uses double the number of interconnects. As the circuit packaging density continues to increase, the number of interconnects will be a limiting factor. It is desirable to send as much data as possible between two points using a minimum number of interconnects. Inserting an extra signal information by using the common mode into the differential signaling is a promising technique [4]. Theoretically, the differential and common mode are orthogonal with each other, thus the two signals can be transmitted on the same physical channel without affecting each other. While in theory the differential and common mode are orthogonal, in practice, inevitable non-idealities, such as mismatch due to vias, connectors, and ground bounce, lead to crosstalk problems. The crosstalk may exist in several different manners. First, signal coupling between modes causes mode conversion between differential and common mode. Furthermore, if a differential pair is near to another differential pair, the crosstalk between them may occur.

In this work, as a preliminary study, we consider the crosstalk between differential lines. First the crosstalk and mode conversion are analyzed. In our analysis, the differential pairs are considered as parallel transmission lines thus the telegrapher's equations for multiconductor lines can be applied [5]. Then the telegrapher's equations are solved by using a mode decomposition technique. The mixed-mode S-parameters are derived to investigate the crosstalk and mode conversion. The measurement of the crosstalk and mode conversion are also conducted. Both the calculated and measured results are presented. The characteristics of the near-end crosstalk (NEXT) and far-end crosstalk (FEXT) are also examined and discussed.

The goal of this work is to find a design of the interconnects that minimizes the crosstalk [6]. Several possible differential-line structures have been considered, including the co-planar lines, stacked-pair lines, diagonal-pair lines. Different structures exhibit different crosstalk characteristics, and the crosstalk can be decreased by properly setting the differential pair. Furthermore, the effect of routing guard traces and ground tracks have also been examined.

REFERENCES

1. Johnson, H. W. and M. Graham, *High Speed Digital Design: A Handbook of Black Magic*, Prentice Hall, NJ, 1993.
2. Hall, S., G. W. Hall, and J. A. McCall, *High-Speed Digital System Design: A Handbook of Interconnect Theory and Design Practices*, John Wiley & Sons, Inc., New York, 2000.
3. Johnson, H. W. and M. Graham, *High Speed Signal Propagation: Advanced Black Magic*, Prentice Hall, NJ, 2003.
4. Gabara, T., "Phantom mode signaling in VLSI system," *Proc. Conf. on Advances Research in VLSI*, 88–100, Salt Lake City, UT, Mar. 2001.
5. Paul, C. R., *Analysis of Multiconductor Transmission Lines*, John Wiley & Sons, Inc., New York, 1994.
6. Kimura, M., H. Ito, H. Sugita, K. Okada, and K. Masu, "Zero-crosstalk bus line structure for global interconnects in Si ultra large scale integration," *Japanese Journal of Applied Physics*, Vol. 45, No. 6A, 4977–4981, 2006.

A Novel Time-domain Approach Using TDR/TDT for Synthesizing SPICE-compatible Models of Power Delivery Networks with Resonance Effect

Chen-Chao Wang[1], **Chih-Wen Kuo**[1], **Alex Wang**[2], **and Hung-Hsiang Cheng**[2]

[1]Department of Electrical Engineering, National Sun Yat-Sen University, Kaohsiung, Taiwan
[2]Advanced Semiconductor Engineering Group, Kaohsiung, Taiwan

Abstract— A novel time-domain approach for synthesizing SPICE-compatible models of power delivery networks with resonance effect based on time-domain reflected/transmitted waveforms is presented. The applied time-domain waveforms can be acquired either by TDR/TDT measurements or FDTD simulations. The step responses of the power/ground planes with resonance effect are solved in terms of rational functions by the generalized Pencil-of-Matrix (GPOM) method, and the pole-residue representation of the time-domain step responses of the structure is obtained. The macro-π model in terms of the rational function pairs is then obtained through a Y matrix transformation. The equivalent lumped circuits of the macro-π model are finally synthesized by a lumped circuit extraction method. It is found that the extracted models accurately predict the power/ground bouncing or resonance behavior in a wide-band range. The developed models can be efficiently incorporated to the HSPICE simulator for considering the power/ground bouncing noise in high-speed circuits.

A Study of Layout Strategies in RF CMOS Design

John Richard E. Hizon, **Marc D. Rosales**, **Honee Lynn B. Tan**
Maria Cecilia N. Gutierrez, **Louis P. Alarcon**, **and Delfin Jay Sabido IX**
Microelectronics and Microprocessors Laboratory
Department of Electrical and Electronics Engineering
University of the Philippines, Diliman, Quezon City, Philippines

Abstract— In this paper, the different issues confronting designers of RF blocks in digital CMOS are presented. These issues include the various implementations for the successful integration spiral inductors and capacitors in CMOS for RF operation as well as the evaluation of Q enhancement techniques to improve inductor Q. Another barrier considered is RF MOSFET modeling because MOSFET parasitics become important as the operating frequency increases and enters the GHz range. Likewise, knowledge of the effects of layout on these parasitics is vital in improving RF design efficiency. To improve RF design capability, it is therefore essential that actual measurement results be done to quantify realizable performance for both passive and active devices in CMOS. Structures presented in this paper were fabricated on a 0.25 μm digital CMOS process.

A Fully Integrated CMOS RFIC Ultra-wideband Low Noise Amplifier with Transformer Feedback Matching Topology

Ming-Hsien Hsieh and Fu-Chiarng Chen

National Chiao Tung University, Taiwan

Abstract— This paper presents a novel low-noise amplifier (LNA) with transformer feedback technology used in the ultra-wideband (UWB) communication systems. Using shunt transformer feedback and the architecture of current reuse can achieve broadband matching, low noise figure, low power consumption, and good gain performance over the operating bandwidth. A fully integrated UWB LNA is fabricated using TSMC 0.18 µm CMOS technology.

In general, a broadband input matching network is realized using multi-section passive LC network or RC feedback technology. However, a large number of components is inevitable, and results in bad noise figure performance and large chip area. We therefore develop a transformer feedback network to reach equivalent characteristic compared to the above mentioned matching topologies. The circuit is shown in Fig. 1. The transformer consists of two inductors, where one is shunted at the input port, and the other is put in the first stage as source degeneration. The transformer employing square inductors is used to reduce the Q factor. Self inductances are appropriately selected by their turn numbers, and mutual inductance is dependent on the distance between the adjacent conductors.

In order to reduce power consumption, the two stages of the circuit are stacked so that bias current of the second stage is reused in the first stage. Thus, the circuit is treated as a cascode circuit in DC biasing and a cascade amplifier in AC analysis. Furthermore, some circuit components are added for bandwidth enhancement. Shunt inductive peaking put on the drain of the second stage is applied to generate extra zero-point frequency. L2 is used to ameliorate the parasitic capacitance which is caused by the large drain-to-substrate capacitance introduced by M2 and loading of the buffer stage.

The simulation results of our 3.1 GHz to 10.6 GHz UWB LNA are shown in Fig. 2. It is performed by Agilent ADS®. The results show that the input and output return loss are less than −10 dB, and the gain is up to 12 dB. The noise figure is 3.2 dB least and less than 5 dB over the entire band. The transformer feedback topology is proved to be efficient in wideband matching and noise reduction. As to in-band linearity, the 1-dB compression point is −14 dBm at best and the IIP3 ranges from −10 to −4 dBm. The total chip occupies 0.69 mm^2 including test pads and consumes power less than 9 mW from a 1.2 V voltage supply. The measurement data will be presented and discussed in our presentation.

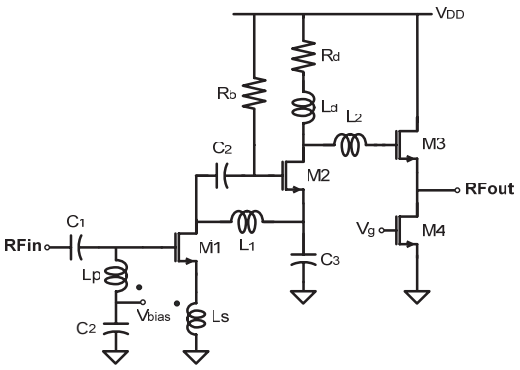

Figure 1: The proposed schematic of UWB LNA.

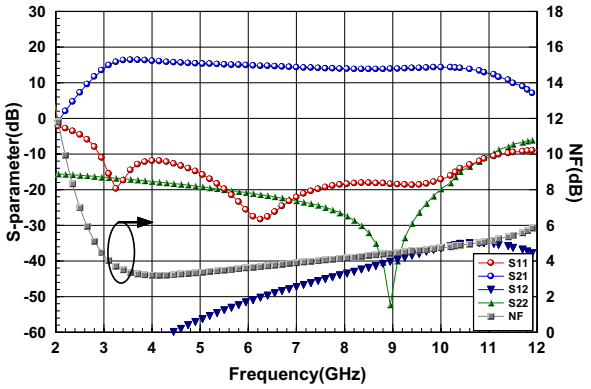

Figure 2: Simulation performance of UWB LNA.

ACKNOWLEDGMENT

The authors would like to thank National Chip Implementation Center (CIC) for technology support and chip fabrication.

Ultra-wide Band Noise-signal Radar Utilizing Microwave Chaotic Signals and Chaos Synchronization

Shan Qiao[1], **Tao Jiang**[2], **Lixin Ran**[1, 2], **and Kangsheng Chen**[1]

[1]Department of Information and Electronic Engineering, Zhejiang University, Hangzhou, 310027, China
[2]The Electromagnetics Academy at Zhejiang University, Zhejiang University, Hangzhou, 310058, China

Abstract— In this paper, we present a new scheme for the realization of a wide-band noise-signal RADAR utilizing wide-band chaotic signal generated from microwave chaotic Colpitts oscillator. System simulations show that such RADAR can still work in an environment when the signal-to-noise ratio (SNR) is −20 dB.

High-dimensional Chaotic Regimes in Distributed Radiophysical Systems Operating near the Cutoff Frequency

A. A. Balyakin and E. V. Blokhina
Saratov State University, 83 Astrakhanskaya St., Saratov 410012, Russia

Abstract— We present the results of computer modeling of chaotic dynamics in several radiophysical models (nonlinear ring cavity under external driving, one-dimensional Fabri-Perrot resonator and a gyrotron with non-fixed field structure). We calculated the set of Lyapunov exponents of chaotic attractors for these systems and estimated the dimensions of chaotic attractors from the Kaplan-Yorke formula. The dimensions were found to be anomalously high. We suppose this phenomenon to occur because all these systems operate near a critical frequency.

Spatio-temporal chaos in distributed systems belongs to the most challenging and promising problems of nowadays physics. Its importance is proved to be doubtless since its obvious connection with such fundamental problems as rise of turbulence and pattern formation. Recently, ideas and methods of nonlinear dynamics have been used extensively in application to distributed radiophysical systems as BWOs, gyrotrons, delayed feedback oscillators based on traveling-wave tubes (TWTs), klystrons and various distributed nonlinear resonators. By now it has been established definitely that for certain domains in parameter space these systems can demonstrate single-mode or multimode and chaotic oscillations. For investigation of the dynamics and illustrative representation of the results, it is conventional to use amplitude versus time plots, spectra, phase portraits, and bifurcation diagrams. As believed, analysis of Lyapunov exponents would provide valuable complementary information concerning nature of the regimes observed in such systems.

In the presented work we discuss the results of numerical studying of three systems operating near a cutoff frequency. The first system belongs to classical electron devices where active medium is represented by electron beam interacting with electromagnetic wave. The second one is well-known Ikeda system — a nonlinear ring cavity filled with medium with modulation instability — driven by an external harmonic signal. The last one is the distributed resonator filled with passive medium, where the rise of instability is caused by end reflections and interaction between forward and backward waves. They all, however, have one similar feature which is the presence of critical frequency (stopband) in the dispersion diagram.

We have developed a code to calculate Lyapunov exponents spectra in such systems, based on a adapted Benettine algorithm [1]. To check the preciseness of our program we have tested it in application to some well-known model systems of nonlinear dynamics, including both finite and infinite dimensional systems.

First, let us consider the simple model of distributed system: the piece of nonlinear medium with end reflections driven by an external harmonic signal. That is well known resonator of Fabri-Perrot type, described by a system of coupled nonlinear Schroedinger equations. In our previous work we studied this system in a wide range of parameters [2]. We have found that when operating near cut-off frequency with increase of the input intensity there take place the transition between different regimes: from periodic to chaotic ones. We applied the developed algorithm to this system. In periodic regimes all Lyapunov exponents were proved to be negative, in chaotic regimes we obtained positive Lyapunov exponents. The typical situation is that the number of positive exponents is very high (hyperchaotic regimes), so the dimension, calculated with the help of Kaplan-Yorke formula, turns to be extremely high (more than 10).

To describe the dynamics of a nonlinear ring cavity we used a nonlinear Schroedinger equation with a delay term. Our calculations of the Lyapunov exponents spectrum revealed that hyperchaotic regimes occur only if the modulation instability in such a system turns from a convective to absolute type (that can take place only near a critical frequency), and dimension of the attractor increases significantly (from 1–2 up to 10). In that case there exist a large number of unstable perturbations that get to the other branch of a dispersion curve and thus propagate towards the main wave.

At last, we examined the complex behavior in a gyrotron with non fixed field structure, operating near a cutoff frequency. Besides various self-modulation and chaotic regimes we have found in this systems the regimes of hyperchaos, characterized by several positive Lyapunov exponents [3]. Applying the Kaplan-Yorke formula we obtained the dimension of chaotic attractors to be anomalously high (more than 10)

Improving the Accuracy of PHEMT Models Using Corrective Artificial Neural Networks

J. Dobeš and L. Pospíšil
Czech Technical University in Prague, Department of Radio Engineering
Technická 2, 16627 Praha 6, Czech Republic

Abstract— In the recent PSpice-family programs, only a class of five types of the MESFET model is available for a pHEMT representation. In the paper, a way is suggested for modeling pHEMT using a corrective neural network working attached to an updated analytic MESFET model. The accuracy of procedures is assessed by extracting model parameters for a typical TriQuint pHEMT. A sequence of analyses is also performed for determining an optimal structure of the artificial neural network.

Introduction The Sussman-Fort, Hantgan, and Huang [1] model equations can be considered a good compromise between complexity and accuracy. Therefore, they can be used as an appropriate base for a corrective neural network, but they must be slightly modified in advance for modeling the special microwave elements as pHEMT working at tens of gigahertz.

However, the accuracy of the updated model functions is still of a percentage order. To be more precise, using the corrective neural network with the suitably modified analytic model can be an effective and relatively simple way to obtain sufficiently accurate model.

Modifying the Static Part of the Mesfet Model The primary voltage-controlled drain-source current source of the MESFET model I_d can be defined for the forward mode ($V_\mathrm{d} \geqq 0$) by the formulae [1] with a simple but efficient update:

$$V_T = V_{T0} - \sigma V_\mathrm{d}, \tag{1a}$$

$$I_\mathrm{d} = \begin{cases} 0 & \text{for } V_\mathrm{g} \leqq V_T, \\ \beta(V_\mathrm{g} - V_T)^{n_2}(1 + \lambda V_\mathrm{d})\tanh(\alpha V_\mathrm{d}) & \text{otherwise.} \end{cases} \tag{1b}$$

The model parameters V_{T0}, β, n_2, λ, and α have already been defined in [1], the parameter σ used in (1a) represents the simple update of the original formulae necessary for modeling potential negative conductance in the output characteristics. Although the updated Equation (1) is relatively simple, it contains an improvement in comparison with the Curtice model (by n_2 parameter which characterizes gate voltage influence on I_d), and also in comparison with the Statz model (by σ parameter that characterizes drain voltage influence on I_d).

The modification (1a) enables the model to be utilized as the pHEMT approximation as shown in Fig. 1. The parameter extraction process has given the values $V_{T0} = -1.64\,\mathrm{V}$, $\beta = 0.102\,\mathrm{A\,V^{-2}}$,

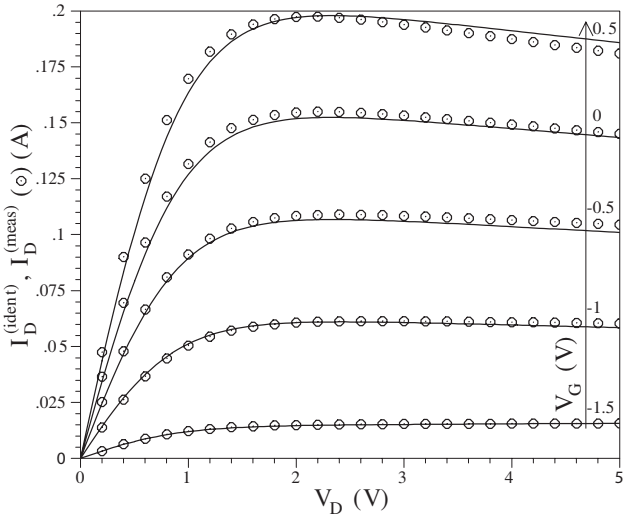

Figure 1: Results of the AlGaAs/InGaAs/GaAs power pHEMT [2] model identification using (1) (rms = 2.38% and $\delta_\mathrm{max} = 8.24\%$).

$n_2 = 0.991$, $\lambda = -0.02884\,\mathrm{V}^{-1}$, $\alpha = 1.16\,\mathrm{V}^{-1}$, $\sigma = 0.00797$, $r_D = 0.3\,\Omega$, and $r_S = 0.2\,\Omega$ with the error of the percentage order.

Selecting the Number of Elements in Layers of ANN Determining the number of elements in the individual layers of the artificial neural networks attached to the modified analytical model is not a simple task. In this section, an illustrative example is demonstrated. The optimal network has been found experimentally in that example. We are now working on an automation of that process with the intention to find the optimal exclusive artificial neural network, or the optimal corrective artificial neural network to a given analytic model.

The tests have been performed for the AlGaAs/InGaAs/GaAs microwave pHEMT, whose analytic model has been identified above. The results are summarized in Table 1. The rms error is the best for the structure MLP-2-4-6-1. However, the very accurate results are also obtained for another structure MLP-2-3-7-1 so we can obtain several networks which get sufficient results.

Table 1: Experimental Searching for Optimal Number of ANN Elements.

Type of network	Relative deviations of networks with 500 training epochs	
	rms (%)	δ_{max} (%)
MLP-2-2-2-1	12.02	192.2
MLP-2-2-3-1	5.683	91.11
MLP-2-2-4-1	2.271	14.98
MLP-2-2-5-1	4.742	36.08
MLP-2-2-6-1	0.9973	**7.196**
MLP-2-2-7-1	2.78	37.67
MLP-2-2-8-1	**0.7249**	9.49
MLP-2-3-2-1	0.8675	5.982
MLP-2-3-3-1	1.418	10.46
MLP-2-3-4-1	0.4432	5.532
MLP-2-3-5-1	0.552	5.728
MLP-2-3-6-1	1.866	14.06
MLP-2-3-7-1	**0.0422**	**0.8029**
MLP-2-3-8-1	1.024	7.29
MLP-2-4-2-1	1.214	13.91
MLP-2-4-3-1	0.2465	2.235
MLP-2-4-4-1	0.3087	4.255
MLP-2-4-5-1	0.0829	1.337
MLP-2-4-6-1	**0.0331**	0.5998
MLP-2-4-7-1	0.1378	2.342
MLP-2-4-8-1	0.0427	**0.4804**

Conclusion The experiments confirm that the precision of the analytic models cannot be better than of a percentage order. Enhancing the precision is possible and relatively easy by corrective artificial neural networks. A sequence of experiments has been performed, which demonstrates that an optimal structure of the network can be systematically found.

REFERENCES

1. Sussman-Fort, S. E., J. C. Hantgan, and F. L. Huang, "A SPICE model for enhancement- and depletion-mode GaAs FET's," *IEEE Trans. Microwave Theory Tech.*, Vol. 34, 1115–1119, Nov. 1986.
2. Cao, J., X. Wang, F. Lin, H. Nakamura, and R. Singh, "An empirical pHEMT model and its verification in PCS CDMA system," *Proc. 29th European Microwave Conference*, 205–208, Munich, Oct. 1999.

Session 4A2
Antenna and Array System 2

A Dual Resonance Three Segment Rectangular Dielectric Resonator Antenna

S. Jarchi[1], **J. Rashed-Mohassel**[1], **M. H. Neshati**[2], **and C. Lucas**[3]

[1]Center of Excellence on Applied Electromagnetic Systems, ECE Department
University of Tehran, Iran
[2]University of Sistan and Baluchestan, Iran
[3]University of Tehran, Iran

Abstract— A three-segment rectangular dielectric resonator antenna with equal segment dimensions and different dielectric constants is investigated. The dielectric constant of each segment is optimized with two different optimization algorithms, genetic algorithm and an optimization algorithm inspired from weed colonization in order to improve bandwidth. A dual resonance frequency response with improved bandwidth is obtained.

Session 4A3
Medical Electromagnetics and Biological Effects

Design and Evaluation of Microwave System for Drying of Textile

Jan Vrba[1], **Marika Pourová**[1], **and Ondřej Žák**[1], **Jan Vrba**[2]

[1]Department of Electromagnetic Field, Czech Technical University in Prague
Technická 2, Prague 6, Czech Republic
[2]ITHE, Aachen University of Technology (RWTH)
Kopernikusstrasse16, Aachen, Germany

Abstract— In this paper we describe our new results dealing with design and evaluation of microwave industrial applicators used for drying of textile materials. We have designed and evaluated two different types of these applicators: open-resonator-type and waveguide-type one. We describe here basic analytical models of the discussed applicators, results of numerical modelling and experimental evaluation as well. Prototype of microwave drying machine working with microwave power of 17 kW at frequency 2.45 GHz is reported.

Introduction: In this contribution we would like to describe our new results dealing with microwave industrial applicators used for drying of textile materials. We have designed and evaluated two different types of these applicators: open-resonater-type and waveguide-type one. We would like to present theoretical models of the discussed applicators, results of numerical modeling and experimental evaluation as well. Protype of microwave drying machine working with microwave power of 17 kW at frequency 2.45 GHz will be reported.

Open Resonator Type Applicator: This type of applicator consists of many drying cells (17 in our prototype machine) — each of them is based on the idea of open resonator (i.e., Fabry-Perrot resonator), see Fig. 1. Each of these cells has its own magnetron placed in waveguide holder. Dryed textile material is in the middle plane between parallel conductive plates, distance between these plates is equal to $(3/2)\lambda$. In the right side of Fig. 1 there is a calculated 2D distribution of electric field strength. Plane of the textile material is in this 2D model given by an abscissa in the middle of the resonator — in the same plane there is an expected maximum of electric field strength.

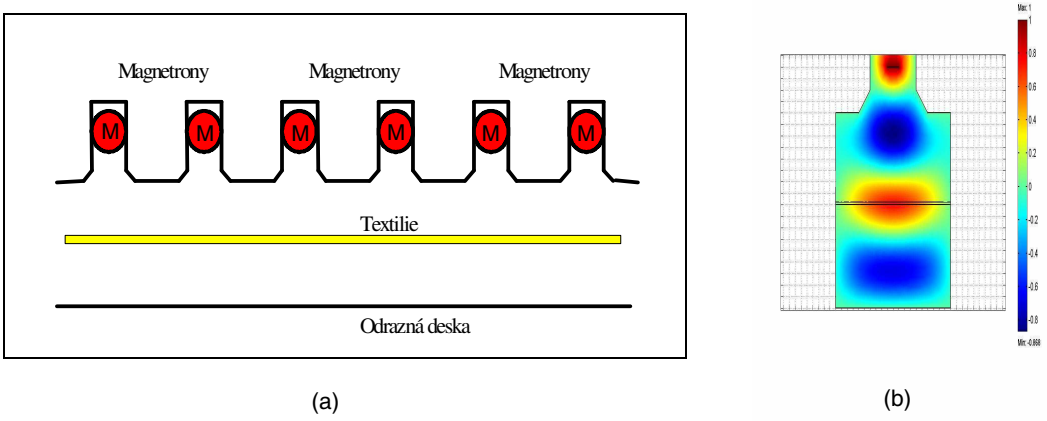

Figure 1: (a) Schematics of 6 cells of open resonator type applicator for drying of textile materials. (b) E field strength 2D distribution in each one of that cells.

For our experiments we have built apparatus with a matrix of 6 cells in first raw, next 5 cells in the second raw and again 6 cells in the third raw — see apertures in the upper conductive plate in Fig. 3. Optimization of overall microwave dryer means to approach to the best possible homogeneity of absorbed microwave energy in the textile material. In the plane of textile material there is shown a calculated distribution of SAR (by aid of software product SEMCAD). Quite a good homogeneity of SAR can be observed and further improvement is obtained thanks to the movement of textile material through microwave drying machine.

Prototype of Microwave Drier: Based on theoretical considerations developed at Czech Technical University in Prague a prototype of microwave drying machine has been built in cooperation of Research Institute of Textile Machines and Technical University in Liberec.

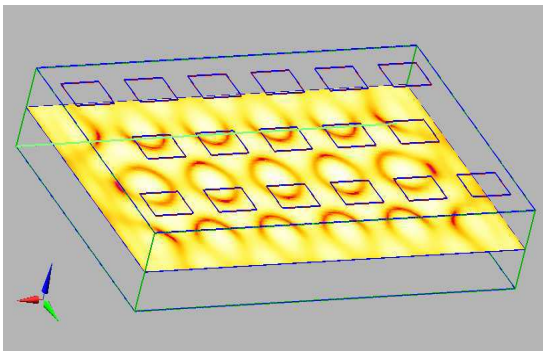

Figure 2: Microwave drying machine 3D schematics and SAR distribution in the plane of the wet textile material (6 cells in first raw, next 5 cells in the second raw and again 6 cells in the last third raw — calculated by SEMCAD).

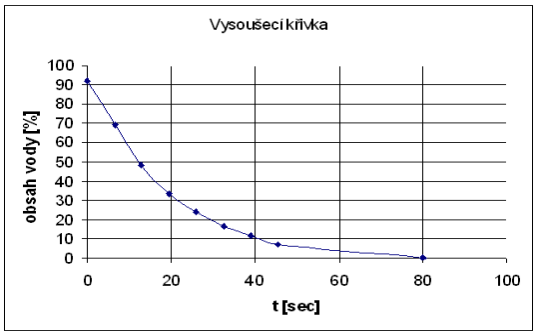

Figure 3: Typical drying characteristics of here described microwave drying systems.

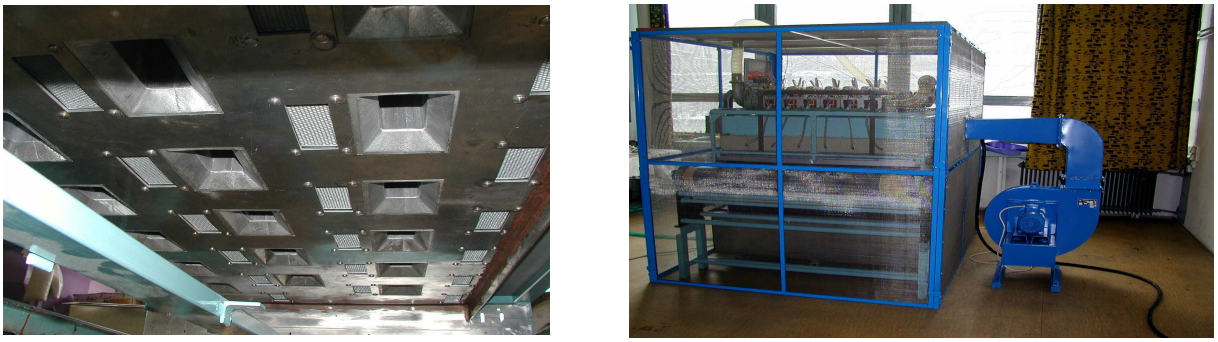

Figure 4: (a) Microwave part of the microwave drying machine. (b) A prototype of microwave drying machine.

In Fig. 4 there is a photo of microwave drier hidden inside a Faraday cage used to reduce leakage of microwave energy (microwave resonator where microwaves are applied on textile is equipped by a set of chokes to prevent the EM energy leakage).

Conclusion, that this assumption is more or less correct can be seen on next figure, where temperature on the drier output has been monitored by infrared camera. In this case velocity of textile belt was 10 cm/s only, and so elementary volume of textile material was inside drier approximately 6 seconds, which was sufficient to increase its temperature from 22 to 61°C.

Basic comparison of classic and microwave drying is given in Tab. 1. We can see quite a big difference in favor of microwave drying.

Table 1: Comparison of classic and microwave drying of textile materials.

ENERGY ABSORBED IN:	CLASSIC DRYING	MICROWAVE DRYING
Mosture in textile	**42 %**	**66 %**
Textile itself	**2 %**	**12 %**
Walls	**5 %**	**1 %**
Others	**51 %**	**21 %**

Effect of Length of Line Source on the Overall Radiation Patterns

Varanasi Shiv Kausik[1,2], **G. S. N. Raju**[1,2], **and R. Ramana Reddy**[1,2]

[1]Department of Electronics and Communication Engineering
Sankethika Vidya Parishad Engineering College, Visakhapatnam, India
[2]Department of Electronics and Communication Engineering, AU College of Engineering
Andhra University, Visakhapatnam530 003, India

Abstract— The linear arrays are popular and their analysis and design are investigated by several authors [1–4]. However, no design is optimum in term of desired directional characteristics. It has been possible to control the radiation patterns by relative element positions, excitation function and the type of element in the array. However, it is of present interest to consider Taylor's method of design of continuous line source to investigate the effect of length of the line source on the overall radiation pattern characteristics.

A line source is considered to be an antenna which is long, narrow with straight geometry. It depends on radiation in fields on current strength with respect to longitudinal coordinate as the basis for its directivity [5]. It is implied that these currents are continuous functions of the longitudinal coordinates.

The expression for radiation pattern as given by Taylor appears in the form of

$$E(u) = \cosh \pi A \frac{\sin u}{u} \prod_{n=1}^{\mathbf{n}-1} \left[\frac{1 - \frac{u^2}{\sigma^2 \pi^2 \left\{ A^2 + \left(\mathbf{n} - \frac{1}{2}\right)^2 \right\}}}{\left(1 - \frac{u^2}{\pi n^2}\right)} \right]$$

where $\mathbf{n}$ is an integer which divides the radiation pattern into uniform sidelobe region surrounding the main beam and the region of decaying sidelobes.

$u = \frac{L}{\lambda} \sin \theta$

L= length of the array

θ is the angle measured from the direction of maximum radiation

A is an adjustable real parameter and

$\cosh \pi A$ gives the sidelobe ratio and

$$\sigma = \frac{\mathbf{n}}{\left[A^2 + (\mathbf{n} - 1/2)^2\right]^{1/2}}$$

for a specified sidelobe ratio the amplitude distributions are numerically computed with length of the line source as a parameter. From the amplitude distribution so designed the patterns are recomputed. From these patterns the effect of length of line source on the overall pattern characteristics is found to vary with $\mathbf{n}$ also.

REFERENCES

1. Woodward, P. M. and J. D. Lawson, "The theoretical precision with which an arbitrary radiation-pattern may be obtained from a source of a finite size," *J. IEE*, Vol. 95, Pt. III, No. 37, 363–370, September 1948.
2. Stegen, R. J., "Excitation coefficients and beamwidths of Tschebyscheff arrays," *Proc. IRE*, 1671–1674, November 1953.
3. Wong, K.-L., F.-R. Hsiao, and T.-W. Chiou "Omni-directional planer dipole array antenna," *IEEE Trans. on Antennas and Propagation*, Vol. 52, No. 2, 624–628, February 2004.
4. Kumar, B. P. and G. R. Branner "Generalized analytical technique for the synthesis of unequally spaced arrays with liner, planar, cylindrical or spherical geometry," *IEEE Trans. on Antennas and Propagation*, Vol. 53, No. 2, 621–634, February 2005.
5. Taylor, T. T., "Design of line source antennas or narrow beamwidth and low sidelobes," *IRE Trans. Antennas Propagat.*, Vol. AP-3, 16–28, January 1955.

Basic Requirements on Applicators for Microwave Thermotherapy, Imaging and Diagnostics

J. Vrba[1], **L. Oppl**[1], **T. Drizdal**[1], **R. Zajicek**[1], **J. Vrba (Jr.)**[2], **P. Togni**[1], **K. Novotna**[1] **L. Visek**[1], **and D. Vrba**[1]

[1]Department of Electromagnetic Field, Faculty of Electrical Engineering
Czech Technical University in Prague
Technická 2, 166 27 Prague 6, Czech Republic
[2]Institute of Theoretical Electrotechnic, RWTH Aachen, Germany

Abstract—

Introduction: Future trends in medical applications of microwave technique and technology can be seen in development of new therapeutic, imaging and diagnostics methods based on high frequency EM field. A significant importance for the future can be identified for the following methods: Microwave radiometry, Measurement of complex permittivity, Microwave tomography, Imaging in the Terahertz waves band and Microwave diagnostic radars. That means to develop very special microwave systems and new types of microwave applicators for such purposes as well. Their common feature is to have a perfect impedance matching in very wide frequency band plus optimized shape of SAR characteristics.

Methods: Microwave radiometry is based on measurement of a very weak EM signal, which radiate any object (e.g., people), whose temperature is superior to absolute zero. It is based on utilization of so-called Planck radiation law. Interest in microwave radiometry is given by possibility of its utilization at diagnostics of cancer and also of inflammatory disorder (e.g., appendicitis, arthritis, atp.) because tumors and inflammatory processes causes temperature rise.

Measurements of complex permittivity "in vivo" seems to be a suitable method for biomedical imaging applications. Usually an open end of coaxial line is used as a very suitable sensor for this measurement. Scanning the studied object by a such probe can bring us a map of the permittivity — we can then evaluate symmetry resp. unsymmetry of the measurement results and from this information we can make hypothesis about possible medical problems.

Microwave tomography is in general application of basic CT principals but by utilization of microwave band. Scattering of EM waves in non-homogeneous human body is however much more complicated than simple attenuation of ionising radiation. Therefore development of microwave tomography is conditioned by new theoretical approach, optimization of evaluation algorythms and more efficient computer technique.

Frequency band of so called Terahertz waves (0.1–10 THz) is being studied during last years We can expect here a lot of new discoveries in material science and in biomedicine as well, especially for imaging purposes. Theoretical models and a feasibility study can be based on similar principles as Microwave Radiometer and Infrared Camera Imaging.

ACKNOWLEDGMENT

This research is supported by Czech Research Program: "Transdisciplinary Research in the Area of Biomedical Engineering II" (MSM6840770012) and by Grant Agency of the Czech Republic project: Medical Applications of Microwaves: "Therapy and Diagnostics" (102/05/0959).

Design and Comparison of Exposure Chambers for Verification of Microwave Influence on Biological Systems

Lukáš Víšek, **Paolo Togni**, **Jan Vrba**, **and Ladislav Oppl**
Department of Electromagnetic Field, Czech Technical University
Technická 2, 166 27 Prague, Czech Republic

Abstract— The main aim of our work is to design and simulate an exposure chamber in order to analyze the influence of electromagnetic field on mice which can simulate mobile phone emission patterns. We use two types of structures and compare their properties to find the best design for our future work.

Comparison between Two Slot-line Applicators for Microwave Hyperthermia

Paolo Togni, **Tomáš Dříž'al**, **and Jan Vrba**
Department of Electromagnetic Field, Czech Technical University
Technická 2, 166 27 Prague, Czech Republic

Abstract— This paper compares two different kinds of slot-line applicators which can be used for microwave hyperthermia treatment, one of the complex methods to treat cancer diseases. During this kind of treatment the biological tissue is exposed to electromagnetic energy in order to enhance its temperature within the range between 41℃ and 45℃. The healing effects are obtained thanks to the higher thermal sensitivity of tumour tissue compared with healthy tissue.

Both planar slot-line applicators are designed for a working frequency of 434 MHz which is one of the allowed frequencies for medical purposes. These applicators are developed on a dielectric board with a 30 µm metallization on one side. Each applicator has three main parts which are respectively: the active part, the ground plane and the slot-line resonator which separates the first two parts. The active part of the first applicator is a squared metal patch with dimensions 30×30 mm while the second one has a circular patch with a diameter of 34 mm. These dimensions allow both structures to resonate at the working frequency in order to radiate the electromagnetic energy to the biological tissue. The biological tissue can be directly in contact with the applicators or eventually with a water bolus inserted between them. The width of the slot-line (7.5 mm for both applicators) gives the correct impedance matching for the working frequency. The rest of the metallization which surrounds the slot lines forms the ground planes. The dimensions of the complete applicators are in the first case a square of 75×75 mm and in the second case a circle with a diameter of 80 mm. The substrate of both applicators is made by a 1.5 mm height dielectric material with relative permittivity 4.3. The impedance matching as well as the SAR distribution inside the biological tissue were first evaluated and then optimized by aid of 3D electromagnetic field simulator. The feeding in simulations was provided by a discrete port with a characteristic impedance of 50 Ω. On the real applicators it was given using coaxial cables cut in such a way to be symmetrical. The impedance matching was measured by network analyzer and the SAR distributions were measured in agar phantom using an IR-camera.

The results of the simulation and measurements have shown similar performance for the both shapes of slot-lines applicators and the possibility to be used for tumours with a dimension of about 50–60 mm which are located on the surface of the body.

The structure of these applicators can be replied in order to compose an array for the treatment of larger areas.

Microwave Time-reversal Hyperthermia

Hana Trefná and Mikael Persson

Department of Signals and Systems, Chalmers University of Technology, Göteborg, Sweden

Abstract— Hyperthermia is presently used as an adjuvant to the radiation therapy in the treatment of certain types of cancers. The goal of hyperthermia treatment is to raise the temperature of a localised cancerous tumour to a therapeutic level without overheating surrounding normal tissue. The necessary temperature range for effective hyperthermia treatment is 40–44°C. One approach for providing the hyperthermia of the deep seated tumours is to employ array of radiators placed circumferencialy around the patient. The idea is to constructively exploit wave interference to selectively heat the tumour.

In this study, we investigate a new beam forming method, which opens up new possibilities in the area of deep heating hyperthermia using a large number of antennas and carefully controlling amplitude and phase of the individual antennas. The method is based on the time-reversal charecteristics of the Maxwell equations. The basic principle of the new method is the electromagnetic modelling of the system. In this modelling, the wave front from a virtual antenna placed in the tumour of the patient is propagated through the patient. The simulated radiated field is then "measured" using the computer model of the surrounding antenna system. The real antenna system is then transmitting the "measured" field in a time reversed order. It is the invariance of the wave equation under time-reversal in lossless media that enables optimal refocusing of time-reversed signal at the original source.

In this contribution, the design of an broadband antenna array for time-reversal based hyperthermia system is presented. Our previous results have showed that for various tumour sizes various frequencies are suitable. In our simulations, we use a computer model of a human body and in particular we focus on treatment of breast and neck tumours. The results include achieved SAR distribution in the treatment areas, which is related to the temperature rise in the tissue. The obtained focusing of the energy in different tumors shows good prospects for a sucessful treatment.

The Effects of 884 MHz GSM Wireless Communication Signals on Spatial Memory Performance: An Experimental Provocation Study

Clairy Wiholm[1,2], **Arne Lowden**[4], **Niels Kuster**[5], **Lena Hillert**[3], **Bengt B. Arnetz**[1,2]
Torbjörn Åkerstedt[4], **and Scott D. Moffat**[6,7]

[1]Department of Family Medicine and Public Health Sciences
Division of Occupational and Environmental Health
Wayne State University, USA
[2]Department of Public Health and Caring Sciences
Uppsala University, Uppsala, Sweden
[3]Department of Public Health Sciences, Division of Occupational Medicine
Karolinska Institute, Stockholm, Sweden
[4]Institute of Psychosocial Medicine (IPM), Karolinska Institutet, Stockholm, Sweden
[5]IT'IS Foundation for Research on Information Technologies in Society
Swiss Federal Institute of Technology (ETH), Zurich, Switzerland
[6]Institute of Gerontology, Wayne State University, USA
[7]Department of Psychology, Wayne State University, USA

Abstract— The effect of electromagnetic fields from digital mobile phones on cognitive functioning is an area receiving increased attention. Several recent studies have examined the effects of radiofrequency fields (RF) during mobile phone use on specific domains of cognitive function. It has been suggested that GSM (Global System for Mobile Communication) RF- emissions improve the speed of information processed and held in working memory (Koivisto 2001). Other authors have reported impairment in reaction time (Preece 1999). However, Wilen et al. (2006) found no differences in reaction time and short term memory in subjects with and without mobile phone related symptoms after exposure to GSM like signals. Most prior laboratory-based exposure studies have been short-term. In most published mobile phone studies, exposure conditions have been non-representative for typical everyday use, the outcome measures have been limited to only some of the purported cognitive effects, and/or they lacked sufficient control conditions. Studies have rarely checked for participants' self-reported symptoms in their regular use of mobile phones. We investigated the effects from a double-blind radio-frequency exposure (884 MHz, /2W peak power, 217 Hz pulse-modulated and 2 Hz DTX signals) on spatial memory. The exposure was conducted in the evening between 7.30 p.m. until 10.30 p.m. (i.e., for three hours).

Purpose: The purpose of this study was to further investigate whether exposure to radio RF fields equal to GSM mobile phone use had any direct impact on learning in a spatial memory performance test and, whether RF exposure, time and sensitivity affect the rate of spatial memory performance in human adults.

Material: The participants were daily mobile phone users, men and women age 18 to 45, with and without symptoms (headache, dizziness and concentration difficulties) they associated with mobile phone use.

Methods: The primary outcome measure was a computerized "virtual" spatial navigation task modeled after the Morris Water Task (Morris et al., 1982) administrated on a standard desktop computer. The task environment was a circular arena surrounded by several cues, which could be used to guide navigation. Hidden beneath the surface of the arena was a platform, and participants were required to locate the platform as quickly as possible. On each of seven trials participants were placed in a different position of the area and facing a different orientation and were informed to locate the platform as quickly and as accurately as possible. The primary dependent variable used in the analysis was the distance traveled on each trial and the amount of improvement (i.e., learning) from trial 1 to 7.

Statistics: Repeated measures ANOVA's were used. Variables in the models included: Sensitvity (Sensitive vs. Non-Sensitive), Exposure (RF vs. Sham), Time (Early 6 p.m. vs. Late 10 p.m.) and Trial (Distance Traveled on each of 7 vMWT trials). Statistical significance was set to $p < .05$.

Results: Subjects showed very good evidence of learning on the vMWT at baseline as revealed by decreases in distance traveled as a function of trial. There were no baseline differences between

the groups (symptomatic vs. non-symptomatic). To assess the amount of learning in the task, the percentage of improvement between the first and last trial was calculated for each subject. Individuals exposed to RF had significantly improved learning compared to sham exposure $p <$ .05, (61% vs. 29% improvement). Although there was no main effect of RF exposure on distance traveled, there was a significant (Trial * Exposure * Time) interaction ($p = .03$).

Discussion: The results of this double-blind intervention study suggest that exposure to 884 MHz, DTX signals may improve learning in a classic measure of spatial memory. Dosimetry modeling of GSM RF suggest that parts of the brain of relevance for executive functioning, including the pre-frontal cortex and the para-limbic area are exposed. This is compatible with the known dependence of spatial memory performance on limbic/hippocampal and pre-frontal systems. Our findings suggest that, under conditions representative of real-life mobile phone exposure, certain cognitive functions of interest are affected. Further studies are needed to pin point the brain mechanisms that may underlie these effects, for example identifying which spepcfic parts of the brain are most affected by GSM exposure.

Modeling of Electromagnetic Sources with Huygens Principle

Markus Johansson, **Jesús Alonso Macías**, **Yngve Hamnerius**, **and Mikael Persson**

Chalmers University of Technology, Sweden

Abstract— It is important to be able to model the field distribution from electromagnetic sources, in dosimetry studies, to make it possible to determine whether exposure safety guidelines, such as the EU directive 2004/40/EC, are complied with. Measured fields on a Huygens surface enclosing a source can be numerically propagated to arbitrary locations on the outside of the surface [1]. The Huygens surface can be approximated by a planar surface positioned between the source and the near-field area of interest. If the total field is known on a large enough surface, the field beyond this can be obtained numerically. When accessing the fields at a workplace usually only the RMS values of the fields are measured.

Therefore a method of determining the complete field, including the phase information, when only field amplitudes have been measured on a set of parallel planes close to the source, see Figure 1, has been developed. The method makes use of the field components on the first plane to calculate the total field on the other planes. First some initial values of the phase angles are chosen. Then the field that the chosen phase angles give can be calculated. To find correct phase angles, the initial angles are changed in small steps, so that they give field amplitudes that come closer and closer to the real amplitudes. An optimization algorithm based on the phase angles, is used to search for those angles that give field amplitudes as close to the correct ones as possible. When the total field is known on one of the planes, an electromagnetic solver with a model of the dielectric properties of a human can be used to calculate the field inside the human.

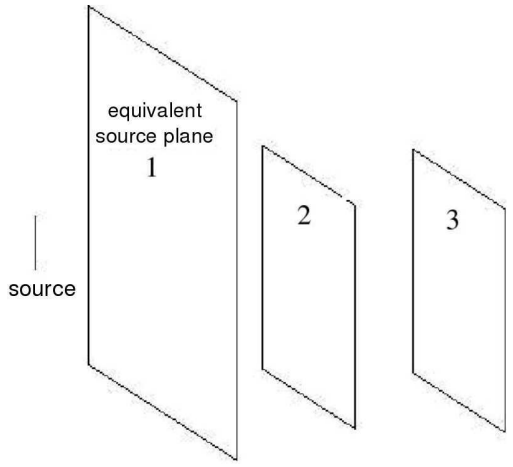

Figure 1: Source in front of planes where field amplitudes can be measured.

Results for a test case, with a robot moving a measurement probe between the measurement points in front of an electromagnetic source, will be presented.

REFERENCES

1. Balanis, C. A., *Antenna Theory Analysis and Design*, John Wiley and Sons, Inc, New York, 1997.

Effects of Dielectric Properties on Radiofrequency Exposure Compliance Using an Alternative Human Head Model

Maia Sauren, **Ray McKenzie**, **and Robert McIntosh**
Australian Centre of Radiofrequency Bioeffects Research (ACRBR), Australia

Abstract— It is difficult to compare studies regarding energy absorption in humans from various radiofrequency (RF) sources due to the contradictions and inconsistencies in RF dosimetry literature. Assumptions used in Specific Absorption Rate (SAR) studies have been insufficiently explored, particularly with regard to the effect of natural variation in the human population of potentially key parameters such as morphology, internal tissue and bone thicknesses and location, dielectric parameters of tissues and overall size. Most studies assume that the average human is a Caucasian male and that all members of the general population, including children and females, are adequately treated as scaled male adults. Dielectric properties of tissues found in the literature are measured using different equipment, from dead tissue or from animal tissue. Frequently, data from a single subject has been used to draw generalized conclusions. The implication is that a randomly chosen individual will provide sufficient information regarding the spread of human anatomical variation.

Due to the nature of available computational models based on either complex realistic models such as Visible Human (Brooks Air Force) or the simple single tissue SAM phantom model (Specific Anthropomorphic Mannequin; IEEE) this issue is not easily explored since the identified parameters are not easily varied within the models. To overcome these deficiencies, we have proposed an alternative compromise model which includes a reduced set of tissues in a semi-homogeneous, simplified geometry for which the key parameters may be varied parametrically. Such adjustments are difficult to achieve using complex realistic models such as Visible Human, which consist of many complex three-dimensional shapes.

We have reviewed some of the available data of human anatomic variations in the tissues of interest and have used this to populate the new model. Using this data we have begun to investigate which of these assumptions are appropriate; what approximation can be used in physical and computational modelling of humans for SAR calculations; and what trade-offs can be made between accuracy and modelling requirements for practical considerations. Key issues being investigated are how SAR varies between children and adults, between males and females, and how to model SAR in the foetus of pregnant females.

It is hoped that this study will produce a model and methods which allow for faster, more accurate and more efficient assessment of compliance with radiofrequency exposure limits. We have previously completed work on the effect of adult cranial and adult skin thickness, and here we present results pertaining to the effects of dielectric properties on SAR.

Session 4A4
EBG, Electromagnetics Wave & Media

Design and Development of Carbon-Nanotube EBG's and Sensors

T. Thai, **A. Traille**, **and M. M. Tentzeris**
School of ECE, Georgia Institute of Technology, Atlanta, GA 30332-0250, USA

Abstract— Carbon nanotubes (CNTs) have been found to have many distinct properties that may enable next generation of sensors with very high sensitivity up to 1 ppb (part per billion). Most CNT-based active sensors employ the change in resistance, thermoelectric power, electrical breakdown voltage, or dielectric properties of the nanotubes for detection. Recently, a resonator-based gas sensor has demonstrated, that enables remote sensing in which the resonator is coated with CNT composite. The operation is based on the change of the effective relative permittivity of the resonator which results in a resonant frequency shift of 1–4 MHz when exposed to different gases including NH3 and CO at several hundreds ppb to several ppm (part per million) for a center resonant frequency of 3.88936 GHz.

The goal of the presented effort is the design and development of a sensing device that features a better detection performance than the traditional ones that rely on small shifts in resonant frequency. The device consists of spatially configurations of passive antennas, that give rise to changes of radiation pattern and gain whenever exposed to gases such as NH3 or NO2. CNT composites may be used as dielectric spheres for three dimension structures or dielectric cylinders for two dimension ones in uniform dielectric substrates. These periodic dielectric structures give rise to an electromagnetic/photonic bandgap (EBG/PBG) in which certain frequencies are forbidden to propagate. The bandgap is determined by the periodic lattice structure and the dielectric contrast which is the refractive index ratio between the background dielectric and lattice dielectric. There's a sharp cutoff for dielectric contrast at which bandgap starts to appear. The gap exists for refractive index contrast as low as 2 for three dimension structure; whereas the gap exist for the contrast at 7.2 for two dimension structure.

The dielectric constant of CNT composites has been reported to be in the range 2–5, depending on different composites and operating frequencies. When SWNTs get coated with different materials, their composites exhibit selectivity in sensing the gases. The change of dielectric constant is about 1% when exposed to NH3 or CO2, leading to a change in dielectric contrast about 0.02–0.08 (estimated). It can be estimated that a change of 0.02 in dielectric contrast gives a change of about 0.078% in the maximum bandgap expressed as percentage of the midgap frequency (13 GHz), which gives a change of 10 MHz to 40 MHz bandgap. If the CNT composite dielectric lattice and the back ground dielectric are chosen to have the dielectric contrast near the low cut off of the bandgap, then a change of 10–40 MHz can yield a notable change in observable spectrum; while at the frequency that is cut off, the radiation pattern and gain may change significantly as well. In the presentation, we will give results about two dimensional EBG/PBG structures (with a midgap frequency of 13 GHz) since all CNT composite "atoms" in this type of lattice can be exposed to the sensed gases, maximizing the sensitivity.

EBG Substrate in Unilateral Fin Line Resonator

Humberto C. C. Fernandes, Davi B. Brito, and Joêmia L. G. Medeiros

Department of Electrical Engineering, Universidade Federal do Rio Grande do Note
P. O. Box 1583, 59.078-970-Natal/RN, Brazil

Abstract— The aim of this work is to characterize and to use the characteristic parameters of the planar structures, constructed with fin lines, looking for their applications in devices, using EBG — *Electromagnetic Band Gap* photonic materials as substrate, operating in the millimeter and optic wave bands. The parameters considered in the structures characterization are the complex propagation constant and the characteristic impedance of unilateral and bilateral fin lines that were obtained by the use of the TTL — Transverse Transmission Line method, together with the method of the Moments. New results are presented.

The electromagnetic band gap have emerged as a new class of periodic dielectric structures where the electromagnetic waves propagation is forbidden for all frequencies in the electromagnetic band gap (EBG) materials, have created innovative methods for controlling the electromagnetic behavior of antennas and other electronic devices. Created from periodic dielectric and/or metallic structures these materials are characterized by a band of frequencies where no propagating modes exist, known as the EBG. In different implementations, the EBG properties may be used to guide wave, filter, store, reflect or collimate electromagnetic waves. This paper demonstrates an application of the 2D layer-by-layer EBG crystal as substrate: an efficient unilateral fin line resonator. The unilateral fin line resonator consists of a rectangular wave guide in which exist three dielectric regions, the second being a substrate placed in the guide most central part, and having a conductor fin longitudinally placed throughout the guide. The method utilized to analyze the structure is the Transmission Line Method — TTL, which is a full wave method in the spectral domain. From the Maxwell's rotational equations the electromagnetic fields equations are developed, then separating the x and z components the final equations in the Fourier Transform Domain considering the structures ith regions. Appling the boundary conditions and after algebraic developing, the unknown constants are obtained. With this, the general equations of the electromagnetic fields as function of E_{xt} and E_{zt}, which are the tangential components of the electric field, are obtained. The initial step to calculate the propagation constant is isolate, the still unknown, E_{xt} and E_{zt} components in the magnetic field equations of the slot regions. Substituting the magnetic field equations and isolating the terms in the electric fields, were find the equations that can be written through the admittance functions. Continuing, the scalar product of the admittance matrix is made by the conjunct of base functions according to the Gallerkin method, the particular case of moment method. With this, the current densities are annulated and a new matrix equation is obtained. So the system has a non trivial solution, the matrix determinant coefficients must be equal to zero. This determinant is represented by a transcended equation that has as roots the attenuation constant "α" and phase constant "β", and the complex propagation constant $\Gamma = \alpha + j\beta$. Once the propagation constant is obtained the effective dielectric constant, "ε_{eff}", is calculated. Finally new results can be obtained for this structure.

Meta-material Multilayer Substrate Planar Resonators with Superconductive Patch

H. C. C. Fernandes and G. D. F. Alves

Electrical Engineering Department, Federal University of Rio Grande do Norte
Lagoa Nova, P.O.Box 1583, 59.078-970-Natal/RN, Brazil

Abstract— The rectangular discretized multilayer microstrip resonators, analyzed using the full wave TTL — Transverse Transmission Line method in the spectral domain, jointly with the moment method is presented. The Superconductive Material (YBCO) is utilized as patch irradiate. The focus of this paper is to introduce novel, artificial periodic magneto-dielectric meta-material structures that exhibit new electromagnetic functionality and previously unobtainable figures of merit. The main objectives are to accurately characterize the meta-materials and present the behaviors of electromagnetic waves within such composite structures. The powerful computational techniques based on the anisotropic effective medium theory (AEMT), and finite difference time domain (FDTD) broadband analysis with periodic boundary condition/perfectly matched layer (PBC/PML) are applied to characterize the periodic materials. The obtained results can be integrated into the design of novel materials with potential applications in wireless systems. Some applications of meta-materials in the areas of electromagnetic band-gap (EBG) structures and antenna miniaturization are highlighted in this work.

In recent years there have been significant amount of research in the area of functional meta-materials. The Superconductive Material (YBCO) is utilized as patch irradiate. The inclusion of the superconductor characteristics is obtained through complex resistive boundary conduction. The focus of this paper is to introduce novel, artificial periodic magneto-dielectric meta-material structures that exhibit new electromagnetic functionality and previously unobtainable figures of merit.

The aim of meta-material development is to propose novel periodic configurations of available materials for achieving new media with desired figures of merit. Different material properties such as Double Negative (DNG), Double Positive (DPS), Epsilon Negative (ENG), and Mu Negative (MNG) parameters have been investigated and many novel applications for them in the areas of RF and optical systems have been proposed.

However, most of the designs are still in the stage of theory and there is a big challenge to integrate.

Antennas with dielectric multilayer have advantages, such as, the flexibility in the operation frequency band, and a smaller physical size.

The TTL — Transverse Transmission Line method is used in the determination of the electromagnetic fields components in the Fourier transform domain (FTD), for the three regions of the structures. The moment method is applied and adequate basis functions are used to expand the current densities in the metallic strip.

The transmission amplitude and phase for a plane wave propagating through the meta-material are obtained and the results are successfully compared with the performance of an equivalent medium with $\varepsilon_{eff} - \mu_{eff}$ constitutive parameters.

Left Handed Effect in a Dielectric PBG-Prism at Microwave Frequencies

S. Massaoudi[1], **A. de Lustrac**[2], **and I. Huynen**[1]

[1]Laboratoire d'Hyperfréquences, Université catholique de Louvain, Louvain-la-Neuve 1348, Belgium
[2]Institut d'Electronique Fondamentale, Université Paris-sud
Bât 220, Département CROQ, Orsay Cedex 91405, France

Abstract— The study concerns the properties of a dielectric Photonic Band Gap Prism (PBG-Prism) at microwave frequencies. We seek to show the effect of Left handed Material between 18 GHz and 27 GHz. The dielectric PBG-prism is made of dielectric rods disposed in an isosceles right-angled triangle.

First, the band diagram and iso- frequency curves are calculated to predict the electromagnetic behavior of these structure. The radiation patterns are calculated with HFSS for different frequencies to show some properties of the dielectric PBG-Prism. In the first allowed frequency band, the dielectric crystals (PC) behave like a homogeneous media. In the second authorized frequency band, the PBG-Prism behaves like a Left Handed Material, i.e., the group velocity and the wave vector are in the opposite direction.

The results of the Dielectric PBG-prism: The Figure 1(a) shows the picture of the dielectric PBG-Prism. The dielectric prism is made with 136 Nylon's rods disposed in an isosceles right-angled triangle. The permittivity and the diameter of each rod are $e = 3.5$ and $d = 5\,\text{mm}$ respectively. The period is $p = 7\text{mm}$. The calculations are taken in TM polarization, i.e., the Electric Field is parallel to the rods. Figure 1(b) gives the three dimensional dispersion diagram calculated with the Plane Waves Method [1]. Figure 1(c) shows the radiation pattern calculated with HFSS [2] at 18.5 GHz of a prism. The numerical results show that the dielectric photonic band gap prism behaves like a homogenous and classical medium in its first authorized frequency band. In the second authorized band, the group refractive index is negative ($n_g < 0$) and the phase refractive index is positive ($n_\phi > 0$). The group velocity and the wave vector are in the opposite direction. The dielectric photonic band gap material behaves like a Left Handed Material.

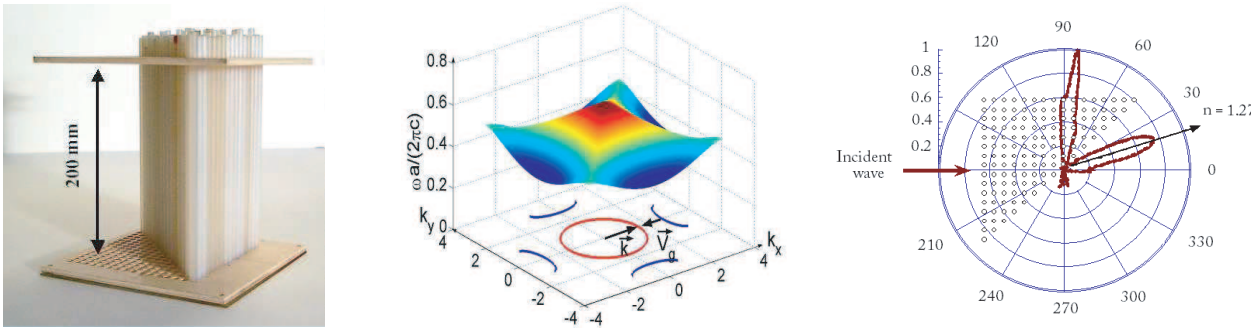

(a) (b) (c)

Figure 1: (a) Picture of PBG-prism, (b) three dimensional dispersion diagram calculated with Plane Wave Method. The blue curves represent the iso-frequency curve of PBG-Prism calculated at 18.5 GHz. The red curve represents the isofrequency curve of vacuum, (c) Radiation pattern calculated at 18.5 GHz with HFSS.

REFERENCES

1. Massaoudi, S., Ph.D. Thesis, Institut d'Electronique Fondamentale, Université Paris-Sud, France, 2005.
2. Remski, R., "Application note, analysis of photonic band gap surfaces using ANSOFT HFSS," *Microwave Journal*, September 2000.

Formulation of Two-dimensional Electromagnetic Scattering from Dielectric Lamellar Grating with Finite Number of Grooves

Koki Watanabe[1] **and Kenji Higa**[2]

[1]Faculty of Information Engineering, Fukuoka Institute of Technology
3-30-1 Wajirohigashi, Higashi-ku, Fukuoka 811-0295, Japan
[2]Graduate School of Engineering, Fukuoka Institute of Technology
3-30-1 Wajirohigashi, Higashi-ku, Fukuoka 811-0295, Japan

Abstract— This paper shows a new approach to the electromagnetic scattering problems from imperfectly periodic structures. As well know, when a plane wave is incident on a perfectly periodic structure, the Floquet theorem claims that the scattered fields are pseudo-periodic (namely, each field component is a product of a periodic function and an exponential phase factor) and the analysis region can be reduced to one periodicity cell. However, in case of structure in which the periodicity is collapsed even if locally, the Floquet theorem is no longer applicable and the computation has been mainly performed with the finite difference time-domain method, the finite element method, the time-domain beam propagation method, the method of the fictitious sources, etc., in which the analysis region has to cover whole scatterers under consideration.

This paper deals with the electromagnetic scattering from a dielectric lamellar grating with finite extent (See Fig. 1). We consider time harmonic fields assuming a time-dependence in $e^{-i\omega t}$. The structure is uniform in the z-direction, and the x-axis is parallel to the direction of periodicity. The cover and the substrate regions are both filled with homogeneous and isotropic materials, and $2M$ grooves are ruled. The incident field, which does not need to be plane wave, is supposed to be a function of x and y only. Therefore the fields are uniform in the z-direction and two-dimensional scattering problem is considered.

The present formulation is based on the pseudo-periodic Fourier transform [1], which makes any function pseudo-periodic. Maxwell's equations and the constitutive relations are transformed and the benefit of the pseudo-periodicity makes us possible to express the transformed field components in the generalized Fourier series [2] without introducing an approximation of artificial periodic boundary. Also, we introduce a discretization of the transform parameter, and then the problem can be solved by using well-known rigorous coupled-wave method [3].

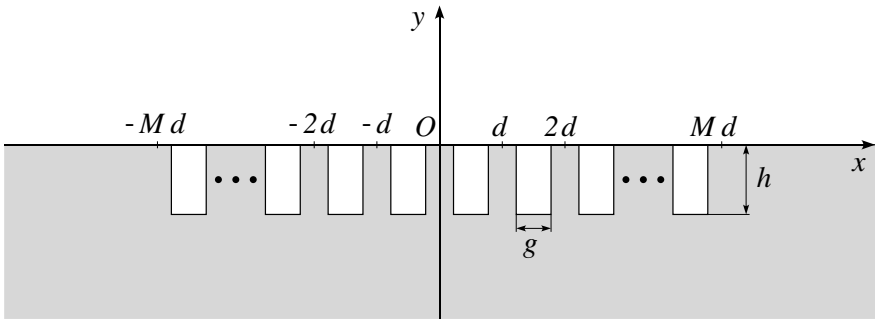

Figure 1: Geometry of lamellar grating with a finite number of grooves.

REFERENCES

1. Watanabe, K., "Optical waveguide analysis using fourier series expansion method based on pseudo-periodic fourier transform," *Proc. 6th Asia-Pacific Eng. Forum on Microwaves and Electromagnetic Theory*, 150–157, 2006.
2. Petit, R., ed., *Electromagnetic Theory of Gratings*, Springer-Verlag, Berlin, 1980.
3. Moharam, M. G. and T. K. Gaylord, "Diffraction analysis of dielectric surface-relief gratings," *J. Opt. Soc. Am.*, Vol. 72, 1385–1392, 1982.

Wave Transport and Time Reversal in Random Structures with Anisotropic Disorder

Gregory Samelsohn

Department of Communication Engineering, Holon Institute of Technology
Holon 58102, Israel

Abstract— Time reversal (TR) is a powerful technique allowing for both space focusing and time compression of (ultra-)wideband signals [1]. Introduced initially in geophysics and ultrasound, it becomes to be used as a practical tool in microwaves and optics [2]. Usually, TR is more effective in strongly scattering disordered media, and is shown to be rather sensitive to the statistics of the structure. In the present work, we investigate time reversal and the phenomena of wave transport (localization, diffusion, ...) for anisotropically disordered structures.

Two closely related problems are considered here. The first one is the relationship between the localization/diffusion and their characteristics (say, localization length and pulse delay time), on the one hand, and the correlation properties of the scattering potential, on the other. To answer this question we have developed a theory [3, 4] that enables a perturbative analysis of the relevant characteristics in random media with continuous type disorder.

It is shown, in particular, that in the long-wavelength limit the radiation is always localized in 2D, and the localization length is independent of the direction of propagation, the latter in contrast to the predictions based on an anisotropic tight-binding model. For shorter wavelengths that are comparable to the correlation scales of the disorder, the transport properties of disordered media are essentially different in the directions along and across the correlation ellipse. There exists a frequency-dependent critical value of the aspect ratio, below which waves are localized at all angles of propagation. Above this critical value, the radiation is localized only within some angular sectors centered at the short axis of the correlation ellipse and is extended in other directions. Analytical results concerning anisotropic time-domain diffusion in both localized and extended regimes have been also obtained. They are in a good agreement with experiments studying light diffusion in anisotropic semiconductors [5].

The second problem investigated here is the effect of structural anisotropy on the time reversal process. It is demonstrated that theoretically predicted anisotropic transport behavior correlates with the results of extensive numerical experiments aimed at studying the time reversal resolution of ultra-wideband signals in 2D random media. A classical FDTD method supplemented by a convolutional stretched coordinate PML has been utilized. An isolated electric (magnetic) dipole and a number of TR transducing arrays with different polarizations have been examined. The results obtained show that the resolution of time reversal, i.e., the ability of the system to refocus the wave in both space and time, depends essentially on the material anisotropy and propagation angle. A pronounced correlation between the localization/diffusion behavior of the wave and time reversal resolution in backpropagated fields is predicted. The analysis can be generalized to 3D anisotropic media.

REFERENCES

1. Fink, M., et al., *Rep. Prog. Phys.*, Vol. 63, 1933, 2000.
2. Lerosey, G., et al., *Phys. Rev. Lett.*, Vol. 92, 193904, 2004.
3. Samelsohn, G., S. A. Gredeskul, and R. Mazar, *Phys. Rev. E*, Vol. 60, 6081, 1999.
4. Samelsohn, G. and V. Freilikher, *Phys. Rev. E*, Vol. 70, 046612, 2004.
5. Johnson, P. M., et al., *Phys. Rev. Lett.*, Vol. 89, 243901, 2002.

Time Reversal in Lossy Material: An Assessment

I. Scott, **A. Vukovic**, **and P. Sewell**
George Green Institute for Electromagnetics Research, School of Electrical and Electronic Engineering
University of Nottingham, University Park, Nottingham, NG7 2RD, UK

Abstract— Time reversal of electromagnetic waves is a promising technique for synthesizing circuits and devices to produce a desired response. However, time reversed simulations are subject to computational errors caused by finite precision floating point representations which limits the fidelity of the approach. By considering canonical configurations for which analytic solutions are available, an assessment of the consequences of the resulting finite spatial and temporal resolution for time reversal simulation is presented. Specifically, a modal decomposition describing the fields within an electromagnetic waveguide [1], naturally quantifies the error after reversal caused by the presence of the evanescent modes of the waveguide. In this paper, the TLM (Transmission Line Modeling) technique for numerical simulations is investigated in this context [2]; however, the same problem is inherent to any numerical time reversal algorithm with fixed (floating point) accuracy.

The paper will progress to observe similar effects in the presence of conductive materials and establish guidelines for determining the viability of time reversal design approaches in this case. The inclusion of loss in time reversal algorithms is usually assumed to be both present in forward and reverse simulations. It will be shown, that under certain conditions, that the loss in the forward simulation can be, balanced by gain in the reverse simulation, in essence creating a controlled instability.

The paper will compare analytic time reversal models for waveguides, with an artificially created precision equal to that of the numerical simulations, re-enforcing the conclusions drawn from the numerical models. An analytic model for a cylindrical problem space will also be given, showing the same effects observed for the waveguide problem. The properties of biological materials, specifically human Grey Matter, in relation to time reversal synthesis will also be analyzed, in the context of optimizing Magnetic Resonance Imaging coils [3].

REFERENCES

1. Cheng, D. K., *Field and Wave Electromagnetics*, 2nd Edition, Addison-Wesley, Reading, Massachusetts, 534–546, 1989.
2. Christopoulos, C., *The Transmission-line Modeling Method: TLM*, Oxford University Press, Oxford, 1995.
3. Gabriel, S., R. W. Lau, and C. Gabriel, "The dielectric properties of biological tissues: II. Measurements in the frequency range 10 Hz to 20 GHz," *Phys. Med. Biol.*, Vol. 41, 2251–2269, 1996.

Eigenfunction Expansions of Source-excited Electromagnetic Fields on Open Cylindrical Guiding Structures in Unbounded Gyrotropic Media

A. V. Kudrin[1], **E. Yu. Petrov**[1], **and T. M. Zaboronkova**[2]

[1]University of Nizhny Novgorod, Russia
[2]Technical University of Nizhny Novgorod, Russia

Abstract— Electromagnetic fields excited by sources in anisotropic media are usually sought using Green's dyadics or Fourier transforms. In the case of gyrotropic anisotropic media, neither of these approaches has substantial advantages over each other, since dyadic Green's functions in such media cannot be expressed in closed forms and are represented in terms of Fourier-type integrals. Moreover, in resonant gyrotropic anisotropic media describable by tensors whose diagonal elements have opposite signs, the Green's functions are singular not only at the source point but also on the surfaces of the so-called resonance cones. Because of these difficulties, an alternative approach based on using eigenfunction expansions of source-excited fields turns out to be more suitable for field evaluations in the aforementioned media. Recent studies of source-excited fields on open magnetized (gyrotropic) plasma waveguides [1] have shown that systematic use of eigenfunction expansions provides a convenient and easily calculated method of finding the total field of a given source located in a magnetoplasma.

In this paper, we extend methods initially developed for representing source-excited electromagnetic fields in the presence of cylindrical guiding structures immersed in a magnetoplasma [1] to the case where spatially bounded, given sources are located in a general gyrotropic medium whose permittivity and permeability are both describable by tensors with nonzero off-diagonal elements. It is assumed that the medium is radially inhomogeneous inside a cylinder of given radius, and is homogeneous outside it. The axis of symmetry of such a cylindrically stratified structure is parallel to the gyrotropic axis of the medium.

The total field is sought in terms of the vector modal solutions of homogeneous Maxwell's equations in cylindrical coordinates ρ, ϕ, and z, assuming that the z axis is aligned with the symmetry axis of the structure. The modes are solutions of source-free Maxwell's equations, have fixed transverse field configurations not varying along the direction of propagation, here taken as z direction, and satisfy the regularity condition at $\rho = 0$ and the boundedness conditions $\rho^{1/2}|\boldsymbol{E}| < C_E$ and $\rho^{1/2}|\boldsymbol{H}| < C_H$ at $\rho \to \infty$ [1, 2]. Here, $\boldsymbol{E}$ and $\boldsymbol{H}$ are the modal fields and C_E and C_H are certain finite constants. By solving this boundary-value problem, it is possible to determine the content of the modal spectrum, which comprises both the discrete and continuous parts, establish orthogonality relations for the modes, and then calculate their excitation factors due to given sources. Note that the modes of the continuous spectrum are grouped into two categories, which is related to the presence of two nondegenerate normal waves in the background medium, in contrast to the case of a gyrotropic cylinder surrounded by an isotropic medium [3]. The resulting field is yielded by summing (integrating) over all modes and is shown to satisfy the radiation condition at infinity. To demonstrate the applicability of the method, representations of total fields due to given sources will be provided for special cases. It is shown that the developed theory makes it possible to immediately obtain source-excited fields in the form of an eigenfunction expansion in terms of the found modal solutions, which allows one to readily perform field evaluations in cylindrically stratified unbounded gyrotropic media without preliminary calculations of dyadic Green's functions or making use of the Fourier transform technique.

REFERENCES

1. Kondrat'ev, I. G., A. V. Kudrin, and T. M. Zaboronkova, *Electrodynamics of Density Ducts in Magnetized Plasmas*, Gordon and Breach, Amsterdam, 1999.
2. Shevchenko, V. V., *Continuous Transitions in Open Waveguides*, Golem Press, Boulder, 1971.
3. Manenkov A. B., "Irregular magneto-optical waveguides," *IEEE Trans. Microwave Theory Tech.*, Vol. MTT-29, No. 9, 906–910, 1981.

Reflection and Transmission in General Single Wire Medium Interface

A. J. Viitanen and I. S. Nefedov
Department of Electrical and Communications Engineering
Helsinki University of Technology, Finland

Abstract— In recent years a lot of research on artificial materials composed of wire lattices have been done. Wire lattice structures behave in certain frequency range like plasma and, hence, the wire media are sometimes called artificial plasma. Because of solid construction with plasma behaviour the wire media are supposed to have practical applications in waveguide structures and in antenna feed constructions, for example, for matching and beam forming. Unlike natural plasma, wire media are strongly spatially dispersive which property make them theoretically and physically very interesting because of new phenomena. In this study we consider the reflection problem from a single wire medium interface when the direction of wires is obliquely oriented to the normal direction of the interface. This is the generalization of our previous studies [1, 2] where the wire directions were normal or perpendicular to the interface. In there we have shown that in wire medium there exist two eigenwaves for the specific polarization. This makes the reflection problem more complicated as usual. The reflection and transmission coefficients are evaluated using the approach introduced by Henneberger [3]. In this method one avoids to use an additional boundary condition by assuming a thin transition layer at the interface when calculating the reflected and transmitted fields.

In the second part of this study the power ow of the transmitted fields are considered. In the wire medium there are propagating two eigenfields. Because of obliquely oriented wires these two fields propagate in different directions. The Poynting vectors for the eigenfields are evaluated. It should be noted that the Poynting vector of each eigenfield has an additional term due to spatial dispersion. These additional terms are evaluated and demonstrated that the direction of the Poynting vector coincides with the direction of the group velocity in wire medium.

REFERENCES

1. Nefedov, I. S., A. J. Viitanen, and S. A. Tretyakov, "Propagating and evanescent modes in two-dimensional wire media," *Physical Review E*, Vol. 71, No. 4, 046612-1-10, April 2005.
2. Nefedov, I. S., A. J. Viitanen, and S. A. Tretyakov, "Electromagnetic wave refraction at an interface of a double wire medium," *Physical Review B*, Vol. 72, 245113-1-9, December 2005.
3. Henneberger, K., *Phys. Rev. Lett.*, Vol. 80, 2889–2892, 1998.

2D Complex Beam Representation in Terms of Cylindrical Harmonics

Raúl Mahillo-Isla, **María-Jesús González-Morales**, **and Carlos Dehesa-Martínez**

Departamento de Teoría de la Señal y Comunicaciones e Ingeniería Telemática
ETSIT Universidad de Valladolid, Spain

Abstract— One of the most interesting approaches when dealing with beams in radiation and scattering problems is the complex source method [2] since it provides exact beam-like solutions to the Helmholtz wave equation in the whole space, known as complex beams. Other popular point of view is to use Gaussian beams. The price paid for the use of Gaussian beams is that they are no longer solutions of the Helmholtz wave equation, they are only an approximation in the paraxial region. On the other hand, the complex beams have other disadvantages such as irregularities (a branch cut) in the beam waist that the paraxial solutions do not have. In this way, severe problems arise when trying to solve scattering problems in which the obstacles are in the beam waist without making paraxial approximations.

The authors' proposal is to provide beam representations based on complex beams with their advantages but without their disadvantages: The beams representations must be exact solutions of the Helmholtz wave equation and must be free of branch cuts. In this essay the authors study how to obtain these representations, based on the plane wave spectrum [1] of solutions of the 2D Helmholtz wave equation.

In the 2D case, two kinds of natural harmonic expansions appear: cylindrical and elliptic-cylindrical harmonics. The first one is the most immediate when dealing with 2D plane wave spectrum, as the plane wave spectrum can be approximated by its Fourier series with each term giving a cylindrical harmonic. This approximation will not take account of the extension of the source since a cylindrical harmonic has an anisotropic point source in the general case. Thus, this expansion will not be able to provide a good description of the beam waist, although far from the waist provide an straightforward representation of the field. The expansion in elliptic-cylindrical harmonics can solve the problem with the beam waist as the equivalent sources of each harmonic have the same length of the support as the complex beam without having a branch cut in the waist of the beam. In order to accomplish the expansion, the plane wave spectrum of an elliptic-cylindrical harmonic is used [3].

The paper will carry out convergence studies for both kind of expansions and comparisons with the complex beam solution.

REFERENCES

1. Clemmow, P. C., *The Plane Wave Spectrum Representation of Electromagnetic Waves*, 1 reissued edition, Oxford University Press & IEEE Press, Oxford & New Jersey, 1996.
2. Felsen, L. B., "Complex source point solutions of the field equations and their relations to the propagation and scattering of gaussian beams," *Symposia Mathematica*, Vol. 18, 39–56, 1976.
3. Stratton, J. A., *Electromagnetic Theory*, 1 edition, McGraw-Hill, New York, 1941.

Author Index